

ISSN 0973-8916

Current Trends in Biotechnology and Pharmacy

Volume- 17

Issue 2

April 2023



www.abap.co.in

Current Trends in Biotechnology and Pharmacy

ISSN 0973-8916 (Print), 2230-7303 (Online)

Editors

Prof.K.R.S. Sambasiva Rao, India
krssrao@abap.co.in

Prof.Karnam S. Murthy, USA
skarnam@vcu.edu

Editorial Board

Prof. Anil Kumar, India
Prof. P.Appa Rao, India
Prof. Bhaskara R.Jasti, USA
Prof. Chellu S. Chetty, USA
Dr. S.J.S. Flora, India
Prof. H.M. Heise, Germany
Prof. Jian-Jiang Zhong, China
Prof. Kanyaratt Supaibulwatana, Thailand
Prof. Jamila K. Adam, South Africa
Prof. P.Kondaiah, India
Prof. Madhavan P.N. Nair, USA
Prof. Mohammed Alzoghaibi, Saudi Arabia
Prof. Milan Franek, Czech Republic
Prof. Nelson Duran, Brazil
Prof. Mulchand S. Patel, USA
Dr. R.K. Patel, India
Prof. G.Raja Rami Reddy, India
Dr. Ramanjulu Sunkar, USA
Prof. B.J. Rao, India
Prof. Roman R. Ganta, USA
Prof. Sham S. Kakar, USA
Dr. N.Sreenivasulu, Germany
Prof.Sung Soo Kim, Korea
Prof. N. Udupa, India
Dr.P. Ananda Kumar, India
Prof. Aswani Kumar, India
Prof. Carola Severi, Italy
Prof. K.P.R. Chowdary, India
Dr. Govinder S. Flora, USA
Prof. Huangxian Ju, China
Dr. K.S.Jagannatha Rao, Panama
Prof.Juergen Backhaus, Germany
Prof. P.B.Kavi Kishor, India
Prof. M.Krishnan, India
Prof. M.Lakshmi Narasu, India
Prof.Mahendra Rai, India
Prof.T.V.Narayana, India
Dr. Prasada Rao S.Kodavanti, USA
Dr. C.N.Ramchand, India
Prof. P.Reddanna, India
Dr. Samuel J.K. Abraham, Japan
Dr. Shaji T. George, USA
Prof. Sehamuddin Galadari, UAE
Prof. B.Srinivasulu, India
Prof. B. Suresh, India
Prof. Swami Mruthinti, USA
Prof. Urmila Kodavanti, USA

Assistant Editors

Dr.Giridhar Mudduluru, Germany

Dr. Sridhar Kilaru, UK

Prof. Mohamed Ahmed El-Nabarawi, Egypt

Prof. Chitta Suresh Kumar, India

www.abap.co.in

ISSN 0973-8916

Current Trends in Biotechnology and Pharmacy

(An International Scientific Journal)

Volume 17

Issue 2

April 2023



www.abap.co.in

Indexed in Chemical Abstracts, EMBASE, ProQuest, Academic SearchTM, DOAJ, CAB Abstracts, Index Copernicus, Ulrich's Periodicals Directory, Open J-Gate Pharmoinfonet.in Indianjournals.com and Indian Science Abstracts.

Association of Biotechnology and Pharmacy (Regn. No. 28 OF 2007)

The Association of Biotechnology and Pharmacy (ABAP) was established for promoting the science of Biotechnology and Pharmacy. The objective of the Association is to advance and disseminate the knowledge and information in the areas of Biotechnology and Pharmacy by organising annual scientific meetings, seminars and symposia.

Members

The persons involved in research, teaching and work can become members of Association by paying membership fees to Association.

The members of the Association are allowed to write the title MABAP (Member of the Association of Biotechnology and Pharmacy) with their names.

Fellows

Every year, the Association will award Fellowships to the limited number of members of the Association with a distinguished academic and scientific career to be as Fellows of the Association during annual convention. The fellows can write the title FABAP (Fellow of the Association of Biotechnology and Pharmacy) with their names.

Membership details

(Membership and Journal)		India	SAARC	Others
Individuals	– 1 year	Rs. 600	Rs. 1000	\$100
LifeMember		Rs. 4000	Rs. 6000	\$500
Institutions	– 1 year	Rs. 1500	Rs. 2000	\$200
(Journal only)	Life member	Rs.10000	Rs.12000	\$1200

Individuals can pay in two instalments, however the membership certificate will be issued on payment of full amount. All the members and Fellows will receive a copy of the journal free.

Association of Biotechnology and Pharmacy

(Regn. No. 28 OF 2007)

#5-69-64; 6/19, Brodipet

Guntur – 522 002, Andhra Pradesh, India

Current Trends in Biotechnology and Pharmacy

ISSN 0973-8916

Volume 17 (2)	CONTENTS	APRIL 2023
	Assessing Zinc Thresholds in Commonly Used Herbs in India and Associated Health Risks <i>Radhika Bansal¹, Pammi Gauba[*]</i>	
	DOI: 10.5530/ctbp.2023.2.15	763-772
	Studies on metabolic regulation of <i>Schizosaccharomyces pombe</i> biomass production for glucan yield improvement <i>Prakasham Reddy Shetty^{a,b*}, Uma Rajeswari Batchu^a, Sudheer Kumar Buddana^{a,b}, Deepthi Pulivarthi^c, Chandrasekhar Cheemalamarri^{a,d}, Linga Banoth^{a,b*}, Suprasanna Penna^e, and Sudhakar Poda^d.</i>	
	DOI: 10.5530/ctbp.2023.2.16	773-787
	Novel Synthesis of Isatin-Thiazole Pharmacophores and their Cytotoxicity Evaluation- <i>Nagaiah Kommu^{a*}, S Srividya Bommakanti^a, Lakshmi Srinivasa Rao Kundeti^a, Tithi Bhat-tacharyya^b and Rajkumar Banerjee^b</i>	
	DOI: 10.5530/ctbp.2023.2.17	788-795
	Development and Optimization of Curcumin and Lycopene Mucoadhesive Buccal Patches Using Response Surface Methodology <i>B. Bhargavi¹, P. Shanmugasundaram^{1*}</i>	
	DOI: 10.5530/ctbp.2023.2.18	796 - 807
	Parkinson's disease Detection Using Tree Based Machine Learning Algorithms <i>Venkata Srinivas Babu Oguri¹, Sudhakar Poda², A. Krishna Satya², NK Prasanna</i>	
	DOI: 10.5530/ctbp.2023.2.19	808 – 818
	Development and Validation of Stability Indicating Rp-hplc Method for Quantitative Estima-tion of Lenalidomide in Lenalidomide Capsules Dosage Form <i>Ponnuri Bharath¹, P V Surendra Gupta¹, *Dittakavi Ramachandran¹</i>	
	DOI: 10.5530/ctbp.2023.2.20	819 – 827
	Simple and Rapid DNA Isolation from Shrimps by Using Single tube extraction buffer with Single step <i>MVSS Pavan Kumar¹, ARanganadhareddy¹</i>	
	DOI: 10.5530/ctbp.2023.2.21	828 -834
	Protective Effect of <i>Annona Squamosa</i> Fruit Pulp on Motor Responses Following Intra-Me-dial Forebrain Bundle Injection of 6-OHda In Rat Model of Parkinson Disease <i>Sudha Muthusamy¹, Shanmuga Sundaram Rajagopal^{2*}, Sambathkumar Ramanathan³</i>	
	DOI: 10.5530/ctbp.2023.2.22	835 - 849
	Properties of Glucose Oxidase produced from a newly isolated strain of <i>Aspergillus niger</i> <i>Okoye Ifeanyi¹, Awhin Prosper Ejiro², Onosakponome Iruoghene^{3*}, Ezugwu Arinze Linus¹, Ajoh Alfred Ikechukwu² and Chilaka Ferdinand Chiemeka¹</i>	
	DOI: 10.5530/ctbp.2023.2.23	850 - 856

-
- Employing Trichoderma to Alleviate Dimethoat Phytotoxicity In Sorghum Bicolor
Archana Kumari¹, Krishna Sundari Sattiraju²
DOI: 10.5530/ctbp.2023.2.24 857 - 872
- Prevalence of Herpes Simplex Virus (HSV) and Cytomegalovirus (CMV) in Oral Squamous Cell Carcinoma patients with a history of Nicotine and Alcohol abuse.
Samata Gadde¹, Sudhakar Poda²
DOI: 10.5530/ctbp.2023.2.25 873 - 884
- Mupirocin Niosomal Gel with Bee Honey & Curcumin as Nano-Drug Delivery in Wound Healing Applications
Srikrishna Theerdhala^{1,2}, Narayanaswamy Harikrishnan³*
DOI: 10.5530/ctbp.2023.2.26 885 -900
- Hypoglycemic and hypolipidemic effects of Oligomeris linifolia in Alloxan- induced diabetic mice
*Aisha Ashiq,¹ Saleem Jan,¹ Yar Muhammad Khan,² Faizan Ullah,³
Ashok Kumar Balaraman⁴, Abul Kalam Azad⁵*
DOI: 10.5530/ctbp.2023.2.27 901 -906
- A Comprehensive Review on Technological Advances in Alternate Drug Discovery Process: Drug Repurposing
Madhuri Pola^{1}, Alok Tiwari¹, Potla Durthi Chandrasai²*
DOI: 10.5530/ctbp.2023.2.28 907 -917
- Bioactive Components of piper betel Could be Potential anticancer Agents: A short Review on Pre-clinical Investigations and Practical Challenges
Bhabani Sankar Satapathy, Sangram Keshari Biswal, Laxmidhar Maharana, Snigdha Pattnaik^{}*
DOI: 10.5530/ctbp.2023.2.29 918 -928
-

Information to Authors

The Current Trends in Biotechnology and Pharmacy is an official international journal of Association of Biotechnology and Pharmacy. It is a peer reviewed quarterly journal dedicated to publish high quality original research articles in biotechnology and pharmacy. The journal will accept contributions from all areas of biotechnology and pharmacy including plant, animal, industrial, microbial, medical, pharmaceutical and analytical biotechnologies, immunology, proteomics, genomics, metabolomics, bioinformatics and different areas in pharmacy such as, pharmaceuticals, pharmacology, pharmaceutical chemistry, pharma analysis and pharmacognosy. In addition to the original research papers, review articles in the above mentioned fields will also be considered.

Call for papers

The Association is inviting original research or review papers and short communications in any of the above mentioned research areas for publication in Current Trends in Biotechnology and Pharmacy. The manuscripts should be concise, typed in double space in a general format containing a title page with a short running title and the names and addresses of the authors for correspondence followed by Abstract (350 words), 3 – 5 key words, Introduction, Materials and Methods, Results and Discussion, Conclusion, References, followed by the tables, figures and graphs on separate sheets. For quoting references in the text one has to follow the numbering of references in parentheses and full references with appropriate numbers at the end of the text in the same order. References have to be cited in the format below.

Mahavadi, S., Rao, R.S.S.K. and Murthy, K.S. (2007). Cross-regulation of VAPC2 receptor internalization by m2 receptors via c-Src-mediated phosphorylation of GRK2. *Regulatory Peptides*, 139: 109-114.

Lehninger, A.L., Nelson, D.L. and Cox, M.M. (2004). *Lehninger Principles of Biochemistry*, (4th edition), W.H. Freeman & Co., New York, USA, pp. 73-111.

Authors have to submit the figures, graphs and tables of the related research paper/article in Adobe Photoshop of the latest version for good illumination and alignment.

Authors can submit their papers and articles either to the editor or any of the editorial board members for onward transmission to the editorial office. Members of the editorial board are authorized to accept papers and can recommend for publication after the peer reviewing process. The email address of editorial board members are available in website www.abap.in. For submission of the articles directly, the authors are advised to submit by email to krssrao@abap.co.in or krssrao@yahoo.com.

Authors are solely responsible for the data, presentation and conclusions made in their articles/research papers. It is the responsibility of the advertisers for the statements made in the advertisements. No part of the journal can be reproduced without the permission of the editorial office.

Assessing Zinc Thresholds in Commonly Used Herbs in India and Associated Health Risks

Radhika Bansal¹, Pammi Gauba*

¹Department of Biotechnology, Jaypee Institute of Information Technology, Noida, India

*Corresponding Author: pammi.gauba@jiit.ac.in

Abstract

Use of herbal medicines has greatly increased as complementary and alternative medicine for the ailment of many diseases. In the present study zinc content was determined in the commonly consumed raw herbs sold over the table in India (East, West, North, South Zones). Zinc is an important micronutrient and plays a vital role in regulation in antioxidant activity and acts as a catalyst. However, excessive absorption of zinc causes suppression of copper & iron absorption, causes GIT disorders and alterations in blood lipoprotein level. The aim of this study was to determine the Zinc concentration in the market samples of raw herbs by ICP-MS (Inductively Coupled Plasma-Mass Spectrometry) and to model the estimated daily intake (EDI).

Keywords: Medicinal Plants, Zinc, Estimated Daily Intake, ICP-MS

Introduction

The Indian form of alternative medicine originated about 2000 years ago which relies on medicinal plants and their formulations (1) (2). According to the World Health Organization (WHO), these plant-based medications are used as primary treatment by around 80% of the world's population (3). These alternative herbal medicines are prepared from medicinal

plants and are generally considered safe for use (4). However, as the need for these therapies is increasing, the natural resources of these herbs are becoming depleted, and in order to fulfil the high demand, herbs are being grown on farms using standard agronomic approaches. Also, for getting high yield, use of chemical fertilizers and pesticides have been increased considerably. This in turn is affecting the overall nutrient status and enhancing the accumulation of some essential nutrients beyond the permissible limits. It is well documented that unethical farm practices and heavy load of chemicals results in the accumulation of toxic substances in the various parts of medicinal plants (5)(6). Apart from this, mining of ores and minerals, heavy industrial practices such as use of foundries, smelters, oil refineries, petrochemical plants, chemical industry, untreated sewage sludge and diffuse sources such as metal piping and combustion by-products from coal-burning power stations etc. are also the major contributors in increasing heavy metal contamination in soil and water (7) (8). This study discusses the zinc status in the commonly used herbs in India shortlisted API Volume I of AYUSH (9). Zinc is essential for overall homeostasis of human body and plays a crucial role in growth and development and acts a signalling factor and is one of the most common trace elements (10). It contributes to the regulation of chronic inflammatory status by

Assessing zinc thresholds in commonly Used herbs in India and associated health risks

decreasing inflammatory cytokines. Additionally, it is known to alleviate oxidative stress by taking part in the synthesis of antioxidant enzymes. It also acts as a catalyst for these enzymes, as well as is involved in lipid, protein, and carbohydrate metabolism (11)(12). Apart from acting as an essential micronutrient and supporting many metabolic processes, numerous studies on lipid and metabolic disorders are been reported with high zinc concentrations. Increased intake of zinc also impacts the immune system of body (13). Nausea, fever and weakness are also some associated side-effects with high zinc consumption (14).

Material and Methods

Study area

Medicinal plants samples in the raw form were procured from the local markets of East, West, North and South zones of India and the passport data for the same was generated. Plant identification and authentication was done from different authorised regional centres by expert botanists from "Regional Ayurveda Research Institute for Gastro-Intestinal Disorders (Guwahati), Regional Ayurveda Institute for Fundamental Research (Pune), Regional Ayurveda Research Institute (Jhansi) and Regional Ayurveda Research Institute for Metabolic Disorders (Bengaluru)"; for East, West, North and South respectively.

Sampling and metal analysis

Raw herbs sold over the table in the Indian market were chosen and collected from the local markets of each region for the analysis of zinc concentration. The names and part used of the respective herb is given in Table 1,2,3&4. The plants were tagged properly, stored in polyethylene bags, and brought to the laboratory.

Reagents

The reagents used were of Supra Grade. HPLC grade water (Rankem) was used. All the glassware soaked overnight in 1% HNO₃

solution and washed with deionized water were used after drying. Hydrogen peroxide (30%) & nitric acid (65%), Merck, Darmstadt, Germany was used.

Digestion of herb samples

The herb samples were grounded into powder and weighed (1g) in PTFE (Teflon) vessels. To this 8ml diacid mixture (2:5 v/v HNO₃ and H₂O₂) was added. The vessels were kept for few hours as such for cold digestion. Samples were digested in a microwave assisted digestion system; Anton Paar Multiwave 7000; with ramp time and hold time of (10, 5 and 5 minutes) for 3 cycles at 90°C, 120°C and 150°C respectively. The digested material was filtered through 0.2 mm syringe filter and was made up to 50 ml in a volumetric flask. The digested samples were stored at 4°C for analysis.

Estimation of zinc concentration

Zinc content determination with the digested leaf samples was performed on a model ICP-MS (Inductively Coupled Plasma Mass Spectrometry) NexION 2000; Germany using Syngistix software; Inductively Coupled Mass Spectrophotometer under an optimized measurement condition with Argon and Helium gas flow. NIST (National Institute of Standards and Technology) certified 1000 ppm zinc standard was used to plot standard graph. The samples were analysed in triplicates and the average values of each sample was used as result.

Estimated daily Intake

Both the metal concentration in plants and the amount consumed of the respective plants influence the average estimated daily intake (EDI). The EDI of Zinc was calculated using Eq.1, recommended by the USEPA (15).

$$EDI = X (FIR/WAB) \dots\dots\dots(1)$$

where EDI is the estimated daily intake (mg/kg bw/day); X is the Zinc concentration in the sample (mg kg⁻¹); FIR is daily

consumption rate for adults. WAB is the average adult body weight (kg) which is considered to be 65 kg.

Results and Discussion

The data for zinc concentration is presented in Tables 1,2,3 & 4 and estimated daily intake in the respective herbs sampled is presented in Table 5. The concentration of zinc (Zn) in the analysed samples ranged between 5.657 and 88 mg kg⁻¹ in East, 4.919 mg kg⁻¹ and 78.089 mg kg⁻¹ in West, 3.44 mg kg⁻¹ and 95.962 mg kg⁻¹ in North, 1.858 mg kg⁻¹ and 78.336 mg kg⁻¹ in South. The maximum concentrations of zinc in Yavani (*Trachyspermum ammi* Linn.); 58.475, 78.089, 95.962, 66.759 mg kg⁻¹, Svetajiraka (*Cuminum cyminum* Linn); 71.389, 60.226, 59.441, 76.145 mg kg⁻¹, Upakuncika (*Nigella sativa* Linn); 130.74, 64.759, 55.021, 57.703 mg kg⁻¹ in all the four zones viz, East, West, North and South respectively and 7 samples in East, West & South Zones and 10 samples in North Zone were found to be above permissible limit of 50 mg/kg (Figure 1-4). Overall, results revealed that of the samples analysed; 9.7% in East, 12.9% in West, 16.12% in North and 11.2% in South had concentrations higher than 50 mg kg⁻¹ (which is the permissible limit (PL)) set for zinc in herbal medicines by FAO/WHO (16)(17). High concentration of Zinc (above 50 mg kg⁻¹) was observed in Mint, Basil, Parsley, Sage and Thyme (52.97, 50.10, 112.19, 58.78, 112.19 mg kg⁻¹ respectively) sampled in UAE (18). Similar to present study, high concentration of zinc, 314.05 mg/kg was found in cumin sampled from Egyptian market (19). The samples of medicinal spices sampled from Polish market were reported with the zinc concentrations with the maximum permissible limits (20).

The EDI's of zinc is calculated on the basis of average concentration of zinc in the herbs and the consumption rate for adults (Table 5). According to the calculated data, the values of the daily intake of zinc were observed to be on the higher side for the medicinal herbs

with high zinc concentrations in the respective zones; with the values ranging from 0.08- 3.29 mg/kg bw/day in east zone, 0.07-4.65 mg/kg bw/day in west zone, 0.05-4.22 mg/kg bw/day in north and 0.03-3.63 mg/kg bw/day in south zones across India. Zinc is a trace element that is essential for normal growth, blood clotting, thyroid function, and DNA & protein synthesis. Excessive zinc consumption has a negative impact on the immune system, blood lipoprotein levels, and copper level (18). Extreme intake of zinc also causes abdominal pain, diarrhoea, vomiting and nausea. High zinc uptake in medicinal plants is due to presence of heavy amount of zinc present in cultivation soil. Therefore, various biological, chemical, and physical strategies are employed to render soil free from zinc contamination. These involve use of hyperaccumulator plants such as *Arabidopsis halleri*, *Noccaea caerulescens* (21), *Thlaspi ochroleucum* (22); apart from this *Dichapetalum subsp. Sumatranum* and *D. subsp. Pilosum* are strong zinc hyperaccumulators (23). Polyaspartate (PASP) synthesized from L-aspartic acid produced by modified thermal procedure has potential to chelate Zinc ions from contaminated soil (24).

Conclusion

The present research based on the zinc estimation in commonly used medicinal plants across four geographical locations across India, showed that the concentration of Zinc in some herbs were beyond the acceptable limits. The findings of the present research also highlight the significance of safety and hygiene practices from harvest to their reaching to consumer end. Therefore, it is utmost necessary to implement the regular monitoring of testing of the quality and mineral content in the raw herbs sold over the table in the Indian markets. It is also to be taken into consideration that the many of the herbs studied in the present research are incorporated in the daily meals. Future prospects regarding the presence of more toxic elements and their impact on overall human health and also on herbs must be studied. Also,

Table 1. Zinc Concentration in the Fruits and Flower Buds of the Herbs Sampled (ppm±SD)

Herb Name	Parst Used	East	West	North	South
Ajamoda (<i>Apium leptophyllum</i>)	Fruit	**	**	43.323±1.1	78.336±0.9
Yavani(<i>Trachyspermum ammi</i>)	Fruit	58.475±1.12	78.089±1.1	91.35±1.2	66.759±0.9
Dhanyaka (<i>Coriandrum sativum</i>)	Fruit	40.49±0.9	60.49±1.12	40.876±0.9	45.809±0.9
Svetajiraka (<i>Cuminum cyminum</i>)	Fruit	71.389±1.23	60.226±1.54	59.441±1.32	76.145±0.9
Krsnajirak (<i>Carum carvi</i>)	Fruit	49.698±1	50.689±1.23	48.723±1.32	43.338±0.9
Amalaki (<i>Embllica officinalis</i>)	Dry Fruits	6.874±1.5	23.34±1.32	7.788±2.1	9.218±1.1
Kankola (<i>Piper chubeba</i>)	Fruit	32.25±0.9	17.13±1.1	65.09±0.9	31.12±0.8
Udumbara (<i>Ficus racemose</i>)	Fruit	8.38±1.12	26.5±1.1	13.23±1.21	13.42±1.1
Jatiphala (<i>Myristica fragrans</i>)	Fruit	20.85±1.56	9.701±1.2	14.491±1.1	9.16±1.1
Suksmaila (<i>Elettaria cardamomum</i>)	Fruit	38.502±1.32	12.984±0.9	51.008±1.2	47.66±1.1
Haritaki (<i>Terminalia chebula</i>)	Fruit	14.05±1.12	14.54±1.1	10.489±1.4	**
Misreya (<i>Foeniculum vulgare</i>)	Fruit	14.917±1.43	14.519±1.1	31.32±1.21	63.77±1.1
Bilva (<i>Aegle marmelos</i>)	Fruit pulp	**	4.919±0.9	13.34±0.9	17.65±0.8
Aragvadha (<i>Cassia fistula</i>)	Fruit pulp	**	7.137±1.32	17.1±0.9	25.85±0.9
Hingu (<i>Ferula foetida</i>)	Oleo-gum-resin	6.36±2.1	9.341±0.7	8.367±1.32	18.401±1.1
Lavanga (<i>Syzygium aromaticum</i>)	Flower bud	12.531±0.9	18.176±1.1	16.171±1.12	18.209±1.1

Table 2. Zinc Concentration in the Root and Rhizomes of the Herbs Sampled (ppm±SD)

Herb Name	Parst Used	East	West	North	South
Haridra (<i>Curcuma longa</i>)	Rhizome	14.248±1.1	11.637±0.9	**	**
Sunthi (<i>Zingiber officinale</i>)	Rhizomes	25.021±1.21	16.818±1.23	**	36.532±0.9
Citraka (<i>Plumbago zeylanica</i>)	Root	6.086±1.13	**	75.32±1.21	14.09±1.1
Aswagandha (<i>Withania somnifera</i>)	Root	44.431±1.13	14.417±1.12	15.753±1.4	15.576±1
Arka (<i>Calotropis procera</i>)	Root	30.94±1.18	29.83±1.12	**	7.35±0.9
Eranda (<i>Ricinus communis</i>)	Root	28.48±1.15	19.85±1.5	14.51±1.3	6.389±0.9
Karavira (<i>Nerium indicum</i>)	Root	**	12.277±1.21	26.43±1.1	31.37±1.2
Nyagrodha (<i>Ficus benghalensis</i>)	Aerial Root	15.06±0.8	12.68±0.9	12.68±0.9	12.27±0.8
Pashanabheda (<i>Bergenia ciliate</i>)	Rhizome	39.96±1.1	15.07±2.1	46.06±0.9	35.77±1
Taamalaki (<i>Phyllanthus fraternus</i>)	Dried Root	**	47.03±0.9	39.41±0.9	**

**The herbs were not available in the respective markets

Table 3. Zinc Concentration in the Stem and Whole Plant of the Herbs Sampled (ppm±SD)

Herb Name	Part Used	East	West	North	South
Kantakari (<i>Solanum surattense</i>)	Whole plant	**	**	**	29.374±0.8
Apaamaarga (<i>Achyranthes aspera</i>)	Whole Plant	17.67±0.9	23.6±1.45	30±0.9	20.81±0.9
Argavadha (<i>Cassia fistula</i>)	Stem Bark	**	12.1±0.9	5.294±1	14.26±1
Ashvattha (<i>Ficus religiosa</i>)	Bark	8.232±0.8	14.712±1.1	**	21.45±1.1
Bilva (<i>Aegle marmelos</i>)	Stem Bark	5.647±1.12	25.37±1.9	22.56±1.1	14.76±1.2
Guduci (<i>Tinospora cordifolia</i>)	Stem	14.39±1.32	52.65±1.12	13.031±1.1	31.09±1.21
Khadira (<i>Acacia catechu</i>)	Heart Wood	8.55±1.12	15.803±1.23	13.23±1.3	21.46±1.1
Kanchanara (<i>Bauhinia variegata</i>)	Stem Bark	16.49±1.15	6.585±1.45	8.353±1.1	14.16±1
Nyagrodha (<i>Ficus benghalensis</i>)	Stem Bark	13.86±0.6	12.7±1.65	12.246±0.9	19.33±1
Taamalaki (<i>Phyllanthus fraternus</i>)	Whole Plant	88.4±1.12	**	**	**
Taamalaki (<i>Phyllanthus fraternus</i>)	Stem	**	11.26±0.9	40.86±1.1	**
Udumbara (<i>Ficus racemose</i>)	Bark	37.89±1.11	14.64±1.2	12.29±1.11	21.14±0.9
Tvak (<i>Cinnamomum zeylanicum</i>)	Bark	14.27±0.9	7.326±1.32	18.07±1.1	8.905±1.2
Babbula (<i>Acacia nilotica</i>)	Stem bark	**	5.94±1.1	3.818±0.9	**
Lodhara (<i>Symplocos racemose</i>)	Stem Bark	**	**	3.44±1.1	1.858±1
Asoka (<i>Saraca asoka</i>)	Stem Bark	**	**	9.78±1.1	4.722±1.1

**The herbs were not available in the respective markets

Table 4. Zinc Concentration in the Seeds and Leaf Samples of the Herbs (ppm±SD)

Herb Name	Part Used	East	West	North	South
Upakuncika (<i>Nigella sativa</i>)	Seed	130.74±0.9	64.759±1.12	55.021±1.1	57.703±0.9
Candrasura (<i>Lepidium sativum</i>)	Seed	**	49.305±1.21	**	58.696±0.9
Atasi (<i>Linum usitatissimum</i>)	Seed	27.14±1.15	53.53±1.11	72.12±0.9	43.72±1.3
Arkaparna (<i>Calotropis procera</i>)	Leaf	51.75±0.9	45.25±1.43	61.5±0.9	35.88±1.1
Eranda (<i>Ricinus communis</i>)	Leaf	23.97±1.11	**	**	14.49±1.1
Eranda (<i>Ricinus communis</i>)	Seed	43.69±1.19	63.76±1.3	73.48±1.1	63.75±0.9

Assessing zinc thresholds in commonly Used herbs in India and associated health risks

Gunja (<i>Abrus precatorius</i>)	Seed	20.22±2.1	29.87±1.21	37.43±1.2	22.03±0.9
Karavira (<i>Nerium indicum</i>)	Leaf	75.44±1.21	26.09±1.43	14.913±1.32	42.5±1.1
Tvakpatra (<i>Cinnamomum tamala</i>)	Leaf	39.125±0.8	32.132±1.32	32.224±1.21	28.857±1.2
Karanja (<i>Pongamia pinnata</i>)	Seed	**	23.95±1.32	**	36.35±0.8
Karpasa (<i>Gossypium herbaceum</i>)	Seed	**	11.95±1.21	34.46±1.1	27.82±0.9
Taamalaki (<i>Phyllanthus fraternus</i>)	Dried Leaf	**	45.62±0.8	12.514±1.1	34.51±1.2
Puuga (<i>Areca catechu</i>)	Seed	19.33±1.13	30.42±1.2	15.1±0.9	47.14±1.1
Kulattha (<i>Macrotyloma uniflorum</i>)	Seed	36.367±1.12	12.279±1.43	54.91±0.9	5.258±0.9
Vijaya (<i>Cannabis sativa</i>)	Leaf	54.79±1.13	**	**	**

**The herbs were not available in the respective market

Table 5. Calculated Daily Intake of Zinc in Respective Herbs

Herb Name	Part Used	Estimated Daily Intake (mg/day kg bw)			
		East	West	North	South
Ajamoda (<i>Apium leptophyllum</i>)	Fruit	**	**	1.33	2.41
Yavani (<i>Trachyspermum ammi</i>)	Fruit	0.90	1.20	1.48	1.03
Dhanyaka (<i>Coriandrum sativum</i>)	Fruit	3.11	4.65	3.14	3.52
Haridra (<i>Curcuma longa</i>)	Rhizome	1.10	0.90	**	**
Hingu (<i>Ferula foetida</i>)	Oleo-gum-resin	0.10	0.14	0.13	0.28
Lavanga (<i>Syzygium aromaticum</i>)	Flower bud	0.19	0.28	0.25	0.28
Tvakpatra (<i>Cinnamomum tamala</i>)	Leaf	0.60	0.49	0.50	0.44
Upakuncika (<i>Nigella sativa</i>)	Seed	2.01	1.00	0.85	0.89
Svetajiraka (<i>Cuminum cyminum</i>)	Fruit	3.29	2.78	2.74	3.51
Sunthi (<i>Zingiber officinale</i>)	Rhizome	0.77	0.52	**	1.12
Krsnajirak (<i>Carum carvi</i>)	Fruit	1.53	1.56	1.50	1.33
Kantakari (<i>Solanum surattense</i>)	Whole Plant	**	**	**	0.45
Candrasura (<i>Lepidium sativum</i>)	Seed	**	0.76	**	0.90
Aswagandha (<i>Withania somnifera</i>)	Root	1.37	0.44	0.48	0.48
Amalaki (<i>Embllica officinalis</i>)	Dry Fruits	0.53	1.80	0.60	0.71
Atasi (<i>Linum usitatissimum</i>)	Seed	1.25	2.47	3.33	2.02
Arka (<i>Calotropis procera</i>)	Root	0.48	0.46	**	0.11
Arkaparna (<i>Calotropis procera</i>)	Leaf	0.80	0.70	0.95	0.55
Apaamaarga (<i>Achyranthes aspera</i>)	Whole Plant	0.27	0.36	0.46	0.32

Argavadha (<i>Cassia fistula</i>)	Stem Bark	**	0.19	0.08	0.22
Ashvattha (<i>Ficus religiosa</i>)	Bark	0.13	0.23	**	0.33
Bilva (<i>Aegle marmelos</i>)	Stem Bark	0.09	0.39	0.35	0.23
Citraka (<i>Plumbago zeylanica</i>)	Root	0.09	**	1.16	0.22
Eranda (<i>Ricinus communis</i>)	Leaf	0.37	**	**	0.22
Eranda (<i>Ricinus communis</i>)	Root	0.44	0.31	0.22	0.10
Eranda (<i>Ricinus communis</i>)	Seed	0.67	0.98	1.13	0.98
Gunja (<i>Abrus precatorius</i>)	Seed	0.31	0.46	0.58	0.34
Guduci (<i>Tinospora cordifolia</i>)	Stem	0.66	2.43	0.60	1.43
Karavira (<i>Nerium indicum</i>)	Leaf	1.16	0.40	0.23	0.65
Karavira (<i>Nerium indicum</i>)	Root	**	0.19	0.41	0.48
Khadira (<i>Acacia catechu</i>)	Heart Wood	0.13	0.24	0.20	0.33
Kanchanara (<i>Bauhinia variegata</i>)	Stem Bark	0.25	0.10	0.13	0.22
Karanja (<i>Pongamia pinnata</i>)	Seed	**	1.11	**	1.68
Karpasa (<i>Gossypium herbaceum</i>)	Seed	**	0.18	0.53	0.43
Kankola (<i>Piper chubeba</i>)	Fruit	0.50	0.26	1.00	0.48
Nyagrodha (<i>Ficus benghalensis</i>)	Ariel Root	0.23	0.20	0.20	0.19
Nyagrodha (<i>Ficus benghalensis</i>)	Stem Bark	0.21	0.20	0.19	0.30
Pashanabheda (<i>Bergenia ciliate</i>)	Rhizome	0.61	0.23	0.71	0.55
Puuga (<i>Areca catechu</i>)	Seed	1.49	2.34	1.16	3.63
Taamalaki (<i>Phyllanthus fraternus</i>)	Whole Plant	1.36	**	**	**
Taamalaki (<i>Phyllanthus fraternus</i>)	Dried Root	**	0.72	0.61	**
Taamalaki (<i>Phyllanthus fraternus</i>)	Dried Leaf	**	0.70	0.19	0.53
Taamalaki (<i>Phyllanthus fraternus</i>)	Stem	**	0.17	0.63	**
Udumbara (<i>Ficus racemose</i>)	Fruit	0.90	2.85	1.42	1.45
Udumbara (<i>Ficus racemose</i>)	Bark	0.58	0.23	0.19	0.33
Vijaya (<i>Cannabis sativa</i>)	Leaf	0.84	**	**	**
Misreya (<i>Foeniculum vulgare</i>)	Fruit	0.46	0.45	0.96	1.96
Jatiphala (<i>Myristica fragrans</i>)	Fruit	0.16	0.07	0.11	0.07
Suksmaila (<i>Elettaria cardamomum</i>)	Fruit	1.18	0.40	1.57	1.47
Haritaki (<i>Terminalia chebula</i>)	Fruit	0.22	0.22	0.16	**
Tvak (<i>Cinnamomum zeylanicum</i>)	Bark	0.22	0.11	0.28	0.14
Kulattha (<i>Macrotyloma uniflorum</i>)	Seed	2.80	0.94	4.22	0.40
Babbula (<i>Acacia nilotica</i>)	Stem Bark	**	0.09	0.06	**
Bilva (<i>Aegle marmelos</i>)	Fruit Pulp	**	0.08	0.21	0.27
Aragvadha (<i>Cassia fistula</i>)	Fruit Pulp	**	0.11	0.26	0.40
Lodhara (<i>Symplocos racemose</i>)	Stem Bark	**	**	0.05	0.03
Asoka (<i>Saraca asoka</i>)	Stem Bark	**	**	0.15	0.07

Assessing zinc thresholds in commonly Used herbs in India and associated health risks

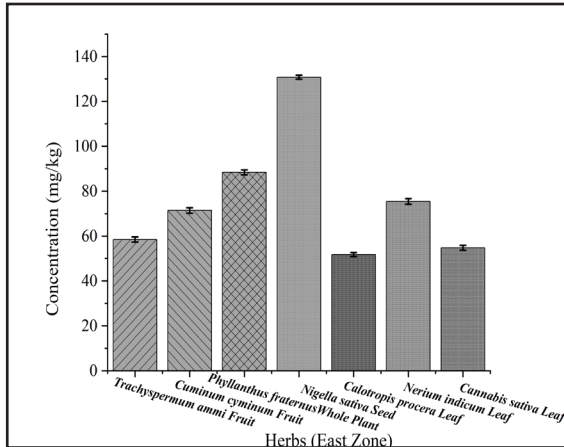


Figure 1. Zinc Concentration above PL in East Zone

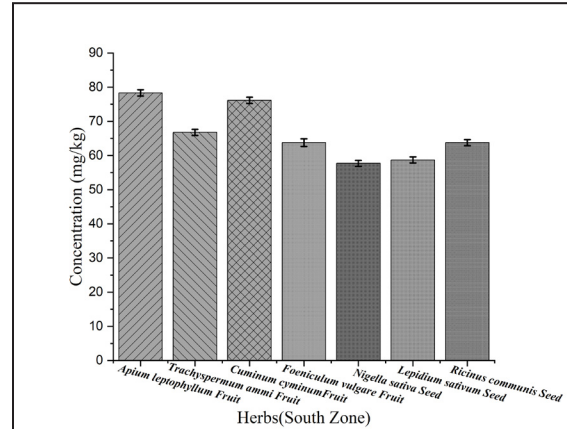


Figure 4. Zinc Concentration above PL in South Zone

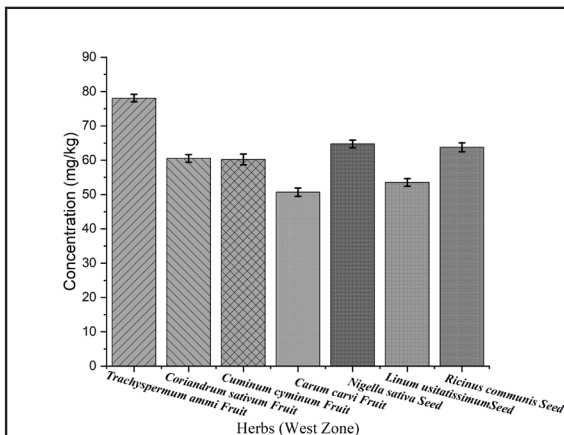


Figure 2. Zinc Concentration above PL in West Zone

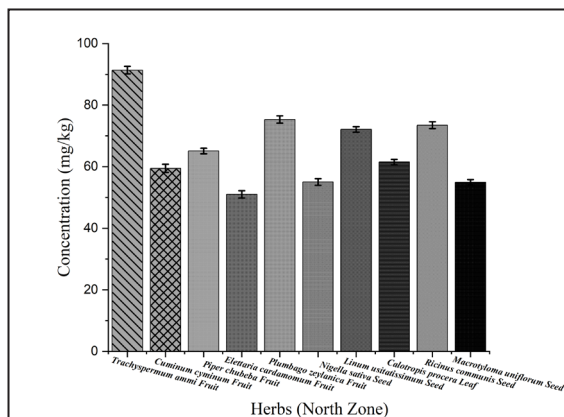


Figure 3. Zinc Concentration above PL in North Zone

remediation measures to reduce contamination of soil should be practiced.

Acknowledgement

The authors thank Jaypee Institute of Information Technology (JIIT), Noida for providing the research facilities and Ministry of AYUSH for giving us the opportunity to work on this project. The authors are also grateful to "Regional Ayurveda Research Institute for Gastro-Intestinal Disorders, Regional Ayurveda Institute for Fundamental Research, Regional Ayurveda Research Institute and Regional Ayurveda Research Institute for Metabolic Disorders" for authentication of the herbs.

References

1. Saper, R. B., Kales, S. N., Paquin, J., Burns, M. J., Eisenberg, D. M., Davis, R. B., & Phillips, R. S. (2004). Heavy metal content of ayurvedic herbal medicine products. *Jama*, 292(23):2868-2873.
2. Chan, K., (2003). Some aspects of toxic contaminants in herbal medicines. *Chemosphere*, 52(9):1361-1371.
3. Behera, B. and Bhattacharya, S. (2016). The importance of assessing heavy metals in medicinal herbs: a quantitative study. *CELLMED*, 6(1):3-1.

4. Gomez, M. R., Cerutti, S., Sombra, L. L., Silva, M. F., & Martínez, L. D. (2007). Determination of heavy metals for the quality control in argentinian herbal medicines by ETAAS and ICP-OES. *Food and Chemical Toxicology*, 45(6):1060-1064.
5. Yu, I.S., Lee, J.S., Kim, S.D., Kim, Y.H., Park, H.W., Ryu, H.J., Lee, J.H., Lee, J.M., Jung, K., Na, C. and Joung, J.Y., 2017. Monitoring heavy metals, residual agricultural chemicals and sulfites in traditional herbal decoctions. *BMC complementary and alternative medicine*, 17(1), pp.1-9.
6. Kan, W.L.T., Ma, B. and Lin, G. (2011). Sulfur fumigation processing of traditional Chinese medicinal herbs: beneficial or detrimental?. *Frontiers in Pharmacology*, 2:84.
7. Zhao, Q., Wang, Y., Cao, Y., Chen, A., Ren, M., Ge, Y., Yu, Z., Wan, S., Hu, A., Bo, Q. and Ruan, L. (2014). Potential health risks of heavy metals in cultivated topsoil and grain, including correlations with human primary liver, lung and gastric cancer, in Anhui province, Eastern China. *Science of the Total Environment*, 470:340-347.
8. Bansal, R., & Gauba, P. (2021). Exploring Phytoremediation Potential of *Vigna radiata* & *Vigna aconitifolia* Under Hexavalent Chromium Induced Stress in Hydroponics. *Current Trends in Biotechnology and Pharmacy*, 15(6), pp. 40-46.
9. The Ayurvedic Pharmacopoeia of India Part-I Volume-I Government of India Ministry of Health and Family Welfare Department of AYUSH.
10. Hara, T., Takeda, T. A., Takagishi, T., Fukue, K., Kambe, T., & Fukada, T. (2017). Physiological roles of zinc transporters: molecular and genetic importance in zinc homeostasis. *The Journal of Physiological Sciences*, 67(2):283-301.
11. Motamed, S., Ebrahimi, M., Safarian, M., Ghayour-Mobarhan, M., Mouhebati, M., Azarpazhouh, M., Esmailie, H., Norouzi, A. and Ferns, G.A. (2013). Micronutrient intake and the presence of the metabolic syndrome. *North American journal of medical sciences*, 5(6):377.
12. de Oliveira Otto, M.C., Alonso, A., Lee, D.H., Delclos, G.L., Jenny, N.S., Jiang, R., Lima, J.A., Symanski, E., Jacobs Jr, D.R. and Nettleton, J.A. (2011). Dietary micronutrient intakes are associated with markers of inflammation but not with markers of subclinical atherosclerosis. *The Journal of nutrition*, 141(8):1508-1515.
13. Orisakwe, O.E., Kanayochukwu, N.J., Nwadiuto, A.C., Daniel, D. and Onyinyechi, O. (2012). Evaluation of potential dietary toxicity of heavy metals of vegetables. *J Environ Anal Toxicol*, 2(3):136.
14. Baby, J., Raj, J. S., Biby, E. T., Sankarganesh, P., Jeevitha, M. V., Ajisha, S. U., & Rajan, S. S. (2010). Toxic effect of heavy metals on aquatic environment. *International Journal of Biological and Chemical Sciences*, 4(4).
15. Zhuang, P., Lu, H., Li, Z., Zou, B. and McBride, M.B. (2014). Multiple exposure and effects assessment of heavy metals in the population near mining area in South China. *PloS one*, 9(4):e94484.
16. Nkuba, L.L. and Mohammed, N.K. (2017). Heavy metals and essential elements in selected medicinal plants commonly used for medicine in Tanzania. *Chemical Science International Journal*, 19(2):1-11.
17. Baba, H.S. and Mohammed, M.I. (2021). Determination of Some Essential Metals in Selected Medicinal Plants. *ChemSearch Journal*, 12(1):15-20.

18. Dghaim, R., Al Khatib, S., Rasool, H., & Ali Khan, M. (2015). Determination of heavy metals concentration in traditional herbs commonly consumed in the United Arab Emirates. *Journal of environmental and public health*.
19. Soliman, N.F., 2015, July. Metals contents in spices and herbs available on the Egyptian market: assessment of potential human health risk. In *The Open Conference Proceedings Journal*, 6(1).
20. Krejpcio, Z., Krol, E. and Sionkowski, S. (2007). Evaluation of Heavy Metals Contents in Spices and Herbs Available on the Polish Market. *Polish Journal of Environmental Studies*, 16(1).
21. Peer, W.A., Mahmoudian, M., Freeman, J.L., Lahner, B., Richards, E.L., Reeves, R.D., Murphy, A.S. and Salt, D.E. (2006). Assessment of plants from the Brassicaceae family as genetic models for the study of nickel and zinc hyperaccumulation. *New Phytologist*, 172(2):248-260.
22. Van der Ent, A., Baker, A. J., Reeves, R. D., Pollard, A. J., & Schat, H. (2013). Hyperaccumulators of metal and metalloid trace elements: facts and fiction. *Plant and soil*, 362(1):319-334.
23. Baker, A. J. M., Proctor, J., Van Balgooy, M. M. J., & Reeves, R. D. (1992). Hyperaccumulation of nickel by the flora of the ultramafics of Palawan, Republic of the Philippines. *The vegetation of ultramafic (serpentine) soils*, 291-304.
24. Mu'azu, N. D., Essa, M. H., Haladu, S. A., Ali, S. A., Jarrah, N., Zubair, M., & Mohamed, I. A. (2019, November). Removal zinc ions from contaminated soil using biodegradable polyaspartate via soil washing process. In *Journal of Physics: Conference Series*, 1349(1):012146. IOP Publishing.

Studies on metabolic regulation of *Schizosaccharomyces pombe* biomass production for glucan yield improvement

Prakasham Reddy Shetty^{a,b*} Uma Rajeswari Batchu^a, Sudheer Kumar Buddana^{a,b},
Sree Harshika Thota^a, Deepthi Pulivarthi^c, Chandrasekhar Cheemalamarri^{a,d},
Linga Banotha^{a,b}, Suprasanna Penna^e, and Sudhakar Poda^d.

^aOrganic synthesis and Process chemistry, CSIR-Indian Institute of Chemical Technology, Hyderabad – 500007 Telangana, India.

^bAcademy of Scientific and Innovative Research (AcSIR), CSIR-Indian Institute of Chemical Technology, Ghaziabad, 201001 New Delhi, India.

^cFluoro-Agrochemicals, CSIR-Indian Institute of Chemical Technology, Hyderabad – 500 007, Telangana, India.

^dDepartment of Biotechnology, Acharya Nagarjuna University, Guntur, Andhra Pradesh, India.

^eNuclear Agriculture and Biotechnology Division, Bhabha Atomic Research Centre (BARC) Mumbai – 400085, Maharashtra, India.

*Corresponding author: prakasam.iict@gov.in

Abstract

Schizo-saccharomyces pombe (*S.pombe*) has been playing a pivotal role in biotech industries as a source of glucans; a biological response modifiers (BRM) and also been studied as a model strain for recombinant proteins in molecular biology. Owing to the presence of > 60% glucans in their cell wall structure, the present research was designed to understand the effect of nutrient regulation on growth of *S.pombe* (*Italic form*) to economize the glucan production. The study was performed using two different media; yeast extract with supplements (YES) and yeast extract-peptone-dextrose (YPD) and the YPD medium was noticed to be the best and cost-effective for maximum growth of *S.pombe*. Thereafter, a sequential optimization studies, starting with one factor at a time (OFAT) methodology followed by two step statistical approach Plackett-burmann design (PBD) and Response surface methodology (RSM) improved the biomass yield from 14-34.5 g/L (1.5-fold) at shake flask level. Mass transfer of media components, temperature, dextrose and yeast extract have

played significant role in metabolism mediated growth of the *S.pombe*. The major finding of the present study is non-significance of peptone in enhancing the *S.pombe* biomass. Validation of the above at bioreactor level with dextrose at 4%, rpm at 200, temperature at 28°C and yeast extract at 2% increased the biomass yield from 34.5 - 52 g/L.

Keywords

Schizosaccharomyces pombe, One factor at a time, Plackett-burmann design, Response surface methodology, Dextrose, Yeast extract.

Introduction

The genus *Schizosaccharomyces pombe* (*S.pombe*)- ancient fission yeast, is a unique species of yeast that has been using in brewing industries since very long time (1). It is an eukaryote with the shortest genome and divides by medial fission to produce off springs of equal size. These characteristics attract the researchers to use it as a model organism to study the eukaryotic genetics and molecular processes (cell cycle) (2) and to produce the

Schizosaccharomyces pombe biomass production for glucan yield improvement

recombinant proteins (Human lipocortin I, Human papillomavirus-type-16 and industrial enzymes) (3). Now a days, *S.pombe* has been gaining importance in health sector as a source of glucans that are used mainly as nutraceuticals and biological response modifiers (BRM) (4-5).

The *S.pombe* is a typical yeast proliferates normally in a haploid state. The cells are grown by extension of tip to attain a critical cell length (7-15 μm) which is followed by mitosis (6). However, under nitrogen limiting conditions, the growth arrests in G2 phase and diploid zygote formation occurs due to the conjugation of opposite cells that can proceed directly to meiosis and divides into four haploid spores (7). Therefore, controlling the cell physiology is the essential factor as it influences the growth state as well as the yield of the *S.pombe* biomass. In general, *S. pombe* cell physiology depends on the choice of nutritional components and culture conditions. It can grow on various nutrient media including complex and diverse sporulation-media which can support sexual differentiation. The rich medium, Yeast extract with supplements (YES) is the preferable media for vegetative growth (8).

The one-factor-at-a-time (OFAT) approach is the traditional method used to optimize the process parameters. However, the drawbacks associated with the OFAT approach compared to factorial designs, resulted the use of statistical methods for improved production yields (9-10). Plackett-Burmann design (PBD) helps in understanding the significance of each variable and selects the significant growth parameters in initial scale up studies whereas the central composite design (CCD) of response surface methodology (RSM) (11) assist to understand the combinatorial role of media components at different concentrations to improve the productivity. Considering the above, the present study aimed to recognize the optimal conditions to improve the *S.pombe* biomass using multi-factorial based designs in sequential manner where OFAT approach followed by combination of PBD and RSM

analysis to improve the yield of biomass as well as glucan production followed by validation at Bioreactor level. This is the first report on maximization of *S.pombe* biomass as a source of glucan.

Materials and methods

The media components such as peptone, yeast extract, malt extract, dextrose, agar used in the present study were obtained from Himedia, India. All chemicals and reagents used were of analytical grade.

Culture collection and morphological characteristics

The glycerol stocks of yeast strain *S. pombe* NCIM 3360 were procured from NCL, Pune. The culture was streaked on MGYD (Malt extract, Glucose, Yeast extract and Peptone) agar slants and incubated at 30°C. Further, the strain was sub-cultured in the same agar medium slants frequently for maintenance and preserved at 4°C.

Media and growth conditions

The growth of *S.pombe* was studied in different yeast media such as YES medium (W/V) containing yeast extract 0.5%, glucose 3%, nitrogen bases as described in ATCC 2064 and YPD medium (W/V) containing 1%, yeast extract, 2%, peptone, 2%, glucose at 30°C, and shaking at 200 rpm for a period of 60 hrs. However, further studies were progressed in YPD medium as it supported the growth of *S. pombe* similar to YES medium.

Growth curve

The growth curve of *S.pombe* was constructed by measuring optical density at different time intervals using double beam UV-Visible spectrophotometer SL 210-Elico at 595 nm.

Morphological characterization

The morphology of *S.pombe* was observed by microscopic method using

Scanning electron microscope (SEM).

Optimization of growth conditions for *S.pombe* biomass production

Influence of and nutritional factors by OFAT approach

The influence of various fermentation physical parameters such as age of inoculum (12, 24, 36, 48, 60 and 72 h), incubation temperature (24, 26, 28, 30, 32, 34 and 36°C), initial pH of the medium (3,4,5,6, 7 and 8), agitation speed (120, 150, 180, 200, 220 and 250 rpm) concentration of inoculum (0.5, 1, 2, 3, 4 and 5%) as well as different carbon (1%) sources (sucrose, dextrose, maltose, fructose, galactose) and various nitrogen (1%) sources (peptone, meat extract, yeast extract, malt extract and beef extract) were investigated by supplementing one factor at a given experiment. Based on the optimized condition, further experiments were performed using best carbon and nitrogen source in the concentration range of 1 to 4% at optimized physiological conditions. Triplicate experiments were performed and the data represented as mean \pm standard deviation.

Identification of significant factors by PBD

In the designing phase, A total of nine variables based on one-at-a-time factorial study were selected and used. Considering each factor concentration at OFAT, the higher level (+1) and lower level (-1) for were selected and used for this study.

Response surface methodology

Only those factors which showed significance in the PB design i.e., dextrose, RPM, temperature and yeast extract were considered for RSM studies. The CCD design was developed with four factors and six replicates at the centre point. The optimum concentration obtained with the OFAT approach was considered as 0 code and two levels below and two levels above were predicted based on the parameter importance on growth of the organism; and coded as -2,-1, 0, +1, and

+2. Based on the software input, a total of 31 experiments were conducted and the response values (Y) were recorded in terms of biomass yield. The presented yield value is the average of the triplicates. By this approach each variable level for maximum response was measured. Thereafter, an experiment was performed to verify the validity of the model using the combination of different optimized variables in order to yield the maximum response. Furthermore, the optimized conditions were evaluated at the level of Bioreactor Biostat B Plus 2010 (Sartorius).

The experimental results of RSM on biomass yield was verified by conducting ANOVA and incorporated into the response surface regression, using the second order polynomial equation:

$$Y = \beta_0 + \sum \beta_i X_i + \sum \beta_{ii} X_i^2 + \sum \beta_{ij} X_i X_j$$

Here Y represents response (biomass, g/L), X_i and X_j represent independent variables, β_0 is the intercept; β_i , and β_j are linear coefficients; β_{ii} and β_{jj} are squared coefficients; β_{ij} is interaction coefficients and the independent variables were coded as X_1 , X_3 , X_7 and X_9 . Thus, the second order polynomial equation can be presented as follows:

$$Y = \beta_0 + \beta_1 X_1 + \beta_3 X_3 + \beta_7 X_7 + \beta_9 X_9 + \beta_{11} X_1 X_1 + \beta_{13} X_1 X_3 + \beta_{17} X_1 X_7 + \beta_{19} X_1 X_9 + \beta_{33} X_3 X_3 + \beta_{37} X_3 X_7 + \beta_{39} X_3 X_9 + \beta_{77} X_7 X_7 + \beta_{79} X_7 X_9 + \beta_{99} X_9 X_9$$

Results and discussion

Growth curve

S.pombe is mostly evaluated as a strain for alcohol production at industrial sector and most of the studies are aimed to improve the alcohol yield rather than improving the biomass yield. Hence the present study is aimed to improve the *S.pombe* biomass and the experiments were conducted to optimize the biomass growth under aerobic conditions. It is evident from the literature that the *S.pombe* growth was studied

in YES medium preferably and a few studies are associated with YPD medium. However, it was proved that YES medium is highly effective in *S.pombe* fermentation studies (8). By considering the above, in the present study, the growth of *S.pombe* was evaluated in YES as well as YPD media at common physiological and nutritional conditions. The data revealed that both the media supported the growth of *S.pombe* in comparable manner; the biomass yield was observed to be 13.5 g/L and 14 g/L with YES and YPD media respectively. The cost effective analysis of the both media components revealed that YES (\$127/ 500g) medium is almost a three-fold higher in cost compared to YPD (\$ 45/500g) medium indicating YPD is the best economic media for *S.pombe* biomass production at industrial sector. Since glucan is the major component (>60%) of *S.pombe* cell wall, the optimization of YPD media components has been the next promising step to reduce the glucan production cost by improving the yield of *S.pombe* biomass. Furthermore, it is apparent to understand the effect of fermentation parameters (physiological, nutritional and biochemical) on the growth of *S.pombe*.

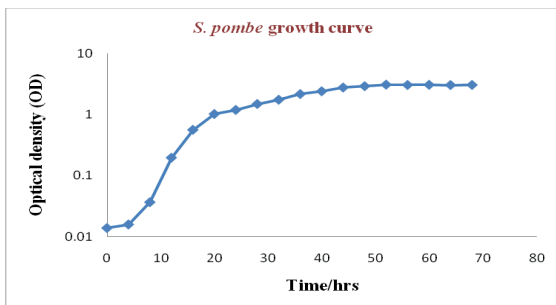


Fig. 1: *S. pombe* growth curve in YPD medium.

The growth curve of *S.pombe* in YPD medium is represented in (Fig 1). It is evident from the data that the growth of *S.pombe* has a lag phase of 0 to 6 hrs followed by 6 to 40 hrs log phase, thereafter the culture entered slowly into stationary phase. Critical observation of the growth pattern at log phase further denoted

that it is bi-phasic in nature; initial fast growth phase (6-12hrs) followed by the second slower growth phase (12 to 40 hrs). This is further evidenced from the growth curve doubling time which was observed as 3.02 hrs at initial fast growth phase, while the same was noticed to be 16.07 hrs at second slower growth phase suggesting nutritional imbalance during the log phase of growth. Further, the specific growth rate (R) was observed to be 0.331/hr and 0.062/hr for faster and slower growth phases respectively. The above data is an indicative of influence of nutrient concentration on growth of *S.pombe* (12). This data is in accordance with the observations noticed by Hayles and Nurse (13) where the authors explain that, initial fast growth phase represent the growth of *S. pombe* through vegetative reproduction (fission) and the second slower growth phase may be associated with meiosis. To evaluate the same, the SEM analysis was performed to understand the morphological nature of the *S. pombe* cells during log phase at initial fast and slower second log phase. (Fig. 2) clearly is an indicative for difference in reproductive pattern (fission type at initial fast log phase (Fig. 2a) and meiosis type at slower second log phase (Fig 2b) regulated by nutritional status of *S.pombe* growth environment.

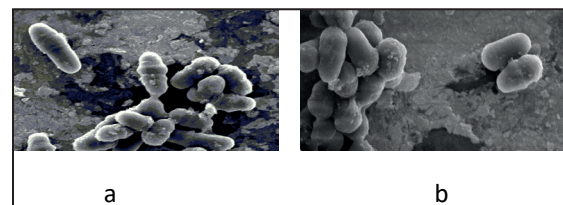


Fig. 2: SEM image of *S. pombe*: a) Fission b) Meiosis.

Effect of bioprocess parameters on *S.pombe* biomass

Any microbial growth is influenced by the fermentation factors and growth of the organism significantly varies based on nutritional status of the medium (14-15) as well as each microbial strain is unique in their

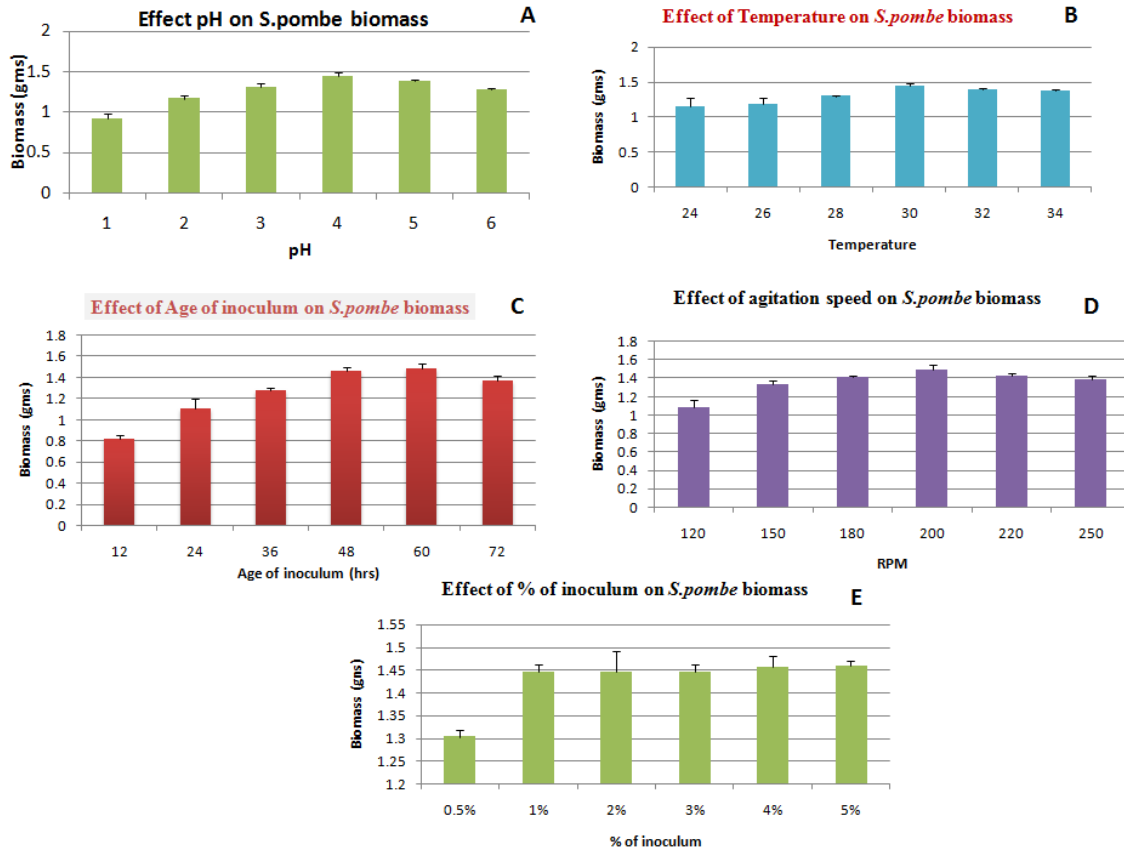


Fig. 3: Effect of physical parameters A) pH B) Temperature C) Age of inoculum D) Agitation speed E) inoculum concentration on *S. pombe* biomass.

growth requirements. Considering the above, the growth of *S.pombe* in terms of biomass yield was evaluated by varying physiological, biological and nutritional parameters one at a time at different experimentation conditions.

Effect of temperature on *S. pombe* biomass

Incubation temperature play vital role in growth and metabolite production in every microbe. Mostly fission yeast cells can grow between the temperature ranges of 18 to 37°C, however, the growth at 37°C or below 20 °C is not ideal for growth (8). Nevertheless, this feature may not be uniform to all strains. Therefore, the effect of incubation temperature on *S.pombe* growth was studied between the temperature

ranges of 24 to 34°C. From the experimental results, the optimum temperature for the maximum biomass production (14.4±0.03) was noticed to be 30°C

Effect of inoculum concentration on *S.pombe* growth

The inoculum concentration is another principal factor which controls the growth state of *S. pombe*. In any microbial growth its effect on growth and metabolite production is significant as inoculum concentration is low, if the culture exhibit longer incubation time and if it is high, there is shorter incubation time these results in faster increase in biomass which ultimately leads to nutrient limitation that effects the product

formation. However, in the case of *S.pombe* the nutrient limitation arrests the growth in G_2 phase and inhibits the mitosis (16). Hence, the effect of inoculum concentration on the growth of *S.pombe* biomass was studied by inoculating the 24 hrs culture at different concentrations (0.5 to 5%). After 60 hours of incubation at 30°C the wet biomass was collected and weighed. The results suggested that growth of biomass was increased from 0.5 to 1.0% inoculum; thereafter the biomass concentration did not show any improvement or remained constant may be due to nutrient limitation.

Effect of initial pH

The medium pH is one of the significant factors that influence the microbial growth mostly by modulating the membrane transport of different nutrient and physiological growth factors. It has been reported earlier that the optimum pH for the growth of yeast is reported between 4.0 to 5.0. Here, the effect of pH on *S.pombe* at 30°C was investigated at the pH range of 3.0 to 8.0 with an increment of 1 pH unit for 60 hours. The results from the study suggested that biomass yield was increased from pH 3 to 6, there after the yield was constant over a broad pH range (6.0 to 8.0). However, a variable trend was reported by Meena et al. (2014), where the growth rate of *S.pombe* in the absence of malate was constant over a broad pH range of 3 to 8 indicating the nutritional parameters especially carbon source do control

the growth of *S.pombe* (17).

Effect of agitation speed

The agitation speed of the incubation plays a major role in the mass transfer of gaseous elements and other fermentation components throughout the culture growth. This impacts the uniform supply of oxygen to the cell culture and leads to appropriate growth rate. The growth of *S.pombe* at different rate of agitation 120 to 250 rpm was studied and results were given in the (Fig.3). From the (Fig. 3) it was evident that 200 rpm is the optimum for maximum biomass production which is found to be 14.9 ± 0.051 g/L.

Effect of different carbon sources

The glucose is the simplest and easy metabolizable carbon source for most of the microbial cells and routinely using carbon source in growth of *S.pombe*. However, it can also use glycerol, sucrose, raffinose, maltose as an energy source (18). Su et al in 1996 explored that absence of glucose arrest the cell division indicating strain dependent variation of growth parameters (12). Considering the above, the effect of different carbon sources like sucrose, fructose, dextrose, maltose and galactose at different concentrations (1 to 4%) were studied. However, the maximum biomass was obtained at 3% concentration of dextrose (17 ± 0.03 g/L) (Fig 4). This result mimics the reports of dextrose effect on ATP production by *S.pombe* (19).

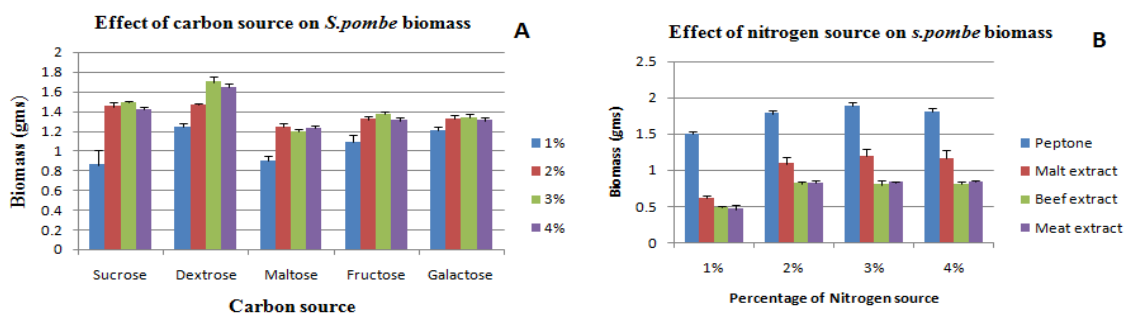


Fig. 4: Effect of nutritional factors A) Carbon source B) Nitrogen source on *S. pombe* biomass.

Effect of nitrogen source and yeast extract

The nitrogen plays a significant role in the cellular processes such as growth and metabolite production of microbes. Each distinct nitrogen source induces significant fluxes through the TOR (expand) and Sty1 growth control pathways to alter the architecture and flux of most cellular processes. Similarly, *S.pombe* growth is also influenced by different nitrogen sources. It is reported that all promote the cell proliferation, but the rate is distinct for different nitrogen sources (20). However, the absence of nitrogen source will arrest the growth in G₁ phase and stops the proliferation (21). Therefore, the present study assessed the influence of various nitrogen sources like peptone, malt extract, beef extract, meat extract on the *S.pombe* growth at different concentrations (1 to 4%). Among the different nitrogen sources peptone showed maximum biomass production (17.5±0.5 g/L) at 3% concentration and thereafter the yield was decreased (Fig 4).

The yeast extract can also used as a complex source to enrich the culture medium with some trace elements and growth factors at low cost to promote the growth of yeast (22). Hence, the effect of yeast extract on *S.pombe* was studied at different concentrations ranging from 1 to 4%. From the results, it was concluded that yeast extract at the concentration of 1% has given higher yield (13.00 g/L) (Fig 5). The result was in accordance with the report of Perez et al.

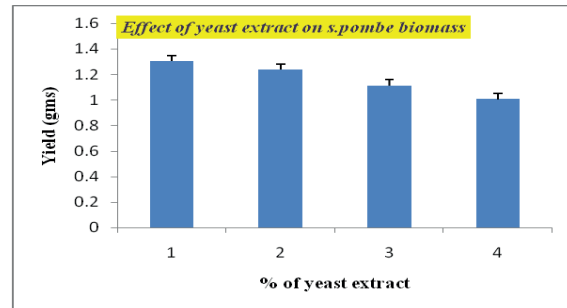


Fig. 5: Effect of yeast extract on *S.pombe* biomass.

(1992) where the effect of yeast extract on growth was influenced by the concentration of glucose. As the concentration of glucose increases, the yeast extract could increase the biomass at low concentration (1%) after that it could not support. However, the absence of yeast extract could not support the growth. Considering the above, it has concluded that yeast extract is one of the essential requirement for the growth of *S.pombe* upto limited concentration only (23).

Selection of significant variables by PBD

Based on the above studies, a total nine variables, i.e., physical parameters such as % of inoculum, age of inoculum, temperature, pH, incubation time and agitation speed as well as nutritional parameters such as dextrose, peptone and yeast extract were found to be effective in *S.pombe* growth. Considering the above and to understand which are the significant factors that influence the *S. pombe* biomass production, all

Table 1: Experimental variables at different levels used for the production of *S. pombe* biomass using Plackett–burmann design.

Variables	Units	Symbol codes	Experimental values	
			Lower	Higher
Temperature	°C	X1	28	32
pH	---	X2	5	7
RPM	---	X3	150	2
Age of inoculum	Hrs	X4	36	60
% of inoculum	MI	X5	0.5	2
Time of growth	Hrs	X6	36	60
Dextrose	% (w/v)	X7	2	4
Peptone	% (w/v)	X8	2	4
Yeast extract	% (w/v)	X9	0.5	2

Schizosaccharomyces pombe biomass production for glucan yield improvement

Table 2: Plackett-burmann design for growth studies of *S. pombe* and yield of the biomass for corresponding trail.

Run order	X1	X2	X3	X4	X5	X6	X7	X8	X9	Biomass (gm/100ml) (Y)	
										Experimental	Predicted
1	32	5	200	36	0.5	36	4	4	2	2.80	2.88
2	32	7	150	60	0.5	36	2	4	2	2.13	2.04
3	28	7	200	36	2	36	2	2	2	1.93	2.13
4	32	5	200	60	0.5	60	2	2	0.5	2.09	2.29
5	32	7	150	60	2	36	4	2	0.5	2.64	2.74
6	32	7	200	36	2	60	2	4	0.5	2.42	2.22
7	28	7	200	60	0.5	60	4	2	2	3.10	2.91
8	28	5	200	60	2	36	4	4	0.5	2.75	2.66
9	28	5	150	60	2	60	2	4	2	1.86	1.95
10	32	5	150	36	2	60	4	2	2	2.95	2.86
11	28	7	150	36	0.5	60	4	4	0.5	2.13	2.32
12	28	5	150	36	0.5	36	2	2	0.5	1.83	1.63

the above effective factors and their initial test ranges were studied and these factors were further subjected to statistical optimization by using PB design to identify the significant variables (Fig.6). All nine variables, each at two levels (lower and higher) were selected for the experimentation. The statistical designing tool

Mintab 18 version used to design the experiment. (Table 1 and 2) represent the design of the experiment (variable name, symbol code, and level of variables). The principal effect of each variable on the biomass yield was calculated by difference between averages of higher and lower level measurement. The significance level

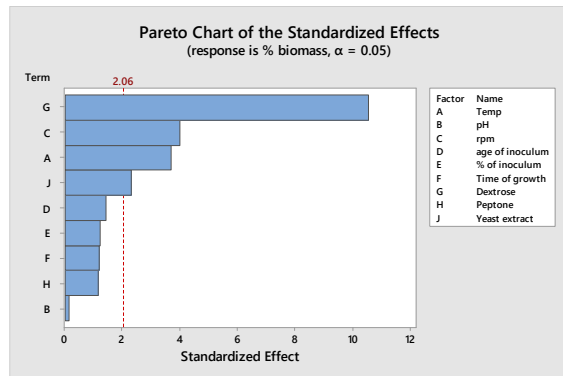


Fig. 6: Pareto chart for estimation of standardized effect of variables.

(P value) of each variable was determined using Student's t-test.

The data obtained by PBD experimentation indicated two-fold increased wet biomass (31g/L) than traditional OFAT (17 g/L) (Table 1; Run order 7) which also further confirmed by validation experiment. The efficiency of the model was evaluated,

Table 3: Estimated effects and coefficients for *S. pombe* biomass (g/l).

Term	Effect	Coef	T-Value	P-Value
Constant		2.3846	73.44	0.000
Temperature	0.2401	0.1200	3.70	0.001
pH	0.0104	0.0052	0.16	0.874
RPM	0.2596	0.1298	4.00	0.000
Age of inoculums	0.0928	0.0464	1.43	0.165
% of inoculums	0.0803	0.0401	1.24	0.227
Time of growth	0.0778	0.0389	1.20	0.241
Dextrose	0.6859	0.3430	10.56	0.000
Peptone	-0.0768	-0.0384	-1.18	0.247
Yeast extract	0.1497	0.0749	2.31	0.029

and the statistically significant variables were further reassured via student's t-test by ANOVA (Table 3). From the (Table 3), it has been concluded that the factors representing $P < 0.05$ were considered as significant factors for the production of biomass and further subjected for optimization studies. Dextrose, agitation

speed with a probability value of 0.000 and temperature, with a probability value of 0.001 were considered as more significant followed by yeast extract (0.029).

The Pareto chart demonstrated influence of each factor represented by alpha value equals to 0.05 i.e., 95% of confidence level and 8 degrees of freedom and t-value (equal to 2.06). The degree of each effect represents the length of the column. In the present study dextrose, revolution per minute, temperature and yeast extract, revealed a significant effect on biomass yield and subjected for further optimization while age of inoculum, incubation time, pH, peptone and % of inoculum did not show any significance.

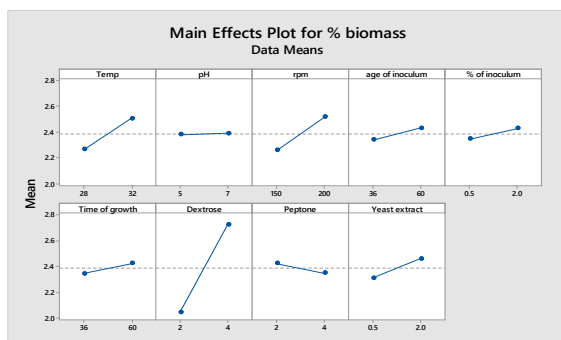


Fig. 7: Main effect plot for *S. pombe* biomass production.

Further the results of the main effect plot (Fig 7) indicated that dextrose at the highest level has a major effect on biomass yield whereas temperature, rpm and yeast extract were significant at lower level while pH, % of inoculum, age of inoculum, incubation time and peptone did not show any significant role on the

biomass yield.

Optimization of significant variables using RSM

Considering significant factors observed by PBD, further optimization studies i.e., interaction between significant variables and their optimum levels for maximum production was studied by the statistical design RSM using CCD design. A quadratic model consisting of 31 trials were applied for experimental studies. The significant variables selected for this purpose include: dextrose, RPM, temperature and yeast extract were represented in (Table 4).

The design and results (mean predicted values) of RSM experiments were shown in (Table 5). The ANOVA data (Table 6) indicated that the most of the model terms, were significant (represent $P < 0.05$), except a few insignificant terms like, $X_7 * X_3$, $X_3 * X_3$, $X_7 * X_9$, $X_7 * X_1$ and $X_3 * X_9$. Further, it explores a significant linear effect of dextrose, yeast extract and temperature ($P < 0.001$) than the rpm. These results inferred a direct relationship between the concentration of the carbon, yeast extract with respect to a temperature in biomass production. Furthermore, the higher F- and P-values (< 0.0001) and lack of fit (0.000) indicated the suitability and good fit of the model for the present study (Table 7). The calculated regression equation (express the response, biomass production (Y) by *S.pombe*) coefficient values were found to be following second-order polynomial equation.

$$\text{Yield} = 2.88952 + 0.36472 X_7 - 0.16639 X_1 + 0.06361 X_3 + 0.11861 X_9 - 0.10092 X_7 X_7 - 0.10092 X_1 X_1 - 0.02842 X_3 X_3 - 0.11176 X_9 X_9 + 0.07375 X_7$$

Table 4: Experimental codes, range of levels of independent variables for RSM experiment.

Variables	Symbol codes	Range of levels				
		-2	-1	0	+1	+2
Temperature	X1	26	28	30	32	34
RPM	X3	125	150	175	200	225
Dextrose	X7	1	2	3	4	5
Yeast extract	X9	0.5	1	1.5	2	2.5

Table 5: CCD matrix with experimental values of biomass production from *S. pombe*

StdOrder	X7	X3	X1	X9	Biomass (Y) (g/100ml)	
					Experimental	Predicted
1	2	150	28	1	2.24	2.31
2	4	150	28	1	3	2.83
3	2	150	32	1	1.87	1.83
4	4	150	32	1	2.6	2.65
5	2	200	28	1	2.23	2.04
6	4	200	28	1	2.73	2.73
7	2	200	32	1	2.05	2.01
8	4	200	32	1	2.84	3.0
9	2	150	28	2	3.09	2.71
10	4	150	28	2	2.95	3.18
11	2	150	32	2	1.61	1.78
12	4	150	32	2	2.58	2.55
13	2	200	28	2	2.48	2.68
14	4	200	28	2	3.45	3.26
15	2	200	32	2	2.18	2.13
16	4	200	32	2	2.96	3.07
17	1	175	30	1.5	1.62	1.75
18	5	175	30	1.5	3.32	3.25
19	3	175	26	1.5	2.6	2.82
20	3	175	34	1.5	2.34	2.15
21	3	125	30	1.5	2.62	2.65
22	3	225	30	1.5	2.89	2.91
23	3	175	30	0.5	2.15	2.21
24	3	175	30	2.5	2.71	2.76
25	3	175	30	1.5	2.91	2.89
26	3	175	30	1.5	2.9	2.89
27	3	175	30	1.5	2.85	2.89
28	3	175	30	1.5	2.96	2.89
29	3	175	30	1.5	2.84	2.89
30	3	175	30	1.5	2.86	2.89
31	3	175	30	1.5	2.85	2.89

$$X_1 + 0.04375 X_7 X_3 - 0.01208 X_7 X_9 + 0.11042 X_1 X_3 - 0.11292 X_1 X_9 + 0.04292 X_3 X_9$$

S = 0.163560 PRESS = 3.17079

R-Sq = 88.98% R-Sq(pred) = 83.25% R-Sq(adj)

The Fisher's test helps to evaluate the statistical significance of the model- equation and term.

The coefficient of determination (R²) and

Table 6: Analysis of variance (ANOVA) for quadratic model.

Source	DF	Seq SS	Adj SS	Adj MS	F	P
Regression	14	16.8473	16.8473	1.20338	44.98	0.000
Linear	4	12.8752	12.8752	3.21881	120.32	0.000
Square	4	2.3265	2.3265	0.58162	21.74	0.000
Interaction	6	1.6456	1.6456	0.27426	10.25	0.000
Residual Error	78	2.0866	2.0866	0.02675		
Lack-of-Fit	10	1.5467	1.5467	0.15467	19.48	0.000
Pure Error	68	0.5400	0.5400	0.00794		
Total	92	18.9339				

the adjusted R^2 values were determined to understand

The quality of fit (second-order polynomial model equation) which was expressed in three-dimensional surface plots. These plots aid to study the interactive relationship between the responses and each variable experimental level utilized in this experiment in terms of biomass production.

The regression equation also displayed the R^2 [multiple correlation coefficient] value as 0.8898 which is an estimate of the fraction of the overall variation in the data whereas the 'adjusted R^2 ' is 87%. This suggested the capability of model which can explain the 88.98 % of the variation in response as well as fitness

of the model (For a good statistical model, the R^2 value should be in the range of 0 to 1.0), The closer the R^2 (near to 1.0), the stronger the model and the better in the prediction of the response (10).

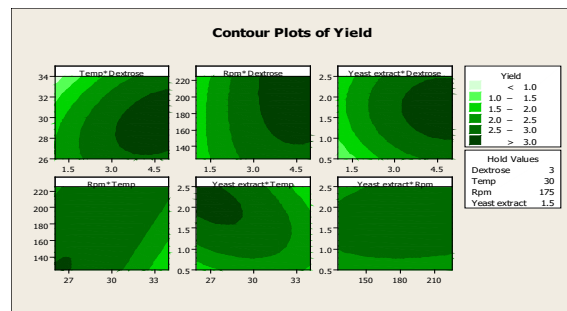


Fig. 8: Contour plots for *S.pombe* biomass optimization.

Table 7: Model coefficient estimated by multiple linear regressions.

Term	Coef	SE Coef	T	P
Constant	2.88952	0.03569	80.958	0.000
X7	0.36472	0.01928	18.921	0.000
X1	0.16639	0.01928	-8.632	0.000
X3	0.06361	0.01928	3.300	0.001
X9	0.11861	0.01928	6.153	0.000
X7*X7	-0.10092	0.01766	-5.715	0.000
X1*X1	-0.10092	0.01766	-5.715	0.000
X3*X3	-0.02842	0.01766	-1.610	0.112
X9*X9	-0.11176	0.01766	-6.329	0.000
X7*X1	0.07375	0.02361	3.124	0.003
X7*X3	0.04375	0.02361	1.853	0.068
X7*X9	-0.01208	0.02361	-0.512	0.610
X1*X3	0.11042	0.02361	4.677	0.000
X1*X9	-0.11292	0.02361	-4.783	0.000
X3*X9	0.04292	0.02361	1.818	0.073

Two-dimensional contour plots showed in (Fig. 8), denote the interaction effect of each independent variable against the biomass yield. For example, contour of glucose (x-axis) and temperature (y-axis) helps in evaluating the contributory role of these two factors at different concentrations on biomass production (>3 g/100 ml) (Fig 8). It also elucidates the direct interaction between dextrose and temperature in maximum biomass production which is further evidenced by their p-value of 0.003 (Table 6) which is significant. Simultaneously, the (Fig. 8) also depicts the significant interaction of temperature with rpm and yeast extract (Table 6). The surface in the other plots indicates that there is no interaction between other factors. Finally, the physical and nutritional parameter variation effect on *S.pombe* biomass production was depicted in (Table 7). It describes the step-by-step improvement of biomass production, where the initial yeast extract-peptone-glucose medium composition by using OFAT method has given the yield of 17 g/L followed by the statistical optimization (PBD & RSM) which yielded 34 g/L. At this step a 2.5-fold rise in biomass production explains the importance of statistical methods to achieve the higher yields of biomass compared to conventional OFAT method.

Validation of model

From the studies it was evident that the experimental biomass production of 34.5 g/L was produced where as predicted value was 32.6 g/L. This indicates a strong agreement between experimental values and predicted values. The optimum levels of tested variables were determined as dextrose (4%), rpm (200), temperature (28° C) and yeast extract (2%). Furthermore, the model was validated by repeating the experiment three times at optimum conditions. This results a biomass yield of 35 g/L, thus proving the validity of the model.

Verification of statistical model by 5L Bioreactor

The optimized levels of significant

variables obtained by RSM were examined using 5L Bioreactor with working volume of 3L. The maximum biomass concentration of 52g/L was produced with in the 10hrs, whereas, the shake flask method produced 34g/L within 60hrs of incubation. This might be due to the oxygenation (0.75vvm) which could resulted in rapid growth rate and high biomass concentrations of *S.pombe* in bioreactor. The same type of effect was observed on *S.pombe* in an ethanol production. From the study, it was evident that aerated cultures were shown higher growth rates in comparison to non-aerated cultures (17).

As several researchers have studied on the growth kinetics of *S.pombe* in relation to ethanol production (17), the studies to improve the biomass were not performed earlier. The present study focused on the optimization studies of *S.pombe* to improve the biomass yield which in turn increases the yield of glucans (Table 8). From these studies, the production media under optimized conditions was designed to have only yeast extract (2%), dextrose (4%) which replaces the commercially used media for the growth of yeast (YPD). Therefore, the production cost of the media for biomass was reduced and that simultaneously reduces the cost of glucan production. Eventhough, the glucans were extracted from different species of higher fungi (*Lentinus edodes*, *Ganoderma lucidium*) (24-25), the simplest structure and rapid growth of *S.pombe* under laboratory conditions will reduce the production cost of glucans compared to higher fungi which require variable environmental conditions for their growth.

Conclusion

To improve the yield of glucan economically, biomass yield should be improved at low production cost. This can be achieved only by using optimization studies of growth as it is directly proportional to yield of glucan. Gene manipulation could not be suitable for economization of glucan production as it is a

Table 8: An overview of step-wise progress in *S. pombe* biomass concentration under batch culture conditions.

Method of optimization	Physical parameters	Nutritional parameters % (w/v)	Biomass (g/L)
OFAT	30°C, 150 rpm, 1% inoculum, 48hrs of age of inoculum, pH -6, 60hrs of incubation time	dextrose-3%, Peptone-2%, Yeast extract-1%,	17
P l a c k e t t - Burman design	28°C, 200 rpm, 0.5 % inoculum, 60 hrs of age of inoculum, pH-7, 60hrs of incubation time	dextrose-4%, Peptone-2%, Yeast extract-2%,	31
R e s p o n s e s u r f a c e methodology	28°C, 200 rpm, 0% inoculum, 48 hrs of age of inoculum, pH-7, 60hrs of incubation time	dextrose-4%, Yeast extract- 2%,	34.5
Bioreactor	26°C, 175 rpm, 0.5% inoculum, 48 hrs of age of inoculum, pH-7, 0.75 vvm	dextrose-4%, Yeast extract- 2%,	52

structural component of cell wall. Therefore, the present combination of statistical optimization and scale up studies could play a significant role in the maximum production (52g/L) of biomass using *S.pombe* which was three fold raised compared to OFAT studies (17g/L).

Acknowledgements

Authors are thankful to the Director, CSIR-IICT Hyderabad. One of the authors, Dr Prakasham Reddy Shetty is thankful to CSIR, New Delhi, Government of India for financial support in the form of CSIR Emeritus Scheme (21(1102)/20EMR-II). The CSIR-IICT manuscript communication number is IICT/Pubs./2021/094.

Conflicts of interest

The authors declared that there are no conflicts of interest.

References

- Benito S, Palomero F, Morata A, Calderon F, Suarez-Lepe JA, New applications for *Schizosaccharomyces pombe* in the alcoholic fermentation of red wines. *International Journal*
- Aravind L, Watanabe H, Lipman DJ and Koonin EV, Lineage-specific loss and divergence of functionally linked genes in eukaryotes. *Proceedings of National Academy of Sciences*. USA 97 (2000) 11319.
- Takegawa K, Tohda H, Sasaki M, Idiris A, Ohashi T, Mukaiyama H, Giga-Hama Y, Kumagai H, Production of heterologous proteins using the fission-yeast (*Schizosaccharomyces pombe*) expression system. *Biotechnology Applied Biochemistry* 53 (2009) 227
- Bush DA, Horisberger M, Horman I, Wursch P, The wall structure of *Schizosaccharomyces pombe*. *Journal of General Microbiology* 81 (1974) 199.
- Sugawara T, Sato M, Takagi T, Kamasaki, T, Ohno N, Osumi M, *In situ* localization of cell wall α -1,3-glucan in the fission yeast *Schizosaccharomyces pombe*. *Microscopy* 52 (2003) 237.

of Food Science Technology 47 (2012) 2101.

6. Mitchison JM, Physiological and cytological methods for *Schizosaccharomyces pombe*. In *Methods in Cell Biology* 4 (1970) 131.
7. Merlini L, Dudin O, Martin SG, Mate and fuse: How yeast cells do it. *Open Biology* 3 (2013) 130008.
8. Petersen J and Russell P, Growth and environment of *Schizosaccharomyces pombe*. *Cold Spring Harbor Protocols* (2016) 1.
9. Adinarayana K and Ellaiah P, Response surface optimization of the critical medium components for the production of alkaline protease by a newly isolated *Bacillus sp.* *Journal of Pharmacology and Pharmaceutical Science* 5(2002) 272.
10. Khuri AI and Cornell JA, Response surfaces: design and analysis. Marcel Dekker, New York (1987).
11. Bhargavi PL, Kumar BS, Prakasham RS, Impact of nutritional factors versus biomass and serralyisin production in isolated *Serratia marcescens*. *Current Trends Biotechnology Pharmacology* 6 (2012) 449.
12. Banoth L, Devarapalli K, Paul I, Thete K.N, Pawar S.V. and Banerjee U.C. Screening, isolation and selection of a potent lipase producing microorganism and its use in the kinetic resolution of drug intermediates. *Journal of the Indian Chemical Society*, 98 (2021)100143.
13. Pai O, Banoth L, Ghosh S, Chisti Y. and Banerjee U.C. Biotransformation of 3-cyanopyridine to nicotinic acid by free and immobilized cells of recombinant *Escherichia coli*. *Process Biochemistry*, 49(2014)655-659.
14. Kamble A L, Banoth L, Meena V.S, Singh A, Chisti Y. and Banerjee, U.C. Nitrile hydratase of *Rhodococcus erythropolis*: characterization of the enzyme and the use of whole cells for biotransformation of nitriles. *3 Biotech* 3(2013)319-330.
15. Ghosh S, Banoth L. and Banerjee, U.C. Biocatalytic deracemization: An efficient one-pot synthesis of (R)- α -methyl-4-pyridinemethanol using whole cells of *Candida parapsilosis*. *Biocatalysis*, 1(2015) 59-66.
16. Egel R, Nielsen O, Weigum D, Sexual differentiation in fission yeast. *Trends in Genetics*. 6 (1990) 369.
17. Meena VS, Banoth L, Banerjee UC. Demonstration of redox potential of *Metschnikowia koreensis* for stereoinversion of secondary alcohols/1,2-diols. *Biomed Res Int*. 2014(2014) 410530.
18. Ravichandra, K., R. Balaji, Kezia D, Chandrasekhar C, Sudhakar P, Linga B, Srinivasa R P, and R. S. Prakasham. Impact of structure and composition of different sorghum xylans as substrates on production of xylanase enzyme by *Aspergillus fumigatus* RSP-8. *Industrial Crops and Products* 188 (2022) 115660.
19. Ravichandra, K., R. Balaji, Kezia D, Uma R B, Sathish T, Linga B, Srinivasa R P, and R. S. Prakasham. Enzymatic production of prebiotic xylooligosaccharides from sorghum (*Sorghum bicolor* (L.) xylan: value addition to sorghum bagasse. *Biomass Conversion and Biorefinery* (2022) 1-9.
20. Kadimpati, K K, Sathish T, Kezia D, Linga B, and Kiran B U. Characterization and hydrolysis optimization of *Sargassum cinereum* for the fermentative production of 3G bioethanol. *Biomass Conversion and Biorefinery* (2021) 1-11.
21. Kumar, R, Linga B, Uttam C B, and Jag-

- deep K. Enantiomeric separation of pharmaceutically important drug intermediates using a Metagenomic lipase and optimization of its large-scale production. *International journal of biological macromolecules* 95 (2017) 995-1003.
22. Patil, R, Linga B, Amit S, Yusuf C, and Utam C B. Enantioselective bioreduction of cyclic alkanones by whole cells of *Candida* Species. *Biocatalysis and Biotransformation* 31(2013)123-131.
23. Perez F, Riba JP, Strehaiano P, Effect of yeast extract concentration on the growth of *Schizosaccharomyces pombe*. *Biotechnology Letters* 14 (1992) 123.
24. Bao X, Duan J, Fang X, Fang J, Chemical modifications of the (1→3)- α -D- glucan from spores of *Ganoderma lucidum* and investigation of their physicochemical properties and immunological activity. *Carbohydrate. Research* 336 (2001) 127.
25. Zhang P and Cheung PCK, Evaluation of sulfated *Lentinus edodes* α -(1→3)-D Glucan as a potential antitumor agent. *Bioscience Biotechnology Biochemistry* 66 (2002) 1052.

Novel Synthesis of Isatin-Thiazole Pharmacophores and their Cytotoxicity Evaluation

Nagaiah Kommu^{a*}, S Srividya Bommakanti^a, Lakshmi Srinivasa Rao Kundeti^a, Tithi Bhattacharyya^b and Rajkumar Banerjee^b

^aCentre for Natural Products and Traditional Knowledge, CSIR-Indian Institute of Chemical Technology, Hyderabad 500007, India;

^bApplied Biology Division, CSIR-Indian Institute of Chemical Technology, Hyderabad 500007, India

*Correspondence author: nagaiah.iict@gov.in

Abstract

Novel synthesis of isatin-thiazole pharmacophores was developed which involves condensation of isatin or halo substituted isatins with phenyl hydrazine, 2-hydrazino-benzothiazole or 2-hydrazino-4-phenyl benzothiazole yielded the corresponding hydrazones which on further di-benzylation or di-methylation yielded 1,2'-dibenzyl or 1,2'-dimethyl substituted hydrazones. Further isatin or 7-Chloroisatin on condensation with 1,2-diaminobenzene yielded corresponding 6H-indolo[2,3-b]quinoxalines. One of the compound 1-benzyl-5-bromo-7-chloroindoline-2,3-dione (23) shows cytotoxicity activity against breast cancer cell line (MCF7) with IC_{50} value $27.23 \pm 3 \mu\text{M}$ and also in colorectal cancer cell line (CT26) with IC_{50} value $17.7 \pm 8 \mu\text{M}$, which was comparable to that of standard Doxorubicin.

Keywords: Halo substituted isatins, Phenylhydrazine, 2-hydrazino benzothiazole, 6H-indolo[2,3-b]quinoxalines, MTT ASSAY.

Introduction

Although there is considerable advance in the field of combinational chemistry related to drug

discovery, the success rate of generating new leads is yet to be achieved. Therefore, there is a necessity to explore focused set of library of compounds starting from therapeutically active heterocycles and make step by step modifications or design hybrid pharmacophore heterocyclic-heterocyclic analogs to make promising molecules.

Isatin (Indolin-1H-2, 3-Dione) is the most promising heterocyclic molecule from the point of exhibiting biological activity. In the past several modifications of isatin molecule were synthesized to study their biological activity. It has chemically three reactive centers, 1-NH, 3-carbonyl and in some reactions 2-carbonyl also. Due to electrophilic character of 3-carbonyl group, isatin or its halo substituted on benzenoid ring have been transformed to 3-substituted-indolin-2-ones like 3-imines (Schiff's bases), 3-hydrazones which on further Mannich reactions by using formaldehyde and secondary amines like diethyl amine, piperidines, morpholines yielded 1-substituted Mannich bases-3-imines/3-hydrazones. Alternatively, isatins were subjected first to Mannich reaction at position 1- of isatin and then 3-imines (schiff bases)/3-thiosemicarbazones or 3-arylhydrazones

were prepared (1-3).

Many of such isatin analogues were reported to possess anti-bacterial (4), anti-fungal (5,6), anti-viral (7), anti-HIV (8), antihelmintic (9), anti-inflammatory (10) and anti-convulsant (11). A novel isatin derivative 6-butyl-9-fluoro-2,3-dimethyl-6H-indolo-2,3-b quinoxaline, obtained by the condensation of 7-fluoro-1- butylisatin with 1,2-diamino-3,5-dimethylbenzene displayed significant in-vitro cytotoxicity against HeLa cells (human cervical cancer cells) (12).

IsatinMannich bases and Schiff bases analogues, obtained .by condensation of Isatin-1- Mannich bases with 2-amino -1- methyl benzothiazole were synthesized and studied for anti-breast cancer activity. For example, 9-chloro-1-dimethylaminomethyl-3-(6-methyl-enzothiazol-2-yl imino)-1,3-dihydro-indol-2-one had the highest activity (13). A spiroisatin derivative, 3H-spiro1,3-benzothiazole-2-3'-indol-2'(1'H)-one obtained by the condensation of isatin with 2-aminothiophenol showed anticancer activity (14). Very recently, after our work was completed the synthesis of spiroimidazopyridineoxindoles multicyclic spirooxindole pyrans and etc., were reported (15,16). Thus synthetic modification of isatin skeleton continues to draw the attention of the chemists and biologists.

Result and Discussion

In recent year's pharmacophore heterocyclic-heterocyclic hybrids gaining importance as practical medicinal agents. For example, several "NIBS" anti-cancer agents are now available commercially. Cytotoxicity evaluation of several heterocyclic compounds for their activity against breast cancer cell line and colorectal cancer cell line are also in progress. NIBS contain two or more than heterocyclic hybrids connected through N=N, NH-NH, =N-NH, -O-CH₂, NH-C and also contain aromatic rings. Some examples are imatinib, erlotinib, dasatinib and importantly sunitinib. Sunitinib featured isatin ring substituted at position-3. For testing biological activity, N-Mannich bases and 3-Aryl-hydrazones are common but N-alkyl, N-benzyl

isatins with substituted 3-aryl- or heteryl- hydrazones do not seem to have been investigated. Therefore, in the present study, 2-hydrazino-benzothiazole, 2-hydrazino-4-phenylthiazole or phenyl- hydrazine and further the resulting 3-hydrazones were successively condensed with 2 moles of benzyl bromide or methyl iodide was studied (Figure 1).

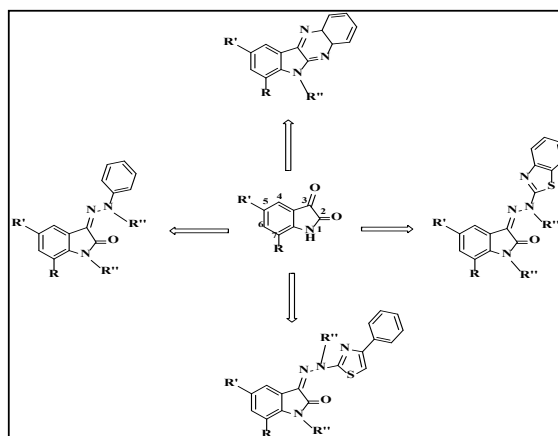
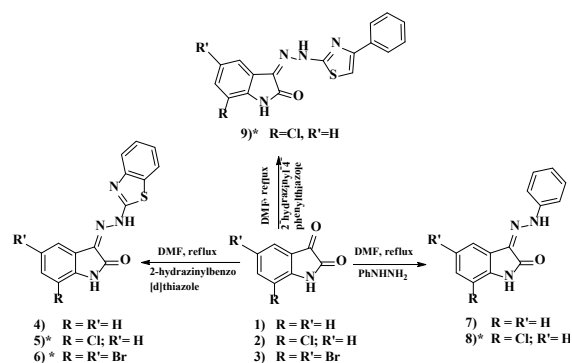


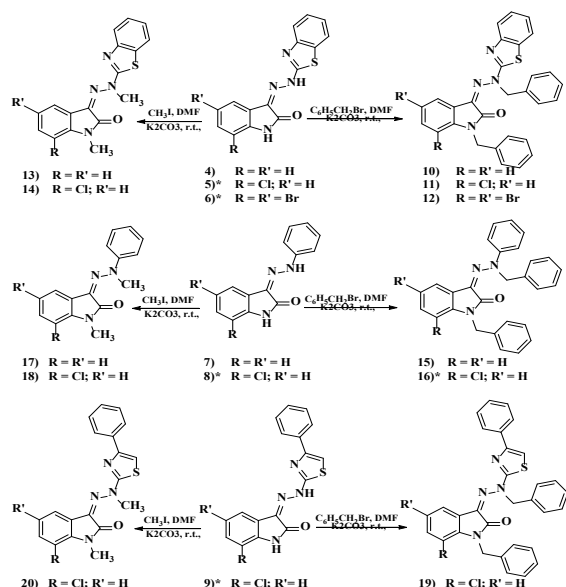
Fig 1: Isatin analogues

The condensation of isatin with heterocyclic hydrazines does not seem to have explored. Benzothiazoles are also well known to exhibit various biological activities. Benzothiazole skeleton show various biological activities such as analgesic (17), antitubercular⁺ (18), antibacterial (19) activities.



Scheme 1: Synthesis of hydrazone derivatives of substituted isatins (*not isolated. The crude compound is used for next step).

The several structural variants developed as a result of this study are (*Z*)-3-(2-(benzodthiazol-2-yl)hydrazono)indolin-2-one, (*Z*)-7-chloro-3-(2-(4-phenylthiazol-2-yl)hydrazono)indolin-2-one and (*E*)-3-(2-phenylhydrazono)indolin-2-one were obtained by successive condensation of isatin (or halo substituted isatins) with 2-hydrazino benzothiazole, 2-hydrazino-4-phenyl-thiazoles or phenyl hydrazine (Scheme 1).



Scheme 2: Synthesis of methylated or benzylated derivatives of isatin hydrazones.

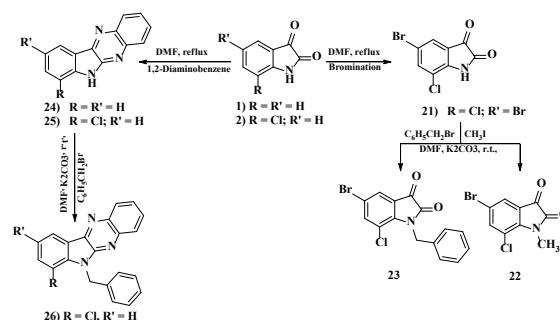
In these compounds isatin-benzothiazole pharmacophores are connected through -C=N-N-H group. Further these compounds were di-benzylated or di-methylated at the two available -NH groups to yield novel compounds (Scheme2).

Thus condensation of isatin with phenylhydrazine yielded isatin -3-phenylhydrazone (20) which on reaction with 2 moles of benzyl bromide yielded (*E*)-1-benzyl-3-(2-benzyl-2-phenylhydrazono) indolin-2-one. Likewise, (*Z*)-1-methyl-3-(2-methyl-2-phenyl hydrazono) indolin-2-one was synthesized in good yield (Scheme-2). Further starting from 7-chloro isatin the corresponding (*Z*)-7-chloro-1-methyl-3-(2-methyl-2-phenylhydrazono)indolin-2-one was

synthesized (Scheme-2). The condensation of 7-chloroisatin-2-hydrazinobenzothiazole with 2 moles of benzyl bromide or 2 moles of methyl iodide furnished (*E*)-3-(2-(benzodthiazol-2-yl)-2-benzylhydrazono)-1-benzyl-7-chloroindolin-2-one or (*Z*)-3-(2-(benzodthiazol-2-yl)-2-methylhydrazono)-7-chloro-1-methylindolin-2-one respectively, were described. Scheme 2 also depicts the synthesis of (*E*)-3-(2-(benzodthiazol-2-yl)-2-benzylhydrazono)-1-benzyl-5,7-dibromo indolin-2-one.

In ¹H NMR of (*E*)-3-(2-(benzodthiazol-2-yl)-2-benzylhydrazono)-1-benzylindolin-2-one, the aromatic protons resonated at $\delta = 7.76$ (dd, $J = 11.1, 7.9$ Hz, 2H), 7.64 (dd, $J = 7.6, 0.7$ Hz, 1H), 7.39 (td, $J = 8.2, 4.9$ Hz, 1H), $7.32-7.22$ (m, 6H), $7.22-7.14$ (m, 6H), 7.03 (td, $J = 7.6, 0.9$ Hz, 1H), 6.66 (d, $J = 7.9$ Hz, 1H). Two N-CH₂ at $\delta = 6.57$ (s, 2H), 4.92 (s, 2H). In ¹³C NMR, 1-N-CH₂-Ph carbon atoms resonate at $\delta = 43.7$ ppm and 2-(2'-N-CH₂-Ph) carbon atom at $\delta = 56.5$ ppm. Isatin 2C=O at $\delta = 170.9$ ppm, thiazole ring C=N at $\delta = 151.9$ ppm and 3C=N of isatin at $\delta = 157.3$ ppm. The aromatic carbons found in the region of $\delta = 108.8$ to 141.5 ppm.

Isatin and 7-Chloroisatin (21) are available in our Laboratory. Further 2-hydrazinobenzothiazole (22), 2-hydrazino-4-phenylthiazole (23) and 5,7dibromoisatin (24) are also synthesized as per literature procedure (Scheme-1). 7-chloro-5-bromo isatin (25) was synthesized by bromination of 7-chloroisatin (Scheme-3).



Scheme 3: Synthesis of methylated or benzylated derivatives of isatin and 6H-indolo 2,3-biquinoxalines

Table 1: Synthesis of hydrazone derivatives of substituted isatins, methylated or benzylated derivatives of isatin hydrazones, methylated or benzylated derivatives of isatin and 6H-indolo[2,3-b]quinoxalines.

Entry	Starting material	Product	Time (h)	Yield (%)
1			8	68
2			8	69
3			5	62
4			5	66
5			6	58
6			5	67
7			5	64
8			5	62
9			5	59
10			5	61
11			5	63
12			5	60
13				70
14			5	67
15			5	71
16			10	65
17			5	67
18			5	69

mo-7-chloro-1-methyl isatin were shown. Further fused isatin-quinoxalines were synthesized as shown in scheme-3. Thus isatin or 7-chloroisatin were condensed with 1,2-diaminobenzene (OPDA) to yield fused isatin-quinoxalines, 6H-indolo2,3-bquinoxaline or 7-chloro-6H-indolo2,3-bquinoxaline respectively. To our knowledge only one such compound was reported earlier¹². In Isatin-quinoxaline fused compound, 6H-indolo2,3-bquinoxaline, in ¹³C NMR, two C=N appeared at $\delta = 145.2, 143.2$ and 3C=O which normally appears at $\delta = 158$ is absent. This confirms the compound is a fused one. Rest of the aromatic protons appeared at $\delta = 139.4, 139.3, 137.9, 130.0, 128.0, 127.4, 126.5, 124.8, 121.3, 119.6, 118.4$ and 111.0.

The typical methods of synthesis of various compounds are given in experimental and in supplementary information. In table 1 the structures and yields are given after chromatography.

*All products were characterised by ¹H, ¹³C NMR, IR and ESI-HRMS spectroscopic techniques

CYTOTOXICITY EVALUATION

Table 2: IC₅₀ values of different isatin derivatives

Compound No.	MCF7	CHO
4	>50	>50
7	>50	34 ± 6
10	>50	>50
13	>50	>50
15	>50	>50
17	>50	>50
18	>50	>50
21	>50	>50
22	34 ± 5	29 ± 4
23	11 ± 5	10 ± 5
25	>50	>50
26	>50	>50
Doxorubicin		

The inhibitory efficiency (IC₅₀ values) was tested for all hydrazone derivatives of substituted isatins, methylated or benzylated derivatives of isatin hydrazones, methylated or benzylated derivatives of isatin and 6H-indolo2,3-bquinoxa-

lines against a panel of two different cancer cell lines such as MCF7 and CT26. This experiment was performed with a positive control in both the cell lines. The results are as follows shown in the following table 2. From the above results we can conclude that compound **23** is cytotoxic on cancer cell lines such as CT26 which is a colorectal cancer and MCF7 which is a breast cancer cell line.

Table 3: IC₅₀ values of compound 23 against MCF7 and CT26

Cell Line	IC ₅₀ of Compound 23 (μ M)	IC ₅₀ of Doxorubicin (μ M)
MCF7	27±3	8.067±0.3
CT26	17±8	7.099±1.43

Table 3 showed the IC₅₀ values of compound **23** against cancer cell lines such as MCF7 which is a breast cancer cell line and CT26 which is a colorectal cancer cell line. A positive control was also taken with compound **23**. The compound showed more cytotoxicity against colorectal cancer CT26 (IC₅₀ = 17.7 ± 8 μ M) with a positive control as Doxorubicin (IC₅₀ = 7.099 ± 1.43).

On breast cancer cell line MCF7, compound **15** is cytotoxic (IC₅₀ = 27.23 ± 3). Here Doxorubicin have (IC₅₀ = 8.067 ± 0.3). Compound **23** includes halogen group and this increases the efficiency of the compound. In fact, the binding efficiency of the compound to its ligand depends on its size.

This leads to a conclusion that compound **23** exhibits cytotoxic nature to different cancer cell lines.

CONCLUSION

Thus, several isatin-benzothiazole/thiazole hybrids were synthesized. Such hydrazones were di-benzylated or di-methylated with 2 moles of benzyl bromide or methyl iodide. Di-benylation or di-methylation took place at position of 1- of isatin and at position 2- of hydrazones resulted, which is an interesting and which is a nov-

el observation. When isatin on condensation with OPDA, resulted in fused isatin-quinoline heterocyclic, 6H-indolo2,3-bquinoline which is also an interesting observation. All the compounds are characterized by spectral data which is incorporated in experimental. In these compounds isatin-benzothiazole pharmacophores are connected through -C=N-N- group. Thus, new pharmacophore isatin-thiazole hybrids and isatin 3-hydrazones were generated in the present study. These compounds evaluated for cytotoxicity activity against different cancer cell lines. One of the compound 1-benzyl-5-bromo-7-chloroindoline-2,3-dione(23) showed cytotoxicity activity against breast cancer cell line (MCF7) with IC_{50} value $27.23 \pm 3 \mu\text{M}$ and also in colorectal cancer cell line (CT26) with IC_{50} value $17.7 \pm 8 \mu\text{M}$, which was comparable to that of standard Doxorubicin.

EXPERIMENTAL SECTION

General chemical methods

All solvents and the reagents were purchased commercially and used without further purification. All moisture sensitive reactions were carried out in anhydrous solvents under N_2 atmosphere. Column chromatography was carried out with silica gel (Merck 60–120 mesh). All reactions were monitored by thin layer chromatography (TLC) on silica gel Merck, Kieselgel 60 F254 plates; both starting material and products were visualized with using UV 254 nm and anisaldehyde stain followed by heating. ^1H and ^{13}C NMR spectra were recorded with an internal deuterium lock on Bruker 300, 400 and 500 MHz instruments, chemical shifts (δ) were measured in parts per million (ppm) and calibrated to the residual proton and carbon resonance of the CDCl_3 ($\delta\text{H} = 7.26$ and $\delta\text{C} = 77.0$ ppm). TOF analyzer technique was used for the HRMS measurement. FTIR spectra were recorded with a Bruker Alpha spectrophotometer and were reported in cm^{-1} .

Experimental and analytical details of three typical compounds are described below and for rest of the compounds the details are given in sup-

plementary information.

Experimental and Analytical data for selected compounds

(1). A mixture of isatin (1 g, 6.80 mmol), 2-phenylhydrazino benzothiazole (880 mg, 8.16 mmol) in DMF (10 mL) with few drops of acetic acid and refluxed for 8 h. After completion of the reaction (monitored by TLC), the reaction mixture was poured into cold water and extracted with ethyl acetate (3 x 20 mL). The combined organic layer dried over Na_2SO_4 and the solvent was removed under the reduced pressure. The residue was purified by silica gel chromatography eluting (EtOAc: hexane, 1:49) leading to (Z)-3-(2-(benzodthiazol-2-yl)hydrazono)indolin-2-one (1.09 g, 68%) derivative as yellow solid (Scheme 1).

(Z)-3-(2-(benzodthiazol-2-yl)hydrazono)indolin-2-one (4).

Yellow solid; mp 249-251 °C; IR (Neat) ν_{max} 2956, 2923, 2853, 1693, 1550, 772 cm^{-1} ; ^1H NMR (CDCl_3 +DMSO, 400 MHz): $\delta = 9.85$ -9.76 (brs, 1H), 8.34 (d, $J = 7.4$ Hz, 1H), 7.79-7.60 (m, 1H), 7.51 (dd, $J = 7.8, 2.2$ Hz, 1H), 7.40-7.19 (m, 3H), 7.16-7.05 (m, 1H), 7.01-6.93 (m, 1H), 6.88 (d, $J = 7.7$ Hz, 1H); ^{13}C NMR (CDCl_3 +DMSO, 75 MHz): $\delta = 173.6, 165.7, 141.7, 141.1, 138.9, 129.7, 126.2, 125.6, 124.5, 121.7, 121.3, 120.7, 117.4, 112.0, 109.2$. HRMS(ESI) m/z calcd for $\text{C}_{15}\text{H}_{10}\text{N}_4\text{OS}$, $\text{M}+\text{H}^+$ 295.0648, found 295.0631.

(2). To a stirred solution of Z)-3-(2-(benzodthiazol-2-yl)hydrazono)-7-chloroindolin-2-one (300 mg, 1.26 mmol) in DMF (8 mL) at 0 °C were sequentially added K_2CO_3 (524 mg, 3.79 mmol) and benzyl bromide (316 μL , 2.65 mmol) and stirring was continued for 5h at room temperature. The reaction mixture was poured into cold water and extracted with ethyl acetate (3 x 20 mL). The combined organic layer dried over Na_2SO_4 , filtered and concentrated. The obtained residue was purified by silica gel column chromatography (EtOAc: hexane, 1:19) to give (E)-3-(2-(benzodthiazol-2-yl)-2-benzylhydrazono)-1-benzyl-7-chloroindolin-2-one (347 mg,

66%) as a yellowish red solid (Scheme 2).

(E)-3-(2-(benzodthiazol-2-yl)-2-benzylhydrazono)-1-benzyl-7-chloroindolin-2-one (11).

Yellowish red solid; mp 192-194 °C; IR (Neat) ν_{\max} 3063, 3031, 2954, 2923, 1697, 1607, 1572, 754 cm^{-1} . ^1H NMR (CDCl_3 , 400 MHz): δ = 7.78 (d, J = 8.0 Hz, 1H), 7.75 (dd, J = 8.1, 0.9 Hz, 1H), 7.58 (dd, J = 7.5, 1.2 Hz, 1H), 7.40 (td, J = 7.4, 1.2 Hz, 1H), 7.31-7.07 (m, 12H), 6.96 (t, J = 7.8 Hz, 1H), 6.56 (s, 2H), 5.37 (s, 2H); ^{13}C NMR (CDCl_3 , 100 MHz): δ = 170.6, 157.7, 151.8, 137.1, 137.1, 134.5, 133.8, 131.8, 129.9, 128.5, 128.4, 127.6, 127.3, 127.1, 126.4, 126.1, 125.8, 123.8, 123.3, 121.8, 121.0, 119.2, 115.3, 56.6, 44.7; HRMS(ESI) m/z calcd for $\text{C}_{29}\text{H}_{21}\text{ClN}_4\text{OS}$, $\text{M}+\text{H}^+$ 509.1197, found 509.1178.(3). To a stirred solution of Z)-3-(2-(benzodthiazol-2-yl)hydrazono)-7-chloroindolin-2-one (300 mg, 1.26 mmol) in DMF (8 mL) at 0 °C were sequentially added K_2CO_3 (524 mg, 3.79 mmol) and methyl iodide (206 μL , 2.43 mmol) and stirring was continued for 5h at room temperature. The reaction mixture was poured into cold water and extracted with ethyl acetate (3 x 20 mL). The combined organic layer dried over Na_2SO_4 , filtered and concentrated. The obtained residue was purified by silica gel column chromatography (EtOAc: hexane, 1:19) to give (Z)-3-(2-(benzodthiazol-2-yl)-2-methylhydrazono)-7-chloro-1-methylindolin-2-one (336 mg, 64%) as a red solid (Scheme 2).

(Z)-3-(2-(benzodthiazol-2-yl)-2-methylhydrazono)-7-chloro-1-methylindolin-2-one (14).

Red solid; mp 204-206 °C; IR (Neat) ν_{\max} 3059, 2921, 2851, 1694, 1609, 1579, 753 cm^{-1} . ^1H NMR (CDCl_3 , 500 MHz): δ = 7.78 (d, J = 7.9 Hz, 1H), 7.72 (d, J = 7.9 Hz, 1H), 7.56 (dd, J = 7.4, 1.2 Hz, 1H), 7.40 (td, J = 7.3, 1.2 Hz, 1H), 7.29-7.22 (m, 2H), 7.01 (t, J = 7.4 Hz, 1H), 4.28 (s, 3H), 3.65 (s, 3H); ^{13}C NMR (CDCl_3 , 100 MHz): δ = 170.1, 157.4, 151.7, 138.0, 133.3, 131.8, 130.0, 126.8, 125.6, 123.7, 123.3, 121.5, 121.0, 119.0, 115.6, 43.3, 29.4; HRMS(ESI) m/z calcd for $\text{C}_{17}\text{H}_{13}\text{ClN}_4\text{OS}$, $\text{M}+\text{H}^+$ 357.0571, found 357.0566.

(4). A mixture of 7-chloro isatin (1 g, 5.53 mmol), *o*-phenylenediamine (775 mg, 7.18 mmol) in DMF (10 mL) with few drops of acetic acid and refluxed for 10 h. The reaction mixture was poured in cold water and extracted with EtOAc (3 x 20 mL). The combined organic layer dried over Na_2SO_4 , filtered and concentrated. The obtained residue was purified by column chromatography (EtOAc: hexane, 1:19) to give quinoxaline (894 mg, 64%) as a light yellow solid. The above obtained quinoxaline (200 mg, 790 μmol) in DMF (2 mL) was treated with K_2CO_3 (218 mg, 1.58 mmol) and benzyl bromide (103 μL , 502 μmol) at room temperature and stirring was continued for 5 h. The reaction was poured in cold water and extracted with EtOAc (3 x 20 mL). The combined organic layer dried over Na_2SO_4 , filtered and concentrated. The obtained residue was purified by column chromatography (EtOAc: hexane, 1:19) to give 26 (184 mg, 68%) as a yellow solid (Scheme 3).

6-benzyl-7-chloro-6,11a-dihydro-4aH-indolo[2,3-b]quinoxaline (26).

Yellow solid; mp 242-244 °C; IR (Neat) ν_{\max} : 3026, 2954, 2921, 1643, 1597, 1582, 1450, 772 cm^{-1} ; ^1H NMR (CDCl_3 , 500 MHz): δ = 8.16 (dd, J = 8.0, 1.3 Hz, 1H), 7.85 (dd, J = 7.9, 1.3 Hz, 1H), 7.48-7.44 (m, 1H), 7.37 (dd, J = 7.9, 1.5 Hz, 1H), 7.35-7.32 (m, 2H), 7.32-7.27 (m, 3H), 6.75 (t, J = 7.9 Hz, 1H), 6.07 (s, 2H), 5.57 (s, 2H); ^{13}C NMR (CDCl_3 , 125 MHz): δ = 154.6, 143.8, 135.1, 132.4, 132.2, 131.2, 130.4, 129.6, 128.9, 127.7, 126.9, 123.9, 120.6, 119.7, 116.5, 114.4, 46.4; HRMS(ESI) m/z calcd for $\text{C}_{21}\text{H}_{14}\text{ClN}_3$, $\text{M}+\text{Na}^+$ 366.0768, found 366.0779.

Declaration of Competing Interest

There are no conflicts to declare. For all the compounds experimental details and spectral data and as well as charts are given in Supplementary information

Acknowledgments

S. S. B and K. L. S. R thank to department of Ayurveda (EMR), India for financial support and

award of senior research fellowship, GAP-0623, Ministry of AYUSH. IICT publication no-IICT/Pubs/2019/286.

References

1. Patro, V. J.; Panda, C. S.; Sahoo, B. M.; Mishra, N. K.; Panda, J. R., *J. Indian Chem. Soc.*, **2012**, *89*, 913-918.
2. Varma, R. S.; Nobles, W. L. *J. heterocyclic. Chem.*, **1966**, *3*, 462-465.
3. Popp, F. D. *J. Med. Chem.*, **1969**, *12*, 182-184.
4. Varma, R. S.; Nobles, W. L. *J. Med. Chem.*, **1967**, *10*, 972-974.
5. Varma, R. S.; Pandey, R. K. *Arch. Pharm (Weinheim)* **1980**, *313*, 352-356.
6. Sarangapani, M.; Reddy, V. M. *Indian J. Pharm. Sci.*, **1994**, *56*, 174-177.
7. Singh, S. P.; Shukla S. K.; Awasthi, L. P. *Curr. Sci.*, **1983**, *52*, 766-769.
8. Pandeya, S. N.; Sriram, D.; Nath, G.; Clercq, E. D. *Eur. J. Med. Chem.*, **2000**, *35*, 249-255.
9. Sarciron, M. E.; Audin, P.; Delebre, I.; Gabrion, C.; Petavy A. F.; Paris, J.J. *Pharm. Sci.*, **1993**, *82*, 605-609.
10. Lingaiah, N.; Narender, R.; Dattatray, A. M. *Indian J. Chem, Sec. B*, **1998**, *37B*, 1254-1257.
11. Sridhar, S. K.; Pandeya, S. N.; Stables J. P.; Ramesh, A. *Eur. J. Pharm. Sci.*, **2002**, *16*, 129-132.
12. Reddy, S. S.; Pallela, R.; Kim, D. -M.; Won M.-S.; Shim, Y. -B. *Chem. Pharm. Bull.*, **2013**, *61*, 1105-1113.
13. Solomon, V. R.; Hu, C.; Lee, H. *Bioorg. Med. Chem.*, **2009**, *17*, 7585-7592.
14. Karali, N.; Guzel, O.; Ozsoy, N.; Ozbey S.; Salman, A.; *Eur. J. Med. Chem.*, **2010**, *45*, 1068-1077.
15. Rahimi, F.; Bayat M.; Hosseini, H.; *RSC Adv.*, **2019**, *9*, 16384-16389.
16. Mohamadi, A.; Bayat, M.; Nasri, S.; *RSC Adv.*, **2019**, *9*, 16525-16533.
17. Wade, J. J.; Toso, C. B.; Matson C. J.; Stelzer, V. L.; *J. Med. Chem.*, **1983**, *26*, 608-611.
18. Bhusari, K. P.; Khedekar, P. B.; Umathe, S. N.; Bahekar R. H.; Rao, A. R. R. *Indian J. Heterocyclic Chem.*, **2000**, *9*, 213-216.
19. Mistry K.; Desai, K. R. *Indian J. Chem.*, **2006**, *45B*, 1762-1766.
20. Azizan, J.; Mohammadi, M.K.; Firuzi, O.; Razzaghi-Asl N.; Miri, R. *Medicinal chemistry research*, **2012**, *21*, 3730-3740.
21. Wang, Z.; Wang, C.; Sun, Y.; Zhang, N.; Liu, Z.; Liu, J.; *Tetrahedron*, **2014**, *70*, 906-913.
22. Mor, S.; Mohil, R.; Nagoria, S.; Kumar, A.; Lal, K.; Kumar, D.; Singh, V.; *J. heterocyclic. Chem.*, **2017**, *54*, 1327-1341.
23. Svetlik, J.; Turecek, F.; Goljer, I.; *J. Org chem.*, **1990**, *55*, 4740-4744.
24. Semenov, B. B.; Novikov, K. A.; Spitsin, A. N.; Azev, V. N.; Kachala, V. V. *Chemistry of Natural compounds*, **2004**, *40*, 585-590.
25. 25 Silva, B. V.; Esteves, P. M.; Pinto, A. C. *J. Braz. Chem. Soc.*, **2011**, *22*, 257-263.

Development and Optimization of Curcumin and Lycopene Mucoadhesive Buccal Patches Using Response Surface Methodology

B. Bhargavi¹, P. Shanmugasundaram^{1*}

¹Department of Pharmaceutical Chemistry and Analysis, School of Pharmaceutical Sciences, Vels Institute of Science, Technology and Advanced Sciences (VISTAS), Chennai-600117, Tamil Nadu, India

*Corresponding author: samsimahe@gmail.com

Abstract

Buccal patches are the ideal mode of delivery for the systemic release of drugs because they give enhanced bioavailability by bypassing hepatic first-pass metabolism and allowing through the jugular vein, direct access to the circulatory system. The present research work is on the development and optimization of a mucoadhesive buccal patch of curcumin and lycopene for embattled release in oral cancer therapy. Using polymers like ethocel and methocel, buccal patches were produced by the solvent-casting method. Buccal patches were evaluated by disintegration time, folding endurance, % drug release, surface pH study, swelling study, mucoadhesive strength and stability studies. The developed buccal patches were evaluated for cytotoxicity in KB cell line using MTT assay. Folding endurance of formulation was found to be 167.66. The disintegration time of buccal patch was found to be 3.34 minutes. Thus, it can be said that the oral cancer treatment using the buccal patch formulation that has been created may be innovative.

Keywords: Buccal patches, Curcumin, Lycopene, Oral cancer, MTT assay.

Introduction

The improvement of controlled medication deliverance systems, either through, the oral mucosa using mucoadhesive polymers has gotten a lot of importance in current years. For local or systemic distribution, the buccal tablets delivery routes are becoming increasingly frequent. (1) The oral cavity, in scrupulous, seems to provide the unique profit of improved availability, a precise yet comparatively penetrable epithelial barrier for delivery of drugs, unidirectional drug instability, fast and simple exclusion of the pharmaceutical formulations leading suggestion, efficient drug permeability, and evade of liver function first-pass metabolism, all of which contribute to enhanced bioavailability and patient compliance. (2) The buccal route has been utilized for both local drug delivery and systemic drug delivery in a variety of dosage form forms, including sticky gels, capsules, films, patches, pastes, mouthwashes, and sprays. (4) Localized aphthous ulcers, gingivitis, periodontal diseases, and xerostomia are all treated using mucoadhesive dosage forms. Due to their outstanding flexibility and simplicity of usage, mucoadhesive tablets appear to be the most popular dose form for buccal administration of medication. They can be used on the cheek, gums, lips, palate, and other parts of the oral cavity. (4)

Oral cancer was among the most recurrent and invasive cancers, accounting for 5% of all cancer deaths globally. Oral cancer is treated with radiotherapy, chemotherapy, and surgical excision, all of which have serious side effects for patients. These unfavourable treatment side effects are caused by the therapeutic drugs' nonspecific activity.(5) Chemotherapy's side effects have been decreased through developments in drug delivery technologies during the last four decades. In addition, the advancement of nanotechnology in anticancer therapy has aided in the development of new diagnostic and treatment procedures. The most desirable treatment for oral cancer is targeted therapy, which focuses on particular site delivery and therefore to reduces side effects and systemic toxicity. The solubility, stability, and bioavailability of therapeutics supplied by nano delivery systems made of polymers were improved, accumulating even inside tumor cells.(6) Oral strips was designed to be applied locally to the tongue or buccal cavity. When compared to traditional measures, mucoadhesive buccal patches provided advantages.(7) Buccal patches provide the advantage of increased residence duration and drug release owing to the narrow holding time of oral gels in the mouth cavity.(8)

One of the most widely utilized methodologies in this design and optimization of targeted drug release is response surface methodology (RSM). The methodology is based on ideology of design of experiments, includes the exploit several forms of trial designs, the development of polynomial numerical equations and the mapping of retort more than experimental province in order to resolve the best formulation (s). The process needs very petite experimentation and time, and it has proven to be significantly more effective and cost-efficient than traditional dosage form formulation procedures. Numerous RSM design types are available for the formulations' quantitative optimization, including the central composite design, 3×3 factorial design, and Box-Behnken design, etc.(9,10)

Polymers are frequently used in con-

temporary pharmaceuticals technology, and they have been crucial to the advancement of medication delivery. Polymers are used as carriers in targeted therapy, allowing for synchronized drug distribution while also lowering medication bitterness.(11) The nature of ethyl cellulose and methylcellulose is hydrophobic. It's a free-flowing white to light powder that's frequently employed in the production of controlled drug release. Ethyl cellulose and methyl cellulose are suitable to be used in tablets, oral capsule, ophthalmic or vaginal formulations, and topical therapies since they have few side effects.(12) A number of natural chemicals built-in the daily diet (or should be present) have been demonstrated to have chemo preventive properties. (13) Numerous biological processes are carried out by polyphenols, including carotenoids (lycopene, carotenoid epigallocatechin-3-gallate, resveratrol, ellagic acid, quercetin, and curcumin), minerals (selenium, zinc), C, D, and E vitamins. Cell growth inhibition, autophagy activation, growth factor decreases, signalling systems that control angiogenesis or tumour growth as well as the suppression of inflammation are only a few of the molecular mechanisms that are involved, have been proven to prevent cancer beginning and progression.(14-18) Aim of this work is development and characterization of buccal patches containing curcumin and lycopene encumbered in ethocel and methocel polymer.

The goal of this study was to characterize buccal patches in assessing their efficacy as targeted drug delivery for oral cancer therapy. A Central merged design was used as computer-aided optimization technique. The quantity of the release retardant served as one of the study's independent variables, polymer-ethocel (X1) and propylene glycol (X2) and carbomer(X3). The dependent variables study was the disintegration time (Y1) and folding endurance (Y2) and % drug release (Y3).

Materials and Methods

Materials and reagents

Development and optimization of curcumin and lycopene mucoadhesive buccal patches using response surface methodology

Curcumin and lycopene were procured from Sigma Aldrich, India. Ethocel and methocel were purchased from TCI chemicals, India. Carbopol and Propylene Glycol were procured from SRL chemicals, India. Millipore water was used in this work. The remaining substances were all of analytical grade.

Development of drug loaded buccal patch

A petri dish was used to make a series of buccal patches using the solvent casting process. The patches were made up of different percentages of ethocel and methocel, which were dissolved in ethanol and then mixed with Curcumin for 30 minutes. Ethanol: water (1:1) Lycopene solution was added to the prior solution and agitated continuously for additional 30 min. The carbopol solution was made by boiling Millipore water with continual stirring before adding it to the polymeric solution. With intermittent shaking, the determined amount of propylene glycol was included to the solution. The casting solvent was therefore reduced to 30ml and agitated for 24 hours to ensure complete dissolution, before being placed in a vacuum

desiccator to eliminate any remaining air bubbles. The rate of evaporation was controlled and prevents patch blistering. Then the solution was cast in a glass petri dish covered with an inverted glass funnel. At room temperature, the solvent was allowed to fade away for 24 hours. The dry patch was isolated, sliced into 2x2 cm square portions. It was covered in aluminium foil and kept in a desiccator.(19-21)

Preparation of buccal patch using experimental design

Utilizing central composite design, the formulation was improved. The selected factors were Ethocel (0.83-1.67gm, factor A), Propylene glycol (4.16-5.84 ml, factor B) and Carbomer 0.66-1.34 gm, factor C). The response studied was Disintegration time, folding endurance and %drug release. The buccal patch was prepared using central composite design (Design expert software version 12.0). The design expert programme displayed the complete 20 runs. The studied response and variables were shown in Table 1.

Table 1: Central composite arrangement for factors and responses

STD	Run	Space type	Factor A: Ethocel (gm)	Factor B :Propylene glycol (ml)	Factor C: Carbomom (gm)	Response 1 Disintegtaion time (Sec)	Response 2 Folding Endurance	Response 3 Drug Release (%)
15	5	Center	1.25	5	1	3.3	206	32.7891
18	8	Center	1.25	5	1	3.3	206	32.7891
19	9	Center	1.25	5	1	3.3	206	32.7891
20	11	Center	1.25	5	1	3.3	206	32.7891
17	13	Center	1.25	5	1	3.3	206	32.7891
16	15	Center	1.25	5	1	3.3	206	32.7891
10	3	Axial	1.956	5	1	6.45	215	41.0472
14	4	Axial	1.25	5	1.57	4	214	43.1234
9	12	Axial	0.543	5	1	6.45	212	42.0240
13	16	Axial	1.25	5	0.428	3	205	33.4518
12	18	Axial	1.25	6.412	1	2.3	202	49.4505
11	20	Axial	1.25	3.587	1	2.6	198	45.123
7	1	Factorial	0.83	5.84	1.34	4.0	209	52.8442

4	2	Factorial	1.67	5.84	0.66	3.0	204	42.8248
5	6	Factorial	0.83	4.16	1.34	3.3	207	92.9218
1	7	Factorial	0.83	4.16	0.66	2.45	203	40.0776
6	10	Factorial	1.67	4.16	1.34	3	208	53.1674
2	14	Factorial	1.67	4.16	0.66	2	200	39.4123
8	17	Factorial	1.67	5.84	1.34	5.1	211	43.9561
3	19	Factorial	0.83	5.84	0.66	2.15	201	18.2612

Table 2: Statistical parameters obtained from ANOVA

Responses	F-value	P-Value	Adjusted R ²	Adequate precision
Disintegration time (DT)	5.11	0.0089	0.9908	8.9078
Folding Endurance	16.02	0.0001	0.8768	14.8771
Percentage Drug Release	4.98	0.0097	0.9534	9.5887

Evaluation of prepared buccal patches

Study of drug–polymer interactions

Fourier Transform Infrared Spectroscopy

Nicolet 520P FT-IR spectrometer wavelength in the range of 4000-500 cm⁻¹ was used for the study of drug and polymer interaction. KBr pellet method was used for sample preparation.

Differential scanning Calorimetry analysis

Differential scanning Calorimetry (DSC) analysis was used to analyze the Drug-polymer interactions. DSC is the one of the thermal analytical techniques. Perkin Elmer Differential Scanning Calorimeter (DSC 6000 – Perkin-Elmer) was used to analyze drug and polymer samples at a heating tempo of 10°C / min under air environment and an air was flushed at a flow rate of 5 mL/ min.

Folding endurance and thickness

It was done to demonstrate the effectiveness of the softener and assess the tensile of the patch made with various polymers. Folding endurance is nothing but the number of folds needed to break any polymer patch. The exact

folding endurance was tested manually by repeated folding of a tiny (2 x 2 cm) section of the film in same spot until it was broken. The folding endurance of patch was determined by how many times it was folded in the same position without breaking or cracking the patch. The same process was repeated for all 3 formulations.

In vitro disintegration time

The interval at which a film disintegrates when it comes into touch with water or a buffer is known as the disintegrating time. A buccal patch of 2 x 2 cm was placed inside the disintegration device, which was kept at 37±0.5°C and filled with pH 7.4 buffer. The time it took for the patch to disintegrate was recorded.

Determination of in vitro drug release

Buccal patch preparations were characterized in vitro using Franz diffusion cells. This is a reliable technique for estimating drug transport from topical formulations through the skin. With a synthetic cellophane membrane and 30.0 ml of phosphate-buffered saline (pH 7.4) injected into the receptors section of the diffusion cell, studies on in vitro drug release were done. A patch of 2 x 2 cm was cut and stitched on. The

membranes in the client compartment received it. The cellophane membrane was then evenly widened. The assembly was continuously kept at 50 rpm at 37.0 ± 0.2°C. In order to keep the receptor phase volume at 30 ml, samples (1.0 ml aliquots) then were set aside at proper times (0, 1, 2, 3, 4, 5, 6, 7, 8, and 10 hr) and supplied with the medium. The patches that contained curcumin and lycopene underwent spectrophotometric analysis at wavelengths of 427 nm, 440 nm, and 375 nm, respectively.

Weight variation

For weight uniformity, all prepared patches were individually weighed. The weight was determined using a weighing balance for analysis (Shimadzu AX 200, Kyoto, Japan). Individual weights were compared to the state median.

Uniformity of drug content

The patches were trampled in a mortar and pestle with water/acetone solvent to check for drug content homogeneity (1.5cm×1.5cm dimension) and water or alcohol as a patch solvent containing curcumin and lycopene. The content was then filtered by using 0.45 µm syringe. Then the solutions were diluted with simulated saliva. Samples were analyzed at a maximum wavelength of 426 and 260.6 nm (Shimadzu, Japan, UV 1800 spectrophotometer) by using solvent plain. Using the calibration curve, the drug substance was calculated.

Surface pH determination study

pH at the surface of the patches were measured at intervals of 1, 2, 3, 4, and 5 hours by inserting them into distilled water in 10 ml glass tubes. Close to the surface with digital pH meters tip allowing the patch to settle. Then it was equilibrating for 1 minute before the recording begins and this determination was carried out in three times.

Swelling study

On petri dishes, 25 mL of artificial saliva

was kept at room temperature. The patch starting weight (W1) was measured. The films with moisture on their surface were gently removed with filter paper after 60 minutes. The swollen patches were weighted (W2), and the formula below was used to estimate the swelling percent.

$$\text{Swelling index} = (W2 - W1) / W1 \times 100$$

Mucoadhesive study of buccal patches

PBS (pH 6.6) was used as the moistening agent, and the modeling substrates were recently excised pig buccal mucosa that was purchased from a slaughterhouse. For a total of 10 minutes, a horizontally positioned crushed buccal patch was "sandwiched" between two or three layers of clipped model tissue substrates. A constant mass of 50 gm was then placed on top. The bio adhesive strength was evaluated using an Exttech 475040 Force Gauge Meter in terms of the force needed to dislodge the patch from the animal buccal mucosa (Exttech Instruments Corp). When the patches were removed from porcine buccal mucosa, upward tension was congested and the force reading was obtained.

Morphology of buccal patches

Morphology of the developed patches were analyzed using scanning electron microscopy (SEM; JEOL JMS-6390 apparatus). In order to ensure the electron beams strong conductivity across the samples, carbon coatings were applied to them. As the electron beam traverses the sample, signals in raster images that contain information about the sample's surface topography and other characteristics are produced.

Stability studies

For the preparation optimized patch, stability studies were conducted over 180 days. Patch was preserved in the incubator, that was maintained at 37 ± 0.05°C and 75 ± 5 RH, for stability studies. The prepared patch medication content and physical appearance were exam-

ined after a 30-days interval. The procedure specified in the section was followed to determine the drug content.

Cytotoxicity assay

Optimized buccal patch 2x2cm was prepared, sterilized by ultraviolet radiation and then incubated with 1ml of DMEM medium at 37°C with 5% CO₂ for 24hrs. Sample solution, from these serial two-fold dilutions (6.25 – 100 µg) was prepared. From NCCS, a KB cell line was purchased. In a medium (DMEM) enriched with 10% inactivated Fetal Bovine Serum (FBS), 100 IU/mL penicillin, and 100 g/mL streptomycin, stock cells were cultivated until confluent. The growing environment consisted of a humidified atmosphere with 5% CO₂.

Using appropriate media containing 10% FBS, the monolayer cell culture was trypsinized and the cell count was adjusted to 1.0 x 10⁵ cells/mL.

About 100 µL of diluted cell suspension (1 x 10⁵ cells/well) was added to each 96 well microtiter plate. A partial monolayer was formed after 24 hours. The monolayer was rinsed with medium once after the excess was flicked off. The partial monolayer in the microtitre plate received 100 L of test samples at various concentrations. The plate was subsequently incubated for 24 h at 37 °C in a 5 % CO₂ environment. (22,23)

Results and Discussion

Drug polymer incompatibility study

The FT-IR and DSC studies were used to determine drug excipient compatibility.

FT-IR

The FT-IR spectrum analysis of the drug and polymer mixture was used to identify any physical or chemical modifications of the drug's properties. Curcumin's FTIR spectra were found to be in the following ranges: -OH group: 3382.67 cm⁻¹; aromatic CH group: 2969.72 cm⁻¹; C=C and C=O group: 1510.60 cm⁻¹; and C-O-C

stretching: 1205.44 cm⁻¹. Lycopene's FTIR spectra were found to be in a range between 282.959 cm⁻¹ and 2005.58 cm⁻¹ for the CH group and 1512 cm⁻¹ for the C=C group. When comparing the spectra of the created films with the original peak of the drug and polymers, it was found that there was no substantial change, indicating that there was no drug-polymer interaction. The IR chromatogram was shown in Figure 2. The final formulation FTIR spectra shown many peaks indicating that the chemical structure of the drug was conserved with efficient loading into the formulation. Curcumin and lycopene had no chemical interaction with the physical mixtures of polymers (ethocel, methocel, carbomer, propylene glycol) utilised in this buccal formulation study.

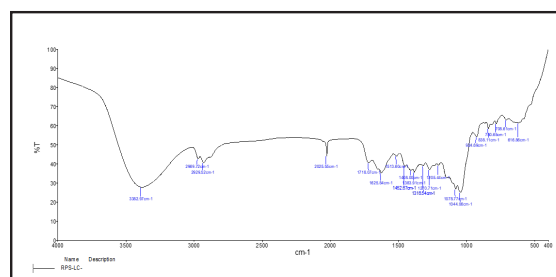


Fig. 2: IR spectrum for Physical mixtures

DSC

DSC thermogram of curcumin, lycopene and polymer was studied. It was found that curcumin shown endothermic peak at 184.81°C, Lycopene shown endothermic peak at 153.11°C, ethocel shown exothermic peak at 348.98°C, methocel shown exothermic peak at 306.22°C, Carbomer showed endothermic peak at 246.70°C. Physical mixture pure drug and polymers showed endothermic peak at 184.81°C, 323.5°C, 153.11°C, 348.98°C, 306.22°C and 246.70°C. This suggests that there were no interactions between drug and polymer as well as excipients used in buccal patch formulations. The DSC thermogram was shown in Figure 3.

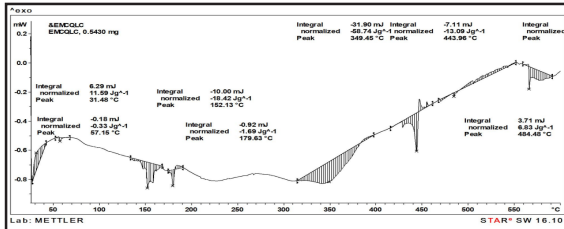


Fig. 3: DSC Thermogram for formulated buccal patch

Evaluation

In this research work, buccal patch of curcumin and lycopene were prepared with polymer combination of ethocel and methocel by using solvent casting technique. A total 20 number formulation were prepared using a central composite design (Table 1). Flat yellow non-transparent patches were obtained and cut into 1.5 cm squares on either side.

Statistical optimization

Disintegration time, folding endurance and % drug release obtained by the various levels of 3 independent variables, ethocel - Polymer, propylene glycol - plasticizer and carbomer - Film thickening agent, were subjected to multiple regressions to yield the final equation.

Disintegration time (DT)

$Y = +3.33 + 0.0940 * A + 0.2193 * B + 0.5478 * C + 0.3375 * AB + 0.0500 * AC + 0.625 * B^2 - 0.8833 * A^2 - 0.5221 * B^2 - 0.5109 * C^2 + 0.3375 * AB$ + Sign of coefficients indicates positive effects of polymer and plasticizer concentration on DT. The model is significant, according to the F-value of 5.11 percent. An F-value this large could only happen to owe to noise 0.89 %. P-values under 0.0500 indicate that the model terms are important.

Folding endurance

$Y = +206.08 + 0.58918A + 1.01 * B + 3.09 * C + 0.8750 * AB + 0.3750 * AC + 0.3750 * BC + 2.15 * A^2 - 2.63 * B^2 + 0.7325 * C^2 + 0.8750 * AB$ + Sign of coefficients indicates positive effects of polymer and plasticizer concentration on folding endurance.

The model is suggested to be significant by the F-value of 16.02 percent. Only 0.01 percent of the time is it possible for noise to cause an F-value this large. The modelling terms are considered significant when the P-value is less than 0.0500.

Percentage drug release

$Y = +32.63 - 2.03 * A - 4.42 * B + 8.68 * C + 7.01 * AB - 9.07 * AC - 3.89 * BC + 4.26 * A^2 + 6.15 * B^2 + 2.97 * C^2 - 9.07 * AC$ negative sign of coefficients indicates negative effects of polymer and thickening agent concentration on percentage drug release. The F-value of 4.98 % suggests that the model is significant. An F-value this large might be caused by noise only 0.97 percent of the time. Model terms that have P-values less 0.0500 are considered significant.

The irrelevant terms ($P > 0.05$) were eliminated from the models to use the backward elimination method to produce an easy-to-understand and practical model. Although in statistical modelling the adjusted R², which takes the number of linear regression variables into account, is commonly chosen, R² always drops when a linear regression variable is removed. The experimental data demonstrated a satisfactory fit to second order polynomial equations because the corrected R² values were well within the allowed bounds of R² 0.90. All of the reduced models had p values below 0.05, indicating that they were all significant models. The signal to noise ratio is measured by the value of appropriate precision. A ratio higher than 4 is desirable. The ratio was found to be in the range from 8.90-14.87 which indicated on adequate signal. Hence the model was significant.

Response surface plot

It is highly helpful to investigate the interaction effects of these factors on the response using 3D surface plots for all response variables. Figure 1 shows 3D response surface plot. From this design optimized formulation was found. The optimized conditions of ethocel 1.67 gm, propylene glycol 5.84 ml and carbom-

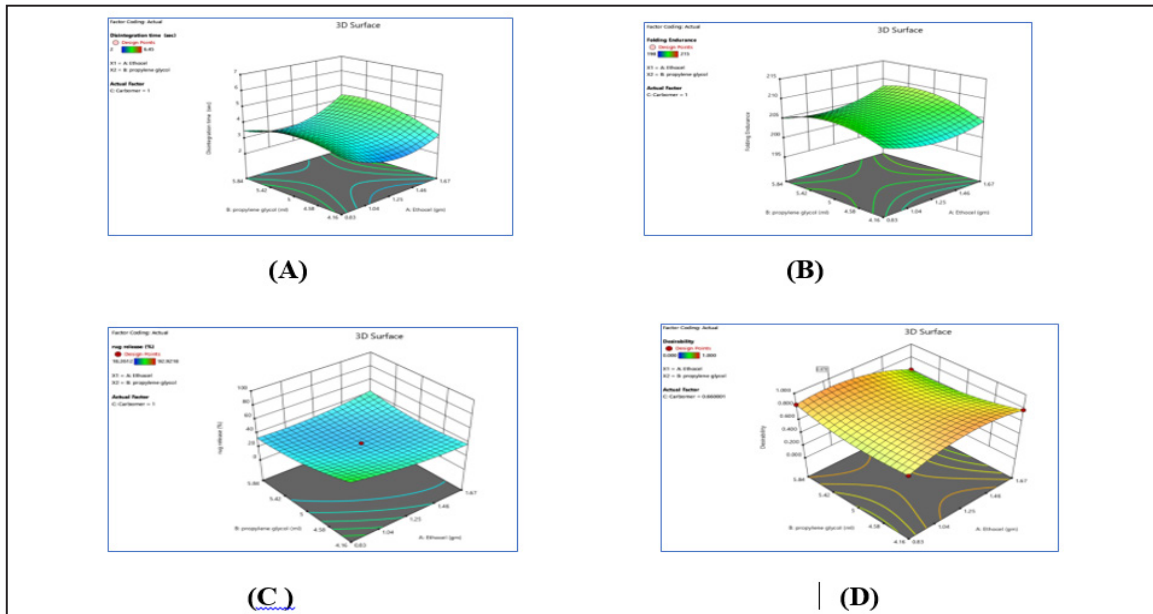


Fig. 1: 3D response plot for (A) Disintegration Time (B) Folding Endurance (C) Percentage Drug Release (D) Desirability function

er 1.34gm used. According to the later value of D, the projected reaction values were DT = 3.34sec, Folding endurance = 167.66, and percent drug release 73.05 %.

Disintegration time (DT):

Decrease the value of DT with the increase the con of plasticizer. At high drug polymer ratio the DT is more. The higher DT is recorded at low con of plasticizer and high drug polymer ratio. But excessive amount of polymer increases the film becomes brittle. Both factors would be considered while controlling the DT. Polymer and Plasticizer at elevated concentration would generate patch which fulfil a prerequisite for rapid disintegration.

Folding endurance

The plasticizer is in charge of giving the film flexibility, while the film forming (Polymer) ensures enough strength. Therefore, a buccal patch with desirable prominence would result from a suitable combination of both of these elements. The findings showed that polymers and plasticizers have a beneficial effect on folding endurance.

The poly nomial equation suggested the concentration of plasticizer has a hopeful influence of the folding endurance. Because plasticizers relax linear polymeric chains, presumably by creating hydrogen bonds that increase flexibility, they are considered to be the key contributing element for folding endurance.

% Drug release

Decreases in the value of the percent drug release with increases in the amount of the film thickening agent and rises in the percent drug release with increases in formulation's polymer content. The highest percentage drug release recorded at low drug polymer ratio and high thickening agent concentration. When con of polymer increases then drug was decreases since drug remains inside the matrix of polymer.

The desirability function of the Derringer D is the geometric mean, weighted average, or the average of the different popularity functions. Desirability has uses D accepts values between 0 and 1. Weight values can range from 0.1 to 10, with weights below 1 denoting less relevance

and weights above 1 denoting higher importance for the aim. The table listed the requirements for each response's optimization.

It was evident from the preceding figure that a particular set of coordinates produced a high Desirability value ($D = 0.879$) were Ethocel 1.06 gm, Propylene glycol 5.84ml and carbomer 0.66gm used. The predicted response values corresponding to the later value of D were $DT = 2$ sec, Folding endurance = 198, % drug release 18.26%. By processing the experimental results under ideal circumstances, the model's prediction effectiveness was verified. Within 1-6 %, it was discovered that the observed and experimental differences were in good agreement.

Physical evaluation of buccal patches

Thickness and folding endurance

The thickness of the patchwork film increases with the weight of the polymer, vice versa. Weight of the batches' films, 260.56 mg. Patch film thickness: As the polymer concentration rises, so does the patch film thickness. The formulation's patch thickness ranges between 0.18- and 0.22-mm. Low standard deviation scores indicate that the movie is physically equal. The folding endurance gauges a film's resistance to rupturing. After manually measuring the folding resistance, it was discovered that the film's folding resistance increases along with the polymer concentration. The film's folding endurance was discovered to be 167.66.

The films' folding endurance values were discovered to be quite favorable, and as a result, they displayed good mechanical and physical properties. The film's surface pH was discovered to be between 6.06 and 6.07 for buccal patch formulations. Table 3 presented the outcomes. All of the films' surfaces had pH values that fell within the range of salivary pH. The pH of the surfaces of all formulations showed no discernible variation. Since the observed surface pH values of all of the formulations were found to be somewhat neutral, they should be quite comfortable and less likely to irritate the

buccal mucosa.

The mucoadhesive strength of buccal patches found to be 6.01 g. The disintegration time of drug loaded buccal patches was found to be 3.34minutes. The Patches disintegration time was within the limit. Hence it was easily dissolved in saliva.

Table 3: Physical evaluation of optimized drug-loaded buccal patches

Evaluation parameter	Result
Disintegration time (min)	3.34
Folding endurance	167.66
Weight (mg)	260.56
Thickness (mm)	0.18
surface pH	6.06
Mucoadhesive strength (g)	6.01
Content uniformity (%)	97.95769

SEM analysis of buccal patches

Figure 4 depicts the cross split of buccal patch compositions seen below a scanning electron microscope. The composition's cross-section inside the patch showed a consistent, non-porous structure. Non-homogeneous texture is visible at greater magnifications was clearly obvious. On evaporation, it is reasonable to suppose that the dissolved curcumin may be affected by the type of solvent used. Micron-sized aggregates have formed as a result of the precipitation. Sizes and are spread throughout the polymer solution. Any there was no texture non-uniformity found suggesting that the medicine has been distributed properly throughout the matrix of polymer.

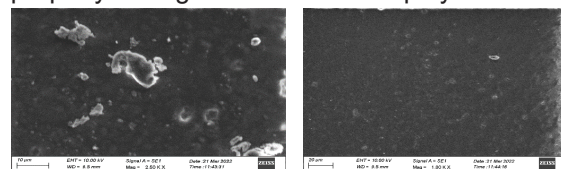


Fig. 4: Scanning electronic microscope image for optimized buccal patch

***in vitro* drug release study**

In-vitro release of curcumin and lycopene encumbered optimized buccal patches was performed in pH 6.8 phosphate buffer. The results were shown in Figure 5 and Table 4. The *invitro* drug release profiles of buccal patches, which is containing ethocel, methocel, propylene glycol and carbomer polymers in the ratio of 1:1,1:2, 2:1, 1:3 and 3:1. The most significant factor disturbing the velocity of drug liberate from the buccal tablets with the drug and polymers ratio. In all the formulations the drug release was ranging from 73.5% to 95.6%.

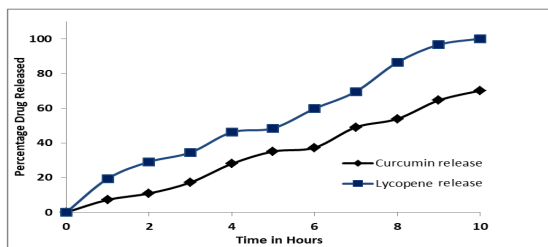


Fig. 5: *In vitro* drug release study of buccal patch

Table 4: Evaluation of the drug-loaded optimized buccal patch's *in-vitro* drug release

Time (Hours)	Curcumin release	Lycopene release
0	0	0
1	7.2	19.4
2	10.9	29.1
3	17.2	34.5
4	28	46.2
5	35.1	48.5
6	37.3	59.8
7	49.1	69.7
8	53.9	86.5
9	64.6	96.7
10	70.2	100.2

Surface pH

The created patch's surface pH was carefully calibrated to account for potential irritability during *in-vivo* tests.

Stability studies

The optimized buccal patch samples were taken after 30 (1 month), 60 (2 months), 90 (3 months) days. For 90 days at 40°C±5°C and 75% RH, the tensile strength, drug content, and percentage of drug release of the sample (optimized) were evaluated. Reports were displayed in Table 5. Stability studies for the formulations of patches were conducted for 90 days. The prepared patches displayed maximum stability with no noticeable physiochemical alterations after defined intervals of 30 days

Table 5: Stability study report of drug-loaded optimized buccal patches

Evaluation parameter	After 30 days	After 60 days	After 90 days
Colour and appearance	No change	No change	No change
% drug content (Curcumin)	96.7±1.66	95.3±1.42	93.2±0.98
% drug content (Lycopene)	97.59±1.98	95.22±1.25	94.3±1.87
% drug release (Curcumin)	70.2±2.69	68.6±2.01	67.4±1.22
% drug release (Lycopene)	100.2±2.55	99.8±1.46	95.1±1.37

Cytotoxicity study (MTT assay)

MTT assay used to measure the cell viability. Cell viability of prepared buccal patches was tested in KB cell lines at various concentrations (Figures 6 and 7). At varying concentrations of 12.5, 25, 50, 100 and 200µg/ml, the prepared buccal patches showed cell viability was reduced in a dose dependent method with a significant difference between the control and test groups. When the drug concentration was increased from 12.5 to 200µg/ml, cell diffusion was improved. The IC50 value of the test sam-

ples for the production of curcumin and lycopene loaded buccal patches was found 2.888.

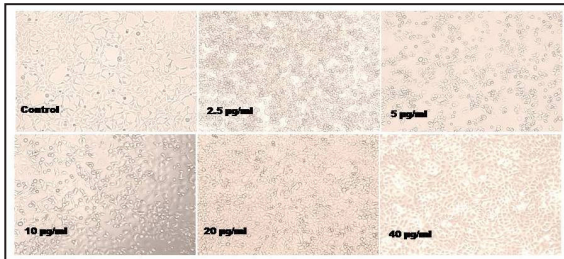


Fig. 6: Cytotoxicity study for different concentration

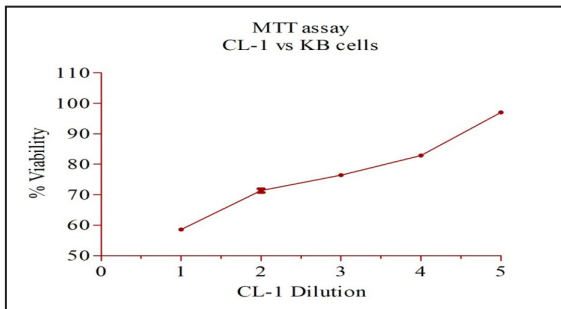


Fig. 7: Cell viability (%) of drug loaded buccal patch formulation

Conclusion

According to the study's findings, in-vitro drug release pattern of the patches were sufficient and good enough ensuring good bio-availability of the drugs. The optimized formulation CL5 had good mucoadhesion, were irritation-free, and released the medication entirely by a diffusion process and this study also recognized the relevance of using curcumin and lycopene combination for formulating buccal patch. As a result, the perspectives and approaches of buccal mucoadhesive patches can be considered as a unique treatment for oral cancer.

References

1. Reddy PC, Chaitanya KS, Rao YM. A review on bioadhesive buccal drug delivery systems: current status of formulation and evaluation methods. DARU Journal of

- Pharmaceutical Sciences. 2011; 19:385.
2. Smart JD. Buccal drug delivery. Expert Opinion on Drug Delivery. 2005; 2:507-17.
3. Sudhakar Y, Kuotsu K, Bandyopadhyay, AK. Buccal bioadhesive drug delivery—a promising option for orally less efficient drugs. Journal of Controlled Release. 2006; 114:15-40.
4. Gavin A, Pham, JT, Wang D, Brownlow B, and Elbayoumi TA. Layered nanoemulsions as mucoadhesive buccal systems for controlled delivery of oral cancer therapeutics. International Journal of Nanomedicine. 2015; 10:1569.
5. Calixto G, Bernegossi J, Fonseca-Santos, B, Chorilli, M. Nanotechnology-based drug delivery systems for treatment of oral cancer: a review. International Journal of Nanomedicine. 2014; 9:3719.
6. Mizrahi B, Domb, AJ. Mucoadhesive polymers for delivery of drugs to the oral cavity. Recent Patents on Drug Delivery and Formulation. 2008; 2:108-19.
7. Adamczak MI, Hagesaether E, Smistad G, Hiorth M. An in vitro study of mucoadhesion and biocompatibility of polymer coated liposomes on HT29-MTX mucus-producing cells. International Journal of Pharmaceutics. 2016; 498:225-33.
8. Reddy PC, Chaitanya KS, Rao YM. A review on bioadhesive buccal drug delivery systems: current status of formulation and evaluation methods. DARU Journal of Pharmaceutical Sciences. 2011; 19:385.
9. Chopra S, Patil GV, Motwani, SK. Release modulating hydrophilic matrix systems of losartan potassium: Optimization of formulation using statistical experimental design. European Journal of Pharmaceutics and Biopharmaceutics. 2007; 66:73-82.

10. Singh B, Chakkal SK, Ahuja N. Formulation and optimization of controlled release mucoadhesive tablets of atenolol using response surface methodology. *Aaps Pharm Scitech*. 2006; 7: E19-28.
11. Malviya R, Sundram S, Fuloria S, Subramaniyan V, Sathasivam KV, Azad AK, Sekar M, Kumar DH, Chakravarthi S, Porwal O, Meenakshi DU. Evaluation and Characterization of Tamarind Gum Polysaccharide: The Biopolymer. *Polymers*. 2021; 13:3023.
12. Rekhi GS, Jambhekar SS. Ethylcellulose-a polymer review. *Drug Development and Industrial Pharmacy*. 1995; 21:61-77.
13. Liu RH. Potential synergy of phytochemicals in cancer prevention: mechanism of action. *The Journal of Nutrition*. 2004; 134:3479S-85S.
14. Thomas R, Butler E, Macchi F, Williams M. Phytochemicals in cancer prevention and management. *British Journal of Medical Practitioners*. 2015; 8:1-8.
15. Lee JH, Khor TO, Shu L, Su ZY, Fuentes F, Kong AN. Dietary phytochemicals and cancer prevention: Nrf2 signaling, epigenetics, and cell death mechanisms in blocking cancer initiation and progression. *Pharmacology & Therapeutics*. 2013; 137:153-71.
16. Heger M. Don't discount all curcumin trial data. *Nature*. 2017; 543:40.
17. Shakibaei M, Buhrmann C, Kraehe P, Shayan P, Lueders C, Goel A. Curcumin chemosensitizes 5-fluorouracil resistant MMR-deficient human colon cancer cells in high density cultures. *PLoS One*. 2014; 9:e85397.
18. Thomas R, Butler E, Macchi F, Williams M. Phytochemicals in cancer prevention and management. *British Journal of Medical Practitioners*. 2015; 8:1-8.
19. Adhikari SN, Nayak BS, Nayak AK, Mohanty B. Formulation and evaluation of buccal patches for delivery of atenolol. *Aaps Pharm Sci Tech*. 2010; 11:1038-44.
20. Alagusundaram M, Chengaiah B, Ramkanth S, Parameswari SA, Chetty CM, Dhachinamoorthi D. Formulation and evaluation of mucoadhesive buccal films of ranitidine. *International Journal of Pharmtech Research*. 2009; 1:557-63.
21. Khana R, Agarwal SP, Ahuja A. Preparation and evaluation of muco-adhesive buccal films of clotrimazole for oral Candida infections. *Indian Journal of Pharmaceutical Sciences*. 1997; 59:299.
22. Sodde VK, Lobo R, Kumar N, Maheshwari R, Shreedhara CS. Cytotoxic activity of *Macrosolenparasiticus* (L.) Danser on the growth of breast cancer cell line (MCF-7). *Pharmacognosy Magazine*. 2015; 1:S156.
23. Khan KA, Khan GM, Shah KU, Niazi ZR, Khan H, Ahmad A, Shah PA, Ullah A, Tahir M, Jan SU. Design, Preparation and evaluation of various parameters of controlled release matrices of losartan potassium using polymers combination. *Pakistan Journal of Pharmaceutical Sciences*. 2020; 3:33.
24. Ullah W, Nawaz A, Akhlaq M, Shah KU, Latif MS, Alfatama M. Transdermal delivery of gatifloxacin carboxymethyl cellulose-based patches: Preparation and characterization. *Journal of Drug Delivery Science and Technology*. 2021; 66:102783.

Parkinson's disease Detection Using Tree Based Machine Learning Algorithms

Venkata Srinivas Babu Oguri¹, Sudhakar Poda², A. Krishna Satya^{*2}, NK Prasanna

¹Department of Computer Science and Engineering, Mahindra University, Bahadurpally Jeedimetla, Hyderabad - 500043 - Telangana, INDIA

²Department of Biotechnology, Acharya Nagarjuna University, Nagarjuna nagar, Guntur-522510, Andhra Pradesh, India

³CSIR- National Institute of Science Communication & Policy Research, New Delhi-110 012, Delhi, India

Abstract

Parkinson's Disease (PD), also known as primary Parkinsonism is a persistent, idiopathic, degenerative nervous disorder which results from lack of dopaminergic neurons in the substantia nigra pars compacta, which is the source of nigrostriatal dopamine pathway within the midbrain. The clinical detection relies on motor symptoms recognition. Significant neurological damage is already done by the time motor symptom occur. Early detection is necessary to stalk the progression of the disease. The problem of detection of PD comes under classification. Several tree-based classification algorithms were applied to the dataset retrieved from UCI machine learning database. The dataset was first split into train and test data. Various models were created using four different algorithms. Correlation coefficients were calculated for each of the features in the dataset. The model was fitted with train data obtained after removing highly correlated features. Predictions were made and various parameters were considered for comparison. Accuracy, precision, recall, F1-Score, Youden Index, error rate and specificity were the parameters calculated. Out of the four algorithms (Decision Tree, Random Forest, XGBoost and LightGBM), LightGBM

achieved the highest accuracy of 97.43%.

Keywords: Parkinson's Disease (PD), LightGBM, Pearson Correlation, Accuracy, Error Rate, Jupyter Notebook.

Introduction

Parkinson's Disease (PD) also known as primary Parkinsonism is a persistent, idiopathic, degenerative nervous disorder which results from lack of dopaminergic neurons in the substantia nigra pars compacta, which is responsible for nigrostriatal dopamine pathway within the midbrain (1). Some of the symptoms of PD include bradykinesia, rigidity, and rest tremor. Resting tremor (initially unilateral), rigidity, bradykinesia (slow movements), dissimilarities in gait, and unstable posture come under the motor symptoms while cognitive changes, behavioural and neuropsychiatric changes, autonomic nervous system failure, sensory and sleep disturbances come under non-motor symptoms (1). Motor and non-motor symptoms are used to diagnose PD. Non-motor issues of the disease can become more troublesome as the disease progresses (2). Also, voice and speech impairment typically occur in PD patients. The loss of ability to communicate properly is the main source of disability in pa-

tients. The multidimensional irregularities in the speech such as hoarse voice, reduced loudness, and restricted pitch variability (Mono pitch and Mono loudness), imprecise articulation and abnormalities of speech rate, and pause ratio can be attributed to the loss of dopaminergic neurons (3). Voice and speech performance will show further deterioration in the course of time which hints at nondopaminergic mechanisms of progression of dysarthrophonia. Early detection reduces the disease progression and limits the treatment expenses. Several machine learning algorithms can be used for the detection of PD in preliminary stages using voice data. Machine learning algorithms have made commendable progress in medical diagnosis in the recent times because of their ease in implementation. The current study aims to utilise the ML algorithms to facilitate early detection of the disease. A total of four ML algorithms were used in this study. They are Decision Tree, Random Forest, XGBoost and LightGBM classifiers.

Review of Literature

10 million people (about half the population of New York) worldwide have PD from the information found in Parkinson's diseases foundation (2015). Death and disability due to PD is increasing faster than any other neurological disease according to WHO. One in every 500 people have PD in Britain and this number is expected to grow threefold by 2050 according to Parkinson's Disease Society website. This illness affects people from 50 -70 years old and becomes worse over time. Diagnosis of PD is heavily reliant on evaluation of motion which is difficult to detect by human sight. This method aims to overcome these difficulties and improve the assessment process by employing machine learning algorithms (6). One attempt was made by implementing Convolutional Neural Networks (CNNs). They were used to classify gait signals converted to spectrogram images by image classification on a big-scale and deep dense Artificial Neural Networks (ANNs) were employed to predict PD at an early stage. Voice recordings were used in this instance. A total of 54 studies in

the category 'Diagnosis of PD' were examined. Out of them 33 studies used datasets from UCI machine learning repository, mPower and PhysioNet databases. In one of the study, data from public repositories was joined with local data bases (7). 14 studies performed diagnosis as well as differential diagnosis. Research articles not written in English were not considered. Most commonly voice data was used, while some studies also used MRI, movement, handwriting patterns and SPECT imaging data. The most common metric used for assessment of performance was accuracy. Most methods are based on speech data (8), gait patterns (9), cardiovascular oscillations (10), smell identification (11) and force tracking data (12). A one-dimensional neural network relying on signals of gait was introduced to detect PD in (13). It should be noted that accuracy is low when using gait analyses because of background noise in voice recordings, causing false positives. Detection of motor impairment based on mobile screen typing was introduced in (14). Four classifiers, namely Decision Tree, Regression, DMneural and Neural Networks (NN) are used and their performances are compared in (15), in which the best accuracy of 92.90% was achieved by NN algorithm. Early and accurate detection of PD is essential to stalk the progression of the disease.

Materials and Methods

The dataset was retrieved from UCI machine learning repository. It was created by University of Oxford and National Centre for Voice and Speech, Denver, Colorado. The dataset contains voice measurements from 31 people, and 23 with PD. It has a total of 195 voice recordings (4). The data aims to discriminate PD people from healthy people. The status column denotes '0' for healthy and '1' for PD affected persons. There are about 5-6 recordings for each patient.

Fig 1 and Fig 2 show a section of the dataset. The problem of diagnosis of PD comes under classification. Classification algorithms come under supervised learning. Several clas-

name	MDVP:Fo(Hz)	MDVP:Fhi(Hz)	MDVP:Flo(Hz)	MDVP:Jitter(%)	MDVP:Jitter(Abs)	MDVP:RAP	MDVP:PPQ	Jitter:DDP	MDVP:Shimmer	MDVP:Shimmer(dB)
phon_R01_S01_1	119.992	157.302	74.997	0.00784	0.00007	0.0037	0.00554	0.01109	0.04374	0.426
phon_R01_S01_2	122.4	148.65	113.819	0.00968	0.00008	0.00465	0.00696	0.01394	0.06134	0.626
phon_R01_S01_3	116.682	131.111	111.555	0.0105	0.00009	0.00544	0.00781	0.01633	0.05233	0.482
phon_R01_S01_4	116.676	137.871	111.366	0.00997	0.00009	0.00502	0.00698	0.01505	0.05492	0.517
phon_R01_S01_5	116.014	141.781	110.655	0.01284	0.00011	0.00655	0.00908	0.01966	0.06425	0.584
phon_R01_S01_6	120.552	131.162	113.787	0.00968	0.00008	0.00463	0.0075	0.01388	0.04701	0.456
phon_R01_S02_1	120.267	137.244	114.82	0.00333	0.00003	0.00155	0.00202	0.00466	0.01608	0.14
phon_R01_S02_2	107.332	113.84	104.315	0.0029	0.00003	0.00144	0.00182	0.00431	0.01567	0.134
phon_R01_S02_3	95.73	132.068	91.754	0.00551	0.00006	0.00293	0.00332	0.0088	0.02093	0.191
phon_R01_S02_4	95.056	120.103	91.226	0.00532	0.00006	0.00268	0.00332	0.00803	0.02838	0.255
phon_R01_S02_5	88.333	112.24	84.072	0.00505	0.00006	0.00254	0.0033	0.00763	0.02143	0.197
phon_R01_S02_6	91.904	115.871	86.292	0.0054	0.00006	0.00281	0.00336	0.00844	0.02752	0.249
phon_R01_S04_1	136.926	159.866	131.276	0.00293	0.00002	0.00118	0.00153	0.00355	0.01259	0.112
phon_R01_S04_2	139.173	179.139	76.556	0.0039	0.00003	0.00165	0.00208	0.00496	0.01642	0.154
phon_R01_S04_3	152.845	163.305	75.836	0.00294	0.00002	0.00121	0.00149	0.00364	0.01828	0.158
phon_R01_S04_4	142.167	217.455	83.159	0.00369	0.00003	0.00157	0.00203	0.00471	0.01503	0.126
phon_R01_S04_5	144.188	349.259	82.764	0.00544	0.00004	0.00211	0.00292	0.00632	0.02047	0.192
phon_R01_S04_6	168.778	232.181	75.603	0.00718	0.00004	0.00284	0.00387	0.00853	0.03327	0.348
phon_R01_S05_1	153.046	175.829	68.623	0.00742	0.00005	0.00364	0.00432	0.01092	0.05517	0.542
phon_R01_S05_2	156.405	189.398	142.822	0.00768	0.00005	0.00372	0.00399	0.01116	0.03995	0.348
phon_R01_S05_3	153.848	165.738	65.782	0.0084	0.00005	0.00428	0.0045	0.01285	0.0381	0.328
phon_R01_S05_4	153.88	172.86	78.128	0.0048	0.00003	0.00232	0.00267	0.00696	0.04137	0.37
phon_R01_S05_5	167.93	193.221	79.068	0.00442	0.00003	0.0022	0.00247	0.00661	0.04351	0.377
phon_R01_S05_6	173.917	192.735	86.18	0.00476	0.00003	0.00221	0.00258	0.00663	0.04192	0.364
phon_R01_S06_1	163.656	200.841	76.779	0.00742	0.00005	0.0038	0.0039	0.0114	0.01659	0.164
phon_R01_S06_2	104.4	206.002	77.968	0.00633	0.00006	0.00316	0.00375	0.00948	0.03767	0.381
phon_R01_S06_3	171.041	208.313	75.501	0.00455	0.00003	0.0025	0.00234	0.0075	0.01966	0.186
phon_R01_S06_4	146.845	208.701	81.737	0.00496	0.00003	0.0025	0.00275	0.00749	0.01919	0.198
phon_R01_S06_5	155.358	227.383	80.055	0.0031	0.00002	0.00159	0.00176	0.00476	0.01718	0.161

Fig1: Dataset Part 1

Shimmer:APQ3	Shimmer:APQ5	MDVP:APQ	Shimmer:DDA	NHR	HNR	status	RPDE	DFA	spread1	spread2	D2	PPE
0.02182	0.0313	0.02971	0.06545	0.02211	21.033	1	0.414783	0.815285	-4.813031	0.266482	2.301442	0.284654
0.03134	0.04518	0.04368	0.09403	0.01929	19.085	1	0.458359	0.819521	-4.075192	0.33559	2.486855	0.368674
0.02757	0.03858	0.0359	0.0827	0.01309	20.651	1	0.429895	0.825288	-4.443179	0.311173	2.342259	0.332634
0.02924	0.04005	0.03772	0.08771	0.01353	20.644	1	0.434969	0.819235	-4.117501	0.334147	2.405554	0.368975
0.0349	0.04825	0.04465	0.1047	0.01767	19.649	1	0.417356	0.823484	-3.747787	0.234513	2.33218	0.410335
0.02328	0.03526	0.03243	0.06985	0.01222	21.378	1	0.415564	0.825069	-4.242867	0.299111	2.18756	0.357775
0.00779	0.00937	0.01351	0.02337	0.00607	24.886	1	0.59604	0.764112	-5.634322	0.257682	1.854785	0.211756
0.00829	0.00946	0.01256	0.02487	0.00344	26.892	1	0.63742	0.763262	-6.167603	0.183721	2.064693	0.163755
0.01073	0.01277	0.01717	0.03218	0.0107	21.812	1	0.615551	0.773587	-5.498678	0.327769	2.322511	0.231571
0.01441	0.01725	0.02444	0.04324	0.01022	21.862	1	0.547037	0.798463	-5.011879	0.325996	2.432792	0.271362
0.01079	0.01342	0.01892	0.03237	0.01166	21.118	1	0.611137	0.776156	-5.24977	0.391002	2.407313	0.24974
0.01424	0.01641	0.02214	0.04272	0.01141	21.414	1	0.58339	0.79252	-4.960234	0.363566	2.642476	0.275931
0.00656	0.00717	0.0114	0.01968	0.00581	25.703	1	0.4606	0.646846	-6.547148	0.152813	2.041277	0.138512
0.00728	0.00932	0.01797	0.02184	0.01041	24.889	1	0.430166	0.665833	-5.660217	0.254989	2.519422	0.199889
0.01064	0.00972	0.01246	0.03191	0.00609	24.922	1	0.474791	0.654027	-6.105098	0.203653	2.125618	0.1701
0.00772	0.00888	0.01359	0.02316	0.00839	25.175	1	0.565924	0.658245	-5.340115	0.210185	2.205546	0.234589
0.00969	0.012	0.02074	0.02908	0.01859	22.333	1	0.56738	0.644692	-5.44004	0.239764	2.264501	0.218164
0.01441	0.01893	0.0343	0.04322	0.02919	20.376	1	0.631099	0.605417	-2.93107	0.434326	3.007463	0.430788
0.02471	0.03572	0.05767	0.07413	0.0316	17.28	1	0.665318	0.719467	-3.949079	0.35787	3.10901	0.377429
0.01721	0.02374	0.0431	0.05164	0.03365	17.153	1	0.649554	0.68608	-4.554466	0.340176	2.856676	0.322111
0.01667	0.02383	0.04055	0.05	0.03871	17.536	1	0.660125	0.704087	-4.095442	0.262564	2.73971	0.365391
0.02021	0.02591	0.04525	0.06062	0.01849	19.493	1	0.629017	0.698951	-5.18696	0.237622	2.557536	0.259765
0.02228	0.0254	0.04246	0.06685	0.0128	22.468	1	0.61906	0.679834	-4.330956	0.262384	2.916777	0.285695
0.02187	0.0247	0.03772	0.06562	0.0184	20.422	1	0.537264	0.686894	-5.248776	0.210279	2.547508	0.253556
0.00738	0.00948	0.01497	0.02214	0.01778	23.831	1	0.397937	0.732479	-5.557447	0.22089	2.692176	0.215961
0.01732	0.02245	0.0378	0.05197	0.02887	22.066	1	0.522746	0.737948	-5.571843	0.236853	2.846369	0.219514
0.00889	0.01169	0.01872	0.02666	0.01095	25.908	1	0.418622	0.720916	-6.18359	0.226278	2.589702	0.147403
0.00883	0.01144	0.01826	0.0265	0.01328	25.119	1	0.358773	0.726652	-6.27169	0.196102	2.314209	0.162999
0.00769	0.01012	0.01661	0.02307	0.00677	25.97	1	0.470478	0.676258	-7.120925	0.279789	2.241742	0.108514

Fig 2: Dataset Part 2

Matrix column entries (attributes):

- name - ASCII subject name and recording number
- MDVP:Fo(Hz) - Average vocal fundamental frequency
- MDVP:Fhi(Hz) - Maximum vocal fundamental frequency
- MDVP:Flo(Hz) - Minimum vocal fundamental frequency
- MDVP:Jitter(%),MDVP:Jitter(Abs),MDVP:RAP,MDVP:PPQ,Jitter:DDP - Several measures of variation in fundamental frequency
- MDVP:Shimmer,MDVP:Shimmer(dB),Shimmer:APQ3,Shimmer:APQ5,MDVP:APQ,Shimmer:DDA - Several measures of variation in amplitude
- NHR,HNR - Two measures of ratio of noise to tonal components in the voice
- status - Health status of the subject (one) - Parkinson's, (zero) - healthy
- RPDE,D2 - Two nonlinear dynamical complexity measures

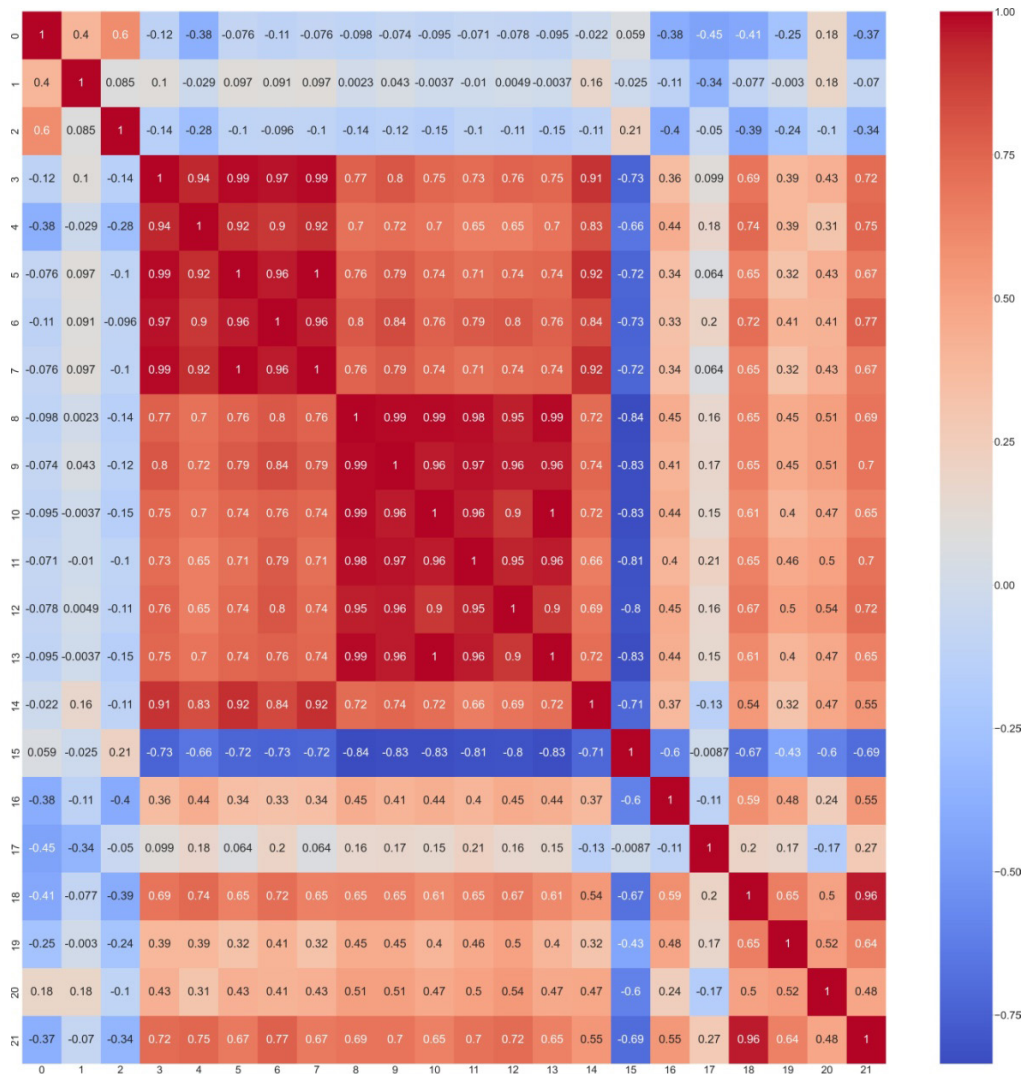


Fig3: Pearson Correlation Heat-map

Parkinson's disease detection using tree based machine learning algorithms

sification algorithms were applied to the dataset. All of them were tree based. DecisionTree, Random Forest algorithms later followed by LightGBM and XGBoost were used to achieve highest accuracy. The reasons behind using tree-based classification algorithms were that they mimic human thinking ability and they can be easily understood [5]. The dataset underwent preprocessing initially. All the work was done in Jupyter Notebook, an interactive python notebook software. Name column(attribute) was removed since it is irrelevant and decreases the accuracy. Next, correlation matrix was generated. Correlation matrix is square and symmetric [16]. It measures the linear dependency between two elements. We were specifically using Pearson's correlation coefficient. The coefficient can be equal to any number between -1 and 1. perfectly negatively linear correlated variables have coefficient equal to -1, highly correlated variables have a correlation of value 1 and 0 indicates no linear correlation between the two variables. After the removal of the Name attribute from the dataset, correlation matrix is generated for the remaining 22 features. The matrix is shown in Fig 3. The matrix was color coded as 'cool warm' to easily understand the strength of relationship. The stronger relations have warmer (red) color grading while the weak ones have cool (blue) color grading. All the diagonal elements will be red in color and have correlation coefficient value of 1 (since each attribute is mapped to itself). The threshold value for removal is set to 0.9. Out of 22 features, 11 were removed. New dataset was created after removal of highly correlated features. This dataset was split into training and testing datasets. 30% was randomly set aside for testing while the remaining was used to train the model. Two Tree based algorithms and two Boosting Algorithms were used. Brief descriptions of the algorithms used in this work are given below.

Decision tree classifier

Decision Tree algorithm breaks a complex problem into a set of decisions which are relatively simpler. Every Decision Tree contains

a Root Node, Leaf Nodes and Internal Nodes. Decision Tree uses Entropy, Information Gain and Gini Index as criteria for evaluating attributes [17]. It comes under Supervised Learning Algorithms. Fig 4 shows the Decision Tree generated on this dataset.

Random forest classifier

Random Forest classification comes under ensemble learning i.e it's an ensemble of Decision Trees. It is a bagging-based algorithm. The fundamental concept used by Random Forest is that a large number of uncorrelated Decision Trees operating as one group will outperform each of the individual constituent tree [18].

XGBoost classifier

XGBoost is Gradient-Boosting algorithm that makes use of Ensemble Learning and is tree-based. Each Decision Tree corrects the errors committed by its predecessor. This method is called Gradient Boosting. XGBoost makes use of Gradient Boosted Decision Trees. Each of these trees then ensemble to give a more accurate model. XGBoost uses Regularization to penalise complex trees and Cross validation to avoid overfitting of the model. performs well because of its handling of data types, distributions and the variety of hyper parameters that can be tuned [19].

Fig 4: Decision Tree Generated

Light BGM classifier

LightGBM is also a Gradient-Boosting algorithm that makes use of Ensemble Learning and is tree-based. This algorithm shares common features such as sparse optimisation, parallel training, multiple loss functions and bagging with XGBoost. But, LightGBM grows trees leaf-wise instead of level-wise [20]. Out of the boosting four types of algorithms available, the default option i.e GBDT (gradient boosting decision tree) was used to implement this model.

Flow chart of the proposed work is depicted in Fig 5

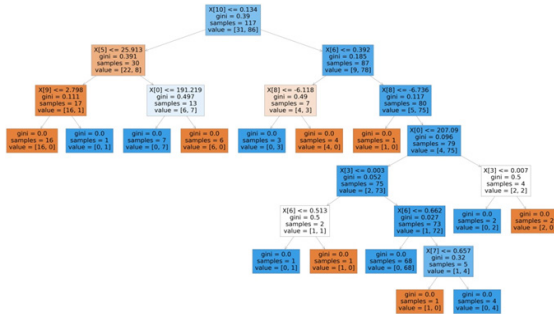


Fig 6: Scatter Plot

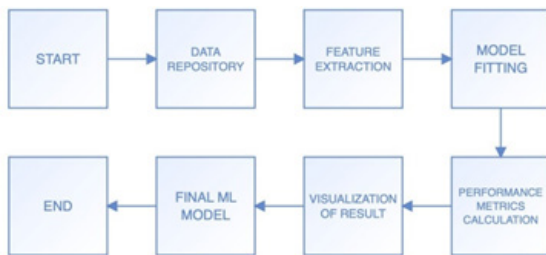
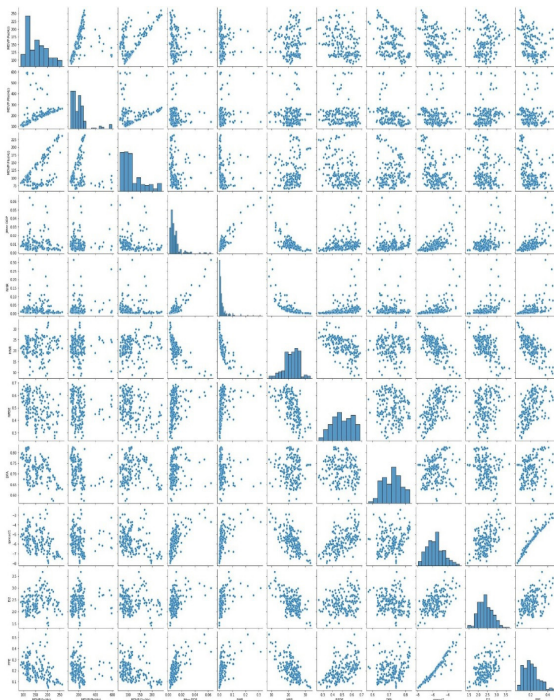


Fig6 shows the scatter plot generated on this dataset; it contains 11 features.



Decision Tree Classification is the least performer of all, scoring 88.46%, while Random Forest

Classification and XGBoost scored 93.58% and 96.15% respectively. Light GBM achieved highest accuracy of 97.43%. Fig 7-10 shows the confusion matrices of all the algorithms used. Confusion Matrix shows the number of True positive (TP), True negative (TN), False positive (FP) and False negative (FN) instances. Decision Tree Classifier has shown 57 True positive, 12 true negative, 5 False positive and 4 False negative instances. Hence a total of 69 instance have been correct out of 78. Therefore, the accuracy is 88.46%.

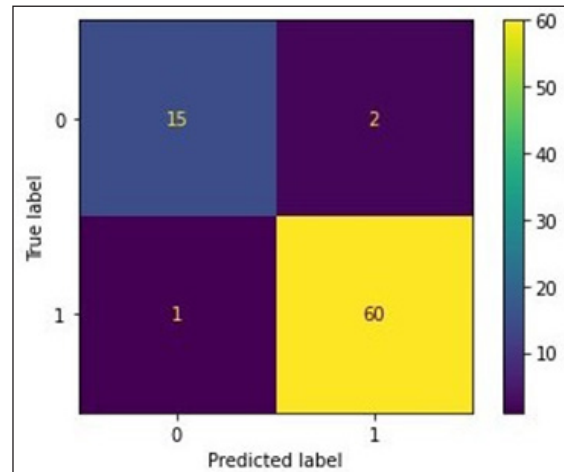


Fig 6 DecisionTree

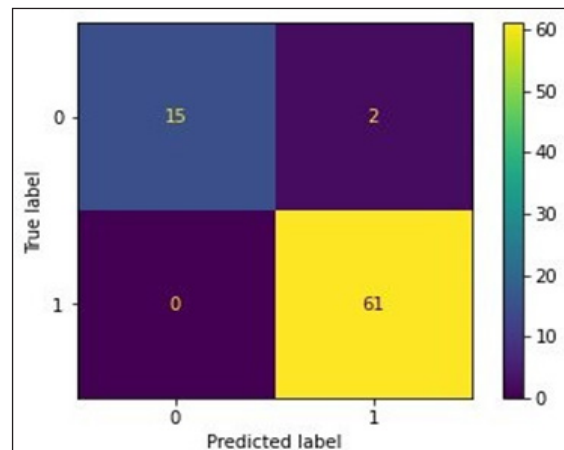


Fig 7 RandomForest

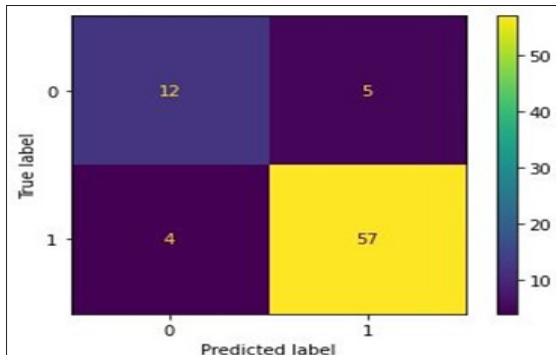


Fig 8 XGBoost

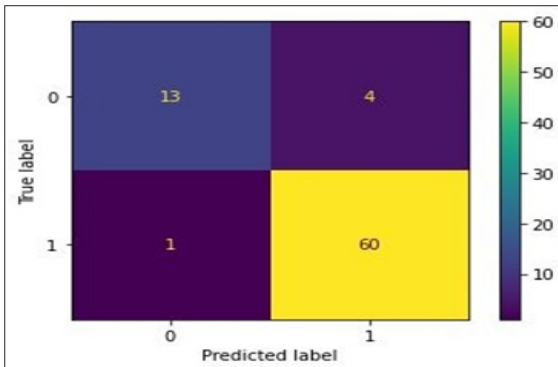


Fig 9 LightGBM

Various other parameters are obtained as well in order to compare the performances. Their formulas are listed below.

$$Accuracy = \frac{TP + TN}{TP + FP + FN + TN}$$

$$Precision = \frac{TP}{TP + FP}$$

$$recall = \frac{TP}{TP + FN}$$

$$F1 - Score = \frac{2 \times Precision \times recall}{Precision + recall}$$

$$YI = recall + specificity - 1$$

$$Specificity = \frac{TN}{TN + FP}$$

$$error_rate = \frac{FP + FN}{TP + TN + FN + FP}$$

The metrics were evaluated and listed in the table below.

Algorithm	Accuracy	Precision	Recall	F1_score	YoudenIndex	Specificity	Error-Rate
Decision Tree	0.8846	0.9193	0.9344	0.9267	0.6402	0.7058	0.1153
Random Forest	0.9358	0.9375	0.9836	0.9599	0.7483	0.7647	0.0641
XGBoost	0.9615	0.9677	0.9836	0.9755	0.8659	0.8823	0.0384
LightGBM	0.9743	0.9682	1.0000	0.9838	0.8823	0.8823	0.0256

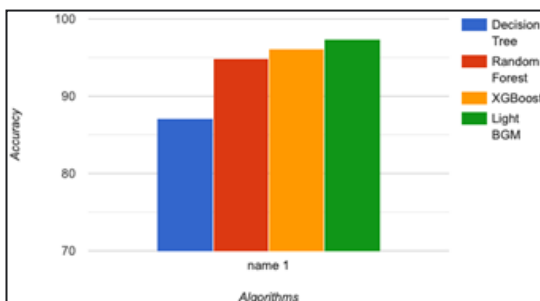


Fig 10: Accuracy

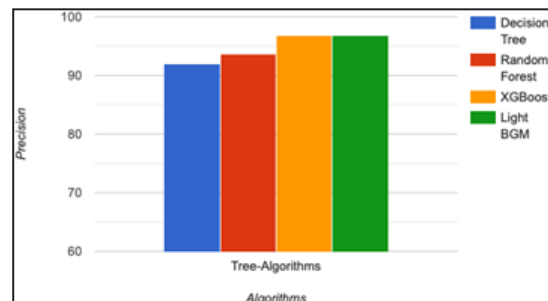


Fig 11: Precision

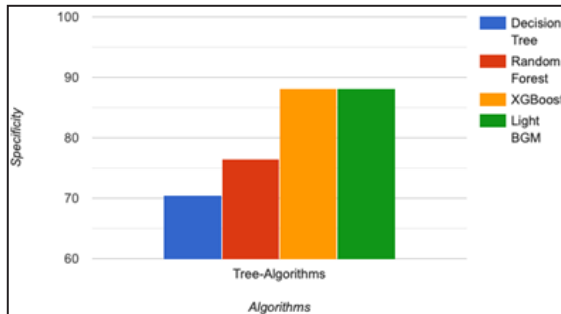


Fig 12: Specificity

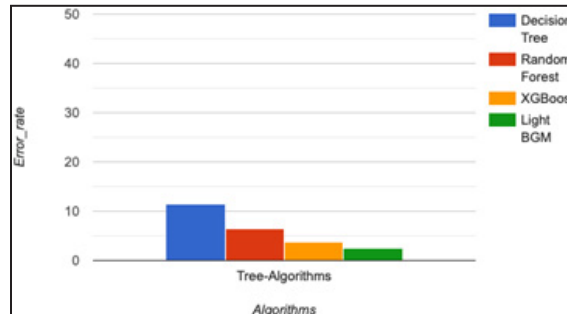


Fig 13: Error rate

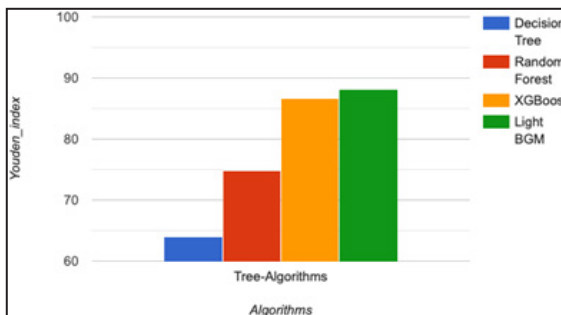


Fig 14: Youden-Index

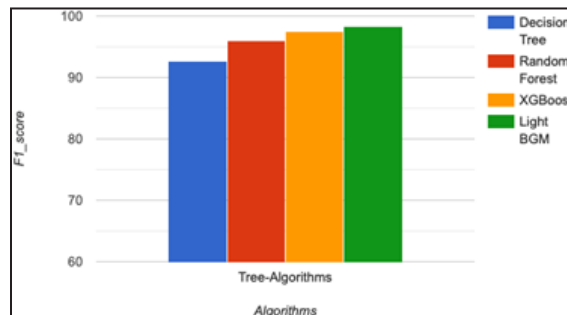


Fig 15: F1_score

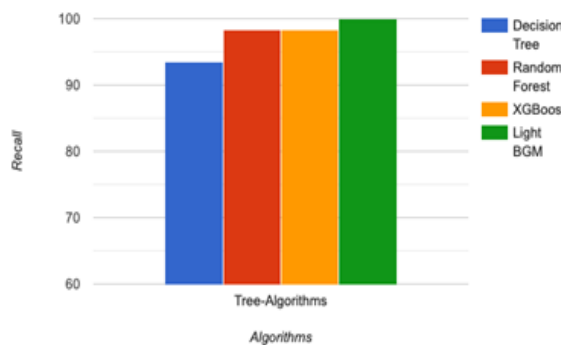


Fig 16: Recall

Fig 17-19 shows the code snippets of this work. They are screenshots of python notebook (.ipynb) file in jupyter notebook workspace.

Comparing with the work done by other researchers, this method achieved highest accuracy of 97.43% using LightGBM. Kuresanet.al [21] got 95.16% percent accuracy using HMM, while the work of other researchers is portrayed in the table below.

The workflow of the proposed model is summarised below:

Author	AlgorithmUsed	Accuracy
Kuresanetal, 2019[21]	HMM	95.16%
Hakan Gunduz[22]	CNN SVM	83.3% 86.9%
Marar et al, 2018[23]	ANN	94.87%
Goyalet.al[24]	XGBoost	91.40%
Mathuretal[25]	KNN+Adaboost KNN+MLP	91.28% 91.28%
KarapinarSen-turk,2020[26]	SVM	93.84%
ProposedWork	LightGBM	97.43%

```
In [1]: import pandas as pd
import numpy as np
import matplotlib.pyplot as plt
data_set = pd.read_csv("parkinsons.data")
data_set2 = pd.read_csv("parkinsons.data")

In [2]: data_set
Out[2]:
   phon_phf1_s501_2  122.400  148.600  113.819  0.00968  0.00008  0.00465  0.00996  0.01394  0.06134  ...
1  phon_phf1_s01_3  116.682  131.111  111.555  0.01050  0.00009  0.00544  0.00781  0.01633  0.02033  ...
3  phon_phf1_s01_4  116.676  131.871  111.306  0.00987  0.00009  0.00502  0.00698  0.01100  0.04482  ...
4  phon_phf1_s01_5  116.074  141.781  110.855  0.01084  0.00011  0.00505  0.00608  0.01066  0.06425  ...
...
190  phon_phf1_s50_2  174.188  230.978  84.261  0.00459  0.00003  0.00263  0.00259  0.00790  0.04087  ...
191  phon_phf1_s50_3  209.516  253.017  86.488  0.00564  0.00003  0.00331  0.00292  0.00994  0.02751  ...
192  phon_phf1_s50_4  174.688  240.005  74.287  0.01380  0.00008  0.00624  0.00564  0.01873  0.02308  ...
193  phon_phf1_s50_5  198.764  396.961  74.904  0.00740  0.00004  0.00370  0.00390  0.01109  0.02096  ...
194  phon_phf1_s50_6  214.289  260.277  77.973  0.00567  0.00003  0.00295  0.00317  0.00885  0.01884  ...
195 rows x 24 columns
```

Fig 17: Importing libraries and loading the dataset

Parkinson's disease detection using tree based machine learning algorithms

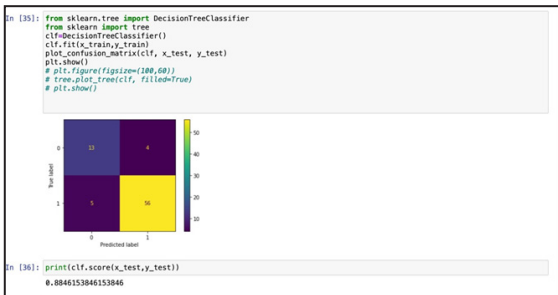


Fig18: Fitting the model with training data

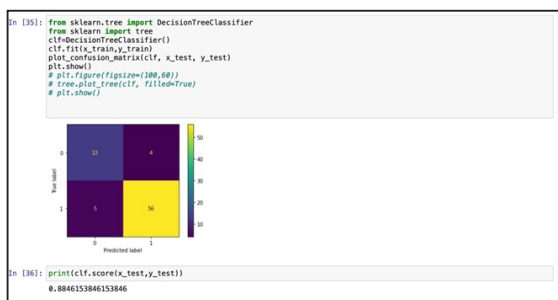


Fig19: Generating the correlation matrix and printing the accuracy

(1)Retrieve the dataset. (2)Calculate Pearson correlation coefficient tand generate cool warm colour graded matrix. (3)Remove one of the highly correlated features(coefficent>0.9). (4)Split the dataset into training and testing data. (5)BuildML model using Decision-Tree, Random Forest, XGBoost, LightGBM algorithms. (6)Fit the models with training data. (7)Obtain the values of Accuracy, Precision, Recall, F1_score, Specificity and Error Rate. (8) Generate confusion matrices of the four models. (9)Compare the models using the obtained parameters.

Conclusion

Early detection of PD is essential to initiate appropriate treatment and to better understand the disease. Voice data is extremely important for this study. Machine Learning algorithms continue to prove useful in the area of medical diagnosis. The present method performs diagnosis of PD by making use of tree-based machine learning algorithms. LightGBM achieved the highest accuracy of 97.43%.

The results show that boosting tree algorithms achieved better accuracy than regular tree-based algorithms as XGBoost and LightGBM performed superiorly. This method provides an automated diagnosis of PD and achieves clinical level accuracy. Application of this work will have great impact on health care system by improving the diagnosis of PD and thereby reduce its severity.

Future Scope

XGBoost and LightGBM can further be hyper parameter tuned in order to produce desired results. Performance of the ML model can further be improved by tuning. This however can vary depending on the dataset taken and the features selected. This Model can further be evaluated on larger datasets and accuracy can be tested.

References

1. Sherer TB, S Chowdhury, K Peabody, D Brooks: Overcoming obstacles in Parkinson's Disease. *Movement Disorders* 27(13), 1606-1611 (2012) .
2. National Institute for Health and Clinical Excellence (2006) *Parkinson's Disease: Diagnosis and Management in Primary and Secondary Care*. London: NICE ([http:// guidance.nice.org. uk/CG35](http://guidance.nice.org.uk/CG35)).
3. Progression of Voice and Speech Impairment in the Course of Parkinson's Disease: A Longitudinal Study S. Skodda, W. Grönheit, N. Mancinelli, and U. Schlegel
4. Exploiting Nonlinear Recurrence and Fractal Scaling Properties for Voice Disorder Detection', Little MA, McSharry PE, Roberts SJ, Costello DAE, Moroz IM. *BioMedical Engineering OnLine* 2007, 6:23 (26 June 2007)
5. Anyanwu MN, Shiva SG. Comparative analysis of serial decision tree classification algorithms. *International Journal*

- of Computer Science and Security. 2009 Jun;3(3):230-40
6. "Parkinson Disease Detection Using Deep Neural Networks", Shivangi, Anubhav Johri and Ashish Tripathi, Department of Computer Science Jaypee Institute of Information Technology Noida, India.
 7. Agarwal, A., Chandrayan, S., and Sahu, S. S. (2016). "Prediction of Parkinson's disease using speech signal with Extreme Learning Machine," in 2016 International Conference on Electrical, Electronics, and Optimisation Techniques (ICEEOT) (Chennai), 3776–3779. doi: 10.1109/ICEEOT.2016.77 55419
 8. H.Gunduz,"Deep learning-based Parkinson's disease classification using vocal feature sets," IEEE Access, vol. 7, pp. 115540–115551, 2019.
 9. A. Zhao, L. Qi, J. Li, J. Dong, and H. Yu, "A hybrid spatio-temporal model for detection and severity rating of Parkinson's disease from gait data," Neurocomputing, vol. 315, pp. 1–8, Nov. 2018.
 10. G. Valenza, S. Orsolini, S. Diciotti, L. Citi, E. P. Scilingo, M. Guerrisi, S. Danti, C. Lucetti, C. Tessa, R. Barbieri, and N. Toschi, "Assessment of spontaneous cardiovascular oscillations in Parkinson's disease," Biomed. Signal Process. Control, vol. 26, pp. 80–89, Apr. 2016.
 11. L. Silveira-Moriyama, A. Petrie, D. R. Williams, A. Evans, R. Katzenschlager, E. R. Barbosa, and A. J. Lees, "The use of a colour coded probability scale to interpret smell tests in suspected Parkinsonism," Movement Disorders, vol. 24, no. 8, pp. 1144–1153, Jun. 2009.
 12. S. Bilgin, "The impact of feature extraction for the classification of amyotrophic lateral sclerosis among neurodegenerative diseases and healthy subjects," Biomed. Signal Process. Control, vol. 31, pp. 288–294, Jan. 2017.
 13. I. El Maachi, G.-A. Bilodeau, and W. Bouachir, "Deep 1D-convnet for accurate Parkinson disease detection and severity prediction from gait," Expert Syst. Appl., vol. 143, Apr. 2020, Art. no. 113075.
 14. T. Arroyo-Gallego, M. J. Ledesma-Carbayo, A. Sanchez-Ferro, I. Butterworth, C. S. Mendoza, M. Matarazzo, P. Montero, R. Lopez-Blanco, V. Puertas-Martin, R. Trincado, and L. Giancardo, "Detection of motor impairment in Parkinson's disease via mobile touchscreen typing," IEEE Trans. Biomed. Eng., vol. 64, no. 9, pp. 1994–2002, Sep. 2017.
 15. R. Das, "A comparison of multiple classification methods for diagnosis of Parkinson disease," Expert Syst. Appl., vol. 37, no. 2, pp. 1568–1572, Mar. 2010.
 16. Cudeck, R. (1989). Analysis of correlation matrices using covariance structure models. Psychological Bulletin, 105(2), 317–327.
 17. Myles, A. J., Feudale, R. N., Liu, Y., Woody, N. A., & Brown, S. D. (2004). An introduction to decision tree modelling. Journal of Chemometrics, 18 (6), 275–285.
 18. Janitza, S., Kruppa, J., König, I.R., & Boulesteix, A.-L. (2012). Overview of random forest methodology and practical guidance with emphasis on computational biology and bioinformatics. WIREs Data Mining and Knowledge Discovery, 2 (6), 493–507.
 19. Chen T and Guestrin C 2016 XGBoost: A Scalable Tree Boosting System[J].
 20. K. Guolin, M. Qi, F. Thomas, W. Taifeng,

- C. Wei, M. Weidong, Y. Qiwei, L. Tie-Yan, "LightGBM: A Highly Efficient Gradient Boosting Decision Tree," *Advances in Neural Information Processing Systems* vol. 30, pp. 3149-3157, 2017. CAT.2018.8933579
21. Kuresan, H., Samiappan, D., and Masunda, S. (2019). Fusion of WPT and MFCC feature extraction in Parkinson's disease diagnosis. *Technol. Health Care* 27, 363–372. doi: 10.3233/THC-181306
 22. Gunduz, Hakan. "Deep learning-based Parkinson's disease classification using vocal feature sets." *IEEE Access* 7 (2019): 115540-115551.
 23. Marar, S., Swain, D., Hiwarkar, V., Motwani, N., and Awari, A. (2018). "Predicting the occurrence of Parkinson's disease using various classification models," in 2018 International Conference on Advanced Computation and Telecommunication (ICACAT) (Bhopal), 1–5. doi: 10.1109/ICA-
 24. Goyal, Jinee, Padmavati Khandnor, and Trilok Chand Aseri. "A Comparative Analysis of Machine Learning classifiers for Dysphonia-based classification of Parkinson's Disease." *International Journal of Data Science and Analytics* 11, no. 1 (2021): 69-83.
 25. Mathur, Richa, Vibhakar Pathak, and Devesh Bandil. "Parkinson disease prediction using machine learning algorithm." In *Emerging Trends in Expert Applications and Security*, pp. 357-363. Springer, Singapore, 2019.
 26. KarapinarSenturk, Z. (2020). Early diagnosis of Parkinson's disease using machine learning algorithms. *Med. Hypoth.* 138:109603. doi: 10.1016/j.mehy.2020.109603

Parkinson's disease Detection Using Tree Based Machine Learning Algorithms

Venkata Srinivas Babu Oguri¹, Sudhakar Poda², A. Krishna Satya², NK Prasanna

¹Department of Computer Science and Engineering, Mahindra University, Bahadurpally Jeedimetla, Hyderabad - 500043 - Telangana, INDIA

²Department of Biotechnology, Acharya Nagarjuna University, Nagarjuna nagar, Guntur-522510, Andhra Pradesh, India

³CSIR- National Institute of Science Communication & Policy Research, New Delhi-110 012, Delhi, India

Abstract

Parkinson's Disease (PD), also known as primary Parkinsonism is a persistent, idiopathic, degenerative nervous disorder which results from lack of dopaminergic neurons in the substantia nigra pars compacta, which is the source of nigrostriatal dopamine pathway within the midbrain. The clinical detection relies on motor symptoms recognition. Significant neurological damage is already done by the time motor symptom occur. Early detection is necessary to stalk the progression of the disease. The problem of detection of PD comes under classification. Several tree-based classification algorithms were applied to the dataset retrieved from UCI machine learning database. The dataset was first split into train and test data. Various models were created using four different algorithms. Correlation coefficients were calculated for each of the features in the dataset. The model was fitted with train data obtained after removing highly correlated features. Predictions were made and various parameters were considered for comparison. Accuracy, precision, recall, F1-Score, Youden Index, error rate and specificity were the parameters calculated. Out of the four algorithms (Decision Tree, Random Forest, XGBoost and LightGBM), LightGBM

achieved the highest accuracy of 97.43%.

Keywords: Parkinson's Disease (PD), LightGBM, Pearson Correlation, Accuracy, Error Rate, Jupyter Notebook.

Introduction

Parkinson's Disease (PD) also known as primary Parkinsonism is a persistent, idiopathic, degenerative nervous disorder which results from lack of dopaminergic neurons in the substantia nigra pars compacta, which is responsible for nigrostriatal dopamine pathway within the midbrain (1). Some of the symptoms of PD include bradykinesia, rigidity, and rest tremor. Resting tremor (initially unilateral), rigidity, bradykinesia (slow movements), dissimilarities in gait, and unstable posture come under the motor symptoms while cognitive changes, behavioural and neuropsychiatric changes, autonomic nervous system failure, sensory and sleep disturbances come under non-motor symptoms (1). Motor and non-motor symptoms are used to diagnose PD. Non-motor issues of the disease can become more troublesome as the disease progresses (2). Also, voice and speech impairment typically occur in PD patients. The loss of ability to communicate

properly is the main source of disability in patients. The multidimensional irregularities in the speech such as hoarse voice, reduced loudness, and restricted pitch variability (Mono pitch and Mono loudness), imprecise articulation and abnormalities of speech rate, and pause ratio can be attributed to the loss of dopaminergic neurons (3). Voice and speech performance will show further deterioration in the course of time which hints at nondopaminergic mechanisms of progression of dysarthrophonia. Early detection reduces the disease progression and limits the treatment expenses. Several machine learning algorithms can be used for the detection of PD in preliminary stages using voice data. Machine learning algorithms have made commendable progress in medical diagnosis in the recent times because of their ease in implementation. The current study aims to utilise the ML algorithms to facilitate early detection of the disease. A total of four ML algorithms were used in this study. They are Decision Tree, Random Forest, XGBoost and LightGBM classifiers.

Review of Literature

10 million people (about half the population of New York) worldwide have PD from the information found in Parkinson's diseases foundation (2015). Death and disability due to PD is increasing faster than any other neurological disease according to WHO. One in every 500 people have PD in Britain and this number is expected to grow threefold by 2050 according to Parkinson's Disease Society website. This illness affects people from 50 -70 years old and becomes worse over time. Diagnosis of PD is heavily reliant on evaluation of motion which is difficult to detect by human sight. This method aims to overcome these difficulties and improve the assessment process by employing machine learning algorithms (6). One attempt was made by implementing Convolutional Neural Networks (CNNs). They were used to classify gait signals converted to spectrogram images by image classification on a big-scale and deep dense Ar-

tificial Neural Networks (ANNs) were employed to predict PD at an early stage. Voice recordings were used in this instance. A total of 54 studies in the category 'Diagnosis of PD' were examined. Out of them 33 studies used datasets from UCI machine learning repository, mPower and PhysioNet databases. In one of the study, data from public repositories was joined with local data bases (7). 14 studies performed diagnosis as well as differential diagnosis. Research articles not written in English were not considered. Most commonly voice data was used, while some studies also used MRI, movement, handwriting patterns and SPECT imaging data. The most common metric used for assessment of performance was accuracy. Most methods are based on speech data (8), gait patterns (9), cardiovascular oscillations (10), smell identification (11) and force tracking data (12). A one-dimensional neural network relying on signals of gait was introduced to detect PD in (13). It should be noted that accuracy is low when using gait analyses because of background noise in voice recordings, causing false positives. Detection of motor impairment based on mobile screen typing was introduced in (14). Four classifiers, namely Decision Tree, Regression, DMneural and Neural Networks (NN) are used and their performances are compared in (15), in which the best accuracy of 92.90% was achieved by NN algorithm. Early and accurate detection of PD is essential to stalk the progression of the disease.

Methodology

The dataset was retrieved from UCI machine learning repository. It was created by University of Oxford and National Centre for Voice and Speech, Denver, Colorado. The dataset contains voice measurements from 31 people, and 23 with PD. It has a total of 195 voice recordings (4). The data aims to discriminate PD people from healthy people. The status column denotes '0' for healthy and '1' for PD affected persons. There are about 5-6 recordings for each patient.

name	MDVP:Fo(Hz)	MDVP:Fhi(Hz)	MDVP:Flo(Hz)	MDVP:Jitter(%)	MDVP:Jitter(Abs)	MDVP:RAP	MDVP:PPQ	Jitter:DDP	MDVP:Shimmer	MDVP:Shimmer(dB)
phon_R01_S01_1	119.992	157.302	74.997	0.00784	0.00007	0.0037	0.00554	0.01109	0.04374	0.426
phon_R01_S01_2	122.4	148.65	113.819	0.00968	0.00008	0.00465	0.00696	0.01394	0.06134	0.626
phon_R01_S01_3	116.682	131.111	111.555	0.0105	0.00009	0.00544	0.00781	0.01633	0.05233	0.482
phon_R01_S01_4	116.676	137.871	111.366	0.00997	0.00009	0.00502	0.00698	0.01505	0.05492	0.517
phon_R01_S01_5	116.014	141.781	110.655	0.01284	0.00011	0.00655	0.00908	0.01966	0.06425	0.584
phon_R01_S01_6	120.552	131.162	113.787	0.00968	0.00008	0.00463	0.0075	0.01388	0.04701	0.456
phon_R01_S02_1	120.267	137.244	114.82	0.00333	0.00003	0.00155	0.00202	0.00466	0.01608	0.14
phon_R01_S02_2	107.332	113.84	104.315	0.0029	0.00003	0.00144	0.00182	0.00431	0.01567	0.134
phon_R01_S02_3	95.73	132.068	91.754	0.00551	0.00006	0.00293	0.00332	0.0088	0.02093	0.191
phon_R01_S02_4	95.056	120.103	91.226	0.00532	0.00006	0.00268	0.00332	0.00803	0.02838	0.255
phon_R01_S02_5	88.333	112.24	84.072	0.00505	0.00006	0.00254	0.0033	0.00763	0.02143	0.197
phon_R01_S02_6	91.904	115.871	86.292	0.0054	0.00006	0.00281	0.00336	0.00844	0.02752	0.249
phon_R01_S04_1	136.926	159.866	131.276	0.00293	0.00002	0.00118	0.00153	0.00355	0.01259	0.112
phon_R01_S04_2	139.173	179.139	76.556	0.0039	0.00003	0.00165	0.00208	0.00496	0.01642	0.154
phon_R01_S04_3	152.845	163.305	75.836	0.00294	0.00002	0.00121	0.00149	0.00364	0.01828	0.158
phon_R01_S04_4	142.167	217.455	83.159	0.00369	0.00003	0.00157	0.00203	0.00471	0.01503	0.126
phon_R01_S04_5	144.188	349.259	82.764	0.00544	0.00004	0.00211	0.00292	0.00632	0.02047	0.192
phon_R01_S04_6	168.778	232.181	75.603	0.00718	0.00004	0.00284	0.00387	0.00853	0.03327	0.348
phon_R01_S05_1	153.046	175.829	68.623	0.00742	0.00005	0.00364	0.00432	0.01092	0.05517	0.542
phon_R01_S05_2	156.405	189.398	142.822	0.00768	0.00005	0.00372	0.00399	0.01116	0.03995	0.348
phon_R01_S05_3	153.848	165.738	65.782	0.0084	0.00005	0.00428	0.0045	0.01285	0.0381	0.328
phon_R01_S05_4	153.88	172.86	78.128	0.0048	0.00003	0.00232	0.00267	0.00696	0.04137	0.37
phon_R01_S05_5	167.93	193.221	79.068	0.00442	0.00003	0.0022	0.00247	0.00661	0.04351	0.377
phon_R01_S05_6	173.917	192.735	86.18	0.00476	0.00003	0.00221	0.00258	0.00663	0.04192	0.364
phon_R01_S06_1	163.656	200.841	76.779	0.00742	0.00005	0.0038	0.0039	0.0114	0.01659	0.164
phon_R01_S06_2	104.4	206.002	77.968	0.00633	0.00006	0.00316	0.00375	0.00948	0.03767	0.381
phon_R01_S06_3	171.041	208.313	75.501	0.00455	0.00003	0.0025	0.00234	0.0075	0.01966	0.186
phon_R01_S06_4	146.845	208.701	81.737	0.00496	0.00003	0.0025	0.00275	0.00749	0.01919	0.198
phon_R01_S06_5	155.358	227.383	80.055	0.0031	0.00002	0.00159	0.00176	0.00476	0.01718	0.161

Fig1DatasetPart1

Shimmer:APQ3	Shimmer:APQ5	MDVP:APQ	Shimmer:DDA	NHR	HNR	status	RPDE	DFA	spread1	spread2	D2	PPE
0.02182	0.0313	0.02971	0.06545	0.02211	21.033	1	0.414783	0.815285	-4.813031	0.266482	2.301442	0.284654
0.03134	0.04518	0.04368	0.09403	0.01929	19.085	1	0.458359	0.819521	-4.075192	0.33559	2.486855	0.368674
0.02757	0.03858	0.0359	0.0827	0.01309	20.651	1	0.429895	0.825288	-4.443179	0.311173	2.342259	0.332634
0.02924	0.04005	0.03772	0.08771	0.01353	20.644	1	0.434969	0.819235	-4.117501	0.334147	2.405554	0.368975
0.0349	0.04825	0.04465	0.1047	0.01767	19.649	1	0.417356	0.823484	-3.747787	0.234513	2.33218	0.410335
0.02328	0.03526	0.03243	0.06985	0.01222	21.378	1	0.415564	0.825069	-4.242867	0.299111	2.18756	0.357775
0.00779	0.00937	0.01351	0.02337	0.00607	24.886	1	0.59604	0.764112	-5.634322	0.257682	1.854785	0.211756
0.00829	0.00946	0.01256	0.02487	0.00344	26.892	1	0.63742	0.763262	-6.167603	0.183721	2.064693	0.163755
0.01073	0.01277	0.01717	0.03218	0.0107	21.812	1	0.615551	0.773587	-5.498678	0.327769	2.322511	0.231571
0.01441	0.01725	0.02444	0.04324	0.01022	21.862	1	0.547037	0.798463	-5.011879	0.325996	2.432792	0.271362
0.01079	0.01342	0.01892	0.03237	0.01166	21.118	1	0.611137	0.776156	-5.24977	0.391002	2.407313	0.24974
0.01424	0.01641	0.02214	0.04272	0.01141	21.414	1	0.58339	0.79252	-4.960234	0.363566	2.642476	0.275931
0.00656	0.00717	0.0114	0.01968	0.00581	25.703	1	0.4606	0.646846	-6.547148	0.152813	2.041277	0.138512
0.00728	0.00932	0.01797	0.02184	0.01041	24.889	1	0.430166	0.665833	-5.660217	0.254989	2.519422	0.199889
0.01064	0.00972	0.01246	0.03191	0.00609	24.922	1	0.474791	0.654027	-6.105098	0.203653	2.125618	0.1701
0.00772	0.00888	0.01359	0.02316	0.00839	25.175	1	0.565924	0.658245	-5.340115	0.210185	2.205546	0.234589
0.00969	0.012	0.02074	0.02908	0.01859	22.333	1	0.56738	0.644692	-5.44004	0.239764	2.264501	0.218164
0.01441	0.01893	0.0343	0.04322	0.02919	20.376	1	0.631099	0.605417	-2.93107	0.434326	3.007463	0.430788
0.02471	0.03572	0.05767	0.07413	0.0316	17.28	1	0.665318	0.719467	-3.949079	0.35787	3.10901	0.377429
0.01721	0.02374	0.0431	0.05164	0.03365	17.153	1	0.649554	0.68608	-4.554466	0.340176	2.856676	0.322111
0.01667	0.02383	0.04055	0.05	0.03871	17.536	1	0.660125	0.704087	-4.095442	0.262564	2.73971	0.365391
0.02021	0.02591	0.04525	0.06062	0.01849	19.493	1	0.629017	0.698951	-5.18696	0.237622	2.557536	0.259765
0.02228	0.0254	0.04246	0.06685	0.0128	22.468	1	0.61906	0.679834	-4.330956	0.262384	2.916777	0.285695
0.02187	0.0247	0.03772	0.06562	0.0184	20.422	1	0.537264	0.686894	-5.248776	0.210279	2.547508	0.253556
0.00738	0.00948	0.01497	0.02214	0.01778	23.831	1	0.397937	0.732479	-5.557447	0.22089	2.692176	0.215961
0.01732	0.02245	0.0378	0.05197	0.02887	22.066	1	0.522746	0.737948	-5.571843	0.236853	2.846369	0.219514
0.00889	0.01169	0.01872	0.02666	0.01095	25.908	1	0.418622	0.720916	-6.18359	0.226278	2.589702	0.147403
0.00883	0.01144	0.01826	0.0265	0.01328	25.119	1	0.358773	0.726652	-6.27169	0.196102	2.314209	0.162999
0.00769	0.01012	0.01661	0.02307	0.00677	25.97	1	0.470478	0.676258	-7.120925	0.279789	2.241742	0.108514

Fig2DatasetPart2

Matrix column entries (attributes):

- name - ASCII subject name and recording number
- MDVP:Fo(Hz) - Average vocal fundamental frequency
- MDVP:Fhi(Hz) - Maximum vocal fundamental frequency
- MDVP:Flo(Hz) - Minimum vocal fundamental frequency
- MDVP:Jitter(%),MDVP:Jitter(Abs),MDVP:RAP,MDVP:PPQ,Jitter:DDP - Several measures of variation in fundamental frequency
- MDVP:Shimmer,MDVP:Shimmer(dB),Shimmer:APQ3,Shimmer:APQ5,MDVP:APQ,Shimmer:DDA - Several measures of variation in amplitude
- NHR,HNR - Two measures of ratio of noise to tonal components in the voice status
- status - Health status of the subject (one) - Parkinson's, (zero) - healthy
- RPDE,D2 - Two nonlinear dynamical complexity measures

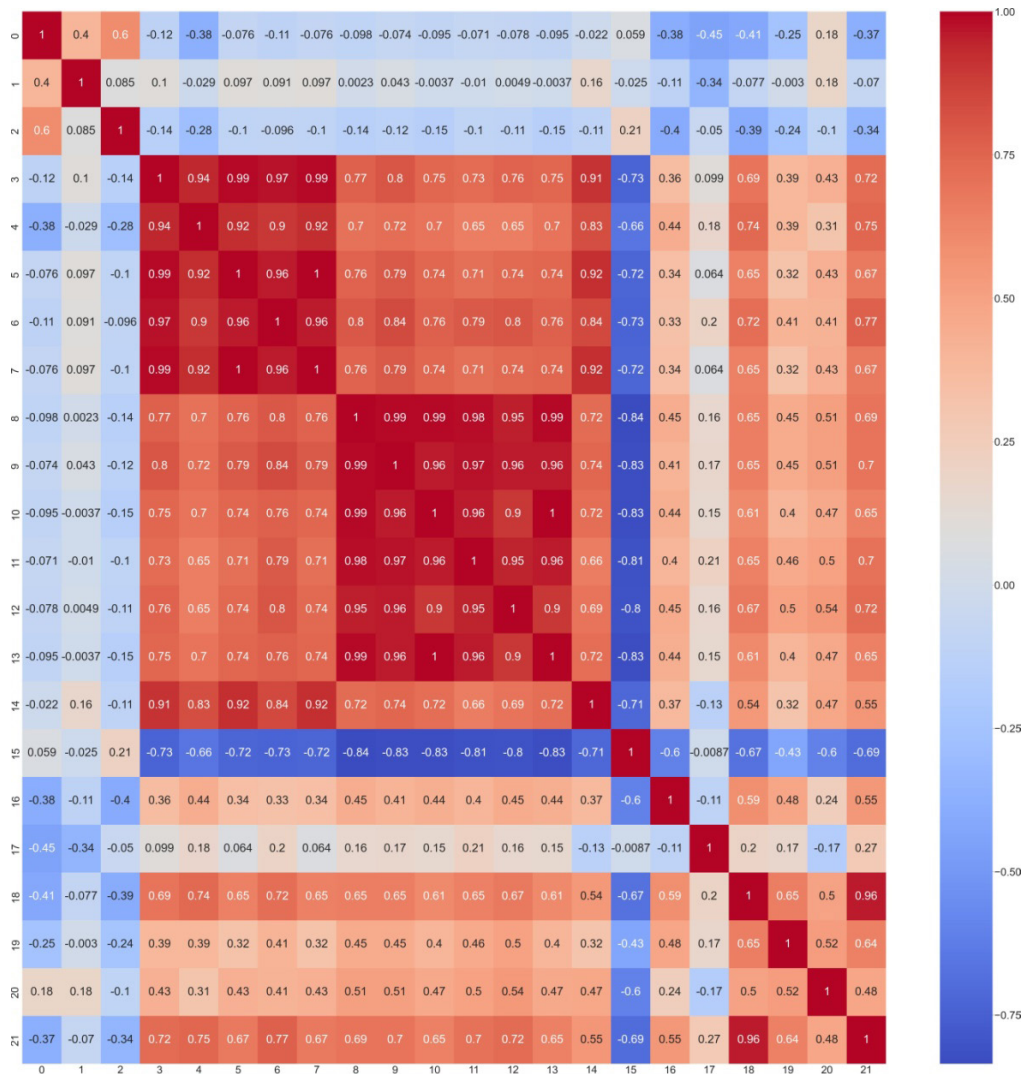


Fig3 Pearson Correlation Heat-map

Fig 1 and Fig 2 show a section of the dataset. The problem of diagnosis of PD comes under classification. Classification algorithms come under supervised learning. Several classification algorithms were applied to the dataset. All of them were tree based. DecisionTree, Random Forest algorithms later followed by LightGBM and XGBoost were used to achieve highest accuracy. The reasons behind using tree-based classification algorithms were that they mimic human thinking ability and they can be easily understood [5]. The dataset underwent preprocessing initially. All the work was done in Jupyter Notebook, an interactive python notebook software. Name column(attribute) was removed since it is irrelevant and decreases the accuracy. Next, correlation matrix was generated. Correlation matrix is square and symmetric [16]. It measures the linear dependency between two elements. We were specifically using Pearson's correlation coefficient. The coefficient can be equal to any number between -1 and 1. perfectly negatively linear correlated variables have coefficient equal to -1, highly correlated variables have a correlation of value 1 and 0 indicates no linear correlation between the two variables. After the removal of the Name attribute from the dataset, correlation matrix is generated for the remaining 22 features. The matrix is shown in Fig 3. The matrix was color coded as 'cool warm' to easily understand the strength of relationship. The stronger relations have warmer (red) color grading while the weak ones have cool (blue) color grading. All the diagonal elements will be red in color and have correlation coefficient value of 1 (since each attribute is mapped to itself). The threshold value for removal is set to 0.9. Out of 22 features, 11 were removed. New dataset was created after removal of highly correlated features. This dataset was split into training and testing datasets. 30% was randomly set aside for testing while the remaining was used to train the model. Two Tree based algorithms and two Boosting Algorithms were used. Brief descriptions of the algorithms used in this work are given below.

Decision tree classifier

Decision Tree algorithm breaks a complex problem into a set of decisions which are relatively simpler. Every Decision Tree contains a Root Node, Leaf Nodes and Internal Nodes. Decision Tree uses Entropy, Information Gain and Gini Index as criteria for evaluating attributes [17]. It comes under Supervised Learning Algorithms. Fig 4 shows the Decision Tree generated on this dataset.

Random forest classifier

Random Forest classification comes under ensemble learning i.e it's an ensemble of Decision Trees. It is a bagging-based algorithm. The fundamental concept used by Random Forest is that a large number of uncorrelated Decision Trees operating as one group will outperform each of the individual constituent tree [18].

XGBoost classifier

XGBoost is Gradient-Boosting algorithm that makes use of Ensemble Learning and is tree-based. Each Decision Tree corrects the errors committed by its predecessor. This method is called Gradient Boosting. XGBoost makes use of Gradient Boosted Decision Trees. Each of these trees then ensemble to give a more accurate model. XGBoost uses Regularization to penalise complex trees and Cross validation to avoid overfitting of the model. performs well because of its handling of data types, distributions and the variety of hyper parameters that can be tuned [19].

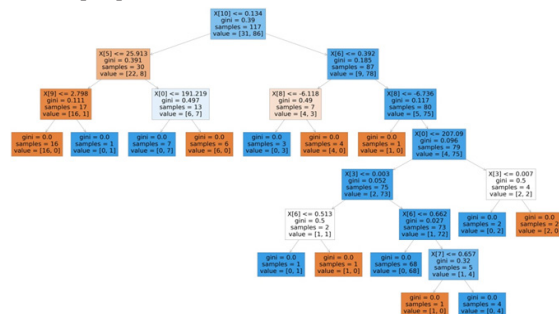
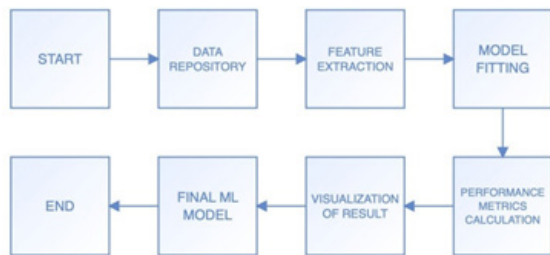


Fig 4: Decision Tree Generated

LightGBM classifier

LightGBM is also a Gradient-Boosting algorithm that makes use of Ensemble Learning and is tree-based. This algorithm shares common features such as sparse optimization, parallel training, multiple loss functions and bagging with XGBoost. But, LightGBM grows trees leaf-wise instead of level-wise [20]. Out of the boosting four types of algorithms available, the default option is eGBDT (gradient boosting decision tree) was used to implement this model.



Flow chart of the proposed work is depicted in Fig 5

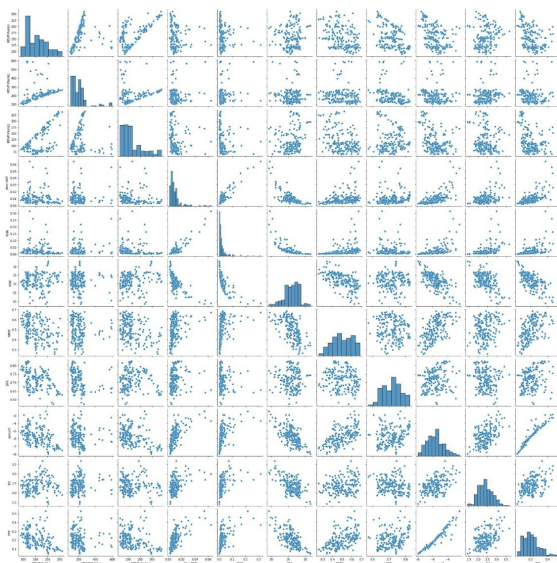


Fig 6 Scatter Plot

Fig 6 shows the scatter plot generated on this dataset; it contains 11 features.

Decision Tree Classification is the least performer of all, scoring 88.46%, while Random Forest Classification and XGBoost scored 93.58% and 96.15% respectively. Light GBM achieved highest accuracy of 97.43%. Fig 7-10 shows the confusion matrices of all the algorithms used. Confusion Matrix shows the number of True positive (TP), True negative (TN), False positive (FP) and False negative (FN) instances. Decision Tree Classifier has shown 57 True positive, 12 true negative, 5 False positive and 4 False negative instances. Hence a total of 69 instance have been correct out of 78. Therefore, the accuracy is 88.46%.

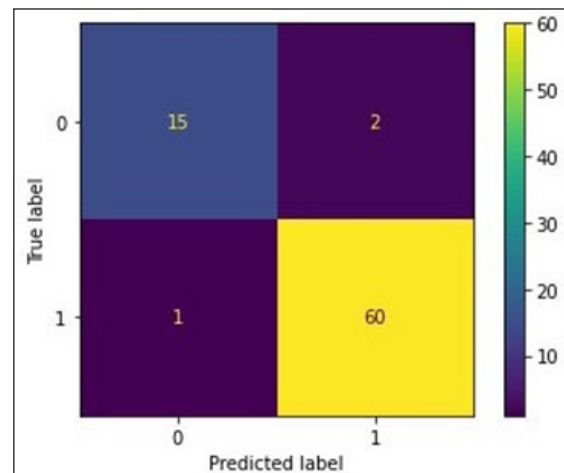


Fig 6 Decision Tree

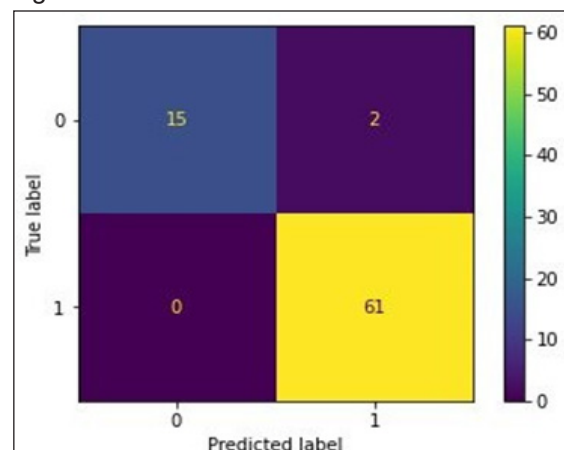


Fig 7 Random Forest

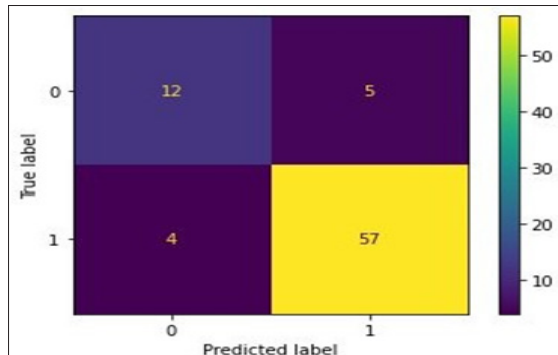


Fig 8 XGBoost

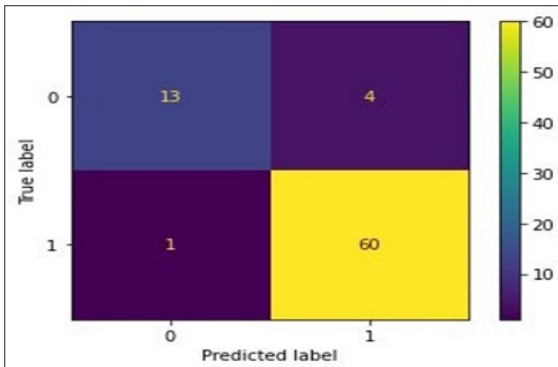


Fig 9 LightGBM

Various other parameters are obtained as well in order to compare the performances. Their formulas are listed below.

$$Accuracy = \frac{TP + TN}{TP + FP + FN + TN}$$

$$Precision = \frac{TP}{TP + FP}$$

$$recall = \frac{TP}{TP + FN}$$

$$F1 - Score = \frac{2 \times Precision \times recall}{Precision + recall}$$

$$YI = recall + specificity - 1$$

$$Specificity = \frac{TN}{TN + FP}$$

$$error_rate = \frac{FP + FN}{TP + TN + FN + FP}$$

The metrics were evaluated and listed in the table below.

Algorithm	Accuracy	Precision	Recall	F1_score	YoudenIndex	Specificity	Error-Rate
Decision Tree	0.8846	0.9193	0.9344	0.9267	0.6402	0.7058	0.1153
Random Forest	0.9358	0.9375	0.9836	0.9599	0.7483	0.7647	0.0641
XGBoost	0.9615	0.9677	0.9836	0.9755	0.8659	0.8823	0.0384
LightGBM	0.9743	0.9682	1.0000	0.9838	0.8823	0.8823	0.0256

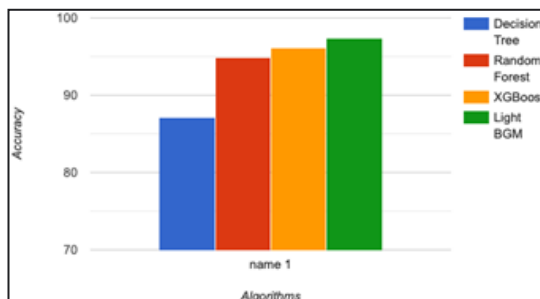


Fig 10 Accuracy

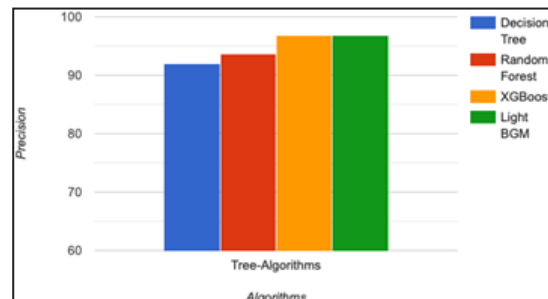


Fig 11 Precision

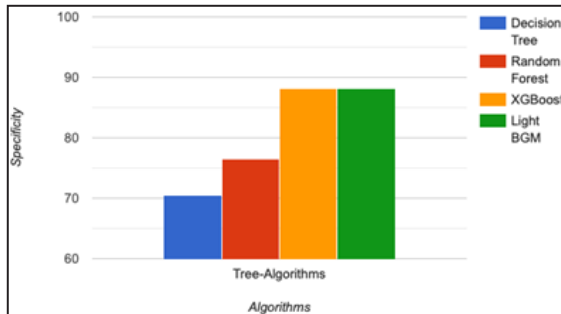


Fig 12 Specificity

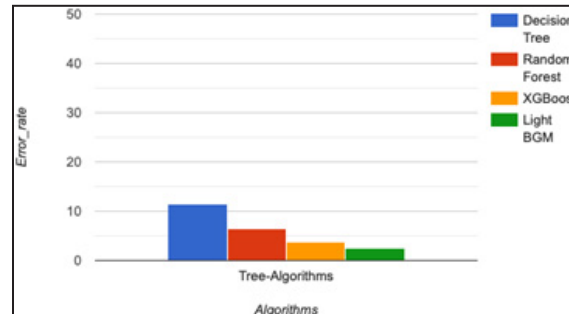


Fig 13 Error rate

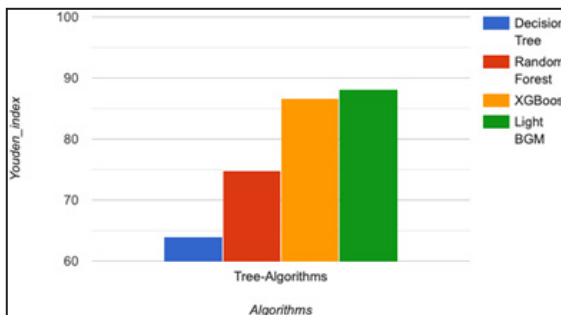


Fig 14 Youden-Index

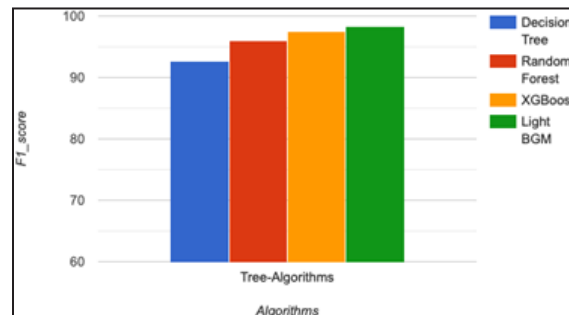


Fig 15 F1_score

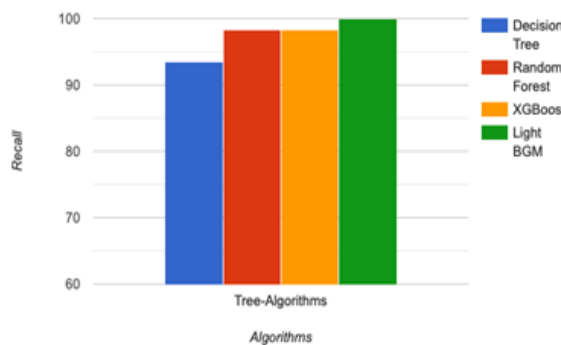


Fig 16 Recall

Fig 17-19 shows the code snippets of this work. They are screenshots of python notebook (.ipynb) file in jupyter notebook workspace.

Comparing with the work done by other researchers, this method achieved highest accuracy of 97.43% using LightGBM. Kuresanet.al [21] got 95.16% percent accuracy using HMM, while the work of other researchers is portrayed in the table below.

Author	AlgorithmUsed	Accuracy
Kuresanetal, 2019[21]	HMM	95.16%
Hakan Gunduz[22]	CNN SVM	83.3% 86.9%
Marar et al, 2018[23]	ANN	94.87%
Goyalet.al[24]	XGBoost	91.40%
Mathuretal[25]	KNN+Adaboost KNN+MLP	91.28% 91.28%
KarapinarSen-turk,2020[26]	SVM	93.84%
ProposedWork	LightGBM	97.43%

```
In [1]: import pandas as pd
import numpy as np
import matplotlib.pyplot as plt
data_set = pd.read_csv("parkinsons.data")
data_set2 = pd.read_csv("parkinsons.data")

In [2]: data_set
Out[2]:
   phon_phf1_S01_2  122.400  148.600  113.819  0.00968  0.00008  0.00465  0.00996  0.01394  0.06134  ...
1  phon_phf1_S01_3  116.682  131.111  111.555  0.01050  0.00009  0.00544  0.00781  0.01633  0.02033  ...
3  phon_phf1_S01_4  116.679  137.871  111.306  0.00987  0.00009  0.00502  0.00698  0.01100  0.04482  ...
4  phon_phf1_S01_5  116.074  141.781  110.855  0.01084  0.00011  0.00505  0.00608  0.01966  0.06425  ...
...
190  phon_phf1_S50_2  174.188  230.978  84.261  0.00459  0.00003  0.00263  0.00259  0.00790  0.04087  ...
191  phon_phf1_S50_3  209.516  253.017  86.488  0.00564  0.00003  0.00331  0.00292  0.00994  0.02751  ...
192  phon_phf1_S50_4  174.688  240.005  74.287  0.01380  0.00008  0.00654  0.00564  0.01873  0.02038  ...
193  phon_phf1_S50_5  198.764  396.961  74.904  0.00740  0.00004  0.00370  0.00390  0.01109  0.02096  ...
194  phon_phf1_S50_6  214.289  260.277  77.973  0.00567  0.00003  0.00295  0.00317  0.00885  0.01884  ...
195 rows x 24 columns
```

Fig17: Importing libraries and loading the dataset

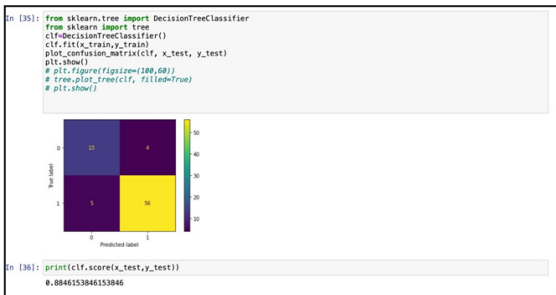


Fig18: Fitting the model with training data

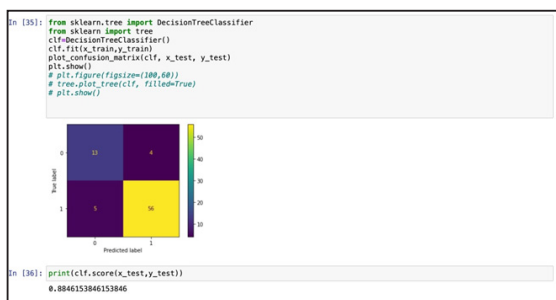


Fig19: Generating the correlation matrix and printing the accuracy

The workflow of the proposed model is summarised below:

- (1) Retrieve the dataset.
- (2) Calculate Pearson correlation coefficient and generate cool warm colour graded matrix.
- (3) Remove one of the highly correlated features (coefficient > 0.9).
- (4) Split the dataset into training and testing data.
- (5) Build ML model using Decision-Tree, Random Forest, XGBoost, LightGBM algorithms.
- (6) Fit the models with training data.
- (7) Obtain the values of Accuracy, Precision, Recall, F1_score, Specificity and Error Rate.
- (8) Generate confusion matrices of the four models.
- (9) Compare the models using the obtained parameters.

Conclusion

Early detection of PD is essential to initiate appropriate treatment and to better understand the disease. Voice data is extremely important for this study. Machine Learning algorithms continue to prove useful in the area of medical diagnosis. The present method performs diagnosis of PD by making use of tree-

based machine learning algorithms. LightGBM achieved the highest accuracy of 97.43%. The results show that boosting tree algorithms achieved better accuracy than regular tree-based algorithms as XGBoost and LightGBM performed superiorly. This method provides an automated diagnosis of PD and achieves clinical level accuracy. Application of this work will have great impact on health care system by improving the diagnosis of PD and thereby reduce its severity.

Future Scope

XGBoost and LightGBM can further be hyper parameter tuned in order to produce desired results. Performance of the ML model can further be improved by tuning. This however can vary depending on the dataset taken and the features selected. This Model can further be evaluated on larger datasets and accuracy can be tested.

References

1. Sherer TB, S Chowdhury, K Peabody, D Brooks: Overcoming obstacles in Parkinson's Disease. *Movement Disorders* 27(13), 1606-1611 (2012) .
2. National Institute for Health and Clinical Excellence (2006) *Parkinson's Disease: Diagnosis and Management in Primary and Secondary Care*. London: NICE ([http:// guidance.nice.org. uk/CG35](http://guidance.nice.org.uk/CG35)).
3. Progression of Voice and Speech Impairment in the Course of Parkinson's Disease: A Longitudinal Study S. Skodda, W. Grönheit, N. Mancinelli, and U. Schlegel
4. 'Exploiting Nonlinear Recurrence and Fractal Scaling Properties for Voice Disorder Detection', Little MA, McSharry PE, Roberts SJ, Costello DAE, Moroz IM. *BioMedical Engineering OnLine* 2007, 6:23 (26 June 2007)
5. Anyanwu MN, Shiva SG. Comparative

- analysis of serial decision tree classification algorithms. *International Journal of Computer Science and Security*. 2009 Jun;3(3):230-40
6. "Parkinson Disease Detection Using Deep Neural Networks", Shivangi, Anubhav Johri and Ashish Tripathi, Department of Computer Science Jaypee Institute of Information Technology Noida, India.
 7. Agarwal, A., Chandrayan, S., and Sahu, S. S. (2016). "Prediction of Parkinson's disease using speech signal with Extreme Learning Machine," in 2016 International Conference on Electrical, Electronics, and Optimisation Techniques (ICEEOT) (Chennai), 3776–3779. doi: 10.1109/ICEEOT.2016.77 55419
 8. H.Gunduz,"Deep learning-based Parkinson's disease classification using vocal feature sets," *IEEE Access*, vol. 7, pp. 115540–115551, 2019.
 9. A. Zhao, L. Qi, J. Li, J. Dong, and H. Yu, "A hybrid spatio-temporal model for detection and severity rating of Parkinson's disease from gait data," *Neurocomputing*, vol. 315, pp. 1–8, Nov. 2018.
 10. G. Valenza, S. Orsolini, S. Diciotti, L. Citi, E. P. Scilingo, M. Guerrisi, S. Danti, C. Lucetti, C. Tessa, R. Barbieri, and N. Toschi, "Assessment of spontaneous cardiovascular oscillations in Parkinson's disease," *Biomed. Signal Process. Control*, vol. 26, pp. 80–89, Apr. 2016.
 11. L. Silveira-Moriyama, A. Petrie, D. R. Williams, A. Evans, R. Katzenschlager, E. R. Barbosa, and A. J. Lees, "The use of a colour coded probability scale to interpret smell tests in suspected Parkinsonism," *Movement Disorders*, vol. 24, no. 8, pp. 1144–1153, Jun. 2009.
 12. S. Bilgin, "The impact of feature extraction for the classification of amyotrophic lateral sclerosis among neurodegenerative diseases and healthy subjects," *Biomed. Signal Process. Control*, vol. 31, pp. 288–294, Jan. 2017.
 13. I. El Maachi, G.-A. Bilodeau, and W. Bouachir, "Deep 1D-convnet for accurate Parkinson disease detection and severity prediction from gait," *Expert Syst. Appl.*, vol. 143, Apr. 2020, Art. no. 113075.
 14. T. Arroyo-Gallego, M. J. Ledesma-Carbayo, A. Sanchez-Ferro, I. Butterworth, C. S. Mendoza, M. Matarazzo, P. Montero, R. Lopez-Blanco, V. Puertas-Martin, R. Trincado, and L. Giancardo, "Detection of motor impairment in Parkinson's disease via mobile touchscreen typing," *IEEE Trans. Biomed. Eng.*, vol. 64, no. 9, pp. 1994–2002, Sep. 2017.
 15. R. Das, "A comparison of multiple classification methods for diagnosis of Parkinson disease," *Expert Syst. Appl.*, vol. 37, no. 2, pp. 1568–1572, Mar. 2010.
 16. Cudeck, R. (1989). Analysis of correlation matrices using covariance structure models. *Psychological Bulletin*, 105(2), 317–327.
 17. Myles, A. J., Feudale, R. N., Liu, Y., Woody, N. A., & Brown, S. D. (2004). An introduction to decision tree modelling. *Journal of Chemometrics*, 18 (6), 275–285.
 18. Janitza, S., Kruppa, J., König, I.R., & Boulesteix, A.-L. (2012). Overview of random forest methodology and practical guidance with emphasis on computational biology and bioinformatics. *WIREs Data Mining and Knowledge Discovery*, 2 (6), 493–507.
 19. Chen T and Guestrin C 2016 XGBoost: A Scalable Tree Boosting System[J].

20. K. Guolin, M. Qi, F. Thomas, W. Taifeng, C. Wei, M. Weidong, Y. Qiwei, L. Tie-Yan, "LightGBM: A Highly Efficient Gradient Boosting Decision Tree," *Advances in Neural Information Processing Systems* vol. 30, pp. 3149-3157, 2017.
21. Kuresan, H., Samiappan, D., and Masunda, S. (2019). Fusion of WPT and MFCC feature extraction in Parkinson's disease diagnosis. *Technol. Health Care* 27, 363–372. doi: 10.3233/THC-181306
22. Gunduz, Hakan. "Deep learning-based Parkinson's disease classification using vocal feature sets." *IEEE Access* 7 (2019): 115540-115551.
23. Marar, S., Swain, D., Hiwarkar, V., Motwani, N., and Awari, A. (2018). "Predicting the occurrence of Parkinson's disease using various classification models," in 2018 International Conference on Advanced Computation and Telecommunication (ICACAT) (Bhopal), 1–5. doi: 10.1109/ICACAT.2018.8933579
24. Goyal, Jinee, Padmavati Khandnor, and Trilok Chand Aseri. "A Comparative Analysis of Machine Learning classifiers for Dysphonia-based classification of Parkinson's Disease." *International Journal of Data Science and Analytics* 11, no. 1 (2021): 69-83.
25. Mathur, Richa, Vibhakar Pathak, and Devesh Bandil. "Parkinson disease prediction using machine learning algorithm." In *Emerging Trends in Expert Applications and Security*, pp. 357-363. Springer, Singapore, 2019.
26. KarapinarSenturk, Z. (2020). Early diagnosis of Parkinson's disease using machine learning algorithms. *Med. Hypoth.* 138:109603. doi: 10.1016/j.mehy.2020.109603

Development and Validation of Stability Indicating Rp-hplc Method for Quantitative Estimation of Lenalidomide in Lenalidomide Capsules Dosage Form

Ponnuri Bharath¹, P V Surendra Gupta¹, *Dittakavi Ramachandran^{1*}

¹Department of Chemistry, University College of Sciences, Acharya Nagarjuna University, Guntur-522 510, Andhra Pradesh, India.

Corresponding author E-mail: dittakavirc@gmail.com

Abstract

Highly sensitive RP-HPLC method developed for the quantification of Lenalidomide in Lenalidomide capsules dosage formulations. Samples are analyzed by means of reverse phase (RP-HPLC) using stationary phase an Kromasil C18 (150 x 4.6 mm, 5 μ m) and the mobile phase consisted of pH 2.5 phosphate buffer and acetonitrile in the ratio of (90:10 volume/volume). The flow rate is 1.0 mL/min. The column temperature was maintained at 30°C and sample cooler temperature was maintained at 5°C, injection volume 10 μ L and wavelength 210 nm. The developed HPLC method was validated with respect to specificity, precision, linearity, accuracy, solution stability and filter study. Validation study compared as per ICH guideline.

Key words: Lenalidomide, Forced degradation, validation and liquid chromatography.

Introduction

Lenalidomide (3-(4-amino-1-oxo-1,3-dihydro-2H-isoindol-2-yl) piperidine-2,6-dione) is an orally available thalidomide analog, which is showing both anti-angiogenic and immunomodulatory/anti-inflammatory properties. Lenalidomide is a drug used to

treat multiple myeloma, smoldering myeloma, and myelodysplastic syndromes (MDS) (1–7). It is marketed under the brand name Revlimid among other names. Figure 1 illustrates its chemical structure.

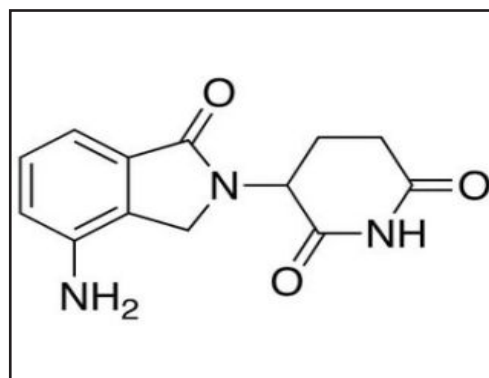


Figure 1. Chemical structure of Lenalidomide

According to an analysis of the literature, significant pharmacopeias, including the USP, EP, JP, and BP, do not include any LC procedures. Lenalidomide and its impurities have only been estimated using a few analytical techniques employing RP-HPLC and LC-MS techniques (8–11).

As a result, we worked to create an HPLC technique for quantifying lenalidomide in dosage forms for lenalidomide capsules. In

accordance with ICH recommendations (12–13), the current study presents a straightforward HPLC approach for the measurement of lenalidomide in lenalidomide capsule dose formulations.

Materials and Methods

Potassium dihydrogen orthophosphate, orthophosphoric acid, Hydrochloric acid, Sodium hydroxide and Hydrogen peroxide purchased from Merck, Mumbai, India. Acetonitrile, Methanol and Milli-Q water HPLC grade procured from Merck, India.

Preparation of pH 2.5 phosphate buffer

Potassium dihydrogen orthophosphate was carefully weighed at 1.3654 g and then added to 1000 mL of water, where it was well mixed. Then a diluted orthophosphoric acid solution was used to get the pH to 2.5. Filtered and sonicated to remove gas using a 0.45 membrane.

Preparation of mobile phase

Prepared a mixture of 900 mL of pH 2.5 phosphate buffer and 100 mL of acetonitrile in the ratio of 900:100 (%v/v).

Preparation of diluent

Mobile phase used as diluent.

Preparation of standard solution

Weighed and transferred 10,418 mg of Lenalidomide standard into a 100 mL volumetric flask, added about 70 mL of diluent, and sonicated until the standard was dissolved. Dilution to volume with diluent and thorough mixing.

Preparation of sample solution for 2.5 mg

Taken 1 capsule was placed in a 25 mL volumetric vial, 15 mL of diluent was added, and the mixture was sonicated for at least 20 minutes with intermittent stirring before being diluted to volume with diluent and thoroughly mixed. 10 minutes of centrifugation at 3000

revolutions per minute.

Preparation of sample solution for 5 mg

Taken 1 capsule was placed in a 50 mL volumetric vial, 30 mL of diluent was added, and the mixture was sonicated for at least 20 minutes with intermittent stirring before being diluted to volume with diluent and thoroughly mixed. 10 minutes of centrifugation at 3000 revolutions per minute.

Preparation of sample solution for 7.5 mg

Taken 1 capsule was placed into a 100 mL volumetric vial, 75 mL of diluent was added, and the mixture was sonicated for at least 20 minutes with intermittent stirring before being diluted to volume with diluent and thoroughly mixed. 10 minutes of centrifugation at 3000 revolutions per minute.

Preparation of sample solution for 10 mg

Taken 1 capsule was placed into a 100 mL volumetric vial, 75 mL of diluent was added, and the mixture was sonicated for at least 20 minutes with intermittent stirring before being diluted to volume with diluent and thoroughly mixed. 10 minutes of centrifugation at 3000 revolutions per minute.

Preparation of sample solution for 15 mg

Taken 1 capsule was placed in a 200 mL volumetric flask along with 150 mL of diluent, which was then sonicated for at least 20 minutes with periodic shaking before being diluted to volume with diluent and well mixed. Centrifuge the mixture for ten minutes at 3000 rpm.

Preparation of sample solution for 20 mg

Taken 1 capsule was placed in a 200 mL volumetric flask along with 150 mL of diluent, which was then sonicated for at least 20 minutes with periodic shaking. The diluent was then diluted to the volume before being mixed. The solution should be centrifuged at 3000 rpm for 10 minutes.

Preparation of sample solution for 25 mg

Taken 1 capsule was placed into a 250 mL volumetric flask, 150 mL of diluent was added, and the mixture was sonicated for at least 20 minutes with intermittent stirring before being diluted to volume with diluent and thoroughly mixed. 10 minutes of centrifugation at 3000 revolutions per minute.

Method development

Lenalidomide drug substance's maximum UV absorbance (max) was found at 210 nm, according to the UV-spectroscopic study.

Different mobile phases were used to generate an ideal peak shape in order to establish an appropriate and reliable HPLC technique for the analysis of lenalidomide in the dose form of capsules. Starting with Zodiac C18 (150x4.6mm, 3.5 m), the technique development was carried out using various mobile phase compositions, such as 0.1% orthophosphoric acid buffer and acetonitrile in an 85:15 volume/volume ratio. It was shown that greater retention times and unsatisfactory peak tailing occurred when lenalidomide was administered. The component was not suited for the stationary phase in the column. Change the column for the next experiment from Inertsil ODS-3V to Hypersil BDS. Lenalidomide was eluted at a void volume with an undesirable peak shape. Change the column for the next experiment from Hypersil BDS to Kromasil C18 (150 x 4.6mm, 5). The peak fronting of the usual Lenalidomide injection was unsatisfactory.

The mobile phase for the following experiment was composed of pH 2.5 phosphate buffer and acetonitrile in a volume-to-volume ratio of 90:10, a flow rate of 1.0 mL/min, a column temperature of 30°C, and a sampler cooler kept at 5°C. At 210 nm, UV detection was carried out. Lenalidomide was eluted at 9.50 minutes, and a satisfactory peak shape was observed. **Figure 2** displays the chromatogram of the Lenalidomide standard generated by

the suggested technique. **Table 1** displays the method's system suitability results.

Optimized chromatographic conditions

A Waters 2489 UV detector/2695 Separation Module with Empower3 software was used for the analysis. A Kromasil C18 (150 x 4.6mm, 5 m) column was employed as the stationary phase. Acetonitrile and pH 2.5 phosphate buffer in the mobile phase at a 90:10 volume/volume ratio. It moves at a rate of 1.0 mL/min. The sample cooler temperature was kept at 5°C, while the column temperature was kept at 30°C. The injection volume was 10 L, and the UV detection wavelength was 210 nm.

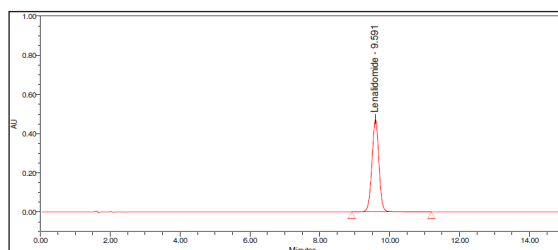


Figure 2. Typical chromatogram of Lenalidomide standard

Results and Discussion

The following parameters were used to thoroughly verify the devised RP-HPLC technique for the assay of lenalidomide in the formulation of lenalidomide capsules.

Specificity and System suitability

Blank and Placebo interference:

The research was done to see if placebo and blank effects interfered. The chromatography was injected with diluent and a placebo at the chromatographic conditions mentioned above, and the chromatograms of the two samples were recorded. The retention period of the signal for lenalidomide was not seen on the chromatogram of the blank solution in **Figure 3**. This shows that the diluent solution used to prepare the sample does not affect the estimate of lenalidomide in the dose form \

of lenalidomide capsules. Similar to this, the chromatogram of the placebo solution (**Figure 4**) did not exhibit any peaks at the Lenalidomide peak retention period. This shows that the placebo used to prepare the sample does not affect how much lenalidomide is estimated in the formulation of the lenalidomide capsules. **Table 2** displays the method's specificity findings.

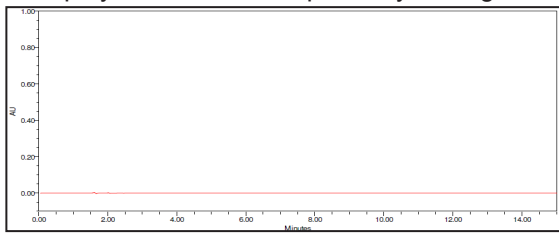


Figure 3. Typical chromatogram blank

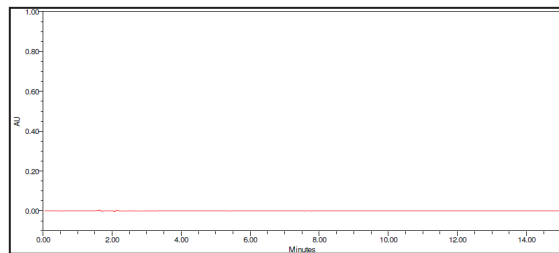


Figure 4. Typical chromatogram placebo

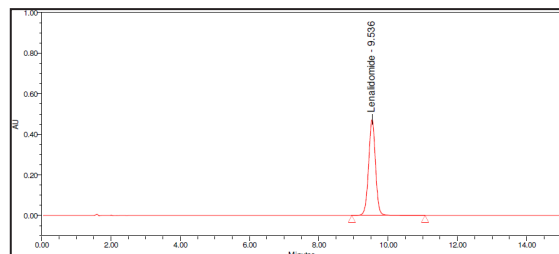


Figure 5. Typical chromatogram standard

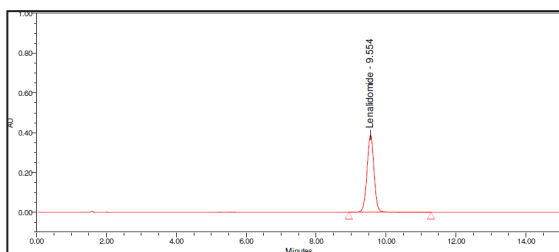


Figure 6. Typical chromatogram sample

Table 1. System suitability results

S.No.	System suitability parameters	Lenalidomide
1	Retention Time	9.591
2	Tailing factor	1.0
3	Theoretical plates	11292
4	%RSD of five replicate standard solution	0.10

Table 2. Specificity results

S. No	Name	Retention Time(min)	Blank	Placebo
1	Blank	ND	NA	NA
2	Placebo solution	ND	NA	NA
3	Standard solution	9.536	No	No
4	Sample solution	9.554	No	No

Force Degradation studies

To effectively separate degradants and contaminants from lenalidomide, research was done. The following stress conditions were applied to separate parts of the sample and placebo solutions in order to cause deterioration. Samples were fed into the HPLC system using a PDA detector, both stressed and unstressed. The findings of the degradation investigation were shown in **Table 3**.

Table 3. Forced degradation results

S.No.	Stress Degradation condition	%Assay	% Degradation
1	Unstressed Sample	100.6	N/A
2	Base stress sample (0.01N NaOH/5mL/15min/BT)	90.6	10
3	Acid stress sample (0.2N HCl/5mL/50°C/2.0 hrs.)	81.5	19.1
4	Peroxide stress sample (30% H ₂ O ₂ /5mL/4hours/RT)	89.9	10.7
5	Thermal stress sample (80°C/48 hours)	95.3	5.3
6	Water degradation at (5mL/50°C/2Hrs)	93.3	7.3

The circumstances of acid, alkali, and peroxide stress showed significant deterioration. Thus, it may be inferred that Lenalidomide is susceptible to oxidation, alkali, and acid.

System precision

The standard solution was made in accordance with the test procedure, administered six times via the HPLC system, and the % RSD for the area responses was assessed. **Table 4** presented the information.

Table 4. System precision results

S.No.	No. of injections	Peak area
1	Inj-1	6690611
2	Inj-2	6693203
3	Inj-3	6673512
4	Inj-4	6665745
5	Inj-5	6680308
6	Inj-6	6696503
Average		6683314
STDEV		12155.4371
% RSD		0.2

Results from six replicates of the standard solution were determined to have a relative standard deviation that was within the permissible range.

Method precision

Six samples of Lenalidomide capsules (2.5, 5.0, 7.5, 10, 15, and 25mg) were assayed to determine the accuracy of the test procedure. For each test preparation, the amount of Lenalidomide in mg and percent was determined. Calculations were used to determine the six preparations' average contents and the six observations' percent RSD. **Table 5** presented the information.

Table 5. Method precision results (% Assay)

S. No	Preparations	2.5 mg	5 mg	7.5 mg	10 mg	15 mg	20 mg	25 mg
1	Preparation 1	99.3	99.4	99.5	99.5	99.6	100.1	100.1
2	Preparation 2	99.7	99.8	99.4	99.4	99.9	100.2	100.2
3	Preparation 3	99.1	99.9	99.9	99.5	99.5	100.6	100.6
4	Preparation 4	100.3	99.2	99.7	99.1	99.6	99.5	100.0
5	Preparation 5	100.1	100.2	100.4	99.0	99.3	99.4	100.3
6	Preparation 6	99.0	100.3	100.5	99.2	99.9	100.8	100.5
Average		99.6	99.8	99.9	99.3	99.6	100.1	100.3
SD		0.5382	0.4336	0.4604	0.2137	0.2338	0.5657	0.2317
%RSD		0.54	0.43	0.46	0.22	0.23	0.57	0.23

Assay compliance rates overall and per person are within the parameters of the test technique. Six test preparations' relative standard deviations were determined to be within the specified range.

Linearity

By preparing solutions with concentration levels ranging from 25% to 150% of the usual concentration level, the linearity of the detector response for lenalidomide was proven. These solutions were added to the HPLC apparatus, and the results of the system's reactions were noted. It was done to plot concentration vs. peak area. It investigated how closely concentration and reaction correlated. As a result, a linear standard curve for the HPLC technique was determined and is

shown in **Figure 7**. **Table 6** is a summary of the observations.

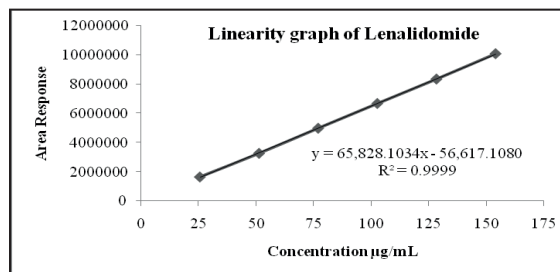


Figure 7. Calibration curve for Lenalidomide

Table 6. Linearity studies for Lenalidomide

S. No	Linearity Level	Concentration (ppm)	Area response
1	Linearity at 25%	25.6447	1668499
2	Linearity at 50%	51.2894	3283725
3	Linearity at 75%	76.9341	5001364
4	Linearity at 100%	102.5788	6693920
5	Linearity at 125%	128.2235	8366385
6	Linearity at 150%	153.8681	10097379
Correlation coefficient (r^2)			0.9999
Intercept			-56.617.1080
Slope			65828.1034
% Y-intercept			0.98

Table 7. Recovery studies for Lenalidomide

% Level	μg added	μg found	% Recovery	Mean % Recovery
50% level-1	50.3168	50.1151	99.6	99.5
50% level-2	50.1723	49.7936	99.2	
50% level-3	49.8353	49.6774	99.7	
100% level-1	101.2113	100.9433	99.7	99.5
100% level-2	101.2595	100.5417	99.3	
100% level-3	101.5484	101.0747	99.5	
150% level-1	150.7095	149.9274	99.5	99.8
150% level-2	150.6132	150.0996	99.7	
150% level-3	150.8540	151.0583	100.1	

Accuracy

By making recovery samples of Lenalidomide at concentrations ranging from 50% to 150% of the intended concentration level, the test method's accuracy was put to the test. For each concentration level of 50% and 150%, the recovery samples were made in triplicate preparations on Lenalidomide API spiked to placebo and then examined in accordance with the suggested procedure. The % recovery of each sample was computed for the quantity added after the chromatography of the aforementioned samples. By calculating the relative standard deviation of six preparations

for 50% and 150% level recovery sample data, it was possible to assess the accuracy of the recovery at each level. The gathered information is shown in **Table 7**.

Solution stability

Standards for solution stability and sample solutions were created under various circumstances, including bench top at ambient temperature and in a refrigerator at 2 to 8°C. The stability of standard and sample solutions was ascertained by contrasting previously created standard and sample solutions with recently prepared standard solutions.

Table 8. Solution stability of standard

Time Interval	Similarity factor	
	Room temperature	Refrigerator
Initial	NA	NA
24hrs	1.09	1.04
48hrs	1.11	1.08

standard and sample solutions are stable when kept on a bench top and in a refrigerator (2-8°C) for up to 48 hours.

Robustness studies

The chromatographic performance under different circumstances was assessed in comparison to the technique's nominal conditions in order to confirm the robustness of the method. At each of the aforementioned altered circumstances, the standard solution was injected.

The procedure can withstand variations in flow rate, pH, and column oven temperature.

Table 9. Solution stability of sample at room temperature

Time Interval	%Assay	%Assay difference
Initial	100.1	NA
24hrs	100.4	0.3
48hrs	100.6	0.5

Filter validation

One portion of the sample solution was centrifuged, while the other half was filtered through 0.45 m PVDF and 0.45 m Nylon filters as part of the filter validation process.

It was determined from the data above that 0.45 m PVDF filters are suitable. Therefore, 0.45 m PVDF filters had to be utilized for sample preparation.

Table 10. Solution stability of sample in Refrigerator

Time Interval	%Assay	%Assay difference
Initial	100.1	NA
24hrs	100.2	0.1
48hrs	100.2	0.1

The previously indicated solution stability parameter was determined. Both the

Table 11. Robustness studies Results

Parameter	Retention time	% RSD of standard	Tailing factor	Theoretical plates
Flow (mL/min)	1.0	9.59	0.20	11334
	1.2	8.99	0.38	12784
	0.8	10.21	0.57	8792
pH	2.5	9.59	0.20	11334
	2.7	9.73	0.46	10981
	2.3	9.11	0.51	9924
Column temperature (°C)	30	9.59	0.20	11334
	35	9.25	0.11	12753
	25	9.64	0.36	10952

Table 12. Results for Filter validation

S.No.	Filter details	Area Response	% Assay	% difference
1	Centrifuged Sample	6595670	100.4	NA
2	0.45 µm PVDF Filtered Sample	6501024	98.3	2.1
3	0.45 µm Nylon Filtered Sample	6590786	100.1	0.3

Conclusion

The new method was validated for several criteria, including accuracy, precision, linearity, specificity, solution stability, robustness, and filter validation, in accordance with ICH guidelines. The obtained results met the acceptance criteria. As a result, it is possible to conclude that the developed approach is simple, precise, cost-effective, environmentally friendly, and safe, and that it may be successfully used for routine analysis of Lenalidomide in Lenalidomide capsule dosage forms.

Acknowledgment

The authors are grateful to the Department of Chemistry, University College of Sciences, Acharya Nagarjuna University, Nagarjuna Nagar, Guntur, Andhra Pradesh, India, for providing the facilities to carry this research work.

Conflict of interests

The authors claim that there is no conflict of interest.

References:

1. Saravanan G, Ra B M, Ravikumar V, Suryanarayana M V, Someswararao N and Acharyulu P V R, *Chromatogr A*, 2007, 66(3/4), 287.
2. Naing A, Sokol L, List AF, *Journal of the National Comprehensive Cancer Network*. 2006; 4(1): 78-82. doi: 10.6004/jnccn.2006.0008.
3. Giagounidis AAN, Germing U, Aul C, *Clinical Cancer Research*. 2006; 12(1):5-10. doi: 10.1158/1078-0432.CCR-05-1437.
4. Anderson KC, *Seminars in Hematology*. 2005; 42(4): 3-8. doi:10.1053/j.seminhematol.2005.10.001.
5. Giagounidis AA, Germing U, Strupp C, Hildebrandt B, Heinsch M, Aul C. Prognosis of patients with del (5q) MDS and complex karyotype and the possible role of lenalidomide in this patient subgroup. *Annals Hematology*. 2005;84:569-71. doi: 10.1007/s00277-005-1054-1060.
6. Dredge K, Horsfall R, Robinson SP, Zhang LH, Lu L, Tang Y, Shirley MA, Muller G, Schafer P, Stirling D, Dalgleish AG, Bartlett JB, *Microvascular Research*. 2005; 69 (1-2): 56-63. doi: 10.1016/j.mvr.2005.01.002.
7. List A, Kurtin S, Roe DJ, Buresh A, Mahadevan D, Fuchs D, et al. Efficacy of lenalidomide in myelodysplastic syndromes. *New England Journal of Medicine*. 2005; 352 (6): 549-57. doi: 10.1056/NEJMoa041668.
8. Masoom Raza S, AlOthman ZA, Rahman N. Analytical techniques in pharmaceutical analysis. *Arabian Journal of Chemistry*. 2017; 10(1): S1409-S1421. <https://doi.org/10.1016/j.arabjc.2013.04.016>.
9. Sastry BS, Gananadhamu S, Prasad SVS, Venu GRK. New spectrophotometric methods for estimation of lenalidomide in pharmaceutical formulations. *Int. J. PharmTech Res*. 2009; 1: 416-419.
10. Saravanan G, Rao BM, Ravikumar M, Suryanarayana MV, Someswararao N, Acharyulu PVR. Development of an HPLC assay method for lenalidomide. *Chromatographia*. 2007; 66: 287-290. 10.1365/s10337-007-0290-y.
11. Maheswara RL, Janardhan RK, Bhaskar RL, Raveendra Reddy P. Development of a rapid and sensitive HPLC assay method for lenalidomide capsules and its related substances. *E-J. Chem*. 2012; 9: 1165-1174. doi:10.1155/2012/673736.

12. Premanand R, Gunasekaran V, Indrajeet S, Javed Ansari M. Development and validation of Lenalidomide in human plasma by LC-MS/MS. Saudi journal of biological sciences., 2018; 26(7):1843-1847. doi.org/10.1016/j.sjbs.2018.02.006.
13. Maher HM, Alzoman NZ, Alshehri MM, Aljohar HI, Shehata S, Alossaimi M, Abanmy NO. Simultaneous determination of dexamethasone and lenalidomide in rat plasma by solid phase extraction and ultra-performance liquid chromatography-tandem mass spectrometry: application to pharmacokinetic studies. Royal Society of Chemistry Advances. 2015; 5: 98600-98609. DOI: 10.1039/C5RA22339C.
14. ICH guidelines, for stability testing of new drug substances and products Q1A (R2), 2004.
15. ICH guidelines for validation of analytical procedures: text and methodology Q2 (R1) 2005.

Simple and Rapid DNA Isolation from Shrimps by Using Single tube extraction buffer with Single step

MVSS Pavan Kumar¹, A Ranganadha Reddy¹

¹. Department of Biotechnology, VFSTR Deemed to be University, Guntur, India 522213.

*Corresponding author: rangaaluri@gmail.com

Abstract

Aquaculture and aquatic animals are important for national food security since they are a good source of animal meat and protein for mankind. Aquaculture is currently the most economically and financially viable option for farmers, so the majority of them are interested in it. In aquaculture, shrimp farming plays a major role and exists in either a freshwater or marine environment for human consumption. Although shrimps are very susceptible to diseases during breeding and farming, these diseases are identified by several methods, i.e., microbiology test, antigen-antibody test and molecular methods. For molecular screening and testing of shrimps, it is necessary to extract nucleic acid, i.e., DNA (deoxyribonucleic acid). So many traditional and commercial methods are available on the market for nucleic acid extraction. In our study, we developed a simple, rapid, efficient, and effective nucleic acid extraction method. DNA was isolated from shrimps and shrimp seeds using this method (A_{260/280} range: 70 ng/uL to 350 ng/uL) and tested using molecular (PCR-Polymerase Chain Reaction) methods, specifically the SYBR Green assay on Real Time PCR.

Key words: Aquaculture, Shrimp, PCR, SYBR Green assay

Introduction

Aquaculture is the managed procedure of cultivating aquatic organisms which includes fish, aquatic plants, Molluscs and especially shrimp for human consumption(1). Shrimp is one of the most commercialized seafood products and shrimp farming is growing on a global scale(2). As a result of increasing consumer demand, the shrimp industry has become a large-scale operation. Shrimp aquaculture provides high-quality food products, socioeconomic development and significant employment opportunities for skilled and unskilled workers (3). In worldwide, the shrimp aquaculture industry faces many challenges, most importantly various bacterial, fungal & viral diseases. Viruses are considered the major pathogenic agent affecting shrimp aquaculture (4). To date, over 20 viral diseases have affected shrimp, primarily white spot disease and hepatic microsporidiosis. White spot disease caused by the white spot syndrome virus (WSSV), a double-stranded DNA virus that can cause 100% mortality in 2 to 10 days. The major targets of WSSV infection are ectodermic and mesodermic tissues in shrimp. Recent studies estimate the total economic loss of WSSV at USD 8-15 billion and it continues to increase by 1 billion a year (5). *Enterocytozoon hepatopenaei*(EHP) is an intra-

cellular microsporidian parasite that lyses epithelial cells in the liver and pancreas tubules in shrimp (6). Still, the life cycle of EHP & the way of eradication of this virus is completely obscure. So, the prevention and control of EHP is a challenge for the shrimp Industry (7). The key step in disease management requires that accurate and reliable diagnostic methods are available. To date, various diagnostic methods have been used for the detection of EHP and WSSV in shrimp, but it is crucial to choose the best methodology for the application. Molecular detection of shrimp diseases via PCR and LAMP is the most reliable method (8-9). Nucleic acid extraction is the preliminary step for every PCR based molecular assay. In conventional DNA isolation method and other chemical method has some disadvantages, i.e., phenol chloroform based extraction is time consuming, laborious & hazardous (10). Meanwhile, other commercial DNA extraction kits are available, but they are labour-intensive and costly for a large number of animal samples. It is therefore very important to develop a method for the rapid, simple and cost-effective detection of EHP and WSSV infection to prevent disease epidemics and economic losses associated with growing shrimp (11). In this study, we demonstrate the single-tube extraction method for DNA isolation of shrimp tissue. Our protocol does not require any hazardous organic solvents and has been deemed suitable for a PCR method. Our method will help shrimp farming communities find a less expensive and user-friendly diagnostic tool for detecting shrimp DNA viral disease.

Materials and Methods

Sample collection

Accurate sampling is one of the most important steps for determining the shrimp diseases. Prior to sampling, take note of any changes in the colour, appearance, or lesions of the shrimp (12). In our study, adult shrimps were collected from a farm area and shrimp seed from a hatchery. Samples were collected in sterile container with 1X PBS saline buffer (130

mM sodium chloride, 2 mM KCl, 10 mM sodium phosphate dibasic, 2 mM potassium phosphate mono basic and pH 7.4). After collection of samples, stored in a cold container maintain 2-8°C (13).

Nucleic acid extraction

Nucleic acid extraction is one of the major steps for molecular detection. Nucleic acids can be extracted from all living kingdoms like bacteria, virus, yeast, Plants, animals, human and also some dried samples. Several methods are used to extract the nucleic acids, i.e. chromatography based, alkaline based, silica based, salting out, CTAB, phenol-chloroform, magnetic bead based, filter based and paper based methods (14). So many commercial extraction method kits available in market like QIAamp, Roche MN kits etc., and different kinds protocols also available on web sites. Whatever, any extraction methods aim was to isolate good yield and purity of nucleic acid with minimal inhibitors. Nucleic Acid (either DNA or RNA) have to be extracted based on the study & targeted organism. In our study, WSSV & EHP viruses has a DNA as a genetic material. So we developed single tube shrimp DNA extraction method with simple, reliable, fast & cost-effective (15-16).

Single Tube Shrimp DNA Extraction Protocol (17):

The shrimp seeds (10 -12 nos) & specimen of adult shrimp was separately transferred to the 50 ml tube containing single step extraction Buffer solution as mentioned in Table 1. The tube was incubated at heating block at 65°C for 30 min. After incubation the required volume of upper clear solution was taken for the further analysis.

Evaluation of DNA Quantity

Nucleic acid quantification is crucial to obtaining precise and reliable data for many molecular biology tests, including PCR (polymerase chain reaction) and real-time PCR assays (18). Quantitative analysis carried out for 21 DNA

Simple and rapid dna isolation from shrimps by using single tube extraction buffer with single step

Table 1: Single tube extraction buffer composition:

Components	Concentration
KCl	100 mM
Tris-HCl	2 mM
MgCl ₂	10 mM
Glycerol	0.1%
NP 40	0.2%
Tween 80	0.1%
pH	7.0

samples which are extracted from shrimp seed and specimen of adult shrimp by using a UV visible spectrophotometer (Eppendorf BioPhotometer D30). The concentration and purity of DNA were determined from the A260/A280 ratio. The concentrations of the sample were in the range of 80 ng/uL to 365 ng/uL and an absorbance quotient value of 1.8 < ratio consider to be good purified DNA.

Real Time PCR

However, Animal tissues can contain inhibitory molecules that can affect PCR. Therefore, we tested if DNA from single tube extraction can be amplified directly by Real Time PCR (19). Real Time PCR is the result of PCR's incredible sensitivity as well as real-time monitoring of its products (20). In Real Time PCR, SYBR Green & TaqMan based methods are more more popularity & sensitivity. In current study, we used the SYBR Green assay for real-time PCR because it is inexpensive and simple to use. SYBR Green assay was performed on BIO-RAD CFX95 Real time System with using specific primers (21). Primers for housekeeping gene β -actin was (5'CAACCGTGAGAAGATGACTC3') and (5'AGCATGAGGAAGAGCATAAC 3'). Reaction mixture containing 10 uL of 2X TB Green Mix (Cat No. 1234), 1 uL of forward primer (10uM), 1 uL of reverse primer (10uM) and 8uL of single tube DNA. The condition used for the amplification was followed: Initial Denaturation 95°C for 3 mins, followed by 40 cycles of 94°C for 15 sec and 60°C for 30 sec. At the end of each

amplification cycle's extension phase, the fluorescence signal was acquired using 465 nm excitation and 510 nm emission wavelengths(22).

Evaluation of SYBR Green assay with melt curve

After the amplification, a melting curve analysis was done to confirm that only one gene-specific product had been synthesized. For each gene, a standard curve was generated to estimate amplification efficiency as shown in Figure 1.(23).

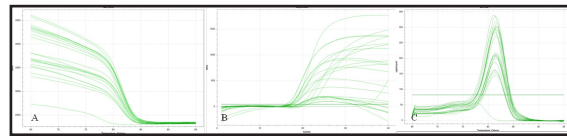


Fig 1: Amplification plot of shrimp DNA extracted by single tube extraction buffer. A. shows amplification plots on linear scale with fluorescence B. shows amplification plot on melt curve with linear scale C. shows determine melting temperature on melt curve analysis scale.

Results and Discussion

DNA Estimation

The results of this study showed that the single tube extracted shrimp DNA samples of 21 subjects ranged approximately 160 ng/uL(24). On purity assessment of shrimp samples we found that all 21 samples were within the optimal range of 1.5-2.4 as mentioned in Table 2.

Table 2: Quantitative results of Shrimp DNA samples extracted by single tube extraction buffer:

S.No.	Samples	Concentration (ng/uL)	A(260/280)
1	01	143	1.5
2	02	200	1.6
3	03	213	1.7
4	04	198	1.8
5	05	175	1.7
6	06	126	1.9
7	07	100	2.0
8	08	168	2.2

9	09	172	1.5
10	10	220	1.8
11	11	210	1.7
12	12	154	1.8
13	13	164	1.8
14	14	209	1.9
15	15	202	2.0
16	16	135	2.4
17	17	139	1.6
18	18	148	1.7
19	19	155	1.8
20	20	168	2.0
21	21	173	1.9

SYBR Green assay with melt curve

For set up of SYBR Green assay to detect beta actin gene from shrimp DNA by single tube extraction buffer. Satisfactory results were obtained as mentioned in Table 3.(25).

Conclusion

The performance of SYBR Green assay has been evaluated by amplification curves and melting temperatures. The melting curves of the SYBR Green assay with shrimp DNA isolated

Table 3: Melt curve temperatures of amplification of shrimp DNA samples

S.No.	Well	Fluorophore	Content	Sample	MeltTemp
1	A01	SYBR	Unkn	01	81.50
2	A02	SYBR	Unkn	09	81.50
3	A03	SYBR	Unkn	17	81.50
4	B01	SYBR	Unkn	02	81.00
5	B02	SYBR	Unkn	10	81.50
6	B03	SYBR	Unkn	18	81.50
7	C01	SYBR	Unkn	03	81.50
8	C02	SYBR	Unkn	11	81.50
9	C03	SYBR	Unkn	19	81.50
10	D01	SYBR	Unkn	04	81.50
11	D02	SYBR	Unkn	12	81.50
12	D03	SYBR	Unkn	20	81.50
13	E01	SYBR	Unkn	05	81.50
14	E02	SYBR	Unkn	13	81.50
15	E03	SYBR	Unkn	21	81.50
16	F01	SYBR	Unkn	06	81.50
17	F02	SYBR	Unkn	14	81.50
18	F03	SYBR	Unkn	22	81.50
19	G01	SYBR	Unkn	07	81.50
20	G02	SYBR	Unkn	15	81.00
21	G03	SYBR	Unkn	PC	81.50
22	H01	SYBR	Unkn	08	81.50
23	H02	SYBR	Unkn	16	81.50
24	H03	SYBR	NTC	NTC	None

Simple and rapid dna isolation from shrimps by using single tube extraction buffer with single step

by single tube extraction buffer were successfully evaluated. The evaluation of the SYBR Green assay on shrimp seed and tissue of adult shrimp samples already quantified by Biophometer method.

References

1. Wagner, C.V., Helenice, P.B., Patricia, M.V., Guilherme, W.B. and Ronaldo, O.C. (2021). Aquaculture in Brazil: past, present and future. *Aquaculture Reports*, 19: 100611. doi.org/10.1016/j.aqrep.2021.100611.
2. Boyd, C.E., McNevin, A.A. and Davis, R.P. (2022). The contribution of fisheries and aquaculture to the global protein supply. *Food Security*. 14: 805–827. doi.org/10.1007/s12571-021-01246-9
3. El-Saadony, M. T. , Swelum, A. A. , Abo Ghanima, M.M., Mustafa, S., Omar, A.A., Taha, A.E., Salem, H.M., El-Tahan, A.M., El-Tarabily, K.A. and Abd El-Hack, M.E. (2022). Shrimp production, the most important diseases that threaten it, and the role of probiotics in confronting these diseases: A review. *Research in Veterinary Science*, 144: 126-140. doi.org/10.1016/j.rvsc.2022.01.009.
4. Chellapandi, P. (2021). Development of top-dressing automation technology for sustainable shrimp aquaculture in India. *Discover Sustainability*, 2: 26. doi.org/10.1007/s43621-021-00036-9
5. Jun, W., Youjia, H., Kaihang, X., Xiaoyong, Z., Hongyan, S., Lanfen, F. and Muting, Y. (2019). White spot syndrome virus (WSSV) infection impacts intestinal microbiota composition and function in *Litopenaeus vannamei*. *Fish & Shellfish Immunology*, 84: 130-137. doi.org/10.1016/j.fsi.2018.09.076.
6. Werawich, P., Natthinee, M., Siripong, T., Kallaya, S. and Aldama-Cano, D.J. (2022). Shrimp microsporidian EHP spores in culture water lose activity in 10 days or can be inactivated quickly with chlorine. *Aquaculture*, 548, 2: 737665. doi.org/10.1016/j.aquaculture.2021.737665.
7. Shuhong, Z., Mengqiang, W., Mei, L., Keyong, J., Baojie, W. And Lei, W. (2020). Rapid detection of *Enterocytozoon hepatopenaei* in shrimp through an isothermal recombinase polymerase amplification assay. *Aquaculture*, 521: 734987. doi.org/10.1016/j.aquaculture.2020.734987.
8. Panchal, V., Kumar, S., Hossain, S.N. and Vasudevan, D. (2021). Structure analysis of thymidylate synthase from white spot syndrome virus reveals WSSV-specific structural elements. *International Journal of Biological Macromolecules*, 167: 1168–1175. doi.org/10.1016/j.ijbiomac.2020.11.071
9. Parisa, E., Mandana, B., Hassan, M. and Ghasem, D. (2022). Field-usable aptamer-gold nanoparticles-based colorimetric sensor for rapid detection of white spot syndrome virus in shrimp. *Aquaculture*, 548(2):737628. doi.org/10.1016/j.aquaculture.2021.737628.
10. Simon, S., Shamsul, A.B., Thompson, N., Nguyen, N.T., Rebecca, F. and Shiddiky, M.J.A. (2022). Latent potential of current plant diagnostics for detection of sugarcane diseases. *Current Research in Biotechnology*, 4: 475-492. doi.org/10.1016/j.crbiot.2022.10.002.
11. Chaijarasphong, T., Munkongwongsiri, N., Stentiford, G.D., Aldama-Cano, D.J., Thansa, K., Flegel, T.W., Sritunyaluksana, K. and Itsathitphaisarn, O. (2011). The shrimp microsporidian *Enterocytozoon hepatopenaei* (EHP): Biology, pathology, diagnostics and control. *Journal of Invertebrate Pathology*, 186: 107458. doi.org/10.1016/j.jip.2020.107458.

12. Kumar, V., Roy, S., Behera, B.K. and Das, B.K. (2021). Disease Diagnostic Tools for Health Management in Aquaculture. In: Pandey, P.K., Parhi, J. (eds) *Advances in Fisheries Biotechnology*. Springer, Singapore. doi.org/10.1007/978-981-16-3215-0_21
13. Ward, A., Hollister, J.R., McNally, K., Ritchie, D.L., Zanusso, G. And Priola, S.A. (2020). Transmission characteristics of heterozygous cases of Creutzfeldt-Jakob disease with variable abnormal prion protein allotypes. *Acta neuropathologica communications*, 8: 83. doi.org/10.1186/s40478-020-00958-x
14. Rajesh, P., Emily, O. and Qingshan, W. (2020). Advances in point-of-care nucleic acid extraction technologies for rapid diagnosis of human and plant diseases. *Biosensors and Bioelectronics*, 169: 112592. doi.org/10.1016/j.bios.2020.112592.
15. Zhi, C., Xuan, D., Pei-Zhuo, Z., Xiao-Yuan, W., Chen, L. and Jie, H. (2020). Development of a cost-efficient micro-detection slide system for the detection of multiple shrimp pathogens. *Analytical Biochemistry*, 599: 113735. doi.org/10.1016/j.ab.2020.113735.
16. Mishra, S.S., Rakesh D., Sahoo, S.N. and Swain, P. (2020). Chapter 14 - Biotechnological tools in diagnosis and control of emerging fish and shellfish diseases, Editor(s): Yashpal Singh Malik, Debmalya Barh, Vasco Azevedo, S.M. Paul Khurana, *Genomics and Biotechnological Advances in Veterinary, Poultry, and Fisheries*, Academic Press, 311-360. doi.org/10.1016/B978-0-12-816352-8.00014-X.
17. Lee, L. T., Ahmed, S.A., Siew, K.N., Marimuthu, C., Carsten, A.R., Timofey, S. R. and Thean, H.T. (2020). Rapid detection of porcine DNA in processed food samples using a streamlined DNA extraction method combined with the SYBR Green real-time PCR assay. *Food Chemistry*, 309: 125654. doi.org/10.1016/j.foodchem.2019.125654.
18. Nacham, O., Clark, K.D. and Anderson, J. L. (2016). Extraction and Purification of DNA from Complex Biological Sample Matrices Using Solid-Phase Microextraction Coupled with Real-Time PCR. *Analytical Chemistry*, 88: 7813–7820, doi.org/10.1021/acs.analchem.6b01861 (2016)
19. Amy, S.H., Madeline, G.R. and Hughes-Stamm, S. (2018). In-field collection and preservation of decomposing human tissues to facilitate rapid purification and STR typing, *Forensic Science International: Genetics*, 36: 124-129. doi.org/10.1016/j.fsigen.2018.06.015.
20. Zhang, H., Xu, Y., Fohlerova, Z., Chang, H., Iliescu, C. and Neuzil, P. (2019). LAMP-on-a-chip: Revising microfluidic platforms for loop-mediated DNA amplification, *TrAC. Trends in Analytical Chemistry*, 113: 44-53. doi.org/10.1016/j.trac.2019.01.015.
21. Zhang, D., Bai, C., Ge, K., Li, Y., Gao, W., Jiang, S. and Wang, Y. (2020). Establishment of an SYBR Green-based real-time PCR assay for porcine circovirus type 4 detection. *Journal of Virological Methods*, 285: 113963. doi.org/10.1016/j.jviromet.2020.113963.
22. Cruz-Flores, R., Mai, H.N. and Arun, K. D. (2019). Multiplex SYBR Green and duplex TaqMan real-time PCR assays for the detection of *Photobacterium* Insect-Related (Pir) toxin genes *pirA* and *pirB*. *Molecular and Cellular Probes*, 43: 20-28. doi.org/10.1016/j.mcp.2018.12.004.
23. Doan, P.T.K., Low, W.Y. and Ren, Y. (2022). Newcastle disease virus genotype VII

Simple and rapid dna isolation from shrimps by using single tube extraction buffer with single step

- gene expression in experimentally infected birds. *Science Reports*, 12: 5249. doi.org/10.1038/s41598-022-09257-y
24. Wu, X., Guangkun, T., Yang, J., Guo, Y., Huang, C., Sha, W. and Fangyou, Y. (2022). Prediction of Mycobacterium tuberculosis drug resistance by nucleotide MALDI-TOF-MS. *International Journal of Infectious Diseases*, 121, 47-54. doi.org/10.1016/j.ijid.2022.04.061.
25. Gulshan, K., Gireesh-Babu, P., Rajendran, K.V., Mukunda, G. and Aparna, C. (2022). Gain of function studies on predicted host receptors for white spot virus, Fish & Shellfish. *Immunology*, 131: 196-205. doi.org/10.1016/j.fsi.2022.09.010.

Protective Effect of *Annona Squamosa* Fruit Pulp on Motor Responses Following Intra-Medial Forebrain Bundle Injection of 6-OHda In Rat Model of Parkinson Disease

Sudha Muthusamy¹, Shanmuga Sundaram Rajagopal^{2*}, Sambathkumar Ramanathan³

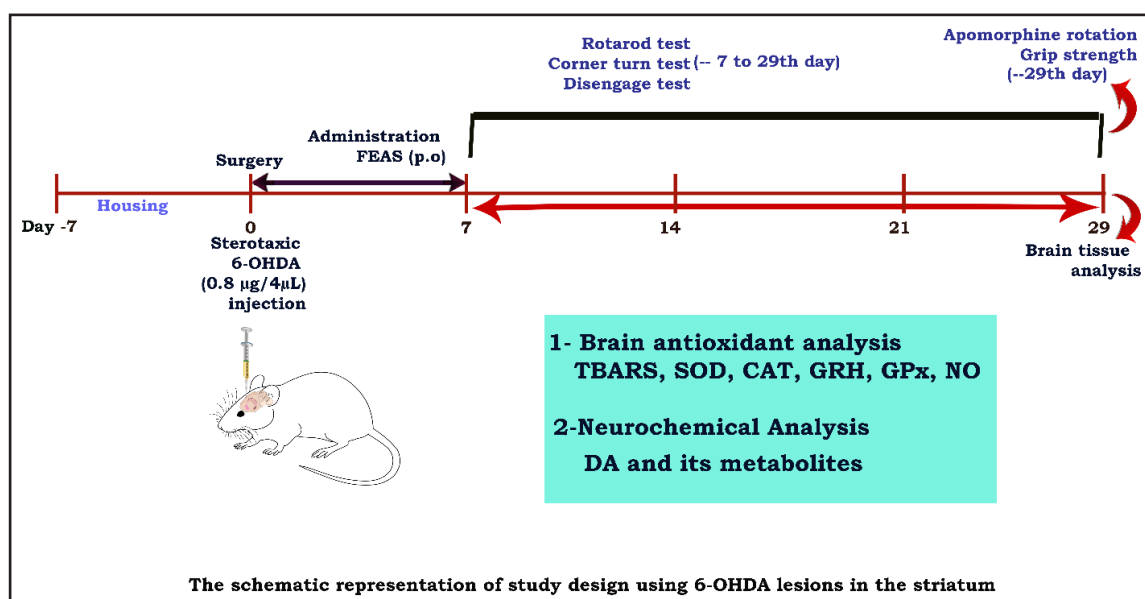
¹Department of Pharmacology, The Erode College of Pharmacy, Veppampalayam – 638 112

²Department of Pharmacology, J.K.K. Nattraja College of Pharmacy, Kumrapalayam – 638 183

³Department of Pharmaceutics, The Erode College of Pharmacy, Veppampalayam – 638 112

*Correspondent author: shansun34@gmail.com

Graphical Abstract



Abstract

Objective: The present study investigated the ethanolic extract of fruit pulp of *Annona squamosa* that ameliorates the 6-OHDA-induced behavioural, biochemical, and neurochemical changes which resemble Parkinson's disease (PD)-like symptoms.

Materials and Methods: Various behavioural

and biochemical parameters were carried out to evaluate the activity of ethanolic extract of fruit pulp of *Annona squamosa* (FEAS) on 6-OHDA treated rats. To determine the therapeutic significance of FEAS on PD, different behavioural tests such as apomorphine rotation, narrow beam maze, rotarod, grip strength, sensorimotor and disengage test and some biochemical tests along with neurochemical findings were

done. **Results:** 6-OHDA caused physical and behavioral abnormalities in animals, including abnormal posture, weak grip strength, and motor deficit. Biochemical analysis of brain homogenates in FEAS treated rats showed altered oxidative stress and elevated lipid biomarkers. Neurochemical alterations of the striatum of FEAS treated rats exhibit altered levels of catecholamines. FEAS administered for 07 days significantly enhanced motor function and behaviour tasks and further restored the invitro antioxidant changes in the brain. Furthermore, FEAS-II treatment significantly improved oxidative damage, which is denoted by the alterations in neurochemical changes of rat brain. **Conclusion:** In this research work, FEAS-I & II (200 mg/kg & 400 mg/kg) provided a remarkable neuroprotective impact, which was evidenced by behavioural and biochemical tests. It restored the behavioural and biochemical alterations caused by 6-OHDA and confirmed the strong neuroprotective mechanism of FEAS in 6-OHDA-intoxicated behavior and motor abnormalities.

Keywords: 6-hydroxydopamine, Annona squamosa Fruit, Parkinson's disease, Dopamine, Neurological disorder,

Introduction

Parkinson disease (PD) is characterised by the progressive degradation of dopamine (DA) neurons in the basal ganglia that innervate substantia nigra pars compacta (SNc)(1) which causes movement abnormalities, cognitive impairment, and sleep disturbances.(2)

Neurological disorders are currently one of the highest global causes of disability.(3) Parkinson's disease is the most prevalent movement disorder, excluding essential tremor, and the second most prevalent neurodegenerative disease after Alzheimer's disease.(4,5) Global PD prevalence estimates for 2019 exceeded 8.5 million individuals (6). PD affects 1-2 people per 1000 at any given moment. PD prevalence increases with the age, and from that 1% of the population older than 60 years is affected (7). PD is pathologically characterized by the loss

of nigrostriatal dopaminergic innervation; however, neurodegeneration does not include only nigral dopaminergic neurons but also cells from other parts of the neural network.

The premotor or prodromal phase of PD may begin 12–14 years prior to diagnosis (8). There is now substantial evidence that the disease may begin in the peripheral autonomic nervous system and/or the olfactory bulb, before spreading to the central nervous system and affecting the lower brainstem structures prior to affecting the substantia nigra.(9)

The majority of degenerative PDs belong to one of the two molecular classes -tauopathies or α -synucleinopathies – because of the pathological accumulation of the microtubule-associated tau protein or the presynaptic protein α -synuclein within vulnerable neurons and frequently glial cells as well. α -synuclein folds into β -helical structures through its N-terminus upon interaction with negatively charged lipids, like the phospholipids that form cell membranes upon interaction with negatively charged lipids. (10,11) In PD, α -synuclein adopts an amyloid-like β -sheet-rich structure that is prone to aggregate. Indeed, misfolded α -synuclein is found within Lewy Bodies (LBs) as filaments measuring 5–10 nm in length. Serine 129 phosphorylation, ubiquitination, and C-terminal truncation have all been proposed as mechanisms for the conformational changes that lead to abnormal α -synuclein aggregation. (12,13) Different species of α -synuclein, including unfolded monomers, soluble oligomers, protofibrils, and high molecular weight insoluble fibrils, are therefore present in the PD brain.(14)

Mitochondrial dysfunction is considered as a key factor in both idiopathic and familial PD pathogenesis.(15) Both PINK1 and parkin (PARK2 and PARK6, respectively) are essential components of the pathway that controls the removal of dysfunctional mitochondria, a process known as mitophagy.(16) Loss-of-function mutations in either gene cause defective mitochondrial quality control and autosomal recessive PD.(17, 18)

Mitochondrial complex-I deficiency may play a crucial role in DA cell death caused by energy depletion.⁽¹⁵⁾ Neurodegenerative diseases characterized by proteinopathies, which are abnormal protein accumulation, share proteasomal abnormalities as a common characteristic.⁽¹⁹⁾

In addition to a decrease in activity, the SNpc of PD brains also exhibits a lower expression of various proteasomal components. In particular, the 20S proteasome α -subunit⁽²⁰⁾ and other molecules involved in the regular function of the Ubiquitin-proteasome system (UPS), such as PA700 and PA28 (protease activators), are diminished.⁽²¹⁾ Genetic studies and the discovery that two of the PARK genes linked to monogenic PD encode proteins involved in UPS function, namely parkin (PARK2; E3 ubiquitin ligase)^(17,22) and UCH-L1, provide additional evidence (PARK5; Ubiquitin C-terminal hydrolase).⁽²³⁾

Similar to the UPS system, numerous lysosomal and autophagy-related components are dysfunctional or variably expressed in PD. In nigral neurons of PD brains, the autophagosome marker LC3-II was elevated, indicating an aggregation of autophagic vacuoles.^(24,25) At postmortem examination, vital lysosomal membrane proteins (LAMP1 and LAMP2A) and several heat-shock protein family molecular chaperones (such as hsc70 and hsp35) were found to be reduced.^(26,27)

Initially believed to be a secondary phenomenon, there is updated evidence that inflammatory responses can contribute to the pathogenesis of the disease on their own. In early studies with rodent models of PD (6-hydroxydopamine and MPTP), inhibition of microglial activation with minocycline pre- and post-neurotoxic insult significantly reduced DA cell death in the SNpc, suggesting that microglia-induced inflammatory processes may be contributing to the degeneration of these cells.^(28,29) Survival of dopamine neurons challenged under oxidative stress conditions.

It is essential to have the relevant disease models in order to comprehend the pathogenesis

of PD and develop potential therapies for improved symptom management. The neurotoxin 6-hydroxydopamine (6-OHDA) provides useful animal models of PD by inducing dopaminergic neuronal degeneration in the substantia nigra pars compacta (SNpc), which leads to a depletion of dopamine level in the striatum.⁽³⁰⁻³²⁾ To elucidate the underlying neuroprotective mechanism, we studied the effect of *Annona squamosa* fruit pulp extract (FEAS) on 6-OHDA-induced oxidative stress in rat dopaminergic neurons by examining the post-treatment effects of FEAS therapy on behavioral dysfunction, biochemical alterations, and dopamine level in the rat brain.

Materials and Methods

Extract preparation

The fruits of *Annona squamosa* Linn. (FEAS) were retrieved from the region of Namakkal District, Tamil Nadu, India. And obtained authentication from Botanical survey of India, Coimbatore. The fresh fruits were washed, and the pulps were scraped from the seeds using a glovebox under vacuum, lyophilized at -50°C , and ground into a powder. This mixture was then extracted with cold maceration by using 70% ethanol for 48 hours while being continuously stirred, yielding a viscous brownish yellow mass. A small proportion of the extract was subjected to preliminary phytochemical analysis, free radical scavenging activity and the other part was kept for future use in a vacuum desiccator.

Free Radical scavenging activity

The extract FEAS was analysed for free radical scavenging activity such as DPPH radical scavenging, hydroxyl radical scavenging, and superoxide scavenging activities are analysed.⁽³³⁾

Animals

Twenty-four adults male Wistar rats weighting 230-250 g were housed in a temperature-controlled room (at approximately 25°C), under 12-h light/dark cycle, with free access to food and water, at $21-22^{\circ}\text{C}$ and 50-55% humidity. The animal experiments were carried out in ac-

cordance with the approval of Institution animal ethical committee (KMCRET/Ph.D/07/2015-16). According to OECD 423 guidelines, the acute toxicity study was done.

Experimental Design

The experimental rats were divided into the following groups i) Sham operated received saline treatment ii) 6-OHDA lesioned group + saline iii) 6-OHDA lesioned group + Fruit pulp of ethanolic extract of *Annona squamosa* 200 mg/kg (6-OHDA + FEAS – I) iv) 6-OHDA lesioned group + Fruit pulp of ethanolic extract of *Annona squamosa* 400 mg/kg (6-OHDA + FEAS – II)

Each group consisted of 4–6 animals. After surgical procedures for the intra-striatal injection of 6-hydroxydopamine (6-OHDA) with saline, the animals were divided into four groups (n = 6 per group). Group I that received saline alone instead of 6-OHDA as a unilateral lesion. Group II received intra-striatal injection of 6-OHDA as a unilateral lesion. Groups III & IV received ethanolic extract of fruit extract of *Annona squamosa* (FEAS) 200 & 400 mg/kg for 07 days, consecutively after 6-OHDA injection.

0.8 µg 6-OHDA, dissolved in 4 µL physiological saline containing 0.1% ascorbic acid were administered through Hamilton syringe over 4.50 min; the syringe was left in place for 5 min after injection before being slowly removed. Sham-operated rats injected with saline. The sequence of experiments carried out in this study is graphically outlined in graphical abstract. At the seventh, fifteenth, and twenty-ninth day after surgery, behavioural tests were performed to evaluate the motor abilities of the animals. The animals were sacrificed at 29th day following the beginning of the treatment.

Behavioural assessments:

After receiving a 6-OHDA treatment, the animals' general behaviour was monitored for 4 weeks continuously, including body weight, food and water intake, body temperature, and urine output.⁽³⁴⁾ All animals underwent baseline meas-

urements of their behaviour in the following behavioural studies (Fig. 1-6).

Apomorphine turning behavior

The evaluation of motor function was carried out by apomorphine-induced rotation test on day 29 after 6-OHDA injection (Fig. 7). Apomorphine hydrochloride (0.5 mg/kg, i.p.) causes rotation in rats. After one-minute administration of apomorphine, the rotations were recorded; perfect and complete rotations were counted in a cylindrical container (33 cm diameter and 35 cm height) for 1 h in a noiseless separated room. Net numbers of rotations by turning contralateral & ipsilateral to the side of lesion were noted.⁽³⁵⁾

Rotarod

Motor performance was also evaluated with a Rotarod equipment, under the protocol which were previously described by Monville C.⁽³⁶⁾ Before administering 6-OHDA, the first three testing days provided as a training period. The animals were put through a four-trial test using an accelerating protocol that lasted 4 to 40 rpm in 5 minutes and given at least 20 minutes rest between trials. On the 7th, 15th, 21st, and 29th day, using the similar protocol, the latency to fall was then recorded.

Narrow beam maze

Animals were positioned on a narrow beam that was 1 m long and 80 cm above the ground. To ensure that the animal wouldn't be hurt if it fell, a 12 cm thick foam was placed exactly beneath the beam. The animal was set at one end of the beam, while the animal's residence cage was set at the other. A stopwatch was used to measure how long it took the animals to travel from their initial starting positions to the other end. The test was recorded as "timed out" at 2 minutes if animals refused to finish a beam run. The latency to start and total time to cross the beam were both recorded throughout this test.⁽³⁷⁾

Grip strength

Forelimb strengths of rats were measured using a grip strength meter.⁽³⁸⁾ To produce a reliable assessment of holding capability, the animals were pretrained for six training sessions on 1st-day, and the grip strength test was carried out on 29th day. Rat forelimbs were placed on the tension bar as they were positioned facing the grip strength meter's T bar. The rat was gently and steadily dragged away from the T bar by the root of the tail when it grabbed the bar. The grip strength meter was automatically calculated and recorded the force that each animal could produce in grams. Each animal measures were computed. Between measurements, the rats were given 30s to rest.

Sensorimotor test

The corner test assesses the direction pattern of sensorimotor dysfunction. It was initially applied on rats. It has been an established technique for evaluating sensory-motor function which is a valid way to spot and measure sensory and postural asymmetry.^(39,40) It offers a quick approach for identifying ipsilateral and contralateral steering deviation.

Disengage test

A tactile stimulus was placed towards the vibrissae, and a stopwatch was used to measure how long it took the rat to turn around and touch the probe with a paw. Paw extension was thus measured for the disengage test.⁽⁴⁰⁾

Biochemical Studies

After behavioral assessment (i.e., 29 days after surgery), the animals were deeply anesthetized. The brains were quickly removed and placed on an ice-cold Petridish. Rat brains will be fixed using a Microwave Fixation System. Striata from both sides are dissected from sham-operated, 6-OHDA-treated, extracts treated group of animals.⁽⁴¹⁾ To eliminate debris, the striatal tissue is homogenized in 250 μ l acetonitrile before being centrifuged at 13,000 g for 30 min. A stream of nitrogen is used to evaporate the acetonitrile after the supernatant has been collected and

cleaned with heptane. Re-suspending the sample in 75 μ l of mobile phase (37.5 mM phosphoric acid, pH 8.5) for the estimation of total protein and lipid peroxidation. The supernatant was again centrifuged at 15000 rpm for 1 h at 4°C. The supernatant obtained was used for further estimation of superoxide dismutase (SOD), catalase (CAT), glutathione (GSH), and lipid peroxidation (TBARS).

TBARS activity

Thiobarbituric acid reactive substances (TBARS) in the homogenate were estimated by the method of Ohkawa *et al.*,⁽⁴²⁾ The amount of lipid peroxidation was determined by using $\epsilon = 1.56 \times 10^5 \text{M}^{-1}\text{cm}^{-1}$ and expressed as TBARS nmoles/mg of protein.

Superoxide dismutase activity

Superoxide dismutase activity was determined based on SOD's potential to stop adrenaline's auto-oxidation to adrenochrome in an alkaline pH. The SOD activity (U/mg of protein) was calculated using the usual plot.⁽⁴³⁾

Catalase activity

The Caliborne method was used to analyze the catalase activity.⁽⁴⁴⁾ Changes in absorbance were noticed at 240 nm. nM H_2O_2 consumed/min/mg protein was used to measure catalase activity.

GRH activity

Glutathione reductase (GRH) activity was determined spectrophotometrically as described previously by Carlberg I.⁽⁴⁵⁾ The amount of nmol NADPH \cdot min \cdot mg⁻¹ protein used to express the enzyme activity.

GPx activity

The dismutation of H_2O_2 at 340 nm was used to measure GPx activity spectrophotometrically using the approach previously described by Wendel A.⁽⁴⁶⁾ The enzymatic activity was denoted as nmol NADPH \cdot min \cdot mg⁻¹ protein.

Total protein content

Total thiols were assayed on the principle of formation of relatively stable yellow color by sulfhydryl groups of DTNB. Protein content in the samples was determined by the method of Lowry et al.,⁽⁴⁷⁾

Nitric oxide estimation

The level of nitrite in the rat striatal tissue is an indicator of the production of nitric oxide (NO), which was determined according to the method of Kumar et al. (2012). By measuring nitrite, nitrate, and total nitrite indirectly in rat brain extract supernatants that were produced after centrifugation, nitric oxide was detected. The absorbance was then noted at 620 nm and 550 nm, respectively.⁽⁴⁸⁾

Neurochemical estimation

The method described by Patel was used to estimate the levels of brain catecholamines with a little modification.⁽⁴⁹⁾ By employing an electrochemical detector and a C18 reverse phase column, HPLC was used to determine the concentrations of catecholamines (DA) and their metabolites (DOPAC, HVA) in the striatum. Based on the standard curve created by employing standards with concentrations of 10-100 ng/ml that were homogenized in a solution containing 0.2 M perchloric acid, the quantities of the neurotransmitter and its metabolites were determined.

Statistical Analysis

The results were expressed as mean \pm standard error mean (SEM). Behavior parameters were analyzed by ordinary and repeated measures of one-way ANOVA (analysis of variance), followed by Dunnett's post hoc test, $p < 0.05$ was considered significant throughout the analysis.

Results and Discussion

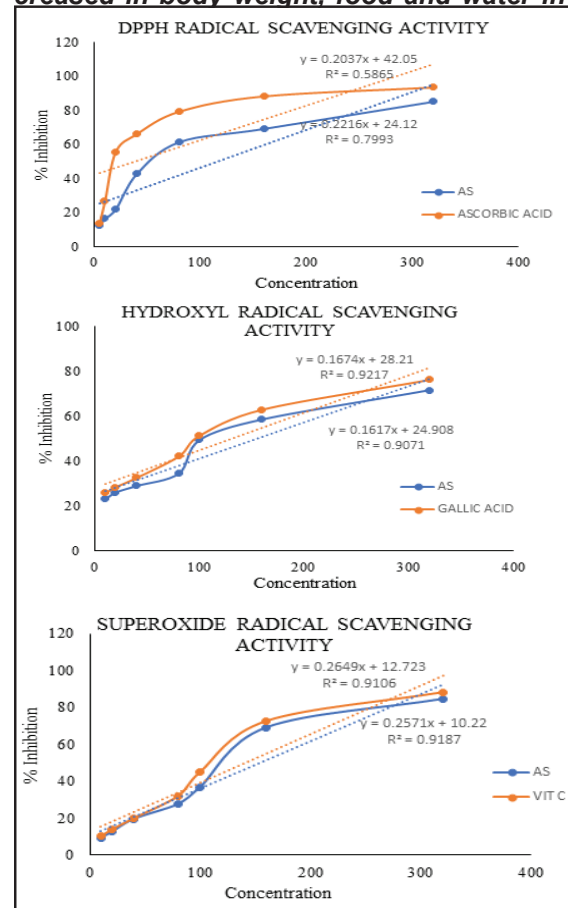
Effect of FEAS on preliminary phytochemical analysis

The extract was subjected to preliminary phytochemical screening. Tests for alkaloids, proteins, steroids, phenols, tannins, flavonoids,

gums and mucilage, glycosides and saponins were tested positive using Trease GE and Evans WC methods. And from the radical scavenging activity the IC₅₀ value was found to be 116.78, 155.17, and 140.72 respectively, which shows that the inhibitory concentration of FEAS was higher than that of standards. (Fig.1)

Fig 1. Effect of FEAS on free radical scavenging activity such as DPPH, and superoxide Scavenging activities.

Effect of FEAS on 6-OHDA induced decreased in body weight, food and water in-



take, body temperature, and urinary output

It was observed that administration of 6-OHDA significantly reduced the body weight, food and water intake, urinary output ($p=0.2080$;

$p=0.0223$; $p=0.0337$; $p=0.1272$) but increased body temperature ($p<0.0001$) when compared to sham operated group respectively. However, treatment with FEAS-I & II (200mg/kg & 400 mg/kg) started to restore the body weight, food and water intake, and volume of urine output compared to the 6-OHDA treated group. Moreover, treatment with FEAS-II (400 mg/kg/day) significantly and dose-dependently ameliorated the loss in body weight compared to FEAS-I (200 mg/kg/day) treated group (Figs. 2, 3, 4, 5, 6).

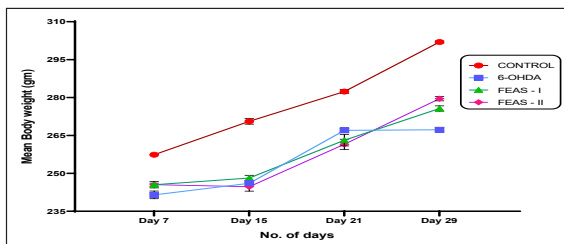


Fig 2. Effect of 6-OHDA and FEAS post-treatment on the body weights (Mean \pm SEM) of each group of rats were recorded. Data are shown as Mean \pm SEM; $n = 06$ rats for each group. * $p \leq 0.05$, ** $p \leq 0.01$, *** $p \leq 0.001$, **** $p \leq 0.0001$, as compared with sham groups. Statistical analysis was done by one-way analysis of variance (ANOVA) and Dunnett's post hoc comparison test.

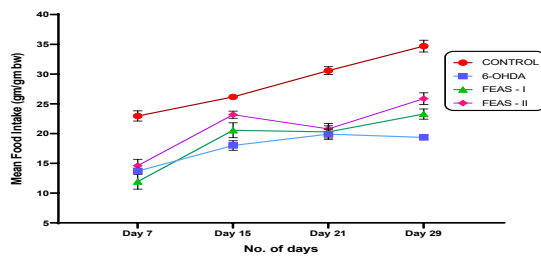


Fig 3. Effect of 6-OHDA and FEAS post-treatment on the food intake (Mean \pm SEM) of each group of rats were recorded. Data are shown as Mean \pm SEM; $n = 06$ rats for each group. * $p \leq 0.05$, ** $p \leq 0.01$, *** $p \leq 0.001$, **** $p \leq 0.0001$, as compared with sham groups. Statistical analysis was done by one-way ANOVA and Dunnett's post hoc comparison test.

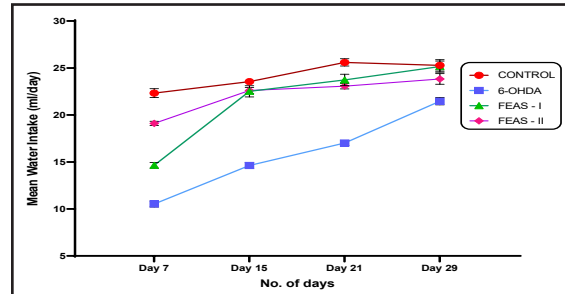


Fig 4. Effect of 6-OHDA and FEAS post-treatment on the water intake (Mean \pm SEM) of each group of rats were recorded. Data are shown as Mean \pm SEM; $n = 06$ rats for each group. * $p \leq 0.05$, ** $p \leq 0.01$, *** $p \leq 0.001$, **** $p \leq 0.0001$, as compared with sham groups. Statistical analysis was done by one-way ANOVA and Dunnett's post hoc comparison test.

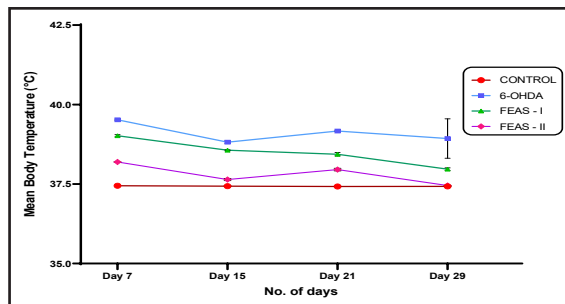


Fig 5. Effect of 6-OHDA and FEAS post-treatment on the body temperature (Mean \pm SEM) of each group of rats were recorded. Data are shown as Mean \pm SEM; $n = 06$ rats for each group. * $p \leq 0.05$, ** $p \leq 0.01$, *** $p \leq 0.001$, **** $p \leq 0.0001$, as compared with sham groups. Statistical analysis was done by one-way ANOVA and Dunnett's post hoc comparison test.

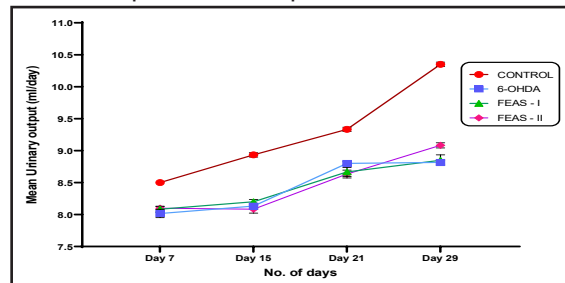


Fig 6. Effect of 6-OHDA and FEAS post-treatment on the urinary output (Mean \pm SEM) of each group of rats were recorded. Data are shown as Mean \pm SEM; $n = 06$ rats for each group. * $p \leq 0.05$, ** $p \leq 0.01$, *** $p \leq 0.001$, **** $p \leq 0.0001$, as compared with sham groups. Statistical analysis was done by one-way ANOVA and Dunnett's post hoc comparison test.

ment on the urinary output (Mean \pm SEM) of each group of rats were recorded. Data are shown as Mean \pm SEM; n = 06 rats for each group. *p \leq 0.05, **p \leq 0.01, ***p \leq 0.001, ****p \leq 0.0001, as compared with sham groups. Statistical analysis was done by one-way ANOVA and Dunnett's post hoc comparison test.

Effect of FEAS on 6-OHDA induced changes in apomorphine activity, rotarod and grip strength, and narrow beam walk performance of rats

Apomorphine activity and narrow beam maze (NBM) walk performance was significantly increased on 6-OHDA administration (on the 29th day) as compared to sham operated group (p < 0.001). Treatment with FEAS-I & II (200 and 400 mg/kg) significantly attenuated the total turns per hour in apomorphine rotation and latency to start and transfer latency in NBM as compared to 6-OHDA group (p < 0.001). Moreover, concomitant administration of FEAS-II (400 mg/kg/day) significantly reduced the turns start latency and transfer latency as compared to FEAS-I (200 mg/kg/day) treated group (Figs. 7, 8).

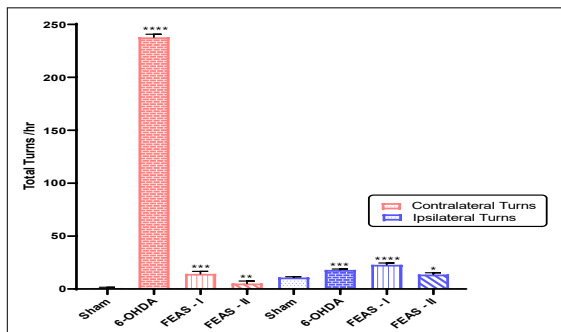


Fig 7. Effect of 6-OHDA and FEAS post-treatment on the apomorphine rotation (Mean \pm SEM) of each group of rats were recorded. Data are shown as Mean \pm SEM; n = 06 rats for each group. *p \leq 0.05, **p \leq 0.01, ***p \leq 0.001, ****p \leq 0.0001, as compared with sham groups. Statistical analysis was done by one-way ANOVA and Dunnett's post hoc comparison test.

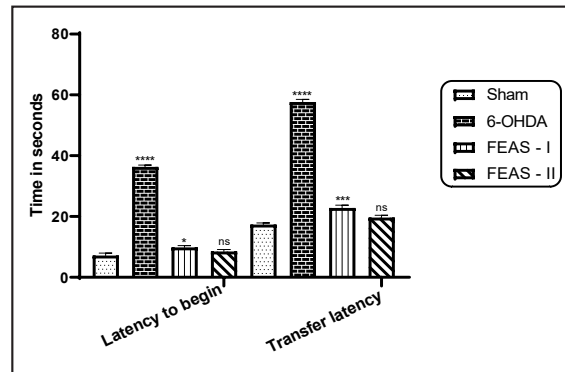


Fig 8. Effect of 6-OHDA and FEAS post-treatment on the activity on narrow beam maze (Mean \pm SEM) of each group of rats were recorded. Data are shown as Mean \pm SEM; n = 06 rats for each group. *p \leq 0.05, **p \leq 0.01, ***p \leq 0.001, ****p \leq 0.0001, as compared with sham groups. Statistical analysis was done by one-way ANOVA and Dunnett's post hoc comparison test.

Rotarod activity and grip strength performance were decreased with 6-OHDA administration (on the 29th day) compared to sham-operated group (p = 0.004; p < 0.0001). Treatment with FEAS-I & II (200 and 400 mg/kg) significantly improved the latency to fall, impaired grip strength, and locomotor activity as compared to 6-OHDA group. Furthermore, continuous administration of FEAS-II (400 mg/kg) extremely attenuated the duration of fall, latency and impaired grip strength compared to FEAS-I (200 mg/kg) treated group. (Figs. 9, 10).

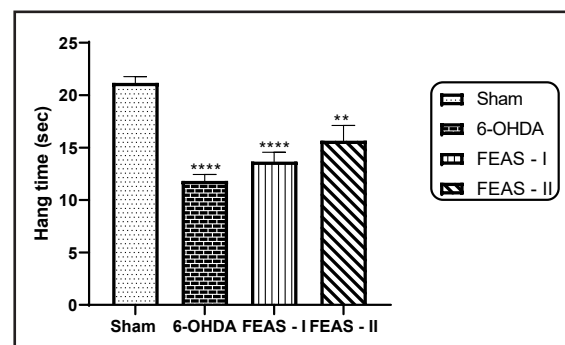


Fig 9. Effect of 6-OHDA and FEAS post-treatment on the rotarod activity (Mean \pm SEM) of

each group of rats were recorded. Data are shown as Mean \pm SEM; n = 06 rats for each group. *p \leq 0.05, **p \leq 0.01, ***p \leq 0.001, ****p \leq 0.0001, as compared with sham groups. Statistical analysis was done by one-way ANOVA and Dunnett's post hoc comparison test.

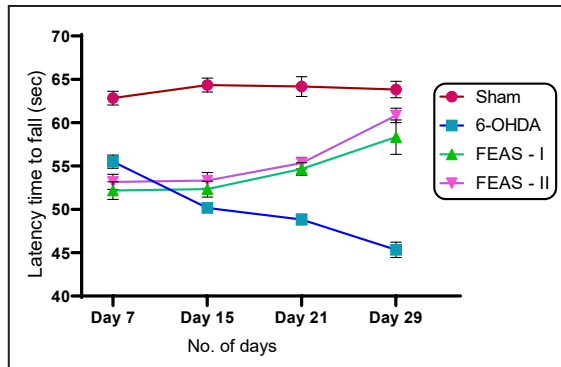


Fig 10. Effect of 6-OHDA and FEAS post-treatment on the grip strength activity (Mean \pm SEM) of each group of rats were recorded. Data are shown as Mean \pm SEM; n = 06 rats for each group. *p \leq 0.05, **p \leq 0.01, ***p \leq 0.001, ****p \leq 0.0001, as compared with sham groups. Statistical analysis was done by one-way ANOVA and Dunnett's post hoc comparison test.

Effect of FEAS on 6-OHDA induced changes in sensorimotor and disengage activity of rats

In sham-operated rats, the turns on both sides were equal. The total count was calculated by applying the formula, which denotes the spontaneous turning latency. Thus, the turning latency noted in rats lesioned with 6-OHDA developed a preference for spontaneous turning towards the contralateral side and the latency(0 to 29th day) was significantly increased on 6-OHDA administration as compared to sham operated group (p = 0.0005) as the lesioned rats turns more on contralateral side. Treatment with FEAS-I & II (200 and 400 mg/kg) significantly attenuated the turn latency on the single side.

Duration of forelimb paw extension was increased on 6-OHDA administration (on the 29th day) due to disengage activity compared to

sham-operated group (p = 0.0196). Treatment with FEAS-I & II (200 and 400 mg/kg) significantly attenuated the latency of paw extension as compared to 6-OHDA group. (Figs. 11, 12).

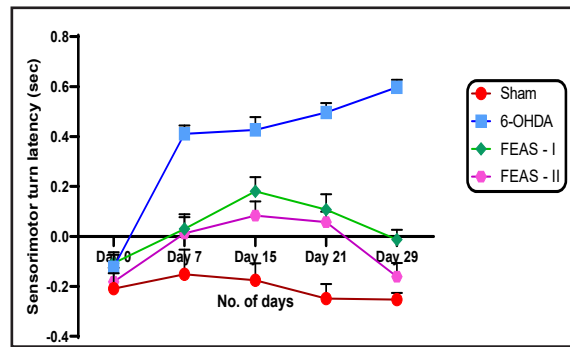


Fig 11. Effect of 6-OHDA and FEAS post-treatment on the sensorimotor turn latency (Mean \pm SEM) of each group of rats were recorded. Data are shown as Mean \pm SEM; n = 06 rats for each group. *p \leq 0.05, **p \leq 0.01, ***p \leq 0.001, ****p \leq 0.0001, as compared with sham groups. Statistical analysis was done by one-way ANOVA and Dunnett's post hoc comparison test.

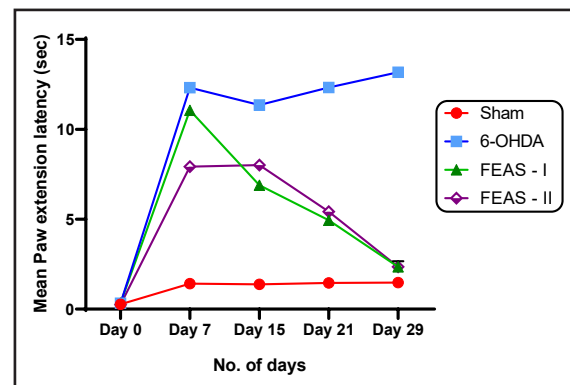


Fig 12. Effect of 6-OHDA and FEAS post-treatment on the forelimb paw extension latency (Mean \pm SEM) of each group of rats were recorded. Data are shown as Mean \pm SEM; n = 06 rats for each group. *p \leq 0.05, **p \leq 0.01, ***p \leq 0.001, ****p \leq 0.0001, as compared with sham groups. Statistical analysis was done by one-way ANOVA and Dunnett's post hoc comparison test.

Effect of FEAS on 6-OHDA induced changes in brain antioxidant levels in rats

Systemic administration of 6-OHDA had a significantly elevated level of oxidative stress parameters, i.e., TBARS and nitrite levels in the striatum with fall of SOD, CAT, GRH, GPx levels

as compared to the sham-operated group ($p < 0.0001$). However, treatment with FEAS-I & II (200 and 400 mg/kg) significantly ameliorated the oxidative stress with restoration of SOD, CAT, GRH, GPx levels as compared to 6-OHDA treated group ($p < 0.0001$). (Fig. 13).

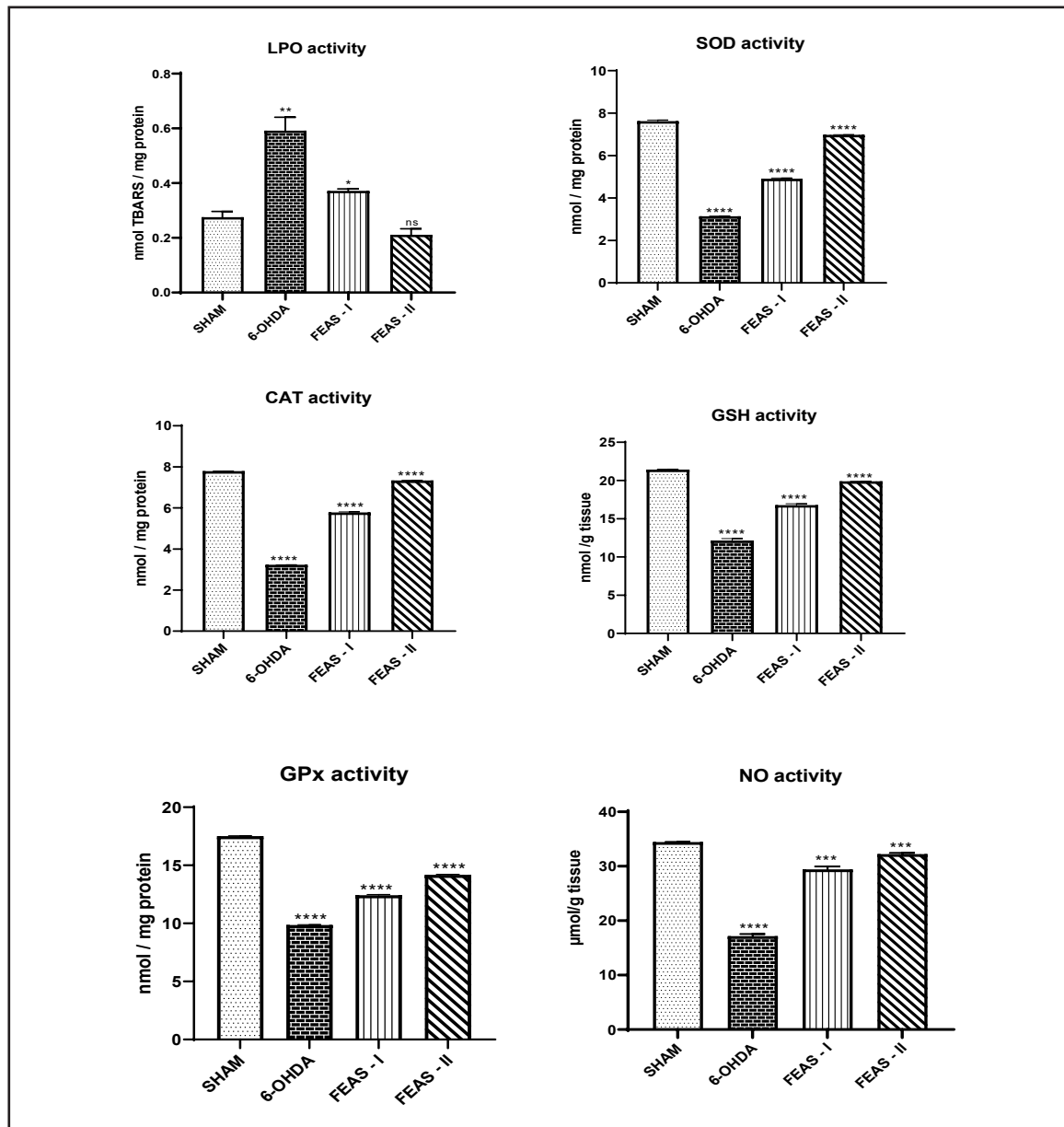


Fig 13. Effect of 6-OHDA and FEAS post-treatment on the brain antioxidant levels (Mean \pm SEM) of each group of rats were recorded. Data are shown as Mean \pm SEM; n = 06 rats for each group. *p

≤ 0.05 , $**p \leq 0.01$, $**p \leq 0.001$, $***p \leq 0.0001$, as compared with sham groups. Statistical analysis was done by one-way ANOVA and Dunnett's post hoc comparison test.

Effect of FEAS with 6-OHDA on striatal dopamine and its metabolites

The level of catecholamine (dopamine) was found to be significantly decreased in the striatum after treatment with 6-OHDA as compared to sham operated group. But its metabolites (DOPAC and HVA) were observed to be elevated in the striatum after treatment with 6-OHDA compared to sham-operated group ($p < 0.0001$). Treatment with FEAS-I & II (200 and 400 mg/kg) significantly and dose dependently ameliorated the alteration in catecholamine and its metabolite level in the striatum as compared to 6-OHDA alone treated group. (Fig. 14)

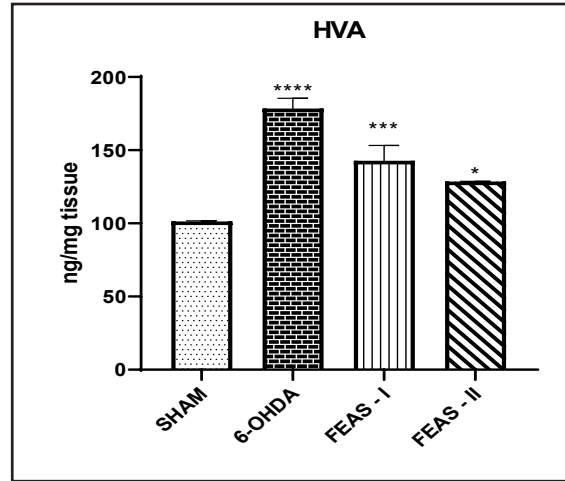
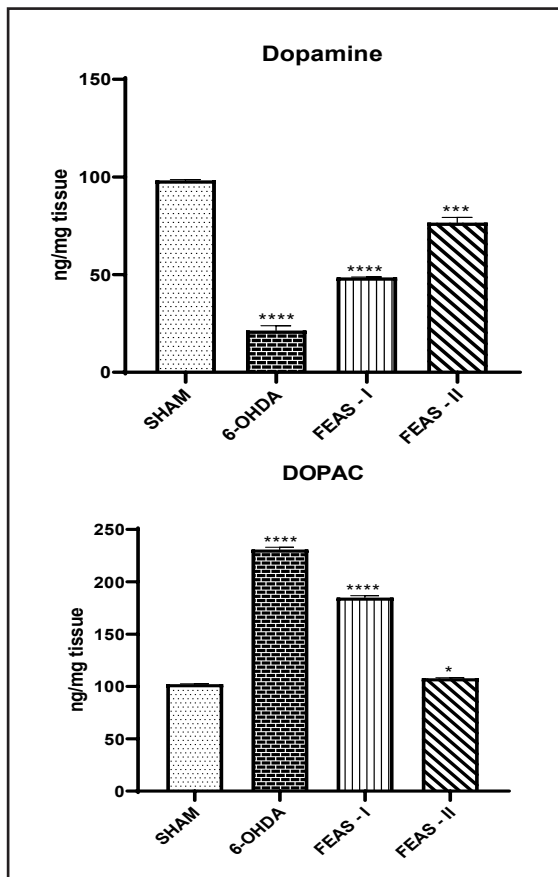


Fig 14. Effect of 6-OHDA and FEAS post-treatment on the neurochemicals (Mean \pm SEM) of each group of rats were recorded. Data are shown as Mean \pm SEM; $n = 06$ rats for each group. $*p \leq 0.05$, $**p \leq 0.01$, $**p \leq 0.001$, $***p \leq 0.0001$, as compared with sham groups. Statistical analysis was done by one-way analysis of variance (ANOVA) and Dunnett's post hoc comparison test.

An investigation using UPLC-ESI-MS/MS sheds new light on the phenolic composition of *Annona squamosa* fruit pulp. And found a total of 16, 15 and 13 free, bound, and esterified phenolic compounds, respectively, in the extracts of *Annona squamosa* Linn. fruit pulp. From Fig. 1, it is also confirmed that the IC₅₀ value of the extract was found to be higher against DPPH, hydroxyl, and superoxide radical scavenging activity.

When 6-OHDA injected directly into the hypothalamus, it had a profound effect on behavioral studies even when injected in a volume smaller. But this study demonstrates the effect of *Annona squamosa* Linn. fruit pulp in 6-OHDA induced Parkinson disease, and it is confirmed from the behavioral analysis, biochemical and neurochemical analysis.

Treatment with FEAS-I & II (200 and 400 mg/kg) significantly attenuated the 6-OHDA induced motor deficit, oxidative damage, neuroinflammation and alterations in striatal neurotransmitter

levels in rats. A single intranigral administration of 6-OHDA to experimental rat's cause PD like symptoms due to its selectivity for striatal dopaminergic neurons, serve as widely accepted experimental model of PD. Through the early onset of hyperkinetic movements followed by hypokinesia, it causes chronic motor deficit and replicates many characteristics of PD patients.⁽⁴⁹⁾ Similarly, in the present study treatment with 6-OHDA produces stable motor deficit as confirmed by increase in transfer latency in narrow beam walk, loss of grip strength, decrease in fall of time in rotarod indicate the motor impairment and dysfunctioning of striatal nuclei.

Additionally, earlier research suggested that the main pathophysiological causes of PD were oxidative stress, mitochondrial dysfunction, excitotoxicity, and neuroinflammation. Oxidative stress in neurons is further facilitated by faulty mitochondrial action and low ATP levels. This further contributes to excessive Ca^{2+} discharge via NMDA. Literature of this sort demonstrates that 6-OHDA injection considerably retards striatal cholinergic and dopaminergic neurons, which lowers catecholamine levels (dopamine) and increased the level of DOPAC and HVA in the striatum nuclei.⁽⁵⁰⁾ This study found that acute 6-OHDA injection significantly increased levels of lipid peroxidation (LPO) and nitrite while depleting antioxidants like SOD, CAT, GSH, and GPx suggested that oxidative stress may play a role in PD.⁽⁵¹⁾

CONCLUSION

The results of the current study indicate that FEAS-I & II (200, 400 mg/kg) corrected the behavioral, biochemical, neuroinflammatory, and chemical deficits brought on by 6-OHDA. FEAS-I & II have been shown to have neuroprotective effects, and these effects are related to their antioxidant and anti-inflammatory properties as well as their ability to modify neurotransmitter levels in the basal ganglia circuit. Also, it is confirmed that FEAS-II (400 mg/kg) is proved to have the therapeutic effect for the treatment of Parkinson's disease (PD), although more re-

search is needed to delve into obscure targets.

REFERENCES

1. Hornykiewicz, O.(2002). Dopamine miracle: from brain homogenate to dopamine replacement. *Movement Disorders*, 17:501–508.
2. Falquetto, B., Thieme, K., Malta, M.B., E. Rocha, K.C., Tuppy, M., Potje, S.R., Antoniali, C., Rodrigues, A.C., Munhoz, C.D., Moreira, T.S., Takakura, A.C. (2020). Oxidative stress in the medullary respiratory neurons contributes to respiratory dysfunction in the 6-OHDA model of Parkinson's disease. *The Journal of Physiology*, 598(22):5271-5293.
3. Elbaz, A., Nichols, E., et al. (2018). GBD 2016 Parkinson's Disease Collaborators ER. Global, regional, and national burden of Parkinson's disease, 1990-2016: a systematic analysis for the global burden of disease study 2016. *Lancet Neurology*, 17:939-953.
4. Alves, G., Forsaa, E.B., Pedersen, K.F., DreetzGjerstad, M., Larsen J.P. (2008). Epidemiology of Parkinson's disease. *Journal of Neurology*. 255:18-32.
5. Ascherio, A., Schwarzschild, M.A. (2016). The epidemiology of Parkinson's disease: risk factors and prevention. *Lancet Neurology*, 15:1257-1272.
6. Parkinson disease - key facts. Published on 13th June 2022. Available at <https://www.who.int/news-room/fact-sheets/detail/parkinson-disease> (Accessed on 16 November 2022).
7. Tysnes, O.B., Storstein, A. (2017). Epidemiology of Parkinson's disease. *J Neural Transm (Vienna)*. 124(8):901-905.

8. Postuma, R.B., Aarsland, D., Barone, P., Burn, D.J., Hawkes, C.H., Oertel, W., et al. (2012). Identifying prodromal Parkinson's disease: Pre-motor disorders in Parkinson's disease. *Movement Disorder*, 27(5):617–26.
9. Katzenschlager, R., Head, J., Schrag, A., Ben-Shlomo, Y., Evans, A., Lees, A.J., et al. (2008). Fourteen-year final report of the randomized PDRG-UK trial comparing three initial treatments in PD. *Neurology*, 71(7):474–80.
10. Dickson, D.W. (2012). Parkinson's disease and parkinsonism: neuropathology. *Cold Spring Harbor Perspectives in Medicine*. 2(8):a009258.
11. Eliezer, D., Kutluay, E., Bussell, R., Browne, G. (2001). Conformational properties of α -synuclein in its free and lipid-associated states. Edited by P. E. Wright. *Journal of Molecular Biology*, 307(4):1061–73.
12. Fujiwara, H., Hasegawa, M., Dohmae, N., Kawashima, A., Masliah, E., Goldberg, M.S., et al. (2002). Alpha-Synuclein is phosphorylated in synucleinopathy lesions. *Nature Cell Biology*, 4(2):160–4.
13. Barrett, P.J., Timothy, G.J. (2015). Post-translational modification of α -synuclein in Parkinson's disease. *Brain Research*, 1628(Pt B):247–53.
14. Baba, M., Nakajo, S., Tu, P.H., Tomita, T., Nakaya, K., Lee, V.M., et al. (1998). Aggregation of alpha-synuclein in Lewy bodies of sporadic Parkinson's disease and dementia with Lewy bodies. *The American Journal of Pathology*, 152(4):879–84.
15. Pickrell, A.M., Youle, R.J. (2015). The roles of PINK1, Parkin and mitochondrial fidelity in Parkinson's disease. *Neuron*, 85(2):257–73.
16. Kitada, T., Asakawa, S., Hattori, N., Matsumine, H., Yamamura, Y., Minoshima, S., et al. (1998). Mutations in the parkin gene cause autosomal recessive juvenile parkinsonism. *Nature*, 392(6676):605–8.
17. Moon, H.E., Paek, S.H. (2015). Mitochondrial dysfunction in Parkinson's disease. *Experimental Neurobiology*, 24(2):103–16.
18. Valente, E.M., Bentivoglio, A.R., Dixon, P.H., Ferraris, A., Ialongo, T., Frontali, M., et al. (2001). Localization of a novel locus for autosomal recessive early-onset Parkinsonism, PARK6, on human chromosome 1p35-p36. *The American Journal of Human Genetics*, 68(4):895–900.
19. McKinnon, C., Tabrizi, S.J. (2014). The Ubiquitin-Proteasome system in neurodegeneration. *Antioxidants Redox Signaling*, 21(17):2302–21.
20. McNaught, K.S.P., Belizaire, R., Jenner, P., Olanow, C.W., Isacson, O. (2002). Selective loss of 20S proteasome alpha-subunits in the substantia nigra pars compacta in Parkinson's disease. *Neuroscience Letters*, 326(3):155–8.
21. McNaught, K.S.P., Belizaire, R., Isacson, O., Jenner, P., Olanow, C.W. (2003). Altered proteasomal function in sporadic Parkinson's disease. *Experimental Neurology*, 179(1):38–46.
22. Um, J.W., Im, E., Lee, H.J., Min, B., Yoo, L., Yoo, J., et al. (2010). Parkin directly modulates 26S proteasome activity. *Journal of Neuroscience*, 30(35):11805–14.
23. Nishikawa, K., Li, H., Kawamura, R., Osaka, H., Wang, Y-L., Hara, Y., et al. (2003). Alterations of structure and hydrolase activity of parkinsonism-associated human ubiquitin carboxyl-terminal hydrolase L1 variants. *Biochemical and Biophysical Re-*

- search Communications, 304(1):176–83.
24. Tanji, K., Mori, F., Kakita, A., Takahashi, H., Wakabayashi, K. (2011). Alteration of autophagosomal proteins (LC3, GABARAP and GATE-16) in Lewy body disease. *Neurobiology of Disease*, 43(3):690–7.
 25. Dehay, B., Bove, J., Rodriguez-Muela, N., Perier, C., Recasens, A., Boya, P., et al. (2010). Pathogenic lysosomal depletion in Parkinson's disease. *Journal of Neuroscience*, 30(37):12535–44.
 26. Chu, Y., Dodiya, H., Aebischer, P., Olanow, C.W., Kordower, J.H. (2009). Alterations in lysosomal and proteasomal markers in Parkinson's disease: Relationship to alpha-synuclein inclusions. *Neurobiology of Disease*, 35(3):385–98.
 27. Alvarez-Erviti, L., Rodriguez-Oroz, M.C., Cooper, J.M., Caballero, C., Ferrer, I., Obeso, J.A., et al. (2010). Chaperone-mediated autophagy markers in Parkinson disease brains. *Archives of Neurology*, 67(12):1464–72.
 28. He, Y., Appel, S., Le, W. (2001). Minocycline inhibits microglial activation and protects nigral cells after 6-hydroxydopamine injection into mouse striatum. *Brain Research*, 909(1–2):187–93.
 29. Jackson-Lewis, V., Vila, M., Tieu, K., Teismann, P., Vadseth, C., Choi, D-K., et al. (2002). Blockade of microglial activation is neuroprotective in the 1-methyl-4-phenyl-1, 2, 3, 6-tetrahydropyridine mouse model of Parkinson disease. *Journal of Neuroscience*, 22(5):1763–71.
 30. Kirik, D., Rosenblad, C., Bjorklund, A. (1998). Characterization of behavioral and neurodegenerative changes following partial lesions of the nigrostriatal dopamine system induced by intrastriatal 6-hydroxydopamine in the rat. *Experimental Neurology*, 152(2):259-277.
 31. Blum, D., Torch, S., Lambeng, N., Nissou, M.F., Benabid, A.L., Sadoul, R., Verna, J.M. (2001). Molecular pathways involved in the neurotoxicity of 6-OHDA. Dopamine and MPTP: contribution to apoptotic theory in Parkinson's disease. *Progress in Neurobiology*, 65(2):135-172.
 32. Deumens, R., Blokland, A., Prickaerts, J. (2002). Modeling Parkinson's disease in rats: an evaluation of 6-OHDA lesions of the nigrostriatal pathway. *Experimental Neurology*, 175(2):303-317.
 33. Rahman, M.M., Islam, M.B., Biswas, M., et al. (2015). In vitro antioxidant and free radical scavenging activity of different parts of *Tabebuia pallida* growing in Bangladesh. *BMC Research Notes*, 8: 621.
 34. Truong, L., H. Allbutt, M. Kassiou, J.M. Henderson. (2006). Developing a pre-clinical model of Parkinson's disease: A study of behaviour in rats with graded 6-OHDA lesions. *Behavioural Brain Research*.169:1–9.
 35. Haddadi, R., Nayebi, A.M., Brooshghalan, S.E. (2018). Silymarin prevents apoptosis through inhibiting the Bax/caspase-3 expression and suppresses toll like receptor-4 pathway in the SNc of 6-OHDA intoxicated rats. *Biomedicine & Pharmacotherapy*, 104:127–136.
 36. Monville, C., Torres, E.M., Dunnett, S.B. (2006). Comparison of incremental and accelerating protocols of the rotarod test for the assessment of motor deficits in the 6-OHDA model. *Journal of Neuroscience Methods*, 158:219-223.
 37. Baiba, J., Zane, D., Kaspars, J., Vladimirs, P., Ulrika, B., Ingrida, M., et al. (2016).

- Spruce needle polyphenols protect against atorvastatin-induced muscle weakness and do not influence central nervous system functions in rats. *Proceedings of the Latvian Academy of Sciences*, 70(1):13–20.
38. Li, Q., Wan, J., Lan, X., Han, X., Wang, Z., Wang, J. (2017). Neuroprotection of brain-permeable iron chelator vK-28 against intracerebral hemorrhage in mice. *Journal of Cerebral Blood Flow & Metabolism*. 37:3110–23.
39. Schaar, K.L., Breneman, M.M., Savitz, S.I. (2010). Functional assessments in the rodent stroke model. *Experimental & Translational Stroke Medicine*, 2:13.
40. Schallert, T., Hall, S. (1988). 'Disengage' sensorimotor deficit following apparent recovery from unilateral dopamine depletion. *Behavioral Brain Research*, 30:15-24.
41. Katalin, M., Bernadett, M., Nora, S., Istvan, G., ZsoltJuranyi, G.L. (2007). Effects of 2, 3-benzodiazepine AMPA receptor antagonists on dopamine turnover in the striatum of rats with experimental Parkinsonism. *Brain Research Bulletin*, 71:501–507.
42. Ohkawa, H, Ohishi, N, Yagi, K. (1979). Assay for lipid peroxides in animal tissues by thiobarbituric acid reaction. *Analytical Biochemistry*, 95(2):351-8.
43. Misra, H.P., Fridovich, I. (1972). The role of superoxide anion in the auto-oxidation of epinephrine and a sample assay for superoxide dismutase. *Journal of Biological Chemistry*. 247:3170–75.
44. Claiborne, A. (1985). Catalase activity. In: Greenwald RA, editor. *CRC Hand Book of Methods for Oxygen Radical Research*. Boca Raton, Florida, USA: CRC Press; 283–84.
45. Carlberg, I., Mannervik, B. (1985). Glutathione reductase. *Methods in Enzymology*, 113:484-490.
46. Wendel, A. (1981). Glutathione peroxidase. *Methods in Enzymology*, 177:325-333.
47. Lowry, O.H., Rosebrough, N.J., Fair, A.L., Randall, R.J. (1951). Protein measurement with Folin phenol reagent. *Journal of Biological Chemistry*, 193:265–75.
48. Kumar, P., Kalonia, H., Kumar, A. (2012). Possible GABAergic mechanism in the neuroprotective effect of gabapentin and lamotrigine against 3-nitropropionic acid induced neurotoxicity. *European Journal of Pharmacology*. 674(2):265–274.
49. Patel, A.B., de Graaf, R.A., Mason, G.F., Rothman, D.L., Shulman, R.G., Behar, K.L. (2005). The contribution of GABA to glutamate/glutamine cycling and energy metabolism in the rat cortex in vivo. *Proceedings of the National Academy of Sciences of the United States of America*, 102:5588–5593.
50. Mabrouk, O.S., Mela, F., Calcagno, M., Budri, M., Viaro, R., Dekundy, A., Morari, M. (2013). GluN2A and GluN2B NMDA receptor subunits differentially modulate striatal output pathways and contribute to levodopa-induced abnormal involuntary movements in dyskinetic rats. *ACS Chemical Neuroscience*, 4(5):808–816.
51. Mercanti, G., Bazzu, G., Giusti, P. (2002). A 6-hydroxydopamine in vivo model of Parkinson's disease. *Neurotrophic Factors, Methods and Protocols*, 846:355–364.
52. Magalingam, K.B., Radhakrishnan, A., Haleagrahara, N. (2014). Protective effects of flavonolisoquercitrin, against 6-hydroxydopamine (6-OHDA)-induced toxicity in PC12 cells. *BMC Research Notes*, 7(1):1–8.

Properties of Glucose Oxidase produced from a newly isolated strain of *Aspergillus niger*

Okoye Ifeanyi¹, Awhin Prosper Ejiro², Onosakponome Iruoghene^{3*}, Ezugwu Arinze Linus¹, Ajoh Alfred Ikechukwu² and Chilaka Ferdinand Chiemeka¹

¹University of Nigeria, Nsukka, Enugu State, Nigeria

²Delta State University, Abraka, Delta State, Nigeria

³Dennis Osadebay University, Anwai, Asaba, Delta State, Nigeria

*Corresponding author: iruoghene.onosakponome@dou.edu.ng,

Abstract

Glucose oxidase (GOx) is a key enzyme used in many industries worldwide. To identify the GOx producer strain, *Aspergillus niger* was isolated from the Beehive and screened for its glucose oxidase-producing capability. Glucose oxidase was mass-produced by a submerged fermentation system. The activity of glucose oxidase was ascertained by the continuous spectrophotometric rate determination method. GOx was purified by (70%) ammonium sulphate precipitation, dialyzed, and gel filtration with 2.82, 3.54, and 3.69U/mg specific activity respectively. The enzyme exhibited an optimum pH range of 5.5 and a temperature optimum of 40°C. Ag²⁺ and Hg²⁺ had a remarkably inhibitory effect on the partially purified GOx, whereas Ca²⁺, Zn²⁺, and Mg²⁺ do not affect the enzyme activity. Cu²⁺ and Co²⁺ have a slight inhibitory effect on GOx. Kinetic characteristics of GOx from *Aspergillus niger* display V_{max} as 40 U/ml, and K_m as 0.12 mM. The findings on the properties of GOx exhibited optimum conditions for industrial applications

Keywords: *Aspergillus niger*, Glucose oxidase, Characterization, Purification, Bee Hive

Introduction

Glucose oxidase (EC 1.1.3.4) is a principal commercial enzyme due to its numerous applications in diverse industries. As an oxidant, GOx is used for bread production with improved quality and loaf volume in the baking industry [1, 2]. GOx extends the shelf-life by removing oxygen and glucose from foods [3]. GOx is effective in the production of H₂O₂ for bleaching in the textile industry [4-6]. GOx is produced by some insects and fungi [7]. Glucose oxidase (EC 1.1.3.4) catalyzes the oxidation of β-D-glucose using oxygen as an electron acceptor, to yield D-gluconolactone and hydrogen peroxide [7]. The cofactor of GOx, flavin-adenine dinucleotide (FAD) is reduced along the reaction mechanism. Muller [8] was the first to isolate GOx from the mycelium of *Aspergillus niger*. A single polypeptide chain of one subunit of GOx contains 583 amino acid residues [9]. The ability of GOx to remove oxygen and generates hydrogen peroxide underline the trait utilized in food preservation. Other applications of GOx are in the food, pharmaceutical and medical industries [10]. Notable in these applications, is the fabrication of glucose biosensors for the measurement of glucose levels in serum. There are few

reports on high catalytic properties of GOx from various fungi, thus this research was designed to produce and characterize GOx from *Aspergillus species* isolated from Beehive to meet the demand for enhanced properties such as elevated catalytic activity for effective production of GOx for industrial purposes. This study aimed to produce and characterize glucose oxidase produced from *Aspergillus niger* under a submerged fermentation system for special application in biotechnology and industries.

Materials and Methods

Materials

Horseradish peroxidase, O-dianisidine dihydrochloride, and Folin-Ciocalteu phenol were purchased from Sigma, USA. All other analytical chemicals used in this study such as D (+)-glucose, glycerol, peptone, and ethanol were purchased from Merck (Germany), May and Baker Limited (England) and Sigma, USA.

Isolation and maintenance of the Organism

In this study, the fungi were isolated from a beehive bought from Opi market, Nsukka, Enugu State, Nigeria. Using a light microscope, the fungi were identified as *Aspergillus sp.* according to Martin *et al.* [11]. The screening of the fungi was carried out using the method of Eun-Ha *et al.* [12]. The isolated fungi were then grown on the medium of sodium acetate buffer pH 5.5 consisting of 80g Glucose, 3.0g peptone, 0.388g $(\text{NH}_4)_2\text{HPO}_4$, 0.188g KH_2PO_4 , 0.156g $\text{MgSO}_4 \cdot 7\text{H}_2\text{O}$, 20.0g Agar. From the peripheral zone of the pure culture colony, a disc of fungal culture was taken and transferred to the middle of the Petri plate containing the above medium, one pure culture for each plate after which the plates were incubated at 35°C. After 3 days, the fungal culture was treated with a mixture (prepared in sodium acetate buffer (pH 5.5) containing (5%) glucose, (2%) glycerol, (0.1%) O-dianisidine, (60IU/ml) Horse radish peroxidase, (1%) agar after which the culture was incubated for one hour. The fungus that gave the highest GOx production was sustained on Potato

dextrose agar (PDA) and stored at 4°C.

Production of Glucose oxidase

A submerged fermentation system was used for the production of GOx. The medium for the production consists of (80%) glucose, (0.3%) peptone, (0.04%) $(\text{NH}_4)_2\text{HPO}_4$, (0.0188%) KH_2PO_4 , (0.0156%) $\text{MgSO}_4 \cdot 7\text{H}_2\text{O}$, (3.5%) CaCO_3 in 50mM sodium acetate buffer pH 6.0 [9]. Four discs of the pure culture were inoculated into 100ml of a sterilized cultivation medium broth contained in 250ml Erlenmeyer flasks after which the flasks were incubated at 30°C. The fermented biomass in each flask was harvested, filtered and centrifuged at 15000 rpm for 15 min [13]. The supernatant constituted the crude enzyme.

Glucose oxidase assay

GOx activity was measured according to the method by Bergmeyer *et al.* [14] using continuous spectrophotometric rate determination at 500nm wavelength. Solution A (0.05M Sodium acetate buffer of pH 5.5), solution B (0.21mM O-dianisidine solution dissolved in 100ml with reagent A), solution C (10% β -D-glucose of Millipore water), and solution D (a mixture of reagent B [24ml] and reagent C [5ml]), solution E (a freshly prepared solution of 60 purpurogallin units/ml of horseradish peroxidase type II) were all prepared. The enzyme reaction contained 2.9ml of solution D and 5ml of solution E. Reagent E. The reaction was measured using a UV-Visible spectrophotometer at 500nm.

Purification of GOx

Ammonium sulphate precipitation and dialysis

Ammonium sulphate precipitation of GOx and dialysis was done as described by Chilaka *et al.* [15]. The suitable percentage of ammonium sulphate to precipitate GOx in this study was Seventy (70%). Dialysis was carried out on the precipitated enzyme against 0.01M sodium phosphate buffer pH 7.0 for 12 hours

with a change of buffer every 6 hours. The dialysate was assayed for GOx activity and protein concentration as earlier described.

Gel Filtration

The dialyzed enzyme (10ml) was introduced into a (2.0 × 80 cm) gel chromatographic column, pre-equilibrated with sodium phosphate buffer (50mM, pH 7.0). At room temperature, fractions were collected at a flow rate of 5ml/15min. The protein concentration and enzyme activity of each fraction were monitored as earlier described. Peaks with the highest GOx activity were pooled and stored at -10°C for further studies.

Characterization of the partially purified *Aspergillus niger* GOx

***Effect of pH on Aspergillus niger* GOx activity**

The optimal pH for GOx activity was monitored using 50mM sodium acetate (pH 3.5 – 5.5), 50mM Sodium phosphate (pH 6.0 – 7.5) and 50mM Tris-HCL (8.0 – 10.0) as described by Simpson *et al.* [16]. The GOx activity was assayed as earlier described.

***Effect of temperature on Aspergillus niger* GOx activity**

The optimum temperature for GOx activity was monitored at temperatures ranging from 30 – 75°C at the interval of 5°C in a water bath using 50mM sodium acetate pH 5.5. The reaction was initiated with the addition of GOx (0.15Uml⁻¹) as described by Singh and Verma [17]. The GOx activity was assayed as earlier described.

***Effect of glucose concentration on Aspergillus niger* GOx activity**

The effect of glucose concentrations (4.0 – 25%, m/v) on GOx activity was monitored as described by Sandalli *et al.* [18] at pH 5.5 and 40°C. The maximum velocity (V_{max}) and Michaelis constant (K_m) were gotten from Lineweaver–Burk plot of initial velocity data of differ-

ent glucose concentrations.

Effect of divalent metal ions on GOx activity

The effect of metal ions on GOx activity was monitored as described by Yanmis *et al.* [19]. The partially purified enzyme (10ml) was incubated for 20mins in different concentrations of metal ions (10 to 30mM). The enzyme activity was assayed at the established optimum temperature and pH in this study.

Results and Discussion

Using a light microscope, the GOx-producing fungi isolated were identified as *Aspergillus* species. The chromosomal DNA of the *Aspergillus* strain was extracted after which the 18S rDNA was amplified with PCR. The product of the PCR was then subjected to agarose gel electrophoresis. A clear band was found at approximately 500bp when compared to the DNA ladder (Figure 1). The multiple alignments of the sequence were compared with 21 other known sequences of *Aspergillus* species gotten from the NCBI data bank. The phylogenetic tree confirmed the strain H1 as *Aspergillus niger* as it showed 99% similarity with *Aspergillus niger* strains AN4, A sp-7136 and IHBF 2920 (Figure 2).

***Molecular Identification of Aspergillus niger* H1**

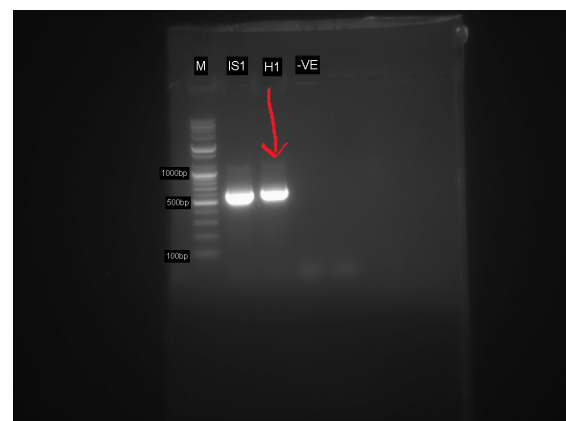


Figure 1: Agarose gel electrophoresis showing PCR amplification of *Aspergillus niger*

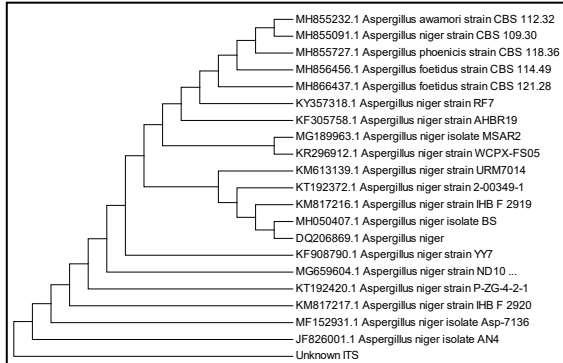


Figure 2: Phylogenetic Tree of *Aspergillus niger* H1 with other *Aspergillus* species

Enzyme production

The crude enzyme has a specific activity of 3.03U/mg.

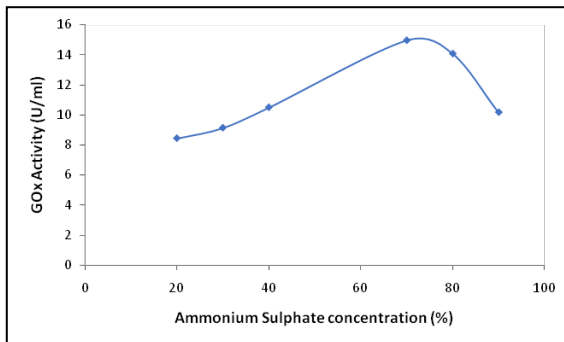


Figure 3: Ammonium Sulphate profile

Purification of *Aspergillus niger* GOx

Seventy-70 % (w/v) of ammonium sulphate precipitation was observed to be suitable for the first purification step with a specific activ-

ity of 2.82U/mg. The precipitated GOx was subjected to dialysis. The specific activity of 3.52 U/mg was obtained after dialysis. Dialysis of protein is encouraged after ammonium sulphate because it stimulates ionic scrambling leading to an aggregate formation with incorrect ionic bond pairing [20]. For further purification, the dialyzed enzyme underwent Gel-filtration equilibrated with 50mM sodium acetate pH 5.0. In the final purification step of Gel-filtration, specific activity increased from 3.54 to 3.69U/mg protein indicating the removal of impurities.

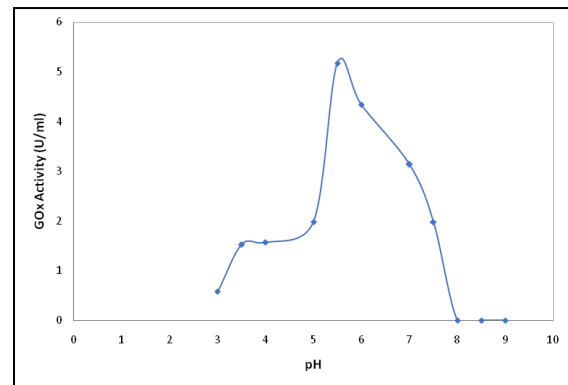


Figure 4: Effect of pH on GOx activity

Optimum pH and temperature determination

In this study, optimum pH of 5.5 was obtained. An increase in pH from 3.0 to 5.5 accompanied by an increase in GOx activity was observed after which the GOx activity started declining. High GOx activity was maintained from 5.0 - 7.0 beyond which, it decreases rapidly as shown in figure 4. GOx has many amino and carboxyl groups which are sensitive to different

Table 1: Purification table of *Aspergillus niger* GOx

	Volume (ml)	Activity (Units/ml)	Total Activity (Units)	Protein Conc. (mg/ml)	Total Protein (mg)	Specific Activity (U/mg)	Yield	Purification fold
Crude enzyme	1000	16.22	16220	5.36	5360	3.03	100	1
NH ₄ SO ₄ Precipitate	120	7.70	924	2.73	327.6	2.82	12	0.931
Dialyzed	50	9.62	481	2.72	136	3.54	5	1.170
Gel Filtration	30	7.85	236	2.13	63.9	3.69	3	1.220

pH values, thus affecting its conformation. Ozyilmaz *et al.* [21] also reported the optimum pH of GOx to be 5.5. An optimum of 5.5 for GOx produced from *Aspergillus fumigatus* AFS4 was also reported by Onosakponome *et al.* [20]. Also, the increase from 20 to 40°C in temperature was accompanied by a rise in GOx activity after which there was a decrease in GOx activity making 40°C the optimum temperature. In this study, GOx maintained high activity over a temperature range of 30 - 70°C as shown in figure 5. The rapid decline in GOx activity after the optimum temperature may be due to subunits dissociation. Like other multimeric enzymes, the subunits dissociation may be involved in *Aspergillus niger* GOx inactivation. Sukhacheva *et al.* [22] reported optimum temperature range of 40–60 °C for GOx from *Aspergillus niger* and *Penicillium amargasakense* ATCC 28686.

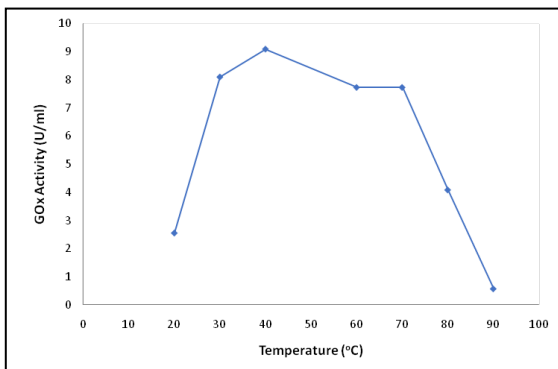


Figure 5: Effect of temperature on GOx activity

Metal ions on GOx activity

The effect of metal ions on *Aspergillus niger* GOx activity showed that Ag^{2+} and Hg^{2+} had a notably inhibitory effect on partially purified GOx, whereas Ca^{2+} , Zn^{2+} and Mg^{2+} do not affect the enzyme activity. Cu^{2+} and Co^{2+} have a modest inhibitory effect on GOx. This study is by Kusai *et al.* [23] who reported that Ag^{2+} and Hg^{2+} are inhibitors of GOx. The Inhibitory Effect of GOx by Ag^{2+} ions may be a result of the reaction of Ag^{2+} with the thiol group of GOx essential for catalysis, which is in proximity to the FAD-binding region of GOx (20). Yuan *et al.* [24]

reported a similar result for recombinant GOx.

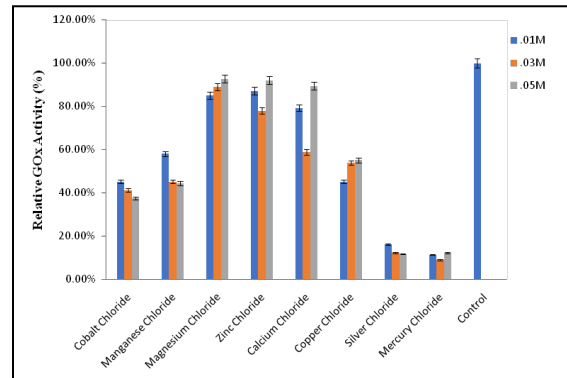


Figure 6: Effect of divalent metal ions on GOx activity

Kinetic characterization

The Michaelis mentens constant (K_m) and maximum velocity (V_{max}) were 0.12mM and 40U/ml respectively. This property indicated that GOx produced from *Aspergillus niger* has a high affinity for β D-glucose oxidation.

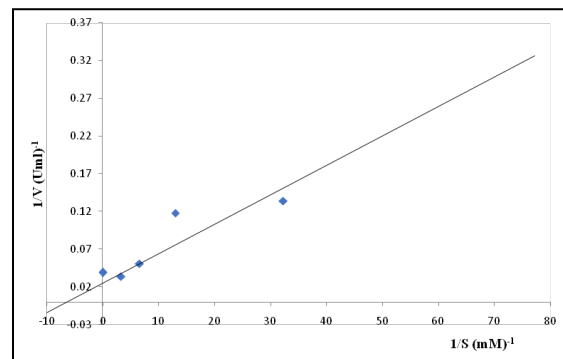


Figure 7: Lineweaver-Burk of initial velocity values at various glucose concentrations

Conclusion

The findings from this study suggest that the *Aspergillus niger* strain isolated from a local beehive was capable of producing glucose oxidase with an optimum pH and temperature of 5.5 and 40°C respectively. The wide range of optimal temperatures (30 - 70°C) and pH (5 - 7.5) give this enzyme an edge in industrial applications, especially in diagnostic applications.

Conflict of interest

No conflict of interest was declared

References

1. Wong, C.M., Wong, K.H. and Chen, X.D. (2008). Glucose oxidase: natural occurrence, function, properties and industrial applications. *Applied Microbiology and Biotechnology*, 78: 927–938.
2. Steffolani, M.E., Ribotta, P.D., Pérez, G.T. and León, A.E. (2010). Effect of glucose oxidase, transglutaminase, and pentosans wheat proteins: relationship with dough properties and bread-making quality. *Journal of Cereal Science*, 51: 366–373.
3. Zia, M.A., Ain, Q., Iftikhar, T., Abbas, R.Z. and Rahman, K. (2012). Production of rabbit antibodies against purified glucose oxidase. *Brazilian Archives of Biology and Technology*, 55: 69–74.
4. Saravanan, D., Vasanthi, N.S., Raja, K.S., Das, A. and Ramachandran, T. (2010). Bleaching of cotton fabrics using hydrogen peroxide produced by glucose oxidase. *Indian Journal of Fiber and Textile Research*, 35: 281–283.
5. Mojsov, K. (2011). "Application of enzymes in the textile industry: a review," in *II International Congress "Engineering, Ecology and Materials in the Processing Industry"* (Jahorina), 230–239.
6. Soares, J.C., Moreira, P.R., Queiroga, A.C., Morgado, J., Malcata, F.X. and Pintado, M.E. (2011). Application of immobilized enzyme technologies for the textile industry: a review. *Biocatalysis and Biotransformation*, 29: 223–237.
7. Bankar, S., Bule, M., Singhal, R. and Ananthanarayan, L. (2008). Optimization of *Aspergillus niger* fermentation for the production of glucose oxidase. *Food and Bioprocess Technology*, 19: 47-56.
8. Müller, D. (1928). Oxidation von Glukose mit Extrakten aus *Aspegillus niger*. *Biochemische Zeitschrift* 199: 136–170.
9. Fiedurek, J. and Szezodrak, J. (1995). Glucose Oxidase biosynthesis about bio-chemical mutation in *A. niger*. *Acta Biotechnology*, 15(1): 107-115.
10. Decamps, K., Joye, I.J., Rakotozafy, L., Nicolas, J., Courtin, C.M. and Delcour, J.A. (2013). The bread dough stability improving effect of pyranose oxidase from *Trametes multicolour* and glucose oxidase from *Aspergillus niger*: unravelling the molecular mechanism. *Journal of Agricultural and Food Chemistry* 61: 7848–7854.
11. Martin, N., de Souza, S.R., da Silva, R. and Gomes, E. (2004). Pectinase production of fungal strains in solid state fermentation using agro-industrial bioproduct. *Brazilian Archives of Biology and Technology*, 47(5): 813-819.
12. Eun-Ha, P., Young-Mi, S., Young-Yi, L., Tae-Ho, K., Dae-Hyuk, K. and Moon-Sik, Y. (2000). Expression of glucose oxidase by using recombinant yeast. *Journal of Biotechnology*, 81: 35–44.
13. Kim, K.K., Fravel, D.R. and Papavizas, G. (1990). Production, purification, and properties of glucose oxidase from the biocontrol fungus *Talaromyces flavus*. *Canadian Journal of Microbiology*, 36: 199–205.
14. Bergmeyer, H., Gawehn, K. and Grassl, M. (1974). *Methods of Enzymatic Analysis* Bergmeyer, HU (2nd edition), vol. 1. Academic Press Inc., New York, USA, p. 457–458.
15. Chilaka, F., Nwachukwu, A. and Uvere, P. (2002). Thermal stability studies of β -galactosidase from germinating seeds of the brown beans, *vigna unguiculata*. *Nigerian Journal of Biochemistry and Molecular Biology*, 17(1): 51-56.

16. Simpson, C. (2006). Isolation, purification and characterization of a novel glucose oxidase from *Penicillium canescens* Tt42: Rhodes University.
17. Singh, J. and Verma, N. (2013). Glucose Oxidase from *Aspergillus niger*: Production, characterization, and immobilization for glucose oxidation. *Advances in Applied Science Research*, 4(3): 250-257.
18. Sandalli, C., Sarai, A., Ulker, S., Karaoglu, H., Belduz, A.O. and Copur-Cicek, A. (2014). Cloning, expression and characterization of a novel CTP synthase gene from *Anoxybacillus gonensis* G2. *Turkish Journal of Biology*, 38: 111-117.
19. Yanmis, D., Karaoglu, H., Colak, N., Ay-Sal, F., Canakcl, S. and Belduz, A. (2014). Characterization of a novel Xylose isomerase from *Anoxybacillus gonensis* G2. *Turkish Journal of Biology*, 38: 586-592.
20. Onosakponome, I., Ezugwu, A.L., Eze, S.O.O. and Chilaka, F.C. (2022). Kinetics and Thermodynamic Properties of Glucose Oxidase Obtained from *Aspergillus fumigatus* ASF4. *Tropical Journal of Natural Product Research*, 6(3): 438-445.
21. Ozyilmaz, G., Tukul, S. and Alptekin. O. (2005). Activity and storage stability of immobilized glucose oxidase onto magnesium silicate. *Journal of molecular catalysis B: Enzymatic*, 35: 154-160.
22. Sukhacheva, M.V., Davydova, M.E. and Netrusov, A.I. (2004). Production of *Penicillium funiculosum* 433 glucose oxidase and its properties. *Applied Biochemistry and Microbiology*, 40(1): 25-29.
23. Kusai, K., Sekuzu, I., Hagihara, B., Okunuki, K., Yamauchi, S. and Nakai, M. (1960). Crystallization of glucose oxidase from *Penicillium amagasakiense*. *Biochimica et Biophysica Acta*, 40: 555-557.
24. Yuan, M., Ning, C., Yang, S., Liang, Q., Mou, H. and Liu, Z. (2020). A new cold-active glucose oxidase from *Penicillium*: High-level expression and application in fish preservation. *Frontiers in Microbiology*, 11(606007): 1-14.

Employing Trichoderma to Alleviate Dimethoate Phytotoxicity In *Sorghum Bicolor*

Archana Kumari¹, Krishna Sundari Sattiraju²

¹Coordinator Plant and Microbial Biotechnology Centre, Biotechnology Department, Jaypee Institute of Information Technology, A-10, Sector 62, 201309, Noida, Uttar Pradesh, India.
Biotechnology Department, Jaypee Institute of Information Technology, A-10, Sector 62, 201309, Noida, Uttar Pradesh, India.

*Corresponding author: Krishna.sundari@jiit.ac.in

Abstract

Dimethoate is a broad spectrum organophosphate pesticide which is used to control pests of order hemiptera, diptera, orthoptera, and araneae. In *Sorghum bicolor* it is found to control green bugs, aphids, spider mites, and grasshoppers. The present study details the impact of dimethoate (30% EC) on *S. bicolor* through a short term (a fortnight study) *in-vivo* bioassay and an extended soil microcosm study (7 weeks study). Experiments were simultaneously carried out at low (10 ppm, 50 ppm) and high (300 ppm, 600 ppm) range of dimethoate. The *in-vivo* bioassay provided evidence of increasing dimethoate toxicity on *Sorghum bicolor* ranging from 19 % to 70 % at 10 ppm and 300 ppm respectively. *Trichoderma harzianum* T103, a plant growth promoting fungus (PGPF) with proven monocrotophos (organophosphate pesticide) tolerance, was engaged to verify its potential to support plant growth under dimethoate stress. Rhizospheric administration and seed biopriming with T103 improved growth of *Sorghum bicolor* by a factor of; root length (1.6, 1.8), shoot length (1.1, 1.2) and biomass (1.4, 1.4) at 10 ppm and 300ppm respectively. LD₅₀ of T103 value for dimethoate is ~ 300 ppm. T103 was observed to sporulate under dimethoate stress (at con-

centrations as high as 1000 ppm), however, the spore density was lesser as compared to unchallenged isolate growth. FTIR spectra indicated ongoing dimethoate degradation registering change in peaks at 1043 (-C-O stretching), 1235 (-OH, -NH deformation), and 1737 cm⁻¹ (C=O stretching). In addition, appearance of new peak at 3456 cm⁻¹ (-OH, -NH stretching) also suggest formation of intermediate and end product. Concentration of proline, a biochemical stress indicator, was greater in untreated plants than in treated plants suggesting signs of phytotoxicity in the absence of T103. The findings demonstrate that, at both low and high concentrations of dimethoate T103 can reduce dimethoate-induced growth retardation in *S. bicolor*.
KEYWORDS: DIMETHOATE, PGPF, *Sorghum bicolor*, PHYTOTOXICITY, PROLINE, CHLOROPHYLL

Introduction

Sorghum is the world's fifth-most important cereal crop after maize, rice, wheat, and barley. India is the second-largest producer of sorghum in the world, with a yield of more than 7.5 million metric tons recorded in 2021 [1]. Major insect pests of sorghum are stem and stalk borers, shoot flies, aphids, and shoot/ear head bugs. In India, infestation

of insect pests causes the loss of the sorghum crop more than 30% and even upto 84% under certain conditions. Losses linked to insects are estimated to reach more than \$1 billion annually in semi-arid tropical regions [2, 3]. *Sorghum bicolor* is chosen in the study as a model plant, as it can be easily grown in a lab and greenhouse with low irrigation and fertilizer requirements, apart from being one of the most important cereal crops in India [4]. Insect pest populations that cause economic damage can be managed with a variety of organophosphate pesticides (OPPs) [5]. These pesticides accumulate in the soil when they are used in excess, causing a variety of stress responses in host plants. Under abiotic stress conditions, plants redistribute majority of the nutrients and energy towards overcoming stress, resulting in a much lower percentage of nutrients and energy going towards biomass accumulation. This would reflect as a significant decrease in yield due to compromised host metabolic activities [6-8]. Most common OPPs used in sorghum are dimethoate, chlorpyrifos, phorate, phosalone and so on [9, 10]. Research studies reported DM residues in soil (58.63 mg/kg), honey (1–10 mg/kg), spinach (2.54 mg/kg) and many other edible substances. As the maximum residue limit for DM is 0.04 mg/kg, the reported residue values in food materials are alarming. Table 1 represents the data on DM chemistry, rate of application, residues reported [11, 12]. The effects of DM on the human immunological, neurological, and reproductive systems were thoroughly reviewed by Eken, 2017 [13]. Kumari and John, 2019; Katsikantami et al., 2019 threw light on health risks associated with dietary exposure to

pesticides [14, 15]. Therefore, it is required to study the change in morphological, biochemical, and stress parameters of plants in the presence of pesticides at both low and high concentrations. However, to date, research publications demonstrating the pesticide toxicity in plants is comparatively less, even though they form the principal routes of

accidental entry of these toxic substances in food chain. Number of scientific records in PubMed, Web of Science, Google Scholar and Science Direct database is evidence. Though some researchers have demonstrated the presence of pesticide residues in various crops as well as their negative effects on plant growth; still, more research work needs to be done in order to understand the actual impact on various morphological and biochemical parameters in many staple food crops owing to their consumption in large quantities. Nine out of ten fractions of the pesticide volume sprayed drift towards non-target plants and eventually sink into the soil. The pesticide enters the plant from the soil and causes several alterations to its physiological, metabolic and mitotic functions [16, 17]. Contrary to occupational direct contact exposure, which is frequently experienced by farmers, dietary exposure is involuntary and cannot be prevented by using external safeguards like wearing masks, gloves, and other safety equipment. Plant growth promoting fungi (PGPF) are important partners for enhancing plant productivity in a sustainable and environment friendly manner. *Trichoderma harzianum*, a prominent PGPF, is extensively known for its biotic stress tolerance/ biocontrol potential. Moreover, reports also exist for its potential to mitigate drought and salt stresses faced by the plants [18, 19]. Employing plant growth promoting microorganism for pesticide bioremediation is a comparatively new trend. Dimethoate (organophosphate pesticide) remediation using *T.harzianum* is a step forward in this orientation. *T.harzianum* isolate T103 used in the present study has demonstrated potential to support the plant growth by providing a. better nutrient access, b. better resistance to the soil competitors, and c. breaking down complex substrate in order to provide plant ready nutrients [20]. This is the reason in choosing the isolate for the current investigation to mitigate DM stress via plant-microbe interaction. The manuscript attempts to provide a definitive experimental evidence for asserting the potential of PGPF-T103 as prob-

able soil remediator, particularly in agricultural soils that have a continuous buildup of residual pesticides reaching either as direct application residues or irrigation surplus. The purpose of this study was (i) to check the impact of dimethoate pesticide on the morphological (R/S ratio, biomass), biochemical (Chlorophyll a), and stress indicative parameters (phytotoxicity and proline content) of *Sorghum bicolor* plants, (ii) to explore the pesticide tolerance of PGPF T103 (mitotic activity, sporulation and pesticide bond breakage); and (iii) to validate the protective effect of T103 on *S. bicolor* subjected to low and high concentrations of dimethoate stress, and its role in restoring plant growth at the greenhouse level.

Materials and Methods

Plant material and pesticide

Sorghum bicolor CSH-16 seeds were procured from the Indian Institute of Millets Research (IIMR), Hyderabad. Seeds were surface sterilized with HgCl₂ (0.1%) for

5 minutes and thoroughly rinsed with double distilled water to remove HgCl₂ completely [23]. Dimethoate, 30% EC (Rogor) formulation was procured from Agriberi India. A fresh stock solution of 10,000 ppm was prepared in molecular grade double distilled water for every experiment and diluted to varying concentrations (10 to 600 ppm) as per the dose required.

Plant growth promoting fungi and plant material

PGPF *Trichoderma harzianum* T103 isolate (GenBank ID- KP122935.1) was used in the present study. Culture was grown and maintained on malt dextrose agar (Himedia laboratories private limited, Mumbai). Stocks are maintained for longer periods of time at -80°C in glycerol stock (30%). PGPF isolate T103 was grown on MDA plates for one week at 30°C. Spores were harvested in sterilized saline (0.85% w/v) and further pooled into 1.5% CMC (carboxymethyl cellulose), post centrifugation, at 3000 RPM for 10 minutes. The spore dose was adjusted to 10⁸ spores /

Table 1: Dimethoate application and residues factsheet

Pesticide	Field application levels	DM residue levels	Application frequency
Dimethoate (DM) 1. Molecular formula- C ₅ H ₁₂ N-O ₃ PS ₂ 2. Hazardous substance Class II 3. Readily available in the market and lead agro-chemical produced by Indian agricultural companies (Annual production in India for the year 2021 is 1391 MT)	DM 30% E.C (100mL bottle dissolved in 100 to 500 liters of water)- Concentration of applying solution ranges from 60 ppm to 300 ppm	Concentration range in ppm Soil (58 ppm) Honey (1-10 ppm) Spinach (2.54 ppm) MRL fixed by C.A is 0.02ppm-0.5 ppm in majority of the crops, and 2 to 5 ppm in some citrus fruits and spices	One to 6 times in a crop season, depending on the type of crops and infection.

Source- INCHEM, Codex Alimentarius, Sun et al., 2015 [8, 9, 21, 22].

ml and used for *in-vivo* plant growth assays and greenhouse studies [24].

Dimethoate tolerance study

A 6 mm Agar plug was detached from sterile MDA plate (centrally) and replaced with a T103 culture plug of the same size. Plates were incubated at 30 ± 2 °C for 120 hours, and radial growth was recorded at the interval of 24 h. Average linear growth rate per day was estimated from the growth recorded at 24 and 72 hours. The LD_{50} value for DM in T103 was estimated as previously described by Kumari and Sattiraju, 2022 [20]. In a separate assay, Malt dextrose broth was supplemented with different concentration of DM (0-2100 ppm) and incubated at 30 ± 2 °C for 5 days at 120 RPM. On fifth day, mycelia were harvested, and biomass was recorded in triplicate after drying at 70 °C overnight.

FTIR analysis

The ethyl acetate extracts of DM control (300 ppm) and PGPF treated samples (experiment detailed in section 2.3) were analyzed with a FTIR spectrophotometer (Spectrum two FTIR, PerkinElmer, UK). Quantities of 10 μ L of both samples were placed on a diamond window of the instrument separately at room temperature (25 °C) in the frequency range of 4,000–400 cm^{-1} . The procedure followed was as given by Kathuria et al., 2022 [25].

In-vivo plant growth study with and without PGPF treatment

Surface sterilized sorghum seeds were transferred to 0.25% water Agar and incubated in plant growth chamber for 72 h. Post emergence, seedlings were treated with PGPF inoculum (@ 10^8 cells/ml for 60 minutes. After seedling treatment, seeds were transferred to sterilized ASURE boxes containing 300 ml of PMB media. Detailed information on ASURE assay is published previously [26]. After 15 days, plants were harvested and plant growth parameters were analyzed.

Greenhouse study

Surface sterilized sorghum seeds were sown in plant growth bags of 1 kg containing a sterile mixture of soil and peat moss in the ratio of (7:3). Post 1 week uneven seedlings were removed and 3 seedlings were maintained per pot. Healthy and uniformly grown seedlings were treated with PGPF inoculum as prepared by the method given in Section 2.3. For each treatment, 15 replicates were maintained. DM was added at 50 ppm, 150 ppm, 300 ppm, and 600 ppm, in the rhizospheric region of potted plants. Plants were kept in a greenhouse with a temperature of 28 ± 2 °C and a relative humidity of more than 70%, and watered every alternate day. Plants were harvested and analyzed to observe growth impact on pesticide stress as compared with unchallenged host plants [27].

Statistical analysis

Each experiment was conducted in triplicates, and results are presented as the mean \pm standard deviation. GraphPad Prism version 9.5 (GraphPad, San Diego, CA, USA) was used for the statistical analyses through one-way ANOVA to identify significant differences amongst the treatments followed by Tukey's post hoc test. The values of $P < 0.01$, $P < 0.05$ for biochemical assay and plant based studies, respectively were considered statistically significant.

Results and Discussion

Evaluation of dimethoate tolerance by selected PGPF

To check the impact of pesticide on growth of chosen PGPF T103, DM plate assay was done at the concentration of 0 to 2000 ppm of DM. Average linear growth of PGPF was decreasing with increasing concentration of DM. The maximum ALGR (mm/ Day) was recorded at 0 ppm and the minimum at 1000 ppm. Sporulation was observed to take place even at a concentration as high as 1000 ppm; how-

ever, spore count was reduced. Spores are the seeds for *Trichoderma*, which are required for their propagation [28]. Figure 1 shows that it can produce spores up to 1000 ppm of DM (which is almost 100 times more than the maximum residue reported in crops).

Spore production at 1000 ppm is indicative of the isolates' potential to sustain their growth at higher concentrations of pesticides. Pesticides are known to impact microorganisms, animals and plants at cellular level adversely. According to Ore et al., 2022, pesticide application can influence microbial diversity, which can be detrimental to plant growth and development by decreasing nutrient availability or disrupting the nutrient cycle [29]. Hage-Ahmed et al., 2014 showed that pesticides changed the sporulation and fungal community composition [30]. Therefore, employing microbial bioinoculants with high tolerance that can grow and divide at higher concentrations of pesticides is the need of the hour.

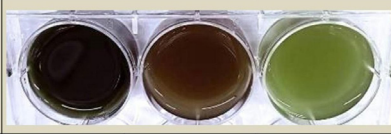
DM (ppm)	T ₀ (0 ppm)	T ₅₀₀ (500 ppm)	T ₁₀₀₀ (1000 ppm)
ALGR (mm/Day)	21±0.96	13.3±0.57	8.3±0.33
Spore suspension			
Spore count	1x 10 ¹⁰	5.5x 10 ⁹	4.4x 10 ⁹

Fig.1. Average linear growth and sporulation of PGPF-T103 under dimethoate stress

The liquid broth assay showed a negative correlation between pesticide concentration and biomass. At 0 ppm, the biomass was around 3.95± g/L which reduced to 1.91±0.18 g/L at 300 ppm, and at 2000 ppm, the concentration was as low as 0.55±0.18 g/L. The estimated LD₅₀ value for DM was near 300 ppm. In both DM plate and broth assays, PGPF strain T103 showed striking pesticide tolerance potential.

Comparative analysis of infrared spectra of control and PGPF treated samples

To observe any structural alterations that occurred due to PGPF-T103 treatment in contrast to untreated DM control, samples were analyzed using FTIR, where spectral readings ranged from 600 to 4000 cm⁻¹. In the PGPF-T103 treated sample, a new peak was recorded at 3456 cm⁻¹ which was absent in the control sample. This peak corresponds to -OH and -NH stretching [31]. Significant variation in the peaks corresponding to 1043 cm⁻¹ and 1235 cm⁻¹ was observed in the treated sample, indicating C-O stretching. Characteristic peak variation at 1737 cm⁻¹ (C=O stretching) was observed, with considerable variation in peak reduction in the PGPF treatment (35%T) compared to the control (28%T) (Figure 2). In the current study, variations in FTIR readings were observed at 1043, 1235, and 1737 cm⁻¹, similar to what was observed in other studies [32, 33]. Prolonged treatment (15 days) with PGPF resulted in effective disappearances of these pesticide specific bonds.

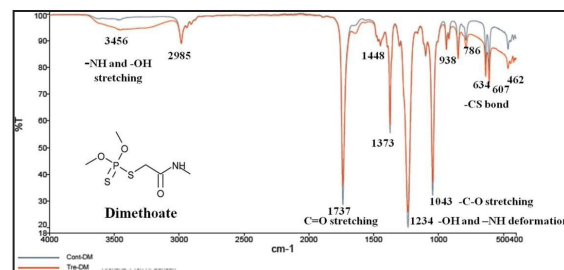


Fig.2. FTIR analysis of the PGPF-T103 treated sample as compared to the DM Control (300 ppm)

Comparative phytotoxicity analysis at low and high concentrations of dimethoate

In comparison to the control (No pesticide) drastic reduction in shoot length, root lengths, biomass and chlorophyll contents were recorded in presence of DM (at both 10 ppm and 300 ppm) (Table 2). Similar to our results Pandey et al, 2022, demonstrated that DM administration on wheat plants for

prolonged periods of time (>10 days) showed an inhibitory effect on plant growth parameters such as root length, shoot length, fresh weight, dry weight and chlorophyll content. DM is water soluble, so it is quickly absorbed by plant roots and accumulates in leaves, where the majority of plant metabolic activities occur. The buildup of DM in plant may impede cell division and elongation, resulting in a reduction in root and shoot length. Lower dosages that had a positive response for a short period of time become harmful if treatment periods are extended beyond 10 days [34]. Even though some scientific groups present an argument that OPPs are water soluble, have shorter half life and thus may not hold greater research emphasis due to lesser retention times in the soil ecosystems. This observation on impact at concentrations that are three times less to field application rate, as evidenced in this study, calls for a concentrated thought on possible future yield impact. Range of DM pesticide applied by farmers and reported residues in soil and plant sample is detailed in Table 1. The exposure to very high pesticide dose may be transient but the impact can be long lasting (Table 2). At higher concentrations there is stark indication of pesticide toxicity on photosynthesis. In this study almost half reduction in chlorophyll a content was recorded at 300 ppm. Chlorophyll is a necessary component of the plant photosystem that is required for photosynthesis. Gitelson et al. (2006) argued that estimating chlorophyll content is critical in determining output. As variations

in canopy Chl are connected to crop phenology, canopy stresses, and vegetation photosynthetic capability, it can also be related to gross primary production (GPP) [35]. The amount of chlorophyll in the leaves determines photosynthetic capacity and is thus one of the most significant physiological factors influencing crop yield [36]. Sharma et al., 2019 proposed that pesticide stress affects photosynthesis for a variety of reasons, including the down regulation of photosynthetic enzymes, which reduces the production of photosynthetic pigments, the decreased stability of protein-pigment complexes, which causes an increase in pigment degradation, the restriction of QA oxidation, which prevents the electron transfer from PSII to PSI, and the production of free radicals [37]. Mishra et al, 2008, demonstrates that DM has an immediate effect on the different locations of the photosynthetic electron transport chain. At all DM concentrations, PS II reduction and chain activity were observed. With rising dimethoate concentrations, there was a considerable decrease in PS II and overall chain activity, which is linked to damage to the oxygen-evolving complex, which eventually gets transferred to the plastoquinone site and the PS II reaction centre [38]. Impacts of pesticides on animal systems are well studied [39-42]. On the contrary, phytotoxicity data is very scarce, which necessitates the studies being conducted on multiple crops. Parween et al, 2014 reviewed the effect of pesticide on plants and concluded that it leads to alteration in biochemical, physiologi-

Table 2: Evaluation of plant growth parameters at field application and at residue levels

Pesticide concentration	Reduction in RL	Reduction in SL	Reduction in DW	Reduction in Chlorophyll content	Percent phytotoxicity
At field residue level	14.6 %	11.7 %	22%	6.8%	15%
At field application level	69.7 %	37.6%	39%	48.8%	70%

cal parameters of plants which might be visible as decrease in yield [43]. The majority of research studies on plants, have focused on pesticide residue detection rather than investigating the physiological phytotoxicity caused by pesticides. The findings of this study will

help researchers better understand the influence of DM on numerous plant development indices, notably in *Sorghum bicolor*, at both the residue and field application levels. **Table 2:** Evaluation of plant growth parameters at field application and at residue levels

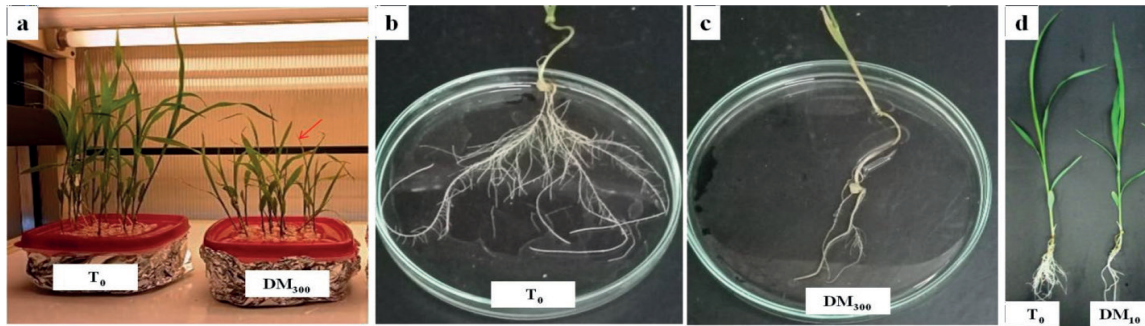


Fig.3.a. Phytotoxic impact of DM on aerial plant parts at field application level; T_0 (No pesticide), DM_{300} (300 ppm of DM), **b.** Phytotoxic impact of DM on root system architecture at field application level **c.** plant phytotoxicity at residue level (10ppm); T_0 (No pesticide), DM_{10} (10 ppm of DM).

Comparative analysis of RSA was done both visibly and by using RhizoVision Explorer version 2.03 software and results are detailed in Table 3. Reductions in root branching and root hairs were clearly visible in the presence of DM (Figure 3). Profuse primary and secondary root branching and extended root system architecture was observed in the absence of pesticide stress. Upon challenging with DM the plant exhibited a severely constricted root architecture, where there is a predominant decrease in the number of primary, secondary and tertiary roots were recorded. The overall root surface area was reduced by >1000 fold in DM challenged plants. As

the root hairs take nutrients and water from the soil, a healthy and robust root system is essential for plant growth. [44]. These morphological changes may have an influence on yield, since biomass was reduced by 22% and 39% at 10 ppm and 300 ppm, respectively. The findings of this study reveal that DM has a detrimental impact on plant development and that the plant cannot overcome it on its own. Therefore, utilizing microorganisms with the ability to protect plants under pesticide stress (DM) would help in alleviation of phytotoxicity due to pesticides. In this study, PGPF-T103 was selected for further *in-vivo* plant growth assays and greenhouse studies.

Table3. Comparative analysis of RSA under no pesticide condition and DM stress

DM (ppm)	R.O.I	No. of roottips	No. of branch points	Total root length. px	Network area.px2	Volume. px3	Surface area.px2
0 ppm	Full	38	40	1956	42701	17315259	476353
300 ppm	Full	2	4	31	247	0.96	427

* Pixel to millimeter conversion factor-25.4, px-pixel, RSA-root system architecture, R.O.I-Region of interest

Employing trichoderma to alleviate dimethoate phytotoxicity

Plant growth support by PGPF under dimethoate stress in in-vivo bioassay

The effects of inoculation with PGPF on plant growth were visible on shoot length, root length, plant biomass, and the root system architecture of sorghum plants at 15 days after germination (Figure 4). Seed priming with PGPF exhibited a significant ($p < 0.05$) improvement in the growth of sorghum plants under normal (no pesticide) and pesticide stress (10 to 300 ppm DM) conditions. It resulted in an increase in root length, of 29%, 53%, 233%, and 119% at 10 ppm, 50 ppm, 100 ppm, and 200 ppm, respectively. However, the increases in shoot length were 15% at 10 ppm and around 3% at 200 ppm. *Trichoderma* was also earlier known to increase root length under drought and salinity stress [45, 46]. Biomass increased by 36%, 10% was recorded at 10 ppm and 200 ppm, respectively (Figure 4). Chlorophyll has direct functions in photosynthesis and is thus strongly related to crop photosynthetic capacity, development, and yield. Ghimire et al, (2015) [47] demonstrated that chlorophyll concentration has a favorable and substantial influence on maize grain production. A significant increase in chlorophyll content was observed in PGPF treatments up to 100 ppm of DM under *in-vivo* conditions. PGPF helps the plants under stress in two main ways, firstly, by giving growth support (increase in root length, shoot length, biomass); and secondly, by alleviating the phytotoxicity and by producing molecules like proline that help them cope with the stressed condition.

Proline is required by plants in a number of stress scenarios. It is a good osmolyte, metal chelator, antioxidant defense molecule, and signaling chemical [48]. In this study, increasing DM concentrations resulted in a steady rise in proline content in untreated plants. Proline is a stress marker and produced under abiotic stress conditions to stabilize proteins, enzymes, to maintain membrane integrity, to detoxify ROS [49]. Pesticide leads to drying of plant which leads to cellular dehydration in such conditions plants produce proline which

act as an osmoprotectant [50]. Shakir et al, 2018, also reported similar results, where imidacloprid pesticide significantly increased proline levels (65% to 138%) in the shoot tissues at all applied concentrations [51]. In this study, PGPF treatment resulted in lower proline levels than the untreated control at each concentration (Figure 5). The values are statistically significant; implicating that PGPF-T103 treatment was effective in easing stress response in plants. Lower proline concentration after PGPF treatment demonstrates the efficacy of PGPF to rescue the plants from DM stress, as greater levels of proline are recorded under various abiotic stresses.

Greenhouse study

A long-term greenhouse assay (45 days) was performed to evaluate the ability of PGPF-T103 to alleviate the DM stress symptoms in *S. bicolor* and support plant growth. Figure 6 shows the phytotoxicity percentage based on RL and SL recorded under varying concentrations of DM. Other investigations also noted a reduction in the length of the shoots and roots under pesticide stress [52, 53]. Phytotoxicity was more visible in roots than shoots. For instance, at 50 ppm DM, phytotoxicity was 29% in roots whereas in shoot phytotoxicity was 9%. A similar pattern was observed at 300 ppm DM, where the phytotoxicity in the root was 76% and that in the shoot was 48%. This could be because roots are highly sensitive in recognizing the physicochemical variations in the soil, and also because they are the principal structures that can influence sustained nutrient and signaling functions of the plants that are challenged with a multitude of abiotic stresses [54]. Thus till a threshold concentration, the pesticide stress might be affecting the plant root system visibly more as compared to its aerial parts. However, once pesticide tolerance is breached the impact is prominent even in the aerial parts of the plant. For instance, browning of shoot tips, necrosis, chlorosis, burning, stunted growth, decrease in number of leaves as well as their width was recorded at higher concentration of DM (300, 600 ppm).

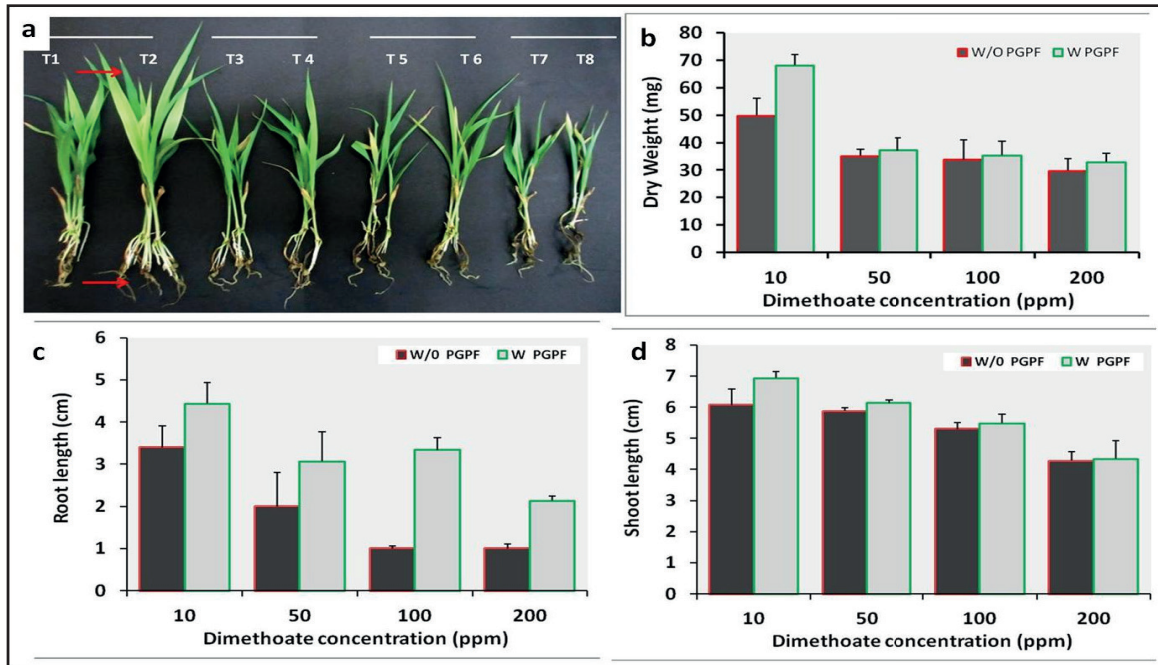


Fig.4. Plant growth support by PGPF-T103 under dimethoate stress **a.** Plant growth under DM stress (10-200 ppm), **T1** (10 ppm DM), **T2** (10 ppm DM+ T103), **T3** (50 ppm DM), **T4** (50 ppm DM+T103), **T5** (100 ppm DM), **T6** (100 ppm+ T103), **T7** (200 ppm DM), **T8** (200 ppm+ T103), **b.** Chlorophyll content, **c.** Root length, **d.** Shoot length and **e.** Dry weight, under DM stress 10 ppm with and without PGPF-T103 treatment. The comparison of treatments was performed by ANOVA single factor, P value <0.05 was considered as statistically significant. Phytotoxicity symptoms were recorded in plants under DM stress, where PGPF treatment is not done. At 10 ppm of DM, phytotoxicity was 10%, and it was around 65% at 300 ppm of DM.

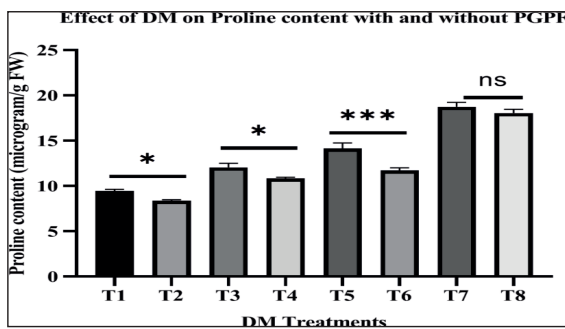


Fig.5. Proline content under DM stress in presence and absence of PGPF-T103, **T1** (10 ppm DM), **T2** (10 ppm DM+ T103), **T3** (50 ppm DM), **T4** (50 ppm DM+T103), **T5** (100 ppm DM), **T6** (100 ppm+ T103), **T7** (200 ppm DM), **T8** (200 ppm+ T103), The comparison of treatments was performed by ANOVA single factor, P value <0.05 was considered as statistically significant. ns- Not significant, *-P<0.05, **-P<0.01, ***-P<0.001

Similar symptoms due to pesticide stress were reviewed by Sharma et al, 2017 [55]. A close observation of Figure 6 reveals this fact, where up to 300 ppm the impact on shoot phytotoxicity was much lesser as compared to impact on root. However, beyond threshold (300 ppm), the adverse impact on the shoot is as strong as the adverse impact on root. PGPF-T103 application resulted in better root systems in *S. bicolor*. Growth parameters, such as the RL, SL and DW recorded from 45 days old plants, are shown in Table 3. Inthama et al, 2021 also observed that application plant growth promoting microbe *B. aryabhatai* in paraquat pesticide contaminated soil, resulted in longer root and shoot lengths in cowpea [55]. In another study *Trichoderma asperellum* increased the phoxim tolerance in *Solanum lycopersicum* by promoting plant detoxification potential [56].

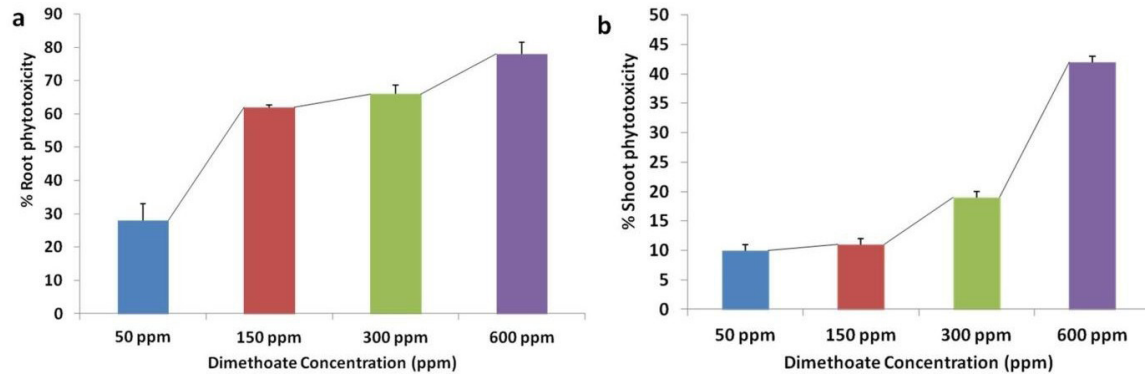


Fig.6. Phytotoxicity based on **a.** root length and **b.** shoot length under DM stress (50 ppm, 150 ppm, 300 ppm and 600 ppm)

Rhizospheric application of PGPF T103 increased the plant growth up to 300 ppm of DM (Figure 7). Findings of our study corroborate the previous findings where application of microbes helped the plants to cope up with phoxim pesticide stress [57]. PGPF-T103 enhances the R/S ratio at each concentration of DM. For instance, without PGPF treatments, the R/S ratio decreased from 5.6 (at 0 ppm), to 4.3 (at 50 ppm), 0.23 (at 150 ppm), and 0.21 (at 300 ppm). Upon PGPF treatment, the R/S ratio was 0.66, 0.35, and 0.34 at 0 ppm, 150 ppm, and 300 ppm, respectively. This could

be because PGPF improves the architecture of root systems, which is evident from the increased root lateral branching and root hair development. Plants with a higher value of R/S indicate their enhanced ability to absorb water and nutrients. The percentage increase in root length, shoot length, and biomass at con

Values are the mean value \pm S.D of three independent replicate. The comparison of treatments was performed by one-way ANOVA followed by Tukey's post hoc test, the values of $P \leq 0.05$ were considered statistically significant*

Table 4. Effect of DM stress on growth parameters of *S. bicolor* in presence and absence of PGPF-T103

Treatments	RL (cm)	% Increase RL upon PGPF treatment	SL (cm)	% Increase in SL upon PGPF treatment	DW(mg)	% Increase in DW upon PGPF treatment
T1 (0ppm)	5.6 \pm 0.5	Control (0ppm)	10 \pm 0.1	Control (0ppm)	202 \pm 2	Control (0ppm)
T2 (0ppm+PGPF)	*7 \pm 0.5	25%	12 \pm 9.1	20%	*227 \pm 6.7	12%
T3 (50 ppm)	4 \pm 0.9	Control (50ppm)	9.1 \pm 0.5	Control (50ppm)	160 \pm 11	Control (50ppm)
T4(50ppm+PGPF)	****7.3 \pm 0.6	82%	11 \pm 0.4	17%	****204 \pm 11	27%
T5 (150ppm)	2.1 \pm 0.1	Control(150 ppm)	9.1 \pm 0.1	.	89 \pm 2.5	Control(150 ppm)
T6 (150ppm+PGPF)	*3.8 \pm 0.6	80%	11 \pm 0.6	17%	107 \pm 4.2	20%
T7 (300ppm)	1.9 \pm 0.3	Control(300 ppm)	8.1 \pm 0.7	Control(300 ppm)	67 \pm 9.3	Control(300 ppm)
T8 (300ppm+PGPF)	* 3.4 \pm 0.1	79%	*10 \pm 0.8	23%	**96 \pm 8.7	43%
T9 (600ppm)	1.2 \pm 0.3	Control(600 ppm)	5.2 \pm 0.2	Control(600 ppm)	33 \pm 5.8	Control(600 ppm)
T10 (600ppm+PGPF)	2.3 \pm 0.5	92%	5.9 \pm 1	14%	50 \pm 6.8	52%

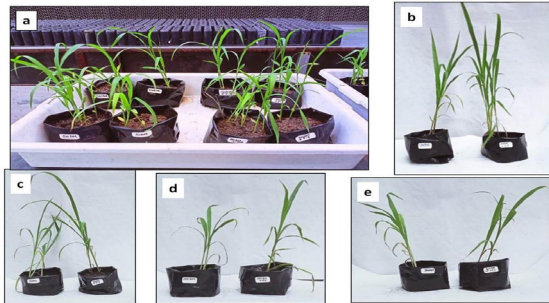


Fig.7. Effect of DM stress on *S. bicolor* grown in the greenhouse at 45 Days; (a) Plants grown in greenhouse (b) untreated control pesticide (0 ppm), treated 0 ppm+ PGPF; (c) 50 ppm, 50 ppm+ PGPF; (d) 150 ppm, 150 ppm+ PGPF; (e) 300 ppm, 300 ppm+ PGPF. In b, c, d and e- Plants on the left side are untreated and on the right side are treated with PGPF-T103 concentrations of 0 ppm, 50 ppm, 150 ppm, and 300 ppm is presented in Table 3. PGPF was able to support plant growth both at 15 days and at 45 days of experiments. Plant growth support by microbes under xenobiotic stress was established by few other researchers [58, 59]

Conclusion

DM influences plant growth and development in terms of both qualitative and quantitative parameters. The deleterious effects of DM are evident right from the concentrations as low as 10 ppm which escalated further as the concentration of DM has increased. PGPF-T103 primed seedlings were successful in overcoming stress due to DM more effectively till a concentration of 100 ppm, beyond 100 ppm and till 300 ppm even though they performed better than PGPF-T103 untreated host they were not completely successful in reversing the impact of DM induced stress. Nevertheless, irrespective of the concentration of pesticide PGPF-T103 treated seedlings invariably suffered less from the DM exposure as compared to those plants that were left untreated. Treated plants were supported by the increased root length; shoot length, Chlorophyll a and drop in the proline content and phytotoxicity. The protective impact and growth support

of sorghum were observed both in *in-vivo* (15 days) and greenhouse (45 days) studies. These results, linked to the PGPF-T103 application, are definitive evidence that *Trichoderma harzianum* isolate T103 can protect the plants under pesticide stress.

Acknowledgements: We would like to thank the Department of Biotechnology (DBT), Government of India, for providing funds and the Jaypee Institute of Information Technology for providing the basic facilities and infrastructure required for the execution of the project.

Conflict of interest statement: The authors declare that they have no conflict of interest in the publication.

References:

1. Arumugam, Y., Chinnusamy, M., Chinnusamy, K., & Kuppasamy, S. (2021). Sorghum as Biofuel Crop: Interdisciplinary Methods to Enhance Productivity (Botany, Genetics, Breeding, Seed Technology, and Bioengineering). In *Biofuels and Biodiesel*, pp.253-270.
2. Hossain, M. S., Islam, M. N., Rahman, M. M., Mostofa, M. G., & Khan, M. A. R. (2022). Sorghum: A prospective crop for climatic vulnerability, food and nutritional security. *Journal of Agriculture and Food Research*, 100300.
3. Reddy, P. S., & Reddy, B. V. Phenotyping in Sorghum [*Sorghum bicolor* (L.) Moench]. Ravikesavan, R., Sivamurugan, A. P., Iyanar, K., Pramitha, J. L., & Nirmalakumari, A. (2022). Millet Cultivation: An Overview. *Handbook of Millets-Processing, Quality, and Nutrition Status*, 23-47.
4. Kaushal, J., Khatri, M., & Arya, S. K. (2021). A treatise on Organophosphate pesticide pollution: Current strategies and advancements in their environmental degradation and elimination. *Ecotoxicology and Environmental Safety*, 207:111483

5. Singh, R. P., Qidwai, S., Singh, O., Reddy, B. R., Saharan, S., Kataria, S. K., ... & Kumar, L. (2022). Millets for food and nutritional security in the context of climate resilient agriculture: A Review. *International Journal of Plant & Soil Science*, 939-953.
6. Hossain, M. S., Islam, M. N., Rahman, M. M., Mostofa, M. G., & Khan, M. A. R. (2022). Sorghum: A prospective crop for climatic vulnerability, food and nutritional security. *Journal of Agriculture and Food Research*, 100300.
7. Fu, H., Tan, P., Wang, R., Li, S., Liu, H., Yang, Y., & Wu, Z. (2022). Advances in organophosphorus pesticides pollution: Current status and challenges in ecotoxicological, sustainable agriculture, and degradation strategies. *Journal of Hazardous Materials*, 424: 127494.
8. Guo, C., Cui, W., Feng, X., Zhao, J., & Lu, G. (2011). Sorghum insect problems and Management. *Journal of integrative plant biology*, 53(3): 178-192.
9. Koli, P., & Bhardwaj, N. R. (2018). Status and use of pesticides in forage crops in India. *Journal of pesticide Science*, 43(4): 225-232.
10. Bagyalakshmi, J., Kavitha, G., & Ravi, T. K. (2011). Residue determination of dimethoate in leafy vegetables (spinach) using RP-HPLC. *International Journal of Pharma Sciences and Research*, 2(2): 62-64.
11. Mohamed, A. O., Abdelbagi, A. O., Abdalla, A. M., Sulieman Ahmed Ishag, A. E., Ali Hammad, A. M., Hamed Gadallah, N. A., & Hur, J. H. (2021). Insecticide Residues in Cotton, Sorghum and Fallow Soil from the Nuba Mountains Cotton Corporation of South Kordofan State, Sudan. *Journal of Health Pollution*, 11(30):210608.
12. Eken, A. (2017). An overview on dimethoate toxicity and human health. *The Turkish Journal Of Occupational/Environmental Medicine and Safety*, 2(4): 32
13. Katsikantami, I., Colosio, C., Alegakis, A., Tzatzarakis, M. N., Vakonaki, E., Rizos, A. K., ... & Tsatsakis, A. M. (2019). Estimation of daily intake and risk assessment of organophosphorus pesticides based on biomonitoring data—the internal exposure approach. *Food and chemical toxicology*, 123: 57-7
14. Kumari D, John S (2019) Health risk assessment of pesticide residues in fruits and vegetables from farms and markets of Western Indian Himalayan region. *Chemosphere* 427 224:162-167 Kamal, A., Ahmad, F., & Shafeeque, M. A. (2020). Toxicity of pesticides to plants and non-target organism: A comprehensive review. *Iranian Journal of Plant Physiology*, 10(4): 3299-3313.
15. Jan, S., Singh, R., Bhardwaj, R., Ahmad, P., & Kapoor, D. (2020). Plant growth regulators: a sustainable approach to combat pesticide toxicity. *3 Biotech*, 10(11), 1-11.
16. Murali, M., Naziya, B., Ansari, M. A., Alomary, M. N., AlYahya, S., Almatroudi, A., ... & Amruthesh, K. N. (2021). Bioprospecting of rhizosphere-resident fungi: their role and importance in sustainable agriculture. *Journal of Fungi*, 7(4): 314.
17. Woo, S. L., Hermosa, R., Lorito, M., & Monte, E. (2022). Trichoderma: a multi-purpose, plant-beneficial microorganism for eco-sustainable agriculture. *Nature Reviews Microbiology*, 1-15.
18. Kumari, A., Sattiraju, K.S. (2022). *In vitro* and *in vivo* evidence for the mitigation of monocrotophos toxicity using native *Trichoderma harzianum* isolate. *Biologia* 77:

- 2335– 2349.
19. Codex Alimentarius (Codex). Emerging Issues in Food Safety and Quality in Countries in the Region. Agenda Item 3.1. In: Joint FAO/WHO Food Standards Programme FAO/WHO Coordinating Committee for Asia, 21st session. September 23–27, Goa, India. Codex Alimentarius, Rome, Italy (2019b)
 20. Sun, X. D., & Dong, X. L. (2015). Quantitative analysis of dimethoate pesticide residues in honey by surface-enhanced Raman spectroscopy. *Guang pu xue yu Guang pu fen xi= Guang pu*, 35(6): 1572-1576.
 21. Sahu, P. K., Tilgam, J., Mishra, S., Hamid, S., Gupta, A., Verma, S. K., & Kharwar, R. N. (2022). Surface sterilization for isolation of endophytes: Ensuring what (not) to grow. *Journal of Basic Microbiology*.
 22. López-Bucio, J., Pelagio-Flores, R., & Herrera-Estrella, A. (2015). Trichoderma as biostimulant: exploiting the multilevel properties of a plant beneficial fungus. *Scientia horticultrae*, 196: 109-123.
 23. Kathuria, D., Bhattu, M., Verma, M., & Billing, B. K. (2022). Chromatographic techniques for the analysis of organophosphate pesticides with their extraction approach: a review (2015-2020). *Analytical Methods*.
 24. Yadav, P., Kumari, A., & Sundari, S. K. (2020). -ASUREII: A multi-potential plant bioassay as a pre-determinative microbial efficiency testing tool for bioinoculant studies. *MethodsX*, 7: 100685.
 25. Illescas, M., Morán-Diez, M. E., Martínez de Alba, Á. E., Hermosa, R., & Monte, E. (2022). Effect of *Trichoderma asperellum* on Wheat Plants' Biochemical and Molecular Responses, and Yield under Different Water Stress Conditions. *International Journal of Molecular Sciences*, 23(12): 6782.
 26. Rawal, R., Scheerens, J. C., Fenstermaker, S. M., Francis, D. M., Miller, S. A., & Benitez, M. S. (2022). Novel Trichoderma Isolates Alleviate Water Deficit Stress in Susceptible Tomato Genotypes. *Frontiers in plant science*, 13:869090-869090.
 27. Ore, O. T., Adeola, A. O., Bayode, A. A., Adedipe, D. T., & Nomngongo, P. N. (2022). Organophosphate pesticide residues in environmental and biological matrices: Occurrence, distribution and potential remedial approaches. *Environmental Chemistry and Ecotoxicology*.1.
 28. Hage-Ahmed, K., Rosner, K., & Steinkellner, S. (2019). Arbuscular mycorrhizal fungi and their response to pesticides. *Pest management science*, 75(3): 583-590. Abderrahim, B., Abderrahman, E., Mohamed, A., Fatima, T., Abdesselam, T., & Krim, O. (2015). Kinetic thermal degradation of cellulose, polybutylene succinate and a green composite: comparative study. *World J. Environ. Eng*, 3(4): 95-110.
 29. Silambarasan, S., & Abraham, J. (2013). Ecofriendly method for bioremediation of chlorpyrifos from agricultural soil by novel fungus *Aspergillus terreus* JAS1. *Water, Air, & Soil Pollution*, 224(1):1-11.
 30. Rearte, T. A., Bozzano, P. B., Andrade, M. L., & Fabrizio de Iorio, A. (2013). Biosorption of Cr (III) and Pb (II) by *Schoenoplectus californicus* and Insights into the Binding Mechanism. *International Scholarly Research Notices*, 2013.
 31. Pandey, J. K., Dubey, G., & Gopal, R. (2022). Prolonged Use of Insecticide Dimethoate Inhibits Growth and Photosynthetic Activity of Wheat Seedlings:

- A Study by Laser- Induced Chlorophyll Fluorescence Spectroscopy. *Journal of Fluorescence*, 32(6): 2159- 2172.
32. Gitelson, A. A., Viña, A., Verma, S. B., Rundquist, D. C., Arkebauer, T. J., Keydan, G., ... & Suyker, A. E. (2006). Relationship between gross primary production and chlorophyll content in crops: Implications for the synoptic monitoring of vegetation productivity. *Journal of Geophysical Research: Atmospheres*, 111(D8).
 33. Jiang, G., Zeng, J., & He, Y. (2014). Analysis of quantitative trait loci affecting chlorophyll content of rice leaves in a double haploid population and two back-cross populations. *Gene*, 536(2): 287-295.
 34. Sharma, A., Kumar, V., Shahzad, B., Ramakrishnan, M., Singh Sidhu, G. P., Bali, A. S., & Zheng, B. (2020). Photosynthetic response of plants under different abiotic stresses: a review. *Journal of Plant Growth Regulation*, 39(2): 509-531.
 35. Mishra, V., Srivastava, G., Prasad, S.M., Abraham, G., 2008. Growth, photosynthetic pigments and photosynthetic activity during seedling stage of cowpea (*Vigna unguiculata*) in response to UV-B and dimethoate. *Pesticide biochemistry and physiology*. 92: 30-37.
 36. Apaydin, F. G., Kalender, S., & Kalender, Y. (2022). Subacute exposure to dimethoate induces hepatotoxic and nephrotoxic effects on male rats: Ameliorative effects of ferulic acid. *Indian Journal of Experimental Biology (IJEB)*, 61(01):51-58.
 37. Al-Ali, A. A., Kata, F. S., & Hussein, S. M. (2016). Biochemical and Histopathological Changes of Dimethoate in some Organ of Laboratory Mice *Mus musculus* L. *Basrah Journal of Agricultural Sciences*, 29(2).
 38. Devi, S., Singh, J., Kumar, V., & Malik, V. (2019). Monocrotophos induced Biochemical and Histopathological alterations in the Kidney tissues of Mice. *Chemical Biology Letters*, 6(2): 39-45.
 39. Martínez-Morcillo, S., Pérez-López, M., Soler-Rodríguez, F., & González, A. (2019). The organophosphorus pesticide dimethoate decreases cell viability and induces changes in different biochemical parameters of rat pancreatic stellate cells. *Toxicology In Vitro*, 54: 89-97.
 40. Parween, T., Jan, S., Mahmooduzzafar, S., Fatma, T., & Siddiqui, Z. H. (2016). Selective effect of pesticides on plant—A review. *Critical reviews in food science and nutrition*, 56(1): 160-179.
 41. Fageria, N. K., & Moreira, A. (2011). The role of mineral nutrition on root growth of crop plants. *Advances in agronomy*, 110: 251-331. Chepsergon, J., Mwamburi, L., & Kassim, M. K. (2014). Mechanism of drought tolerance in plants using *Trichoderma spp.* *Int J Sci Res*, 3(11): 1592-1595.
 42. Khomari, S., Golshan-Doust, S., Seyed-Sharifi, R., & Davari, M. (2018). Improvement of soybean seedling growth under salinity stress by biopriming of high-vigour seeds with salt-tolerant isolate of *Trichoderma harzianum*. *New Zealand Journal of Crop and Horticultural Science*, 46(2): 117-132.
 43. Ghimire, B., Timsina, D., & Nepal, J. (2015). Analysis of chlorophyll content and its correlation with yield attributing traits on early varieties of maize (*Zea mays* L.). *Journal of Maize Research and Development*, 1(1): 134-145.
 44. Ghosh, U. K., Islam, M. N., Siddiqui, M. N., Cao, X., & Khan, M. A. R. (2022). Proline, a multifaceted signalling molecule in plant

- responses to abiotic stress: understanding the physiological mechanisms. *Plant Biology*, 24(2): 227-239.
45. Alhasnawi, A. N. (2019). Role of proline in plant stress tolerance: A mini review. *Research on Crops*, 20(1).
46. Ahluwalia, O., Singh, P. C., & Bhatia, R. (2021). A review on drought stress in plants: Implications, mitigation and the role of plant growth promoting rhizobacteria. *Resources, Environment and Sustainability*, 5: 100032.
47. Shakir, S. K., Irfan, S., Akhtar, B., Daud, M. K., Taimur, N., & Azizullah, A. (2018). Pesticide-induced oxidative stress and antioxidant responses in tomato (*Solanum lycopersicum*) seedlings. *Ecotoxicology*, 27(7): 919-935.
48. Sidhu, G. K., Singh, S., Kumar, V., Dhanjal, D. S., Datta, S., & Singh, J. (2019). Toxicity, monitoring and biodegradation of organophosphate pesticides: a review. *Critical reviews in environmental science and technology*, 49(13): 1135-1187.
49. Kaur, H., Bhardwaj, R., Kumar, V., Sharma, A., Singh, R., & Thukral, A. K. (2015). Effect of pesticides on leguminous plants: an overview. *Legumes under environmental stress: Yield, improvement and adaptations*, 91-101.
50. Franco, J. A., Bañón, S., Vicente, M. J., Miralles, J., & Martínez-Sánchez, J. J. (2011). Root development in horticultural plants grown under abiotic stress conditions—a review. *The Journal of Horticultural Science and Biotechnology*, 86(6): 543-556.
51. Sharma, A., Kumar, V., Thukral, A. K., & Bhardwaj, R. (2019). Responses of plants to pesticide toxicity: An overview. *Planta Daninha*, 37.
52. Inthama, P., Pumas, P., Pekkoh, J., Pathom-Aree, W., & Pumas, C. (2021). Plant growth and drought tolerance-promoting bacterium for bioremediation of paraquat pesticide residues in agriculture soils. *Frontiers in Microbiology*, 12: 604662.
53. Chen, S., Yan, Y., Wang, Y., Wu, M., Mao, Q., Chen, Y., ... & Ahammed, G. J. (2020). *Trichoderma asperellum* reduces phoxim residue in roots by promoting plant detoxification potential in *Solanum lycopersicum* L. *Environmental Pollution*, 259:113893.
54. Abhilash, P. C., Dubey, R. K., Tripathi, V., Gupta, V. K., & Singh, H. B. (2016). Plant growth-promoting microorganisms for environmental sustainability. *Trends in Biotechnology*, 34(11): 847-850.
55. Inthama, P., Pumas, P., Pekkoh, J., Pathom-Aree, W., & Pumas, C. (2021). Plant growth and drought tolerance-promoting bacterium for bioremediation of paraquat pesticide residues in agriculture soils. *Frontiers in Microbiology*, 12: 604662.
56. Chen, S., Yan, Y., Wang, Y., Wu, M., Mao, Q., Chen, Y., ... & Ahammed, G. J. (2020). *Trichoderma asperellum* reduces phoxim residue in roots by promoting plant detoxification potential in *Solanum lycopersicum* L. *Environmental Pollution*, 259:113893.
57. Abhilash, P. C., Dubey, R. K., Tripathi, V., Gupta, V. K., & Singh, H. B. (2016). Plant growth-promoting microorganisms for environmental sustainability. *Trends in Biotechnology*, 34(11): 847-850.
58. Janeeshma, E., & Puthur, J. T. (2021). Potential role of microbial endophytes in xenobiotic stress management. *Sustainable Environmental Clean-up*, 165-185.

Abbreviations:

PGPF-Plant growth promoting fungi

DM-Dimethoate

LD₅₀-Lethal dose 50

FTIR-Fourier Transform Infrared Spectroscopy

MRL-Maximum Residue Limits

OPP-Organophosphate pesticides

EC- Emulsifiable concentrate,

MDB-Malt dextrose broth, **PMB**-Plant microbe bioassay

CMC-Carboxymethyl cellulose

ALGR-Average linear growth rate

RPM-Revolutions per minute

R/S ratio- Root/Shoot ratio

RL-Root length

SL-Shoot length

DW-Dry weight

Chl- Chlorophyll

PMB-Plant microbe bioassay

PPM-Parts per million

PP%-Phytotoxicity %

Prevalence of Herpes Simplex Virus (HSV) and Cytomegalovirus (CMV) in Oral Squamous Cell Carcinoma patients with a history of Nicotine and Alcohol abuse.

Samata Gadde¹, Sudhakar Poda²

¹ Department of Biotechnology, Acharya Nagarjuna University
² HOD, Department of Biotechnology, Acharya Nagarjuna University
*Corresponding author:

Abstract

Several risk factors cause Oral Squamous cell carcinoma such as alcohol and smoking. In considerable studies, patients without exposure to these habits develop OSCC which emphasizes the role of other factors like oncogenic viruses and genetic susceptibility. Several viruses are frequently associated with OSCC along with co-factors on which the viruses are dependent for their carcinogenic abilities. The accurate role of viruses in cancer development is yet to be studied to improve treatment and prognosis of OSCC. In this study, the prevalence of HSV-1, HSV-2, and CMV in the patients diagnosed with OSCC are reported with help of molecular and quantification techniques such as PCR and ELISA which recognize the DNA of the virus in the host and IgG, IgM antibodies of HSV-1, HSV-2 and CMV in the blood serum. The results are statistically analyzed, determining the significance of the results obtained. OSCC occurrence because of HSV infection with risk factors like smoking, alcohol consumption, tobacco chewing was less as compared to the cancer caused by infection of CMV with combination of risk factors. The genetic material of both the studied virus HSV (1 and 2) and CMV were observed to be in majority biopsy samples of the patients.

Keywords: Oral Squamous Cell Carcinoma, HSV, CMV, antibodies, quantification, EBV, Vaccines, oncogenic proteins, OSCC, HPV, oncogenic viruses, head and neck cancers, PCR, tobacco chewing, smoking, oral cancer.

Introduction

Oral cavity cancer is the sixth most recurrent cancer reported worldwide, of which almost 5% has been observed in developed countries. In the Indian subcontinent, due to its large population, it was always regarded as an epicentre for oral carcinomas and a major public health challenge by the WHO¹. There is a vast variation in the global burden of this disease, which has vital incidents in India, South-east Asia, and South Asia being the highest in the world. An increase in the incidences was observed in Latin America, Europe, and other Pacific parts. An enormous effect on the biological system by environment and lifestyle factors carried out a direct or indirect role in cancer development². OSCC is primarily originating from mucosal epithelium that is non-keratinized and stratified. Some similarities to Squamous cell carcinomas occur on other body parts morphologically like the bronchi, anus, and cervix. It was typically assumed that alcohol, tobacco, and betel quid consumption caused the development of OSCC majorly^{3, 4}.

Oral squamous cell carcinoma patients with a history of nicotine and alcohol abuse.

Since the 20th century, studies on the impact of viruses on OSCC were reported, where the infectious agent was identified and isolated, and which was later observed to be able to induce a tumor in chicken⁵⁻⁸. OSCC etiology depends upon several factors which include environment, lifestyle, genetic alterations, and infectious agents. The chief role in etiology is played by viruses. The most typical viruses which cause OSCC are HPV9, Herpes group¹⁰, CMV¹¹, adenovirus¹² and HPV¹³. HSV includes eight viruses which are HSV-1, HSV-2, EBV, CMV, and VZV¹⁴. In the past few years, HSV has been investigated in association with human cancers. HSV-1 antibodies in patients with oral cancers were observed to be high^{15, 16}. Mainly, IgA and IgM classes were observed in the patients, while anti-HSV IgM retained a transient life in the host. The more considerable risk was observed when risky habits like alcohol consumption, smoking, chewing tobacco along with infection with HSV and CMV caused high-risk cancer. Reports were observed where the genetic material of the viruses was found in the oral cancer patients¹⁷⁻¹⁹. It was deemed that the association of HSV and CMV with oral cancers is difficult to study as the transformed cells do not express the antigens or specific genes to viruses.

Recent years have seen little progress in the study of the malignant potential of HSV. The polymerase chain reaction (PCR) assay is a technique that has several advantages over other methods^{4, 20}. It can detect viral presence in initial infections and requires only a limited quantity of biological material. PCR detection of HPV, Epstein-Barr virus (EBV), and HSV are exceptionally sensitive and specific and can supplement the clinical detection of virus-associated oral lesions^{18, 21}. Because the herpes virus subtypes can vary in distinct parts of the world, there have been few studies in Iran about the prevalence of HSV in OSCC^{3, 11, 17}. This study was conducted to determine the prevalence of HSV and CMV in OSCC (in isolation or in combination with tobacco and alcohol) by

PCR technique. The genetic material of both HSV and CMV in the biopsy samples taken from various sources of the oral cavity of patients and healthy controls and the prevalence of IgG and IgM antibodies in the blood serum that were collected from patients as well as control subjects.

Methods

All the OSCC cases were diagnosed during the study which was carried out by following all the ethical committee standards. All procedures were followed in accordance with the standards of the liable hospital or institution committee. All personnel were interviewed with a planned questionnaire to collect information regarding their lifestyle and habits.

Criteria of selection

All patients have been included in the exclusion criteria as well as exclusion criteria with the help of their clinical data acquired. The required information like age, gender, alcohol intake, smoking, and chewing tobacco products was noted. The exclusion criteria included the patients who denied consent and patients who have to undergo radio or chemotherapy or have any pre-existing conditions like heart diseases. The inclusion criteria included the patients who were confirmed with oral carcinoma and who were AIDS and Hepatitis B negative.

Sample collection

Tumour tissue and blood were collected from OSCC patients and healthy patients at the time of the biopsy. The tissue samples were stored in saline and formalin solution till further use. Blood samples were collected in the EDTA coated tubes to prevent coagulation, and serum was separated which is used as a control in several experiments.

Molecular analysis

DNA was extracted from the biopsy samples of both healthy and OSCC patients. Both forward and reverse primers were designed for HSV : (5'-AGCCTGTACCCCAGCATCAT-3' for-

ward and reverse primer 5'-TGGGCCTTCAC-GAAGAACA-3' for HSV-1 DNA and 1 µl each of the forward primer 5'-AGGCCTACCAACAG-GGCG-3' and the reverse primer 5'-CTGGATC-GACGGGATGTGC-3' for HSV-2) and CMV (forward primer 5'-TTT GGA GAA AAC GCC GAC -3' and the reverse primer 5'-CGC GCG GCA ATC GGT TTG TTG TA -3').

The target DNA fragment was amplified using PCR using Bio-Rad kit maintaining appropriate temperature and time cycles for 40 repeats after which the PCR products were analyzed on 3% agarose gel stained with ethidium bromide and visualized under UV transilluminator.

Quantitative determination of Herpes simplex 1,2 and CMV Ig G and Ig M in the blood serum

This assay was performed with DIESSE Diagnostic Senese kit, Italy. This kit is based upon the ELISA technique where the antigen containing the partially purified or inactive virus is bound to the solid phase. Specific immunoglobulins to the selected viruses were bound to the antigen by incubating them together in human serum. Subsequent washes were performed to eliminate any loose proteins. The complex of the antigen and the specific immunoglobulin was incubated along with a conjugate made up of human IgG monoclonal antibodies in a complex with horseradish peroxidase. Peroxidase substrate is added after washing to remove any unconjugated complexes. Development of color was observed which is proportional to the antibody concentration of the serum sample. The reaction is interrupted by adding a stop solution which develops a yellowish color in the samples which can be read using a microplate reader.

Results and Discussion

Demographic characteristics of the population

The current study has employed 100 patient samples of Oral Squamous Cell Carcinoma (OSCC) as well as 100 healthy controls. The

demographic characters and the involved risk factors were already described [Table 1]. The demographic profiles of all the subjects including age, sex, habits that can cause OSCC were noted. 45% of the 100 OSCC patients were male, while the rest 55% were females. In a similar fashion, in the control group, males were 55% while females were 45%. The age groups for patients range from 9-87 while for the control population, age recorded was 21-76. The average age of the patient samples, as well as healthy controls during diagnosis, were recorded as 50.53 and 55.27 respectively. The subjects with carcinomas were divided into four sub-groups which are < 25, 26-45, 46-65, and > 66 age groups. Habits such as tobacco chewing, alcohol, and tobacco chewing, alcohol and smoking, and alcohol, smoking, tobacco chewing in OSCC as well as controls were observed to be 32%, 30% and 17%, 13% and 12%, 6%, and 10%, 6% respectively. The biopsy for the cancer patients was categorized as tongue, buccal mucosa, mandible, oral cavity, retromolar trigone, the floor of the mouth, lip, tongue base, maxilla, and palate which showed incidence as 23%, 35%, 12%, 10%, 8%, 4%, 3%, 2%, 2% and 1% respectively. The tumor was categorized into four stages like stage 1 of 6%, stage 2 of 21%, stage 3 of 39% and stage 4 of 34% [Table 1].

Table 1: Demographic table of patient and healthy population:

Clinical Characteristics	n = 100 (Cases)	n = 100 (Controls)
Gender		
Males	45(45%)	55(55%)
Females	55 (55%)	45 (55%)
Mean age & Range Males	50.53/9-87	
Mean age & Range Females	55.27/30-75	
Age Distribution		
26-45	28 (28%)	22(22%)

Oral squamous cell carcinoma patients with a history of nicotine and alcohol abuse.

46-65	60 (60%)	70(70%)
66 and above	12 (12%)	8 (8%)
Habitual Risk		
Alcoholics	—	3 (3%)
Smokers	6(6%)	13 (13%)
Tobacco chewing	31(31%)	30 (30%)
Alcohol + Smoking	14 (14%)	6 (6%)
Alcohol + Tobacco chewing	26 (26%)	13(13%)
Smoking + Tobacco chewing	2 (2%)	4 (4%)
Alcohol + Smoking + Tobacco chewing	10(10%)	6 (6%)
No Habits	11%(11%)	25(25%)
Site of Diagnosis		
Tongue	23(23%)	
Buccal mucosa (BM)	35 (35%)	
Mandible	12 (12%)	
Oral Cavity	10 (10%)	
Retromolar trigone	8(8%)	
Floor of mouth	4(4%)	
Lip	3(3%)	
Base of tongue	2 (2%)	
Maxilla	2 (2%)	
Palate	1 (1%)	
Staging		
Stage 1	6 (6%)	
Stage 2	21 (21%)	
Stage 3	39 (39%)	
Stage 4	34(34%)	

HSV-1 and HSV-2 genotyping

Among the 100 selected patients, the DNA of Herpes Simplex Virus was found to represent 7% in OSCC and 2% in control samples when the molecular analysis was performed on the samples. 4% incidence of HSV-1 was observed while HSV-2 represented 1% while there was no incidence (0%) in control samples when HSV-2 was present. Both HSV-1 and the two were ob-

served in 2% of the combined patient population and 0% in the control population. The results were statistically significant with the odd ratio of 2.04, CI of 0.36 - 11.4, and p-value of 0.005 when the patients and controls were compared. Differences between the cases and controls were observed to be not significant when the risk was for HSV-2, where the OR = 2.04; CI=0.00-1.04 P=0.4 and for the presence of HSV-1 and 2 were reported as OR=0.02; 95%CI=0.00-1.55; P=0.08. [Table 2, Figure 1]

Table 2 HSV genotyping in OSCC and control group

HSV typing	Cases N (%)	Controls N (%)	Odds Ratio	95% CI	P-Value
HSV-1					
Positive	4	2	2.04	0.36 - 11.4	0.05
Negative	96	98			
HSV-2					
Positive	1	0	0.01	0.00 - 1.04	0.4
Negative	99	0			
HSV-1&2					
Positive	2	0	0.02	0.00 - 1.55	0.08
Negative	98	0			

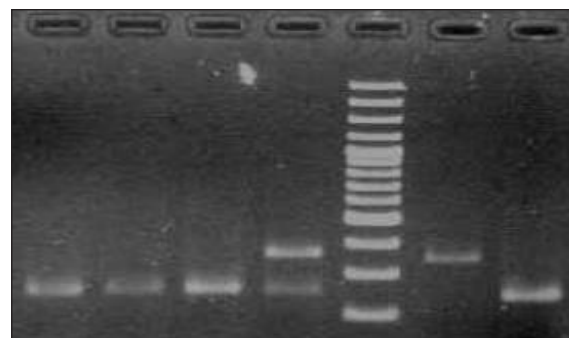


Figure 1: HSV infected OSCC Samples

- 1 – HSV negative
- 2 – HSV negative
- 3 – HSV negative
- 4 – HSV-1 positive
- 5 – Ladder
- 6 – HSV-2 positive
- 7- HSV negative

Genotyping of HSV in OSCC and control groups according to demographics

The presence of viral DNA in the patient and control population was categorized according to the demographics. Under the gender category, three males and 1 female patient have shown HSV-1, 1 male has shown HSV-2, and two females were observed to have both HSV-1 and 2 DNA. The results were not significant as the p-value = 0.232. Underage distribution, 2 falls under 26- 45, 2 under 46-65 for HSV-1. Only one patient was observed to have HSV-2 who falls under 46-65 group. Two patients under the group 46-65 were observed to have both HSV-1 and 2; the results were not significant as the p-value is 0.733. Under the category site of diagnosis, one patient each for the palate, RMT, the oral cavity, and BM samples revealed the presence of HSV-1 DNA. HSV-2 was observed in only one patient whose sample was mandible. Two patients whose tongue sample was taken

have shown the presence of both HSV-1 and two. The results obtained were not significant as the p-value was reported as 0.175. HSV-1 was observed in three patients whose stage is 2 and one patient whose tumour is at stage 4. HSV-2 was observed in only one patient with stage three tumours. Both HSV-1,2 were observed in two patients whose tumour was in stages 3 and 4 respectively. The results when analyzed were not significant as their p-value is 0.595. Under the category of habits, one patient each has alcohol + smoking, alcohol+smoking+chewing, and patients with no habits contain HSV-1 DNA. HSV-2 was observed in the one patient each maintaining habits like alcohol consumption, smoking, and alcohol +smoking. Both HSV-1 and two were observed in one patient each retaining habits like alcohol consumption, smoking, and alcohol+chewing. The results were not statistically significant as their p-value is > 0.05. [Table 3]

Table 3 Correlation of HSV-1 and 2 genotypes with demographical factors of OSCC patients

Demographical Characteristics	HSV-1	HSV-2	HSV-1&2	F-value	P-value
Gender					
Males (n=45)	3	1	0	1.453	0.232
Females (n=55)	1	0	2		
Age Distribution					
<25	0	0	0	0.428	0.733
26-45	2	0	0		
46-65	2	1	2		
66 and above	0	0	0		
Site of Diagnosis					
BM	1	0	0		
Tongue	0	0	2		
BOT	0	0	0		
FOM	0	0	0		
LIP	0	0	0	1.689	0.175
Mandible	0	1	0		
Maxilla	0	0	0		
Palate	1	0	0		
RMT	1	0	0		
Oral Cavity	1	0	0		
Staging					

Oral squamous cell carcinoma patients with a history of nicotine and alcohol abuse.

Stage 1	0	0	0	0.633	0.595
Stage 2	3	0	0		
Stage 3	0	1	1		
Stage 4	1	0	1		
Habitual Risk					
Alcoholics	0	0	1	0.103	0.958
Smokers	0	0	1	0.753	0.523
Chewers	0	0	0		
Combination Risk Factors					
Alcohol+Smoking	1	1	0	0.673	0.571
Alcohol+Chewing	0	0	1		
Smoking+Chewing	0	0	0		
Alcohol+Smoking +Chewing	1	0	0		
No Habits	1	0	0		

Quantification of HSV-1, 2 IgG and IgM in serum

46% of the total OSCC patients and 5% of the control subjects were observed to have HSV-1 IgG antibodies in their serum which was greater than equal to 1.2 Mmol/L while the HSV-1 IgM antibodies were observed in 11% of OSCC patients and 4% of the control population. HSV-2 IgG antibodies were observed in 8% and 3% of patients and control populations respectively

whereas 3% of patients and 2% of the control population were positive for HSV-2 IgM. Univariate analysis was performed which revealed that the results of HSV-1 and HSV-2 IgG, as well as IgM levels, were not significant when the patient samples were compared to controls. The levels were elevated which were significant in the case of HSV-1 IgG (0.001) in OSCC cases as compared to the control groups while there was no association between HSV-1 IgM, HSV-2 IgG, and HSV IgM. [Table 4]

Table 4: Levels of HSV IgG and Ig M 1 &2 in the serum of OSCC and controls

Serum HSV-1	C a s e s n(%)	Mean±SD	C o n t r o l s n(%)	Mean±SD	F-value	P-Value
IgG levels (Mmol/L)						
< 1.2	54	0.58±0.31	95	0.50±0.22	111.2	0.001
≥1.2	46	3.35±1.85	5	3.18±2.32		
IgM levels (Mmol/L)						
< 1.2	89	0.59±0.3	96	0.43±0.19	5.12	0.005
≥1.2	11	3.13±3.3	4	1.86±0.43		
Serum HSV-2 IgG levels (Mmol/L)						
< 1.2	92	0.64±0.24	97	0.53±0.29	47.5	0.001
≥1.2	8	3.72±1.73	3	3.29±2.0		

Serum HSV-2 IgM levels (Mmol/L)						
< 1.2	97	0.45±0.21	98	0.47±0.23	2.69	0.91
≥1.2	3	1.29±0.00	2	1.49±0.14		

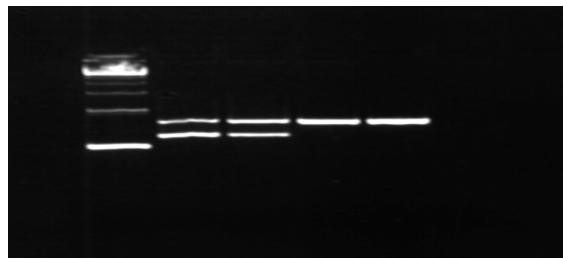
CMV genotyping

In the population of both OSCC patients and control, DNA of CMV was found in 21% of patients and 2% of control when the samples were analysed molecularly. The results obtained were significant statistically with an odd ratio of 13.02, 95%CI range of 2.96-57.2, and the P-value of 0.007. [Table 5, Figure 2]

Table 5 CMV genotyping in OSCC and control group

CMV Typing	Cases N (%)	Con-trols N (%)	Odds Ratio	95% CI	P-Value
Positive	21	2	13.02	2.96 - 57.2	0.0007
Negative	7	98			

Figure 2: CMV infected OSCC Samples



L - 123bp ladder 2 - CMV positive patient 2
 1 - CMV positive patient 1 3 & 4 - CMV negative patient

CMV genotype in association with demographic features

CMV DNA presence in OSCC patients was categorized demographically. Samples of 13 males and 8 females were observed to have the viral DNA; the results obtained are not significant as

the p-value obtained is 0.08. Underage groups, one patient below 25 years, eight patients in the range 26-45, 11 patients in the range 46-65, and one patient in the range 66 and above were reported to have CMV DNA in their samples; these results were not significant as p-value is 0.09. Under the diagnosis site category, five patients of BM, eight patients of the tongue, one patient of FOM, two patients of the mandible, one patient of the palate, one patient of RMT, and three patients of the oral cavity were reported to have the viral DNA. The results obtained were not significant as the p-value was calculated as 0.6. CMV DNA was observed in all 4 stages of tumor groups 3 in stage 1, eight in stage 2, nine in stage 3, and one in stage 4; the p-value was calculated as 0.003 which means the results were significant. Under the category of habits, one patient with a habit of smoking, 10 patients who chew tobacco, four patients who consume alcohol and smoke, two patients who consume alcohol and chew tobacco, one patient who smoke and chew tobacco, one patient who consumes alcohol, chew and smoke tobacco and two patients with no habits were reported to have CMV DNA in their biosamples. The p-value was 0.05 which shows that the results were significant. [Table 6]

Table 6 : Correlation of CMV genotypes with demographical factors of OSCC patients

Demographical Characteristics	CMV N=21 (%)	P-value
Gender		
Males (n=45)	13 (61.90)	0.08
Females (n=55)	8 (38.10)	
Age Distribution		
<25	1 (4.76)	0.09
26-45	8 (38.10)	
46-65	11 (52.38)	
66 and above	1 (4.76)	

Oral squamous cell carcinoma patients with a history of nicotine and alcohol abuse.

Site of Diagnosis		
BM	5 (23.81)	
Tongue	8 (38.10)	
BOT	0 (0.00)	
FOM	1 (4.76)	
LIP	0 (0.00)	
Mandible	2 (9.52)	
Maxilla	0 (0.00)	
Palate	1 (4.76)	
RMT	1 (4.76)	
Oral Cavity	3 (14.29)	0.6
Staging		
Stage 1	3 (14.29)	0.003
Stage 2	8 (38.10)	
Stage 3	9 (42.86)	
Stage 4	1 (4.76)	
Habitual Risk		
Alcoholics	0 (0)	
Smokers	1 (4.76)	
Chewers	10 (47.6)	
Combination Risk Factors		
Alcohol+Smoking	4 (19.05)	
Alcohol+Chewing	2 (9.52)	
Smoking+Chewing	1 (4.76)	
Alcohol+Smoking+Chewing	1 (4.76)	
No Habits	2 (9.52)	0.05

Quantification of CMV IgG and IgM antibodies in serum

28% of the total OSCC patients and 4% control serum samples were observed to be positive for CMV IgG at a concentration less than 1.2 Mmol/l while CMV IgM antibodies were observed in 9% of OSCC patients and 1% control samples. Univariate analysis was performed to the results obtained for IgM of CVM gave a p-value of 0.02 which is significant while for IgG of CVM gave a p-value of 0.45 which is not significant. [Table 7]

Squamous Cell Carcinoma malignancy is primarily associated with gender, geographical region, and location^{22, 23}. Southern Asia was reported to be more prevalent amongst other countries. SCC is observed more in the male gender as compared to females. In India, SCC is more prevalent in the form of Oral and tongue cancers²⁴ mandating focus on associated key genetic players that may contribute to OSCC pathogenesis, and the curative potential²⁵. IgM antibody is important to act against HSV in the pretext of oral cancers²⁶ and HSV enacts a crucial role in cancer incidence²⁷. An association between mandibular OSCC and HSV infection where in the prevalence of HSV-1 was 18% and HSV-2 represented 6% was reported in a study²⁸. HSV prevalence in worldwide patients suffering from OSCC was almost 15% while the highest was observed in the United Kingdom. This clarifies that geographical differences affect HSV prevalence²⁹. 5% of the patients infected with HSV-1 are with OSCC³⁰ and HSV-2 has a

Table 7: Levels of CMV IgG and IgM in the serum of OSCC and controls

Serum CMV	Cases n(%)	Mean±SD	Controls n(%)	Mean±SD	F- value	P-Value
IgG levels (Mmol/L)						
< 1.2	72	0.38±0.22	96	0.40±0.25	1.32	0.25
≥1.2	28	1.37±0.18	4	1.37±0.11	2.67	0.45
IgM levels (Mmol/L)						
< 1.2	91	0.46±0.24	99	0.44±0.2	1.44	0.02
≥1.2	9	1.24±0.02	1	0	--	--

high prevalence in OSCC in the samples which are differentiated tissue with HSV-1 (7.5%) and HSV-2 (15%), while 5% were coinfecting with both HSV-1 and HSV-2³¹. Several studies have reported that HSV-1 and HSV-2 in combination with tobacco usage by chewing or smoking and concurrent alcohol consumption or any other consumption of chemical carcinogens can promote development of OSCC^{11, 27}. CMV was observed to have a high prevalence in OSCC than in other cancers³². Several articles have discussed the presence of CMV in tumors and its involvement in the development of tumors^{33, 34}. Studies have reported that age, gender, location, histological stage, grade, size and distribution of the lesions in patients are associated with CMV prevalence in OSCC patients. It was reported that the general prevalence of CMV in oral cancer patients was different in several areas ranging from 0 to 91.5%³⁵⁻³⁸. In a study, CMV percentage is high in OSCC (42.5%) than in benign (25%) and control samples (7.5). Similarly, CMV DNA was found in OSCC which was nearly 28%³². Many clinical and experimental results have recommended the partial contribution of CMV to malignancy and chemoresistance in tumor cells³⁹, and may play a significant role in modulating the tumor microenvironment⁴⁰. CMV lays dormant in the body after infection, due to the exposure of the squamous cells to tobacco and alcohol consumption. Cell damage and subsequent infection of the damaged cells by CMV was observed in several *in vitro* studies. These infected cells then transform to cancerous cells leading to OSCC in several individuals.

The current study predominantly focuses on the molecular and serological epidemiology of HSV-1, HSV-2, and CMV in patients with Oral Squamous Cell Carcinoma. The risk factors like alcohol consumption, smoking, chewing tobacco were considered individually or in combinations showed that in the combined patient population, HSV-1 (3%), HSV-2 (1%), HSV-1,2 (1%), and CMV (21%) prevalence was observed. Tumors in several stages were tested

for the prevalence where HSV-1 (4%), HSV-2 (1%), HSV-1, 2 (2%), and CMV (21%) of the patient population were observed having viral prevalence. Although there was a reduced rate of HSV infection it could be due to the limited population, size of the sample amongst others. Our findings were in contrast to several studies which reported a majority of OSCC in the male gender. According to the results, patients infected with the HSV genome were less as compared to the patients infected with CMV which means HSV has a low infection rate. Our results are similar to studies³⁰ which confirmed that HSV has a low prevalence rate in patients with OSCC. Results obtained in this study are similar to several studies which have reported that the prevalence of CMV in the OSCC tissue samples was more than other viruses as they can increase the oncogenesis and infect the cancerous tissues opportunistically as monocytes and lymphocytes are the key focus sites of CMV.

Conclusion

Oral cancer is one of the significant reasons for mortality and morbidity mainly in developing countries which can be foreseen as a rise in the near future. Viruses associated with head and neck cancers were studied for several critical insights into the mechanism of oral cancer. Viral infection, as well as co-infections, could provide targets for diagnostic tests and therapy along with understanding the tumor development mechanisms. Diagnosis of Oral Squamous Cell Carcinoma is typically made by oral examination which is then followed by tissue biopsy. Due to this approach, most of the cases go unaffected and are diagnosed at more recent stages, which cause OSCC to metastasize leading to less survival rate in 50% of the diagnosed population. Even though new diagnostic techniques in the detection of oral cancer exist they are incapable of surpassing histopathological, molecular, and biopsy is considered gold in standards. In this study, the prevalence of HSV-1 and HSV-2 along with CMV viruses was studied among the selected patient and control population further associated with several risk

Oral squamous cell carcinoma patients with a history of nicotine and alcohol abuse.

factors observing that the genetic material of the virus is integrated into the host DNA. The quantification of IgG and IgM of both the selected viruses has shown that after the viral infection, the antibodies are present in the blood serum of the patients as well as control subjects.

Conflict of Interest

The authors declare no conflict of interest.

References

1. Kato MG & Day TA, Oral cavity and oropharyngeal cancer: a new staging system for 2017, *Otolaryngology-Head and Neck Surgery E-Update*, 2016.
2. Hwang E, Johnson-Obaseki S, McDonald JT, Connell C & Corsten M, Incidence of head and neck cancer and socioeconomic status in Canada from 1992 to 2007. *Oral Oncol*, 49 (2013) 1072.
3. Siddiqi K, Shah S, Abbas SM, Vidyasagar A, Jawad M & Dogar O, Global burden of disease due to smokeless tobacco consumption in adults: analysis of data from 113 countries. *BMC Med*, 13 (2015) 194.
4. Allen L, Williams J, Townsend N, Mikkelsen B, Roberts N & Foster C, Socioeconomic status and non-communicable disease behavioural risk factors in low-income and lower-middle-income countries: a systematic review. *Lancet Glob Health*, 5 (2017) 277.
5. Ferlay J, Soerjomataram I, Dikshit R, Eser S, Mathers C & Rebelo M, Cancer incidence and mortality worldwide: sources, methods and major patterns in GLOBOCAN 2012: Globocan 2012. *Int J Cancer*, 136 (2015) 359.
6. Bray F, Ferlay J, Soerjomataram I, Siegel RL, Torre LA & Jemal A, Global cancer statistics 2018: GLOBOCAN estimates of incidence and mortality worldwide for 36 cancers in 185 countries. *CA Cancer J Clin*, 68 (2018) 394.
7. Gupta B, Johnson NW & Kumar N, Global epidemiology of head and neck cancers: A continuing challenge. *Oncology*, 91 (2016) 13.
8. Leemans CR, Snijders PJF & Brakenhoff RH, Publisher Correction: The molecular landscape of head and neck cancer. *Nat Rev Cancer*, 18 (2018) 662.
9. Hsu W-L, Yu KJ, Chiang C-J, Chen T-C & Wang C-P, Head and neck cancer incidence trends in Taiwan. *International Journal of Head and Neck Science*, 1 (1980) 180.
10. García-Martín JM, Varela-Centelles P, González M, Seoane-Romero JM, Seoane J & García-Pola MJ, Epidemiology of Oral Cancer, *Oral Cancer Detection*, (Springer), 2019, 81.
11. Johnson S, McDonald JT & Corsten M, Oral cancer screening and socioeconomic status. *J Otolaryngol Head Neck Surg*, 41 (2012) 102.
12. Alam AY, Iqbal A, Mohamud KB, Laporte RE, Ahmed A & Nishtar S, Investigating socio-economic-demographic determinants of tobacco use in Rawalpindi, Pakistan. *BMC Public Health*, 8 (2008) 50.
13. Khawaja MR, Mazahir S, Majeed A, Malik F, Merchant KA & Maqsood M, Chewing of betel, areca and tobacco: perceptions and knowledge regarding their role in head and neck cancers in an urban squatter settlement in Pakistan. *Asian Pac J Cancer Prev*, 7 (2006) 95.
14. Fantom N & Serajuddin U (2016). The World Bank's classification of countries by income: The World Bank. *Policy Research*

Working Paper, 7528.

15. Pradhan NA, Ali TS, Hasnani FB, Bhamani SS & Karmaliani R, Measuring socio-economic status of an urban squatter settlement in Pakistan using WAMI Index. *J Pak Med Assoc*, 68 (2018) 709.
16. Madathil SA, Rousseau M-C, Wynant W, Schlecht NF, Netuveli G & Franco EL, Nonlinear association between betel quid chewing and oral cancer: Implications for prevention. *Oral Oncol*, 60 (2016) 25.
17. Tsai K-Y, Su C-C, Lin Y-Y, Chung J-A & Lian I-B, Quantification of betel quid chewing and cigarette smoking in oral cancer patients. *Community Dent Oral Epidemiol*, 37 (2009) 555.
18. Westra WH & Lewis JS Jr, Update from the 4th edition of the world health organization Classification of Head and Neck Tumours: Oropharynx. *Head Neck Pathol*, 11 (2017) 41.
19. Mummudi N, Agarwal J, Chatterjee S, Mallick I & Ghosh-Laskar S, Oral cavity cancer in the Indian subcontinent-challenges and opportunities. *J Clin Oncol*, 318 (2019) 520.
20. Bhisey RA, Chemistry and toxicology of smokeless tobacco. *Indian J Cancer*, 49 (2012) 364.
21. Ernani V & Saba NF, Oral cavity cancer: Risk factors, pathology, and management. *Oncology*, 89 (2015) 187.
22. Siegel RL, Miller KD & Jemal A, CA: a cancer journal for clinicians, 66 (2016) 7.
23. Gatta G, Botta L, Sánchez MJ, Anderson LA, Pierannunzio D & Licitra L, Prognoses and improvement for head and neck cancers diagnosed in Europe in early 2000s: The EURO CARE-5 population based study. *European journal of cancer*, 51 (2015) 2130.
24. Reddy RB, Bhat AR, James BL, Govindan SV, Mathew R & Ravindra DR, Meta-analyses of microarray datasets identifies ANO1 and FADD as prognostic markers of head and neck cancer. *PLoS One*, 11 (2016) 0147409.
25. Samata Gadde, Sudhakar Poda, Suryanarayana Veeravilli & Lakshmi Addala, Lack of the brafv600e mutation in oral squamous cell carcinoma. *Journal of Medical Science And Clinical Research*, 04 (2016) 14912.
26. Correia AVL, Coêlho MRCD, de Oliveira Mendes Cahú GG, de Almeida Silva JL, da Mota Vasconcelos Brasil C & de Castro JFL, Seroprevalence of HSV-1/2 and correlation with aggravation of oral mucositis in patients with squamous cell carcinoma of the head and neck region submitted to antineoplastic treatment. *Support Care Cancer*, 23 (2015) 2105.
27. Parker TM, Smith EM, Ritchie JM, Haugen TH, Vonka V & Turek LP, Head and neck cancer associated with herpes simplex virus 1 and 2 and other risk factors. *Oral Oncol*, 42 (2006) 288.
28. Osman SA, Enan KA & Mohamed EA, Molecular detection of herpes simplex virus (1, 2) in oral squamous cell carcinoma at Khartoum. *Clinical Medicine Journal*, 2 (2017) 10.
29. Jalouli J, Ibrahim SO, Mehrotra R, Jalouli MM, Sapkota D & Larsson P-A, Prevalence of viral (HPV, EBV, HSV) infections in oral submucous fibrosis and oral cancer from India. *Acta Otolaryngol*, 130 (2010) 1306.
30. Mokhtari M & Beiraghdar M, Evaluation of Oral squamous cell carcinoma patients with a history of nicotine and alcohol abuse.

Oral squamous cell carcinoma patients with a history of nicotine and alcohol abuse.

- the prevalence of herpes simplex-1 infection in oral squamous cell carcinoma specimens in Alzahra and Kashani Hospitals with polymerase chain reaction method in 2012-2013. *Adv Biomed Res*, 4 (2015) 173.
31. Bashir R & Elhag W, Molecular detection of herpes simplex virus types [1 and 2] in oropharyngeal squamous cell carcinoma (OSCC) in Khartoum dental education hospital. *J Adv Med Med Res*, 26 (2018) 1.
 32. Wei, Hou, & Shu Qianqian Xiang Xiaoming, Primary study on human papillomavirus type 16 and human cytomegalovirus infections in oral squamous cell carcinoma. *J Compr Stomatol* , 2 (1996) 001.
 33. Bray F, Ren J-S, Masuyer E & Ferlay J, Global estimates of cancer prevalence for 27 sites in the adult population in 2008. *Int J Cancer*, 132 (2013) 133.
 34. Lambert R, Sauvaget C, de Camargo Cancela M & Sankaranarayanan R, Epidemiology of cancer from the oral cavity and oropharynx. *Eur J Gastroenterol Hepatol*, 23 (2011) 633.
 35. Zheng Y, Xia P, Zheng H-C, Takahashi H, Masuda S & Takano Y, The screening of viral risk factors in tongue and pharyngolaryngeal squamous carcinoma. *Anticancer Res*, 30 (2010) 1233.
 36. de França TRT, de Albuquerque Tavares Carvalho A, Gomes VB, Gueiros LA, Porter SR & Leao JC, Salivary shedding of Epstein-Barr virus and cytomegalovirus in people infected or not by human immunodeficiency virus 1. *Clin Oral Investig*, 16 (2012) 659.
 37. Delavarian Z, Pakfetrat A, Falaki F, Pazouki M & Pazouki N, The role of viruses in oral squamous cell carcinoma in young patients in khorasan (northeast of Iran). *J Appl Sci*, 10 (2010) 981.
 38. Saad Hasan Mohammed A, Majed Mohammed Mahmood Al J& Noor Al Huda Ali AHS, Localization of human cytomegalovirus-late gene DNA, expression of P53 gene and CD8-tumor infiltrating lymphocytes in oral squamous cell carcinoma. *Iraqi Postgrad Med J*, 12 (2013) 296.
 39. Michaelis M, Doerr H.W & Cinatl J, The story of human cytomegalovirus and cancer: Increasing evidence and open questions. *Neoplasia* , 11(2009) 1.
 40. Mitchell D.A, Xie W, Schmittling R, Learn C, Friedman A , LcLendon R.E & Sampson J H, Sensitive detection of human cytomegalovirus in tumors and peripheral blood of patients diagnosed with glioblastoma. *Neuro-Oncol* , 10 (2008) 10 .

Mupirocin Niosomal Gel with Bee Honey & Curcumin as Nano-Drug Delivery in Wound Healing Applications

Srikrishna Theerdhala^{1,2*}, Narayanaswamy Harikrishnan³

¹Research Scholar, Department of Pharmaceutics, Faculty of Pharmacy, Dr. M.G.R. Educational and Research Institute, Deemed to be University, Velappanchavadi, Chennai - 600077, Tamil Nadu, India.

²Department of Pharmaceutics, Ratnam Institute of Pharmacy, Nellore, SPSR Nellore (Dt.) - 524346, Andhra Pradesh, India.

³Department of Pharmaceutical Analysis, Faculty of Pharmacy, Dr. M.G.R. Educational and Research Institute, Deemed to be University, Velappanchavadi, Chennai - 600077, Tamil Nadu, India.

*Corresponding Author: srikrishna.nlr@gmail.com

Abstract

Wound healing research is still aiming toward complete regeneration and restoration of the skin's function and structure with the least amount of scarring. Controlled and targeted medication distribution to wounds is more convenient than systemic administration, which allows for larger drug concentrations to be delivered to the targeted site over time. The nano wound healing gel demonstrated a dependable administration strategy, excellent local tolerability, and superior drug delivery methods, which can promote faster healing. Recently, niosome formulations have been developed to reduce toxicity while increasing accumulation at the target site. Curcuma longa (CU) and honey are effective at inhibiting the growth of wound-associated pathogens and hastening the healing process. The wound healing potential activity of mupirocin-loaded niosomal gel formulated with honey and curcumin, as well as their blends, by ether injection method and investigated for further studies. FTIR and DSC study reveals the compatibility of the drug and other excipients. In the case of post-approval study the parameters evaluated are entrapment efficiency, drug

content, pH, viscosity, spreadability, SEM, in-vitro drug release study, release kinetic study, stability study, and in-vivo wound healing study followed by histopathological study. This study aimed to create an excision wound model in albino rats and compare it to a commercially available ointment (Mupicip by Cipla). The blended formulation (Formulation F7) was administered twice daily, and the wound healing effect was determined by the highest percentage of wound contraction, epithelisation period, and histoarchitecture studies. The obtained results concluded that formulation F7 is considered as best formulation and has shown a higher percentage of wound contraction 99.08%. The histological study also confirms that formulation F7 promotes faster wound healing.

Keywords: Wound healing, Mupirocin, Curcumin, Honey, Niosomal ointment Nano-drug delivery.

Introduction

The wound is the disruption of cellular and anatomic continuity of living tissue, which is the main cause of physical illness. Wound healing is the dynamic process of survival of

a patient by attempting regeneration or restoration of broken tissue and its function (1, 2). Every year, millions of people around the world suffer from acute and chronic wounds and their treatment burden due to its impaired and delayed healing process (3). Different kinds of ulcers including diabetic, vascular, arterial, and pressure ulcers (4-7) are the main factors resulting in complications and intensive treatment in wound healing. Wound healing takes place with three complex interrelated stages, namely inflammation, granulation, and remodeling (8). The mechanism of healing is started due to the secretion of clotting factor fibrin by platelets at the targeted site (9). Growth factors cytokines as a key signal arrives with platelets a source of fibrin clot, helps to treat inflammatory cells in wound healing. The fibroblast is responsible for collagen deposition which helps to provide strength, integrity, and structure to the injured tissue during wound healing and also helps to restore tissue anatomic structure and function (10).

Nanomedicine emerged nanosized particles help in the diagnosis and treat wound healing (11, 12). An optimal drug action application of nanoscience in the pharmaceutical industry is very promising and has grown rapidly. Nano carrier could be a good transporter for drug molecules to achieve action in the targeted site. Non-ionic surfactant vesicles like niosomes (13, 14) can be used as carriers to transport amphiphilic and lipophilic drugs (15, 16). Niosomes are more stable as compared to similar types of vesicles due to the presence of better surfactants and phospholipids available in them.

A variety of drugs are available for wound healing management like analgesics, nonsteroidal anti-inflammatory, and antibiotics but most of them are responsible for unwanted side effects. In recent years, herbal drugs explicate their potential in wound healing management and revived interest in alternative treatment against synthetic drugs (17). The main object of this research study is to introduce a natural antibiotic mupirocin with the combination

of herbal-based products such as curcumin and honey in the form of niosomal gel to control side effects. The significance of this study is to provide quick wound healing of the skin with optimal functional and aesthetic results (18). Mupirocin reversibly inhibits isoleucyl-transfer RNA, which helps in constraining bacterial protein and RNA synthesis. Mupirocin is highly effective against many bacteria (19, 20) and pathogens mostly found in primary and secondary skin infections. Similarly, curcumin and honey have shown anti-inflammatory, antimicrobial, and wound healing properties (21-23) and treat against staphylococcus aureus Pseudomonas aeruginosa and Escherichia coli, the most common causative agent of wound infections (24,25). Curcumin is also used in burn wound infection, sepsis in surgical wounds (26), infections such as bacteremia, septicemia, and wound infection in hospitalized patients (27). Honey free from toxic contaminants, gone through gamma irradiation sterilization technique is safe for medical application (28). Reepithelialization, angiogenesis, and stimulation of skin and immune cells (29) are one of the main wound-healing abilities of honey. The overall aim of this research study is to develop a Niosome, a nanocarrier to improve wound healing treatment by enhancing stability, reducing toxicity, and controlling the release profile of active drugs.

Materials and Methods

Materials

Mupirocin and carbopol are obtained from Divya associates, Vijayawada, India. Miresi is an online site to get organic honey without any preservatives. Curcumin (*Curcuma longa*) was obtained from Sigma-Aldrich, India. Tween 80, Cholesterol, and glycerin are obtained from SD fine chemicals India. All other excipients were of analytical research grade and contain the highest purity.

Curcumin Preparation Process

Curcumin preparation was carried out with a wide-mouth vial. The calculated amount

of cholesterol and surfactant tween 80 have been taken. The mixture was dissolved in diethyl ether and methanol (8:2) solution. Sealed the vial and heat it with a water bath at 60 °C for 10 min until the cholesterol gets dissolved. The required quantity of Curcumin has to be added to the lipid mixture to obtain a creamy yellow gel (30).

Preparation of niosome by ether injection method

Weight amount of polymer and mupirocin taken at different ratios in a 250 ml beaker. Honey is added slowly into the drug and polymeric solution with continuous stirring to obtain a homogeneous mixture. Prepared curcumin gel loaded into a 14-gauge needle and added to mupirocin. The temperature maintained during this mixing is 55-60 °C. Solvents are gradually evaporated from the mixture to obtain a stable vesicle (31). This method also helps to control the size of the formulated niosome, based on the selection of needle and other factors. Formulation codes for different niosomal formulations based on the diverse ratio between polymer, surfactant, and cholesterol are mentioned in Table 1.

Evaluation of Niosomal Gel

Physicochemical evaluation of formulated niosomal gel

All formulated niosomal gels were subjected to visual inspection to determine the homogeneity, color, fluidity, and consistency. Niosomal gel was also viewed under an optical microscope at 50X magnification to further determine the crystallization, agglomeration, and grittiness.

The entrapment efficiency of drug

Niosomal gel from each formulation (1 g) was collected individually and placed in a 100 ml volumetric flask which contain 20 ml buffer solution (pH 7.4) and sonicated for 30 min at room temperature. The mupirocin-loaded niosome were separated from the untrapped drug with the help of centrifugation at 12000 rpm for 20 min. The supernatant with suitable dilution was taken for UV analysis at 226 nm. The % of encapsulated drugs was determined by using the formula given below.

$$\% \text{ Entrapment efficiency} = \frac{\text{(Amount of drug entrapped)}}{\text{(Amount of drug added)}} \times 100$$

Table 1: Formulation of niosomal gel loaded with 2% mupirocin (Net Weight 15 g)

Formulation Code	Drug: polymer ratio	Honey	Curcumin	TWEEN80: Cholesterol ratio	Glycerine	Methylparaben	Distilled water
F1	2:1	-	5	4:8	5	0.22	Q.S
F2	2:0	-	-	5:4	5	0.22	Q.S
F3	2:2	2	2	5:3	5	0.22	Q.S
F4	2:3	5	1	6:8	5	0.22	Q.S
F5	2:2	7	4	6:4	5	0.22	Q.S
F6	2:3	3	2	3:5	5	0.22	Q.S
F7	2:2	5	4	5:8	5	0.22	Q.S
F8	2:2	4	2.5	5:8	5	0.22	Q.S

Drug content

Niosomal gel 1 gm was collected individually from each formulation and dissolved with buffer sample pH 7.4 and made up the volume up to 50 ml. 1 ml of the above solution with suitable dilution was taken for determination of absorbance by UV-Visible spectrophotometer at 226 nm.

pH determination of formulated niosome gel

Calibration should be done for the pH meter before its use. 1 gm of formulated niosomal gel was dispersed in 100 ml water and subjected to calibrated digital pH meter to determine the pH of the sample. To avoid unwanted complications each formulation pH was measured in triplicate.

Determination of viscosity

The selected spindle has been attached with a viscometer to determine the viscosity of the sample. The spindle as a rotating element in a fluid measures torque and indicates the viscosity of the fluid. Various formulated niosomal gels were subjected to a Brookfield viscometer to determine the viscosity. The respective reading was noted and represented in cps. The samples are done in triplicate to avoid the error.

Spreadability

An excess sample was taken from each formulation to determine the spreadability of the niosomal gel. Niosomal gel from various sample were placed in between two glass slides and compressed by 100 gm weight for 5 min to obtain uniform thickness. The weight (125 gm) was applied to the upper glass slide to separate both slides. The time required to separate the slides was individually noted to determine the spreadability.

SEM study

The morphology of the niosomal gel was performed by scanning electron microscope (SEM, Model no. JEOL Model JSM - 6390LV). 1 gm of the sample was added with 100 ml of

buffer solution and mixed for 30 min using a magnetic stirrer. Take the supernatant sample to determine the morphology study. It also gives additional information about the shape and size of the niosome.

In-Vitro release studies

Franz diffusion cell with receptor compartment volume 20 ml used to carry out *in vitro* drug release study. Cellulose dialysis membranes (Sigma-Aldrich, Mumbai, India) were soaked in buffer media (pH 7.4) for 24 h at room temperature before experimenting. From various freshly prepared formulations of niosomal gel 3 mg of the sample was loaded in the donor compartment. In the receptor compartment, the buffer media was continuously stirred at 600 rpm and the temperature was maintained at 37 ± 0.5 °C. After a predetermined time interval, 5 ml samples were collected from the receptor compartment and replaced with the same amount of fresh buffer media. Collected samples were analyzed under a UV Visible spectrophotometer at 226 nm with a suitable dilution. A comparison study of drug release kinetic has been made between formulated niosomal gel concerning commercially available Mupicip manufactured by Cipla. All the experiments were conducted in triplicates and the average were calculated to minimize the error percentage.

Drug release mechanism studies

The drug release mechanism study of mupirocin-loaded niosomal gel was fitted to various release models obtained from *in vitro* dissolution profile. The various kinetic models are zero order, first order, Higuchi model, and Korsmeyer-Peppas model (32). The high correlation coefficient value indicates the best fitting of the release kinetics of any of the models.

Stability studies

The best formulation F7 was packed in an aluminum collapsible tube of 15 gm and considered for the stability test. The stability test was carried out as per ICH guidelines at 25

°C with 60% RH and 40 °C with 75% RH for 3 months. At suitable time intervals, the sample is evaluated for physical appearance, pH, viscosity, spreadability, and drug release profile.

In vivo study

Healthy Wistar albino rats age 8-10 weeks, weight: 200-250g were used to perform the efficacy of formulated niosomal gel (Containing 2% mupirocin) with marketed mupirocin gel on excision wound model.

Animal Preparation

In this current research, all the Wistar albino rats are housed under standard conditions and clinically examined. The animals were acclimatized to the standard laboratory conditions in a cross-ventilated animal house at 25 ± 2 °C, relative humidity 44–56%, and light and dark cycle of 12: 12 hours and fed with a standard diet and water during the study. All the animals were divided into 3 groups having 6 animals each. The animal ethical clearance no IAEC/SCPER/2021-22/13 was approved before performing the study.

Group-I contained control animals (Untreated animals)

Group-II best formulation Niosomal gel (mupirocin, honey, and curcumin loaded gel) was administered

Group-III Application of marketed gel (Mupicip)

Excision wound model preparation

Anesthetic ether (0.05 to 0.1 mg/kg SC) was used to anesthetize the rats (33). Then the rats were subjected to shaving the hair on the back by using a razor. A 15 mm full-thickness wound of 3X3 cm with sterile surgical scalpels was created. The incisions were created in the dorsal lumbar region, 1.5 mm from the midline on the back of rats. Finally, the rats were divided into three separate groups as mentioned earlier. The wounded rats of group I were considered as controlled ones (Left untreated), group II treated with the best formulation F7 (mupirocin, honey,

and curcumin loaded gel), and group III with marketed mupirocin gel (Mupicip) applied twice a day until the complete healing of the wound. The wound contraction was measured every 3 days interval to determine the % of wound contraction. The time for wound closure was noted when total healing occurred.

Histopathological studies

The skin specimens were collected in 10% buffered formalin (34) from rats of the 3 different groups after anesthetized. Then, 5-micrometer-thick sections were sliced and stained with hematoxylin and eosin dye for histological examination. The Olympus photomicroscope (400X magnification) was used to evaluate the sliced sections in terms of collagen formation, fibroblast proliferation, keratinization, and epithelisation.

Results and Discussion

FTIR Study

To investigate the compatibility of drugs and polymers, the pharmaceutical industry frequently uses the potent analytical method known as Fourier transform infrared spectroscopy (FTIR). This method examines the interactions between the drug and the polymer as well as any modifications to the polymer's chemical structure that result from the drug's inclusion. As FTIR is a non-destructive and non-invasive method, the chemical makeup of the materials being examined is not changed. FTIR can also pick up electrostatic, hydrogen bonds and van der Waals interactions between the medication and the polymer. These interactions may have an impact on the mechanical and thermal characteristics of the polymer as well as the stability, solubility, and bioavailability of the medication. FTIR spectra of mupirocin, honey and curcumin, and all other excipients and their compositions were considered for compatibility study shown in Figure 1. Obtained spectra of mupirocin confirm that the peak position and intensity of the peaks don't alter due to the addition of honey, curcumin, and other excipients in different for-

mulations. Mupirocin spectra show major peaks 3471.08, 3304.2 cm^{-1} corresponding to OH-stretching 2934.18, 2850.74 cm^{-1} CH-stretching 1723.98, 1658.68 cm^{-1} belongs to C=O stretching 1449.73 cm^{-1} for C-C stretching. Mupirocin with honey spectra appears at 3471.08, 3310.01, cm^{-1} corresponding to OH-stretching 2928.37, 2860.17 cm^{-1} CH-stretching 1721.80, 1658.68 cm^{-1} belongs to C=O stretching 1402.37 cm^{-1} for C-C stretching. Mupirocin with curcumin spectra appears at 3471.88, 3325.24, cm^{-1} corresponding to OH-stretching 2943.61, 2857.27 cm^{-1} CH-stretching 1718.17 cm^{-1} belongs to C=O stretching 1456.26, 1408.37 cm^{-1} for C-C stretching. FTIR spectrum of mupirocin with carbopol shows at 3471.08, 3298.04 cm^{-1} corresponding to OH-stretching 2928.37, 2844.94 cm^{-1} CH-stretching 1718.17, 1652.88

cm^{-1} belongs to C=O stretching 1449.23 cm^{-1} for C-C stretching. Mupirocin with Tween 80 shows the peak at 3471.08, 3304.20 cm^{-1} corresponding to OH-stretching 2928.37, 2857.27 cm^{-1} CH-stretching 1723.98, 1652.88 cm^{-1} belongs to C=O stretching 1449.23 cm^{-1} for C-C stretching. Similarly, mupirocin with cholesterol composition shows IR frequencies at 3471.08, 3301.30, cm^{-1} corresponding to OH-stretching, 2932, 2859.45 cm^{-1} CH-stretching, 1723.98, 1647.07 cm^{-1} belongs to C=O stretching. The active pharmaceutical ingredient, mupirocin, did not interact chemically with honey, curcumin, or any of the other excipients, according to an FTIR result with a minor change in the FTIR spectrum shown in Figure 2. So, it may be concluded that the active substance is compatible and has retained its functionality.

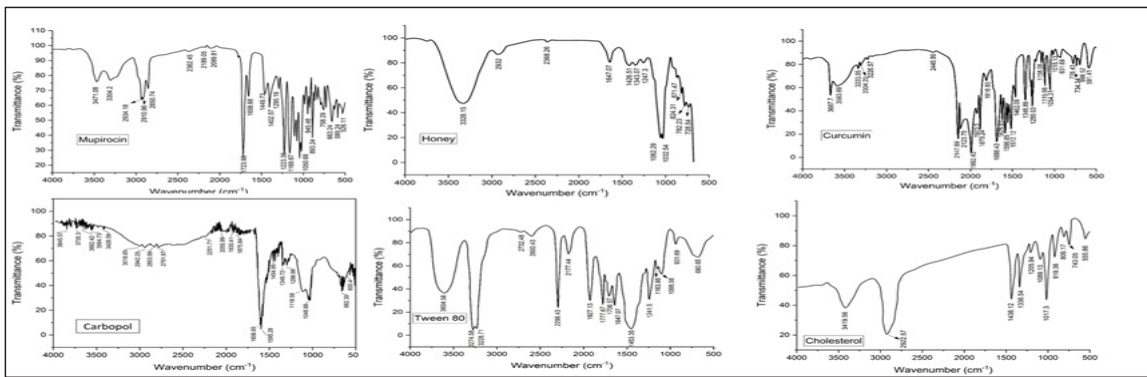


Figure 1: FTIR spectrum of mupirocin, honey, curcumin, and excipients

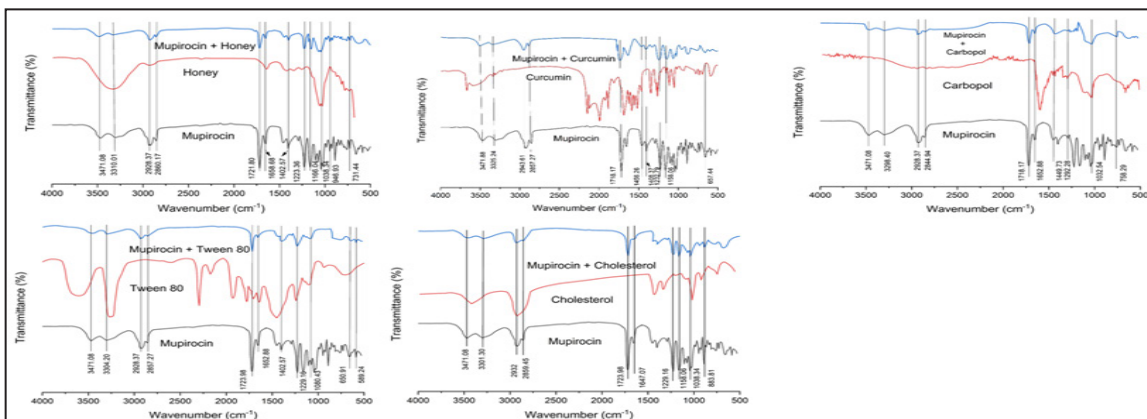


Figure 2: FTIR spectrum of mupirocin mixed with honey, curcumin, and excipients

DSC study

In research on drug-polymer compatibility, differential scanning calorimetry (DSC) is a method that is frequently utilized. DSC can detect any changes in the thermal behavior of the polymer following the addition of the drug since it detects the heat flow connected to thermal transitions in materials, such as melting and solidification. Insights on the compatibility between the medicine and the polymer may be gained by using DSC to identify changes in the glass transition temperature, melting point, and crystallization behavior of the polymer. DSC is more responsive to changes in the polymer's thermal behavior. Changes in these parameters can indicate the formation of new chemical entities resulting from drug-polymer interactions.

Mupirocin, honey, curcumin, carbopol, tween 80, and cholesterol endothermic peaks were observed at 77.78°C, 192.44°C, 172.47°C, 74.39°C, 79.15°C, 149.09°C respectively shown in figure3. Figure 4 represents the DSC curve for a mupirocin mixture with honey, curcumin, carbopol, and other excipients. Mupirocin with honey represents the spectra at 78.42°C, mupirocin with curcumin shows spectra at 77.78°C, mupirocin with carbopol shows spectra at 77.73°C and mupirocin with tween 80 shows spectra at 77.43°C and mupirocin with cholesterol shows spectra at 77.75°C. Obtained results show minor changes in the peak shape and width and intensity, which should be an indication of mupirocin is compatible with other excipients used in different formulations.

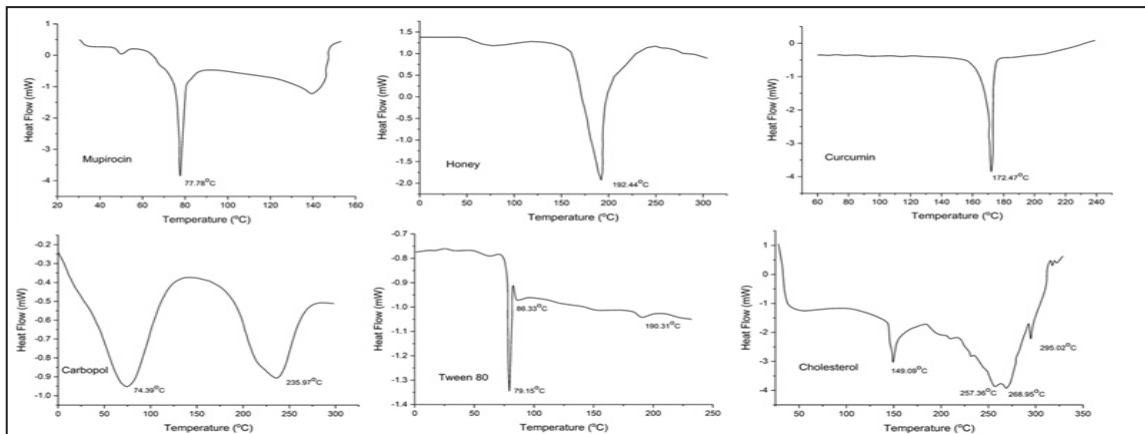


Figure 3: DSC spectrum of mupirocin, honey, curcumin, and excipients

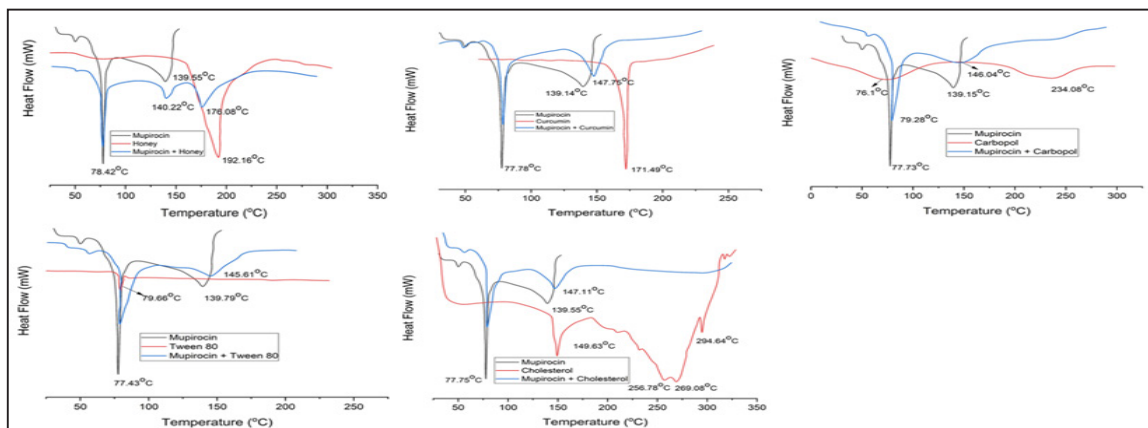


Figure 4: DSC spectrum of mupirocin mixed with honey, curcumin, and excipients

Evaluation study of Mupirocin-loaded niosomal gel

The entrapment efficiency of the drug

Entrapment efficiency (EE) is a measure of the amount of drug mupirocin that is effectively trapped or encapsulated within a drug delivery system, such as formulated niosomal gel. It is an important parameter in drug delivery systems, as it directly affects the drug release rate, bioavailability, and therapeutic efficacy. A high entrapment efficiency is desirable in drug delivery systems, as it indicates that a greater proportion of the drug is being delivered to the target site while minimizing potential side effects from the drug being released in unintended areas. A low entrapment efficiency may result in inadequate drug delivery, lower therapeutic efficacy, and increased toxicity due to higher drug concentrations in non-target areas. Obtained results confirm that 80% to 98% of mupirocin is entrapped in various formulations shown in Table 2. Cholesterol renders the niosomes impenetrable (35) and improves aqueous phase entrapment effectiveness and permeability. With the present formulation of niosome gel (36), nonionic surfactants also significantly improved the drug's ability to be entrapped.

Drug content

Drug content is an important quality control parameter that measures the amount of mupirocin present in a niosomal gel formulation. The drug content of a drug product should be within a specified range. Variations in the drug content of a drug product can occur due to several factors, such as variability in the manufacturing process, changes in the source or quality of the API or excipients, and inadequate mixing or blending of the drug product components. It was observed that a high carbopol content helps to keep more of the medicine in the niosomal gel. The drug concentration was obtained between 84% and 99% shown in Table 2.

Determination of pH

The pH is an important parameter that can affect the stability, solubility, and bioavailability of a drug product. For example, certain drugs may be unstable or insoluble at extreme pH values, and changes in the pH of a drug formulation can affect the rate of drug release and absorption in the body. Therefore, the pH of a drug product is carefully controlled and monitored during the manufacturing process and throughout its shelf life. According to Table 2, all mupirocin-loaded niosome-based gel formulations had a pH between 6.19 and 6.72, which is following the skin pH.

Determination of viscosity

Viscosity is a measure of the resistance of a fluid to flow and is a commonly important parameter in the formulation and processing of various drug products. The viscosity of a semisolid or gel-like drug formulation can affect its spreadability and adhesion to the skin or mucosal surfaces. According to Table 2, the viscosity ranged from 400 to 555 cps.

Spreadability

Spreadability is an important parameter in the development and formulation of topical drug products. The spreadability of a semisolid gel formulation can affect its ease of application, coverage area, and penetration into the skin or mucosal surfaces. The spreadability of a semisolid formulation depends on various factors, such as the viscosity, rheology, surface tension, and particle size distribution of the formulation. Optimization of these factors can ensure optimal spreadability and uniformity of drug distribution on the target surface, which can enhance the efficacy and safety of the drug product. Table 2 shows that the Spreadability of all formulations comprising niosomal gel loaded with mupirocin varied from 4.36 to 5.2 g. cm/s.

Table 2: An evaluation study of mupirocin-loaded niosomal gel

Formulation	Entrapment efficiency (%)	Drug content (%)	pH	Viscosity(cps)	Spreadability (g cm/s)
F1	87.15±0.13	89.25±0.64	6.32±1.36	401.61±3.33	4.79±0.39
F2	93.17±0.72	84.51±0.13	6.31±0.05	400.35±2.94	4.36±0.27
F3	97.73±0.68	96.87±0.19	6.72±0.82	455.51±3.94	4.91±0.86
F4	98.24±0.75	98.82±0.91	6.77±0.36	555.74±5.93	5.2±0.91
F5	97.95±0.83	91.27±0.53	6.19±0.35	538.32±9.97	4.98±1.74
F6	80.03±0.86	98.13±0.61	6.52±0.17	510.02±11.13	4.63±0.62
F7	94.09±0.57	96.31±0.62	6.41±0.94	535.79±5.68	4.71±0.07
F8	95.61±0.53	97.61±0.75	6.71±0.91	540.84±11.76	4.8±0.74

*Results are expressed as of mean ±SD (n=3)

SEM analysis

SEM is a powerful imaging technique that involves scanning a beam of high-energy electrons across a sample surface and detecting the electrons that are scattered or emitted from the surface to generate a high-resolution image. SEM can provide detailed information on the size, shape, and surface characteristics of formulated mupirocin loaded niosome gel. The SEM image of the best formulation F7 was discovered to be a spherical shape and particle sizes ranging from 90 nm to 120 nm. Figure 5 illustrates the SEM image of the best formulation F7, which was found to have a homogeneous distribution of niosome sphere-shaped particles (37).

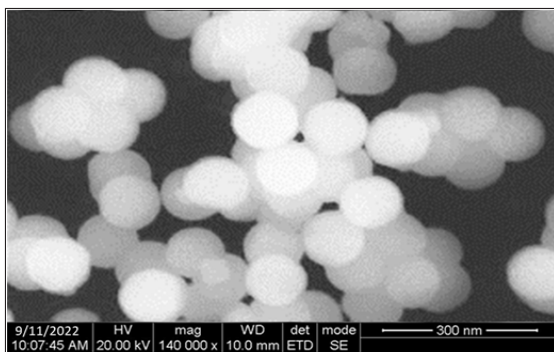


Figure 5: SEM Image of formulation F7 (Mupirocin loaded niosomal gel)

In-Vitro diffusion study

In-vitro diffusion study is a common technique used to assess the rate and extent of drug release from a dosage form. This technique is used to evaluate the release and diffusion of drug molecules from a formulation through a membrane. In this study prepared niosomal gel was placed on one side of a membrane and exposing it to a buffer solution on the other side. The drug molecules then diffuse through the membrane or tissue into the solution, and the concentration of the drug in the solution is measured over time using UV-visible spectroscopy. An *in-vitro* diffusion study was carried out in triplicate using the diffusion medium Phosphate buffer with a pH of 7.4. The percentage of mupirocin drug release at the end of 14 hours varied between 98% and 100% for all niosomal gel formulations shown in Figure 6.

Formulation F1 contains a drug-polymer (mupirocin-carbopol) ratio (2:1) and curcumin without honey shows 98 % drug release at 7h. Formulation F2 contains only drugs without polymer, curcumin, and honey and shows 100 % drug release at 6h. Formulation F2 has shown quick release of mupirocin due to the absence of carbopol in the formulation but the viscosity of honey manages the rate of release till 6h. Formulation F3 contains a drug with an

equal amount of polymer, curcumin, and honey and shows 98% drug release at 8h. Formulation F4 contains a drug-polymer ratio (2:3) high concentration of carbopol and honey and a low concentration of curcumin showing 99% drug release at 9h. Formulation F5 contains an equal amount of drug-polymer ratio (2:2) and a high concentration of honey with a low concentration of curcumin shows 100% drug release at 11h. Honey shows high viscosity and is useful in controlling the release rate of mupirocin at high concentrations. Formulation F6 contains an equal concentration of polymer and honey with a low amount of curcumin showing 99% drug release at 10h. Formulation F7 and F8 contain equal amounts of drug-polymer ratio (2:2) with variation in curcumin and honey showing 100% and 99 % drug release at 14 h and 12 h respectively. Formulation F7 has shown 100% drug release at 14 h, chosen as the best formulation among others.

The retarded release of mupirocin from niosomal gel is due to the concentration and viscosity grade of the polymer used and also due to the addition of a nonionic surfactant in the formulation. Carbopol is a water-soluble polymer that is commonly used as a thickening agent in pharmaceuticals, while honey is a natural product that has been used for medicinal purposes for centuries. Researchers confirm that carbopol and honey were combinedly and used for controlled drug release. The carbopol-honey combination can sustain the release of an active drug with the modulation of ratio. Reports confirm that the carbopol-honey had antibacterial properties, which could be useful in wound healing applications. Mupirocin drug release from niosome gel, which involves the polymer ability to form a gel matrix and its influence on the physicochemical properties of the niosomes. Carbopol can form a gel matrix when it is hydrated, which can entrap the drug and create a network that controls the diffusion and release of drugs. Gelling property of carbopol for topical formulations to preserve the drug molecule for a long time and generate a stable plasma drug concentration. The use of

carbopol in niosomal gels for drug delivery is a promising strategy for achieving controlled drug release, and further, enhancing the safety and efficacy of the gel. Available reports confirm that the non-ionic surfactant tween 80 enhances the entrapment efficiency of the active drug in the formulation. Due to the higher concentration of mupirocin drug getting entrapped inside the niosome, it helps Carbopol to sustain the drug and provide better therapeutic efficacy. Overall, the combination of carbopol and honey with non-ionic surfactant tween 80 in niosomal gel, can control the drug release and shows antibacterial properties towards topical wound healing treatment.

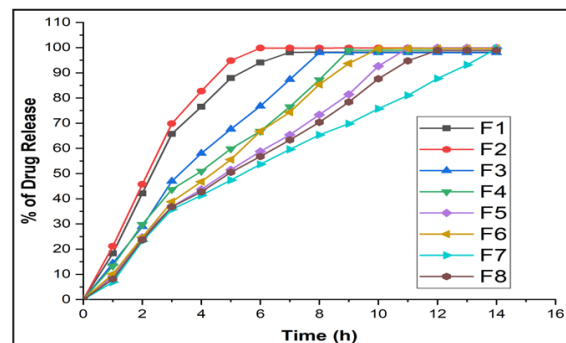


Figure 6: *In-vitro* dissolution of mupirocin-loaded niosomal gel formulations (F1-F8)

Release kinetic study of a mupirocin-loaded niosome-based gel

A release kinetic study is used to determine the release behavior of drugs from drug delivery systems over time. This kinetic study provides important information about the mechanism of the rate of drug release behavior. Obtained drug release data at different time intervals fitting to mathematical models to describe the release kinetics. The mathematical models that can be used to describe the release kinetics of drugs from drug delivery systems, include zero-order, first-order, Higuchi, and Korsmeyer-Peppas models. The greatest R^2 value was used as the best-fit criterion for choosing the optimal model. The Korsmeyer-Peppas model is a more complex model that can describe drug re-

lease from a variety of delivery systems, including matrix and reservoir systems, and assumes that the release rate is controlled by both diffusion and erosion. Table 3 displays the results, the drug release followed zero-order kinetics, independent of concentration. The illustration data fit into Peppas's equation, which depicted non-fickian release,

implying diffusion release and a mixture of diffusion and erosion release of the niosome-based gel.

Stability study

A stability study is an important parameter, which involves evaluating the physical, chemical, and microbiological stability of a drug product over time under specific storage conditions. Stability studies reveal that the drug product maintains its quality, efficacy, and safety throughout its shelf life, and establishes appropriate storage and handling conditions.

To establish its self-life, formulation F7 was

Table 3: Release kinetics of mupirocin-loaded niosomal gel formulation (F1-F8)

Formulation	R ² Values					Order of release
	Zero-order plots	First-order plots	Higuchi plots	Korsmeyer-peppas plots		
				R ²	Diffusional exponent (n)	
F1	0.987	0.961	0.959	0.663	0.983	Diffusion
F2	0.958	0.824	0.956	0.641	0.972	Diffusion
F3	0.972	0.831	0.960	0.726	0.999	Diffusion
F4	0.981	0.943	0.96	0.712	0.983	Diffusion & Erosion
F5	0.989	0.639	0.951	0.791	0.977	Diffusion & Erosion
F6	0.991	0.724	0.947	0.787	0.89	Diffusion & Erosion
F7	0.996	0.992	0.966	0.790	0.894	Diffusion & Erosion
F8	0.985	0.877	0.955	0.798	0.837	Diffusion & Erosion

Table 4: Stability study for mupirocin-loaded niosomal gel formulation F7

Storage condition	Days	Evaluated parameters				
		physical appearance	pH	viscosity	Spreadability	drug release profile (12h)
25°C/60%RH	0	Clear and transparent	6.41	535.79±5.68	4.71±0.07	100%
	30	Clear and transparent	6.49	535.6±5.45	4.69±0.05	98.75%
	60	Clear and transparent	6.5	534.91±5.04	4.68±0.03	98.16%
	90	Clear and transparent	6.5	534.87±5.01	4.68±0.02	97.95%
40°C/75%RH	0	Clear and transparent	6.41	535.79±5.68	4.71±0.07	100%
	30	Clear and transparent	6.46	534.91±5.32	4.70±0.03	97.35%
	60	Clear and transparent	6.51	534.01±5.11	4.69±0.03	96.16%
	90	Clear and transparent	6.52	533.98±4.93	4.69±0.01	95.93%

Results are expressed as of mean ±SD (n=3)

chosen for two different temperatures and related humidity for stability investigation shown in Table 4. The chosen formulation's ultimate purpose is self-life. The results of a 3-month accelerated stability analysis show that there have been no appreciable changes in the physical characteristics (consistency, morphology, and color), pH, viscosity, or spreadability. The drug release profile presented in Table 4 has a slight deviation. The stability of the mupirocin-loaded niosomal gel is confirmed by the obtained findings, which demonstrate no change or a slight deviation in formulation F7.

In vivo wound healing study on an albino rat model

Wound healing is a complex process that involves various cellular and molecular events, including inflammation, angiogenesis, and tissue remodeling. In a rat model study, the niosomal gel loaded with mupirocin, honey, and curcumin (Formulation F7) and marketed available mupicup medicine were applied topically on full-thickness skin wounds considered as group-II and Group-III respectively. Group-I rats are untreated (no application of medicine) and considered a controlled group. Figure 7 depicts the experimental process and the wound healing capability after each treatment. There was no redness, exudation, infection, or suppuration with experimental groups during the monitoring time. All of the wounds had blood scabs on them and were healing. Rats treated with formulation F7 healed wounds more quickly as compared to commercially available mupicup. On the 12th post-operative day, the wound closure area in group II (99.08%) was greater than group III (87.34%), and group-I (80.73%). The niosomal gel showed faster wound closure, increased collagen synthesis, and decreased inflammation compared to the other groups.

Niosomal gel is a novel drug delivery system that can improve the efficacy and bio-availability of drugs by enhancing their penetration into the skin layers and promoting their sustained release. Mupirocin is an antibiotic that

inhibits bacterial protein synthesis, thereby preventing bacterial infection and promoting faster wound healing. Honey shows antibacterial, anti-inflammatory, and antioxidant properties. It enhances wound healing by promoting tissue regeneration and reducing inflammation. The niosomal gel loaded with honey retard the release rate of active ingredients into the wound, which can enhance its therapeutic effect and promote faster wound healing. Curcumin is a polyphenol compound with potent anti-inflammatory and antioxidant properties. It helps in reducing inflammation, promoting tissue regeneration, and increasing collagen synthesis. The niosomal gel loaded with curcumin can enhance its bioavailability and provide better wound-healing properties.

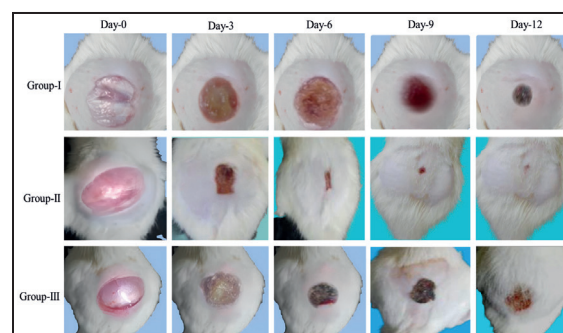


Figure 7: Images represent wound repair on excision wound model days 0-12.

The use of niosomal gel loaded with mupirocin, honey, and curcumin may provide a novel and effective approach to the treatment of skin wounds in animal models. Overall, the niosomal gel (formulation F7) can promote faster wound healing by preventing bacterial infection, reducing inflammation, endorsing tissue regeneration, and increasing collagen synthesis.

Histopathological study

In the case of niosomal gel loaded with mupirocin, honey, and curcumin on a rat model, a histopathological examination can provide insights into the mechanism of action and safety of the treatment. The examination showed a significant increase in the number of fibroblasts,

which are cells responsible for producing collagen, the primary component of the extracellular matrix in wounds. Figure 8 represent the histopathological study of group-I, group II, and group III where (a) Rearrangement of intact epidermis/epithelial cells; (b) Well-developed blood vessel, more organized collagen fibers, formation of mononuclear cells, neovascularisation, and hair follicle growth; and (c) Hair follicle development. Re-epithelization and remodeling of epithelial cells. (d) Maximum number of fibroblasts and newly-formed blood vessels, angiogenesis (H & E photograph captured with an Olympus photomicroscope at 400X magnification)

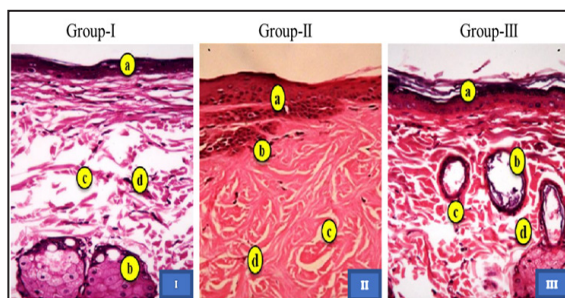


Figure 8: Histopathological photomicrographs of wounded tissue of rats on day 12

Histological examination of the lesion areas of the treated groups confirmed an increase in cellular infiltration, angiogenesis, fibroblast depositions, and collagen depositions. Due to the chemotactic effect of the niosomal gel (Formulation F7) in group II, the mechanisms of topical action on the lesion site may have attracted inflammatory cells. Further mitogenic activity may have increased cellular proliferation and contribute substantially to wound healing. On the 12th day, group II exhibited significantly smaller wound areas than group I & III.

This finding indicates that the niosomal gel may promote tissue regeneration and faster wound healing. Moreover, there was a significant decrease in the number of inflammatory cells, such as neutrophils and macrophages, in the wound site of the rats treated with the niosomal gel. This finding indicates that the niosomal gel may have anti-inflammatory effects, which

can promote faster wound healing by reducing inflammation and preventing the formation of chronic wounds. The histopathological examination also showed that the use of the niosomal gel did not cause any significant adverse effects or tissue damage. This finding indicates that the niosomal gel is safe and well-tolerated in the rat model.

Conclusion

Treatment of wound healing problems depends on the severity of the wound and its treatment procedure such as the application of antibiotics to treat infection, surgical debridement to remove dead tissue, wound dressings to promote healing, and lifestyle changes such as improved nutrition and exercise. In some cases, advanced wound care techniques such as nano drug delivery or growth factor therapy may be necessary to promote wound healing. In conclusion, the combination of mupirocin with honey and curcumin in a niosomal gel has the potential to provide a novel approach to wound healing treatment. Niosomes may serve as an effective drug delivery vehicle because it helps in controlling rapid drug release, targeted drug release and improve penetration. The combination has been shown to provide a synergistic effect in promoting wound healing, due to the antibacterial and anti-inflammatory properties of these compounds. Compatibility studies between drug, polymer, and other excipients, confirm by FTIR and DSC studies. Obtained results reveal entrapment efficiency, drug content, pH, viscosity, spreadability, and *in vitro* diffusion studies within the limit of IP. Formulation F7 is considered the best formulation. SEM analysis confirms the spherical shape of particles in the range of 90-120 nm. Kinetic studies depicted non-fickian release, implying diffusion release and a mixture of diffusion and erosion release of the niosome-based gel. The stability study confirms that obtained niosomal gel is stable with minor deviation. The niosomal gel formulation F7 healed wounds more quickly as compared to commercially available mupirocin gel. On the 12th post-operative day, the wound clo-

sure area in group II (99.08%) was greater than group III (87.34%), and group-I (80.73%). The histopathological examination for formulation F7 showed increased fibroblast activity and decreased inflammation, indicating that the niosomal gel can promote faster wound healing without causing significant tissue damage and has shown superior therapeutic options compared to conventional dose forms.

Ethics

All the *In-Vivo* procedures were approved by the Institutional Animal Ethic Committee (IAEC) as per CCSEA (Committee for Control and Supervision of Experiments on Animals), India.

Acknowledgments

The authors would like to express their gratitude to the administration and Pharma faculty of Dr. M.G.R. Educational and Research Institute, Deemed to be University, Chennai, Tamilnadu, India, and Ratnam Institute of Pharmacy, Nellore, A.P., India for their motivation and encouragement. The authors also thank Dr. Shaikh Ershadul Haque, Krupanidhi College of Pharmacy, Bengaluru, Karnataka, India for proofreading the manuscript.

Funding : None to declare.

Conflict Of Interest

The authors declared no conflict of interest.

References

1. Li, J., Chen, J., and Kirsner, R. (2008). Pathophysiology of acute wound healing. *Clin Dermatol*, 25(5): 9-18.
2. Boateng, J.S., Matthews, K.H., Stevens, H.N., and Eccleston, G.M. (2008). Wound healing dressings and drug delivery systems: a review. *J pharma Sci*, 97(8): 2892-2923.
3. Lazarus, G.S., Cooper, D.M., Knighton, D.R., Margolis, D.J., Percoraro, R.E., and Rodeheaver, G. (1994). Definitions and guidelines for assessment of wounds and evaluation of healing. *Wound Repair Regen*, 2(3):165-70.
4. Harding, K.G., Morris, H.L., and Patel, G.K. (2002). Healing chronic wounds. *Brit Med J*, 32(4): 160-163.
5. Singer, A.J., and Dagum, A.B. (2008). Current management of acute cutaneous wounds. *N Engl J Med*, 359: 1037-1046.
6. Wang, L., Qin, W., Zhou, Y., Chen, B., Zhao, X., and Zhao, H. (2017). Transforming growth factor β plays an important role in enhancing wound healing by topical application of Povidone-iodine. *Scie Reports*, 7 (1): 991-999.
7. Gonzalez, A.C.D.O., Andrade, Z.D.A., Costa, T.F., and Medrado, A.R.A.P. (2016). Wound healing – A literature review. *An Bras Dermatol*, 91(5): 614-620.
8. Moore, K., Callion, R., Searle, R.J., Stacey, M.C., and Harding, K.G. (2006). Prediction and monitoring the therapeutic response of chronic dermal wounds. *Int wound J*, 3(2): 89-98.
9. Eppley, B.L., Woodall, J.E., and Higgins, J. (2004). Platelet quantification and growth factor analysis from platelet-rich plasma: implications for wound healing. *Plast Reconstr Surg*, 114:1502–1508.
10. Farahpour, M.R., and Habibi, M. (2012). Evaluation of the wound healing activity of an ethanolic extract of Ceylon cinnamon in mice. *Vet Med*, 57:53-59.
11. Krausz, A.E., Adler, B.L., Cabral, V., Navati, M., Doerner, J., and Charafeddine, R.A. (2015). Curcumin-encapsulated nanoparticles as innovative antimicrobial and wound healing agent. *Nanomed Nanotec Bio Med*, 11(1):195-206.

12. Losi, P., Briganti, E., Errico, C., Lisella, A., Sanguinetti, E., and Chiellini, F. (2013). Fibrin-based scaffold incorporating VEGF- and bFGF-loaded nanoparticles stimulates wound healing in diabetic mice. *Acta biomater*, 9(8):7814-7821.
13. Allen, T.M. (1998). Liposomal drug formulations, rationale for development and what we can expect for the future. *Drugs*, 56: 747-756.
14. Baillie, A.J., Coombs, G.H., and Dolan, T.F. (1986). Non-ionic surfactant vesicles, niosomes, as delivery system for the anti-leishmanial drug, sodium stibogluconate. *J Pharm Pharmacol*, 38: 502-505.
15. Dinu Pîrvu, C., Hlevca, C., Ortan, A., and Prisada, R. Elastic vesicles as drugs carriers through the skin. *Farmacia*, 58(2): 128-135.
16. Malhotra, M., and Jain, N.K. (1994). Niosomes as drug carriers. *Indian Drugs*, 31(3): 81-86.
17. Madhava Chetty, K., Sivaji, K., and Tulasirao, K. (2008). Flowering plants of Chittoor District, Andhra Pradesh. Tirupati, India. Students offset printers, 277: 103-112.
18. Ukil, A., Maity, S., Karmakar, S., Datta, N., Vedasiromoni, J.R., and Das, P.K. (2003). Curcumin, the major component of food flavour turmeric, reduces mucosal injury in trinitrobenzene sulphonic acid-induced colitis. *Br J Pharmacol*, 139: 209-218.
19. Bagdonas, R., Tamelis, A., and Rimdeika, R. (2003). Staphylococcus aureus in the surgery of burns. *Medicina*, 39: 1078-1081.
20. Sun, M.C., Chen, Y.F., Liu, D., Xu, X.L., You, Y.C., and Lu, W. (2023). Effective decolonization strategy for mupirocin-resistant Staphylococcus aureus by TPGS-modified mupirocin-silver complex. *Mater Today Bio*, 100:53-64.
21. Kundu, S., Biswas, T.K., Das, P., Kumar, S., and De, D.K. (2005). Turmeric (*Curcuma longa*) rhizome paste and honey show similar wound healing potential: a preclinical study in rabbits. *Int J Low Extrem Wounds*, 4(4): 205-213.
22. Shah, A., and Amini-Nik, S. (2017). The role of phytochemicals in the inflammatory phase of wound healing. *Int J mole Sci*, 18(5): 106-108.
23. Kenawy, E.R., Kamoun, E.A., Ghaly, Z.S., Shokr, A.B., El-Meligy, M.A., and Mahmoud, Y.A. (2023). Novel physically cross-linked curcumin-loaded PVA/Aloe Vera hydrogel membranes for acceleration of topical wound healing: In vitro and in vivo experiments. *Arabian J Sci Eng*, 48(1):497-514.
24. Saleem, W., Sarfraz, B., and Mazhar, S. (2022). Combined Effect of Honey, Neem (*Azadirachta Indica*), and Turmeric against Staphylococcus Aureus and E. Coli Isolated from a Clinical Wound Sample. *Bio Sci Rev*, 4(4): 21-44.
25. Rani, G.N., Budumuru, R., and Bandaru, N.R. (2017). Antimicrobial activity of honey with special reference to methicillin resistant Staphylococcus aureus (MRSA) and methicillin sensitive Staphylococcus aureus (MSSA). *J Clinical Diagnostic Res*, 11(8):25-35.
26. Kumari, M., and Nanda, D.K. (2022). Potential of Curcumin nanoemulsion as antimicrobial and wound healing agent in burn wound infection. *Burns*, 4(10): 87-95.
27. Dons, T., and Soosairaj, S. (2018). Evaluation of wound healing effect of herbal lotion in albino rats and its antibacterial activities. *Clin Phytoscience*, 4: 1-7.
28. Hermanns, R., Mateescu, C., Thrasyvou-

- lou, A., Tananaki, C., Wagener, F.A., and Cremers, N.A. (2020). Defining the standards for medical grade honey. *J Apicultural Res*, 59(2): 125-135.
29. Chaudhary, A., Bag, S., Banerjee, P., and Chatterjee, J. (2020). Wound healing efficacy of Jamun honey in diabetic mice model through reepithelialization, collagen deposition and angiogenesis. *J Traditional Complementary Med*, 10(6): 529-543.
30. Shehata, T.M., Ibrahim, M.M., and Elsewedy, H.S. (2021). Curcumin niosomes prepared from proniosomal gels: In vitro skin permeability, kinetic and in vivo studies. *Polymers*, 13(5): 791-799.
31. Ravalika, V., and Sailaja, A.K. (2017). Formulation and evaluation of etoricoxib niosomes by thin film hydration technique and ether injection method. *Nano Biomed Eng*, 9(3): 242-248.
32. Safwat, M.A., Soliman, G.M., Sayed, D., and Attia, M.A. (2016). Gold nanoparticles enhance 5-fluorouracil anticancer efficacy against colorectal cancer cells. *Int J Pharm*, 513: 648-658.
33. John-Africa, L.B., Yahaya, T.A., and Isimi, C.Y. (2014). Anti-ulcer and wound healing activities of *Sida corymbosa* in rats. *Afr J Tradit Complement Altern Med*, 11(1): 87-92.
34. Bayat, S., Amiri, N., Pishavar, E., Kalalinia, F., Movaffagh, J., and Hashemi, M. (2019). Bromelain-loaded chitosan nanofibers prepared by electrospinning method for burn wound healing in animal models. *Life Scie*, 229: 57-66.
35. Nematollahi, M.H., Pardakhty, A., Torkzadeh-Mahanai, M., Mehrabani, M., and Asadikaram, G. (2017). Changes in physical and chemical properties of niosome membrane induced by cholesterol: a promising approach for niosome bilayer intervention. *RSC Adv*, 7(78): 49463-49472.
36. Bhattacharya, M., Malinen, M.M., Lauren, P., Lou, Y.R., Kuisma, S.W., and Kanninen, L. (2012). Nanofibrillar Cellulose Hydrogel Promotes Three-Dimensional Liver Cell Culture. *J Control Release*, 164(3): 291-298.
37. Pripem, A., Janpim, K., Nualkaew, S., and Mahakunakorn, P. (2016). Topical niosome gel of Zingiber cassumunar Roxb. extract for anti-inflammatory activity enhanced skin permeation and stability of compound. *AAPS Pharmscitech*, 17:631-9.

Hypoglycemic and hypolipidemic effects of *Oligomeris linifolia* in Alloxan-induced diabetic mice

Aisha Ashiq,¹ Saleem Jan,¹ Yar Muhammad Khan,² Faizan Ullah,³
Ashok Kumar Balaraman⁴, Abul Kalam Azad⁵

¹ Department of Chemistry, University of Science and Technology, Bannu, Pakistan

² Department of Biotechnology, University of Science and Technology, Bannu, Pakistan

³ Department of Botany, University of Science and Technology, Bannu, Pakistan

^{4,5} Faculty of Pharmacy, MAHSA University, Bandar Saujana Putra, 42610 Jenjarom, Selangor, Malaysia

Corresponding author: azad@mahsa.edu.my

Abstract

The current study was focused to evaluate the hypoglycemic and hypolipidemic effect of methanolic extracts of *Oligomeris linifolia* in Alloxan-induced diabetic mice. Albino mice were orally treated for 15 days with methanolic extract of *Oligomeris linifolia* at dose of 200 mg/kg body-weight. The antidiabetic effect was analyzed by measuring blood glucose (BG) at 0, 3, 6, 9, 12, and 15 days. Total cholesterol (TC), high density lipoprotein cholesterol (HDL-C), low density lipoprotein cholesterol (LDL-C), Serum Bilirubin (SBR), Alkaline Phosphatase (ALP), Alanine Aminotransferase (ALT), Urea, Creatinine, and triglycerides (TG) levels at sacrifice (day 16) were measured. Glibenclamide (10 mg/kg) was used as standard. Alloxan-induced diabetic mice showed adequate to significant increase in the level of BG, TC, TG, LDL-C, SBR, ALT, ALP, Urea, Creatinine, while HDL-C and body-weight were decreased as compared to control group (non-diabetic mice). Administration of plant methanolic extract to Alloxan-induced diabetic mice at a dose of 200 mg/kg body-weight resulted in a notable decrease in BG, TC, TG, LDL-C, SBR, ALT, ALP, Urea and Creatinine whereas HDL-C level and body-weight were increased markedly after 15 days as compared to diabetic control group.

The methanolic extract at the dose of 200 mg/kg, produced similar results compared to group treated with Glibenclamide.

Keywords: *Oligomeris linifolia*, White Albino mice, Antidiabetic activity, Lipid profile

Introduction

Natural source is one of the major hub for medicinal analogue [1]. Diabetes Mellitus is the most common metabolic and chronic disorder indicated by rise in blood glucose level due to relative or complete insulin deficiency [2]. In the long term the disease is associated with various complications including renal, eyes, neurological and cardiovascular disorders [3]. Diabetes Mellitus has symptoms such as excess urination, fatigue, glycosuria (increased urine glucose level), blurry vision, and delayed wound healing [4]. One of the impairments of the immune system is destruction of the β -cells of pancreas within Islets of Langerhans and therefore development of insulin-dependent diabetes. Immune system is affected by several environmental and genetic factors which lead to the attack of lymphocytes, causing pancreatitis. This inflammatory reaction leads to insulinitis and diabetes [5, 6] and without proper treatment, vascular, cardiac, neurological, renal damage and neuropathy can occur. Diabetes Mellitus is

Hypoglycemic and hypolipidemic effects of *Oligomeris linifolia* in alloxan induced diabetic mice

mostly controlled with Treatment of diabetes includes healthy diet, regular exercise, and medication [7]. The primary major treatment is the use of anti-diabetogenic drugs, but side effects of these drugs limits their use [8]. Due to lesser side effects, there is a long history of medicinal plants usage and nowadays, they are being widely used to treat various diseases [9].

Plant *Oligomeris linifolia* Vahl belongs to family Resedaceae which contains 107 species with 8 to 12 genera [10]. Physically *O. linifolia* is like chubby having low height around 50 centimeters with many rigged stems. The leaves size is about 45 mm in length and with 0.52 mm width [11]. It is mostly present in Southeast Asia, Middle East, North America, North Africa and south of Europe [12]. The literature data has revealed that this plant has exhibited various pharmacological activities including antioxidant, antifungal and antibacterial activities [13]. The current study was undertaken to investigate the hypoglycemic effect of methanolic extract of *O. linifolia* in a non-obese diabetes model.

Experimental design collection and Identification

The plant was collected in flowering season from various regions of Bannu District, Khyber Pakhtunkhwa, Pakistan. Plant specimen was identified by Dr. Faizan Ullah, Associate Professor, Department of Botany, University of Science and Technology, Bannu.

Extraction

Plant was initially rinsed through tap water and then with distilled water. The plant was then dried under shade. The shade dried plant material (1.5 kg) was chopped and soaked in 80% aqu. methanol for one week and was filtered by using filter paper. After filtration, rotary evaporator was utilized for evaporation of methanol to obtain crude plant extract [14].

Animals

In current research, White Albino mice (age 3-4 weeks, weighed 20-22 g with a mean

of 21 g) were used. The mice were purchased from National Institute of Health Sciences, Islamabad, Pakistan. The "White albino mice" were placed in controlled conditions i.e., temperature 25C°-27 C° with 12hr darkness photoperiod with rodent-pellets as feed along with water. The Internationally accepted standard ethical guidelines for laboratory animal use and care were adopted in the experiment [14].

Induction of Hyperglycemia

In current study, the investigational mice were abstained from eating for 8-12 hrs, however, there was no restriction on water to drink. "Hyperglycemia" was induced experimentally by a single intraperitoneal dose of 150 mg/kg body weight of freshly prepared alloxan 10% monohydrate obtained from Department of Biotechnology, University of Science and Technology, Bannu. After 48 hrs, blood glucose level of the animals was checked by using glucometer. Mice with blood glucose level of 200mg/dl and above were used for further investigation.

Experimental Design

The experimental models were divided randomly into four groups, each group with five mice (both sex). Group 1 consisted of normal mice orally directed with 0.1 ml "normal saline"; Group 2 consisted of alloxan induced diabetic mice orally managed with 0.1 ml normal "saline"; Group 3 consisted of alloxan treated mice orally managed with 10 mg/kg "Glibenclamide". Group 4 comprised of "alloxan-induced diabetic-mice" (150 mg/kg) orally administered with plant extract of 200 mg/kg body-weight. The investigation was carried out for 15 days. Glycaemia and body weights were measured at an interval of 3 days for 15 days. After one day of last treatment (day 16), all the groups of mice were sacrificed by cervical dislocation. Blood was collected for measuring total cholesterol (TC), high density lipoprotein cholesterol (HDL-C), low density lipoprotein cholesterol (LDL-C), Serum bilirubin (SBR), Alkaline Phosphatase (ALP), Alanine Aminotransferase (ALT), Urea, Creatinine, and triglycerides (TG) levels by using commercial

kits (INMESCO (Germany).

Statistical analysis

The reported data statistically analyzed by ANOVA. The lipid profile parameters were analyzed using one-way ANOVA while for blood glucose determination two ways ANOVA was used.

Results and Discussion

Effects of oligomeris linifolia on Body Weight and lipid profile

In current investigation it was observed that alloxan substantially reduced body-weight of mice-as compared to control group, measured at an interval of 3 days for 15 days. Administration of doses of plant *Oligomeris linifolia* extract rescue remarkably in the body-weight. The plant species *O.linifolia* reduces adverse effects on body weight when supplemented at 200 mg/kg body weight as compared to Glibenclamide. The diabetic condition in mice (untreated diabetics) raised TC, LDL-C and TG concentrations while, the HDL-C level were lower as compared to control mice (nondiabetic mice). As shown in table 1, the elevated level of TC, LDL-C and TG recovered significantly. However, the decrease in HDL level was also restored by effective doses of *O. linifolia* extract.

Effects of oligomeris linifolia on blood glucose

Table 2 shows the effects of methanolic extract of *O. linifolia* on blood glucose levels of White Albino mice after 15 days of continuous treatment. Significant and continuous reduction of blood glucose level was observed in alloxan-treated mice groups after 15 days of the treatment. Groups of mice treated with *O. linifolia* and glibenclamide exhibited significant decrease in blood glucose level as compared to diabetic control, measured at 0th day to 15th day of the experiment.

Alloxan is a toxic glucose analogue that preferentially accumulates in pancreatic beta cells via the GLUT2 glucose transporter. Alloxan selectively inhibits glucose-induced insulin secretion through specific inhibition of glucokinase, and causes a state of insulin-dependent diabetes through its ability to induce ROS formation, resulting in the selective necrosis of beta cells. [15]. Alloxan produces oxygen radicals in the body, which cause pancreatic injury and could be responsible for increased blood sugar as well as lipid peroxidation. In diabetic mice treated with *O. linifolia* extract, a significant decrease in blood glucose level was observed as compared to respective baseline values (day 0). It could be believed that this plant with this

Table 1: Effects of Oligomeris linifolia on body weight, lipid profile on Alloxan-induced diabetic mice

Groups	Body weight(g)			Lipid profile(mg/dl)								Creatinine
	Initial	Final	% Variation	TC	LDL-C	HDL-C	TG	ALT	SBR	ALP	Urea	
Normal Control	21±0.2a	25±0.4a	0.0016	100±0.6	80±0.31a	32±0.15a	200 ±0.447	23±0.02a	0.55±0.08a	223±0.04	40±0.004a	0.40±0.002a
Diabetic Control (Untreated Diabetic)	20±0.19b	16±0.31b	-0.0025	163±0.63b	110±0.24b	20±0.31b	235±0.31b	98±0.31b	0.67±0.002b	283±0.06b	44±0.07b	0.56±0.003b
Diabetic + Glibenclamide (10 mg/kg)	19±0.2c	21±0.44c	0.0009	118±0.24c	73±0.20c	46±0.21c	153±0.002c	59±0.06c	0.80±0.04c	371±0.08c	43±0.020c	0.47±0.004c
Diabetic + Methanolic Extract (200 mg/kg)	19±0.15c	21±0.32c	0.0009	116±0.63d	75±0.22c	45±0.20c	144±0.002d	26±0.04d	0.53±0.002c	259±0.05c	38±0.019c	0.40±0.005c

Hypoglycemic and hypolipidemic effects of Oligomeris linifolia in alloxan induced diabetic mice

Table 2: Effects of *Oligomeris linifolia* on blood glucose in Alloxan-induced diabetic mice

Groups	Fasting blood glucose level (mg/dl)						
	Initial	Day of treatment					
		Day 0	Day 3	Day 6	Day 9	Day 12	Day 15
Normal Control	135 ±3.11	138±1.91	140±3.6	147±2.11	145±2.14	140±3.23	130±2.56
Diabetic Control (Untreated Diabetic)	129 ±2.78	210±2.89	243±3.12	250±2.13	275±3.75	280±3.65	290±4.13
Diabetic+ Glibenclamide (10 mg/kg)	128 ±1.89	210±2.89	197±2.12	180±1.96	150±2.89	140±3.14	129±2.87
Diabetic+ Methanolic Extract (200 mg/kg)	130 ±2.02	210 ±2.89	190±2.9	175±4.12	140±3.11	12±0.91	115±4.21

±standard error.

anti-diabetic potential may contains certain antioxidant constituents which are useful in treatment of diabetes [16-18]. The *in vitro* antioxidant property of *O. linifolia* previously reported [13] further supported our result that the constituents with antioxidant property may have their anti-diabetic potential [19–21].

Conclusion

Results of the current investigation showed that methanolic extract of *Oligomeris linifolia* possess antidiabetic effect and favorable effects on diabetic hyperlipidemia. Alloxan-induced diabetic mice showed adequate to significant increase in the level of BG, TC, TG, LDL-C, SBR, ALT, ALP, Urea, Creatinine, while HDL-C and body-weight were decreased as compared to control group (non-diabetic mice). Administration of the methanolic plant extract to Alloxan-Induced Diabetic mice at a dose of 200 mg/kg body-weight resulted in a notable decrease in BG, TC, TG, LDL-C, SBR, ALT, ALP, Urea and Creatinine; HDL-C level and body-weight were increased markedly after 15 days as compared to diabetic control group. All these effects could be the result of bioactive compounds present in *Oligomeris linifolia* extracts.

References

1. Islam, M. S., Samsudin, S., & Azad, A. K. (2015). Herbal medicinal importance of *Citrullus lanatus* mentioned in the Ahadith: a precise overview. *American Journal of Ethnomedicine*, 2(1), 39-45.
2. Azad, A. K., Azizi, W. S., Ismail, A. F. H., Abbas, S. A., Uddin, J., & Labu, Z. K. (2019). Phytochemical and toxicity evaluation of traditional herb: *Lagerstroemia speciosa* L.(Banaba) by MCF-7 cell line and brine shrimp lethality bioassay. *Bangladesh Pharmaceutical Journal*, 22(1), 45-49.
3. Rao NK, Nammi S. Antidiabetic and renoprotective effects of the chloroform extract of *Terminalia chebula* Retz. seeds in streptozotocin-induced diabetic rats. *BMC complementary and alternative medicine*. 2006;6(1):1-6.
4. Ziamajidi N, Nasiri A, Abbasalipourkabir R, Sadeghi Moheb S. Effects of garlic extract on TNF- α expression and oxidative stress status in the kidneys of rats with STZ+ nicotinamide-induced diabetes. *Pharmaceuti-*

- cal biology. 2017;55(1):526-31.
5. Azad, A. K., & Sulaiman, W. M. A. W. (2020). Antidiabetic effects of *P. macrocarpa* ethanolic fruit extract in streptozotocin-induced diabetic rats. *Future Journal of Pharmaceutical Sciences*, 6, 1-12.
 6. Bwititi P, Musabayane CT, Nhachi CF. Effects of *Opuntia megacantha* on blood glucose and kidney function in streptozotocin diabetic rats. *Journal of Ethnopharmacology*. 2000;69(3):247-52.
 7. Lert-Amornpat T, Maketon C, Fungfuang W. Effect of *Kaempferia parviflora* on sexual performance in streptozotocin-induced diabetic male rats. *Andrologia*. 2017;49(10):e12770.
 8. Yu Z, Gong C, Lu B, Yang L, Sheng Y, Ji L, Wang Z. *Dendrobium chrysotoxum* Lindl. alleviates diabetic retinopathy by preventing retinal inflammation and tight junction protein decrease. *Journal of diabetes research*. 2015;2015.
 9. Das M, Sarma BP, Khan AK, Mosihuz-zaman M, Nahar N, Ali L, Bhounik A, Rokeya B. The antidiabetic and antilipidemic activity of aqueous extract of *Urtica dioica* L. on type2 diabetic model rats. *Journal of Bio-Science*. 2009;17:1-6.
 10. Fallah Huseini H, Fakhrzadeh H, Larijani B, Shikh Samani AH. Review of anti-diabetic medicinal plant used in traditional medicine. *Journal of Medicinal Plants*. 2006;5(17):1-8
 11. Azad, A. K., Rahman, M. K., & Sunzida, N. K. (2015). Acute oral toxicity Study on Malaysian traditional herb: *Lagerstroemia speciosa* L.(Banaba). *Journal of Pharmacognosy and Phytochemistry*, 4(4), 228-232.
 12. Sulaiman, W. M. A. W., Azad, A. K., Daud, N. A., & Khan, N. (2016). Evaluation of skin elasticity after used different seaweed containing products by DermaLab® Combo. *Asian J Pharm Pharmacol*, 3(2), 72-76.
 13. Hussein SR, Elkhateeb A, Marzouk MM, Ibrahim LF, Kawashty SA. "Phytochemical investigation of *Oligomeris linifolia* (Vahl) Macbr. (Resedaceae)". *Biochemical Systematics and Ecology*. 2013; 49: 73–76.
 14. Babar, Z. M., Azizi, W. M., Ichwan, S. J., Ahmed, Q. U., Azad, A. K., & Mawa, I. (2019). A simple method for extracting both active oily and water soluble extract (WSE) from *Nigella sativa* (L.) seeds using a single solvent system. *Natural product research*, 33(15), 2266-2270.
 15. Azad, A. K., Babar, Z. M., Wan Mohd Azizi, W. S., & Sunzida, N. K. (2016). The significance of *murrayakoenigii* (L.) spreng leaves: A mini-Review. *Pharmacologyonline*, 2, 18-25.
 16. Lenzen, S. The mechanisms of alloxan- and streptozotocin-induced diabetes. *Diabetologia*. 2008; 51: 216–226.
 17. Jang YY, Song JH, Shin YK, Han ES, Lee CS: Protective effect of boldine on oxidative mitochondrial damage in STZ-induced diabetic rats. *Pharm Res*. 2000, 42: 361-371.
 18. Sarkhail P, Rahmanipour S, Fadyevatan S, Mohammadirad A, Dehghan G, Amin G, Shafiee A, Abdollahi M: Antidiabetic effect of *Phlomis anisodonta*: Effects on hepatic cells lipid peroxidation and antioxidant enzymes in experimental diabetes. *Pharm Res*. 2007, 56: 261-266.
 19. Azad, A. K., Awang, M., Rahman, M. M., & Akter, F. U. (2012). Biological and pre-clinical trial evaluation of a local medicinal plant *bacopa monnieri* (L.) Penn. *Interna-*

Hypoglycemic and hypolipidemic effects of *Oligomeris linifolia* in alloxan induced diabetic mice

- tional Journal of Current Research and Review, 4(19), 92.
20. Ali Hussain HE: Hypoglycemic, hypolipidemic and antioxidant properties of combination of Curcumin from *Curcuma longa*, Linn, and partially purified product from *Abroma augusta*, Linn. in streptozotocin induced diabetes. *Indian J Clin Biochem.* 2002, 17: 33-43.
 21. Leelavinothan P, Muniappan L: Protective role of *Scoparia dulcis* plant extract on brain antioxidant status and lipid peroxidation in STZ diabetic male Wistar rats. *BMC Complement Altern Med.* 2004, 4: 16-10.
 22. Nain P, Saini V, Sharma S, Nain J: Antidiabetic and antioxidant potential of *Emblica officinalis* Gaertn. leaves extract in streptozotocin-induced type-2 diabetes mellitus (T2DM) rats. *J Ethnopharmacol.* 2012, 142: 65-71.
 23. Pari L, Latha M: Antidiabetic effect of *Scoparia dulcis*: effect on lipid peroxidation in streptozotocin diabetes. *Gen Physiol Biophys.* 2005, 24: 13-26.
 24. Li WL, Zheng HC, Bukuru J, De Kimpeb N: Natural medicines used in the traditional Chinese medical system for therapy of diabetes mellitus. *J Ethnopharmacol.* 2004, 92: 1-21.
 25. Saravanan R, Pari L: Antihyperlipidemic and antiperoxidative effect of Diasulin, a polyherbal formulation in alloxan-induced hyperglycemic rats. *BMC Complement Altern Med.* 2005, 5: 1-8.
 26. Sharma SB, Nasir A, Prabhu KM, Murthy PS, Dev G: Hypoglycaemic and hypolipidemic effect of ethanolic extract of seeds of *Eugenia jambolana* in alloxan-induced diabetic rabbits. *J Ethnopharmacol.* 2003, 85: 201-206.

A Comprehensive Review on Technological Advances in Alternate Drug Discovery Process: Drug Repurposing

Madhuri Pola^{1*}, Alok Tiwari¹, PotlaDurthi Chandrasai²

¹ uGDX School of Technology, ATLAS SkillTech University, Tower 1-Equinox Business Park, Off Bandra-Kurla Complex, LBS Marg, Kurla West Mumbai-400070

²Department of Biotechnology, National Institute of Technology Warangal, Warangal, Telangana, India-506004

*Corresponding author: madhuri.pola@gmail.com

Abstract

The traditional de novo drug discovery is time consuming, costly and in some instances the drugs will fail to treat the disease which result in a huge loss to the organization. Drug repurposing is an alternative drug discovery process to overcome the limitations of the De novo drug discovery process. It helps for the identification of drugs to the rare diseases as well as in the pandemic situation within short span of time in a cost-effective way. The underlying principle of drug repurposing is that most of the drugs identified on a primary purpose have shown to treat other diseases also. One such example is Tocilizumab is primarily used for rheumatoid arthritis and it is repurposed to treat cancer and COVID-19. At present, nearly 30% of the FDA approved drugs to treat various diseases are repurposed drugs. The drug repurposing is either drug-centric or disease centric and can be studied by using both experimental and *in silico* studies. The *in silico* repurpose drug discovery process is more efficient as it screens thousands of compounds from the diverse libraries within few days by various computational methods like Virtual screening, Docking, MD simulations, Machine Learning, Artificial Intelligence, Genome Wide Association Studies (GWAS), etc. with certain limitations. These limitations can be addressed by

effective integration of advanced technologies to identify a novel multi-purpose drug.

Keywords: Drug repurposing, Screening, Drug-centric, Disease-centric, FDA, Pandemic, GWAS, Machine Learning, Artificial Intelligence

Introduction

De novo drug discovery method is the traditional drug discovery process which is tedious, time-consuming and expensive with high attrition values. In De novo drug discovery process of new drug identification, testing drug safety, efficacy and toxicity studies costs up to 2.6 billion dollars and it takes nearly 15 years for its approval from the screening to final approval of a drug candidate (1). Most traditional drugs were not approved or withdrawn because of the toxicity profile, adverse effects (especially hepatotoxicity) and limited financial support (2). The failure of a drug not only results in financial loss but also it costs both the individual health and life in some cases. Besides, it is difficult to find drugs by traditional methods for the pandemics like COVID-19 as it is a phase beyond the containment (3). Hence, there is need to study in detailed about this complex process i.e. drug mechanism of action on humans at gene level by employing various novel strategies.

Most of the pharma companies will invest only in the specific diseases which have the scope

to generate more revenue and hence their treatments are expensive. There are various other rare diseases, where pharma companies would refrain themselves to focus because of low populations. Hence, to meet the unmet medical needs of rare diseases, the researchers have adopted many novel alternate optimization approaches for the discovery of new drugs or drug candidates and found promising results in the identification of multipurpose application of various drugs. Of the different methods adopted by the pharmaceutical companies, the most revolutionized alternate technology is drug repurposing which works on the multiple usage of the drugs that are approved or still under clinical trials(4). The repurposing drug discovery is more efficient because of the existing data (toxicology and pharmacology) of the drugs which are already approved or still in the clinical trials phase. It was reported in the literature that, 30% of the existing FDA approved drugs are the repurposed drugs accounting for 25% of the global pharmaceutical market revenue (5). Hence, to overcome the tedious traditional process many applications based on bioinformatics were developed to screen thousands of the drugs within less time. The time instance for both the De novo drug discovery and drug repurposing is as shown in the below Figure 1.

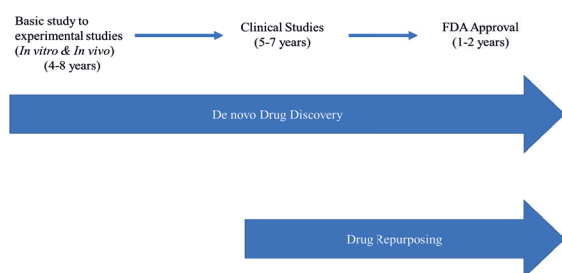


Figure 1. Overview of De novo drug discovery and Drug Repurposing

The *in vitro* and *in vivo* repurposing studies takes longer times and it is difficult to screen thousands of compounds at an

instance. This can be met by the application of computational repurposing methods which can screen thousands of compounds, either based on the disease pathways or gene expression profiles within the less time as it accounts the available research data for screening drug candidates(6).

In addition to drug discovery the computational methods will be helpful in predicting the market value with in less time, if in case the drug fails or gets success by using the existing data. This lays the basis for the computational drug repurposing to study multiple applications in pharmaceutical industry. Hence, it is a potential breakthrough in the drug discovery process of identifying multiple applications for the same drug. Besides, there is need for the identification of drugs having multi disease potential by various computational studies as they require only 2D/3D structures of the targets before it is studied in experiments. The computational tools will help to build 3D structures of the target by using modelling techniques. The interactive effect between the target and the drug can be studied by docking and Molecular Dynamics (MD) and Simulations studies (7). Hence, it is important and will be advantageous to screen the drugs with multiple targets to achieve success.

Many reports were published about the application of the drug repurposing for the FDA approved drugs and other clinical drugs. This will minimize both time and cost of production. In addition to FDA approved and other clinical trials, many researchers are working on the application of the enzymes as alternative medication to minimise the side effects of the chemically synthesised drugs (8-10). So many enzymes as drugs such as L-Asparaginase, L-Glutaminase are currently in use to treat cancer (11-12). Hence many recent technologies based on the Bioinformatics, Cheminformatics, Artificial Intelligence and Systems Biology are being implemented by the researchers across the world to find the multipurpose application of the drugs to treat various diseases (13).

Many examples of the successful application of the repurposed drug as an anticancer, anti-malarial, antibiotic etc. are currently in use (14). The present review will discuss about the principles of drug repurposing, associated methodological strategies, available databases, applications, challenges and recommended solutions to improve effective integration of drug repurposing in pharmaceutical industry.

Principle of Drug Repurposing

Drug repurposing has gained momentum and leveraged by the pharmaceutical companies to improve the drug efficiency and its development (15). The principles on which the drug repurposing is based are: 1. Many drugs have cryptic biological activities with observed side effects-Multiple targets for the same drug. 2. Many diseases share same molecular pathways or genetic factors -Disease similarity. 3. Pleiotropic effects of the target based on their molecular function.

The alternate drug repurposing strategies were successful in identification of various repurposing

drugs in the treatment of diseases like cancer, Cardio Vascular Diseases (CVD), arthritis, COVID-19, etc. by the application of advanced computational studies to find the multiple use of the same drug for various diseases. Table 1 demonstrates the reported applications of drugs for what disease treatment they are synthesized and their repurpose application to treat other diseases. The overview of drug repurposing was shown in the below Figure 2.

The most demonstrated example of the repurposed drug discovery process is Sildenafil (Viagra) which is developed for the treatment of hypertension but its repurposed application is for erectile dysfunction and pulmonary arterial hypertension (16).

The advantages of using drug as a repurposing which in clinical trials not only cut down the time, cost but also associated risks which makes drug repurposing as an attractive alternate drug discovery process.

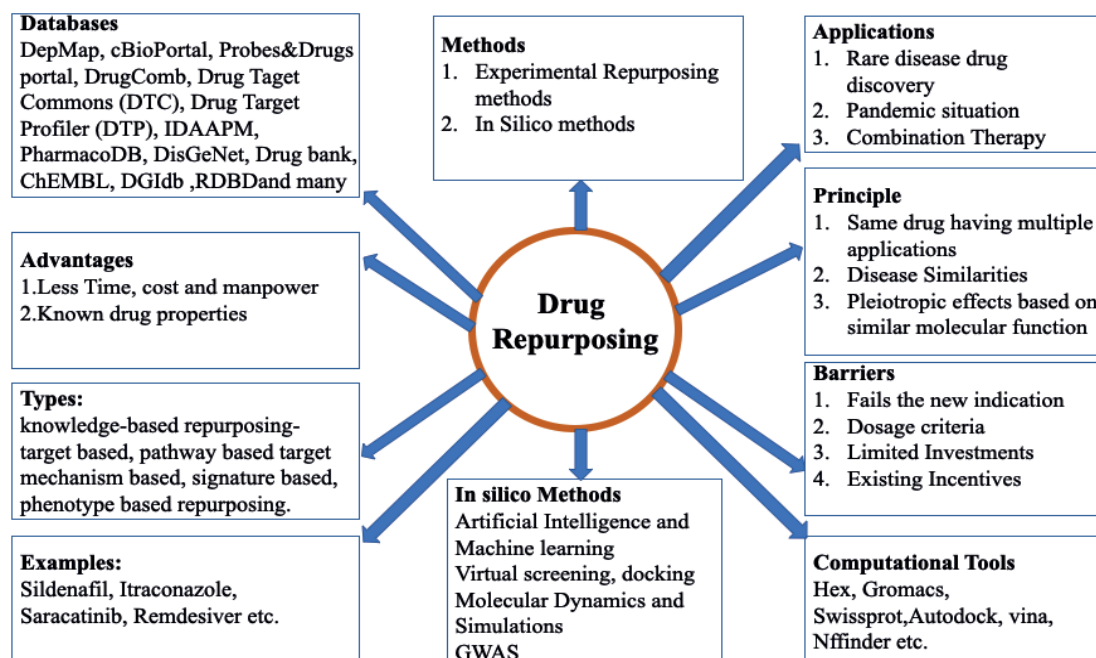


Figure 2. Overview of Drug Repurposing

Table 1: Drugs their primary purpose and Repurpose treatment

S. No	Drug	Purpose	Repurpose
1	Sildenafil	Hypertension & Angina	Erectile Dysfunction
2	Itraconazole	Anti-Fungal	Lung and Prostate Cancer
3	Saracatinib	Failed Anti-Cancer	Alzheimer's Disease
4	Remdesivir	Ebola	COVID-19
5	Toremifene	Breast Cancer	COVID-19
6	Hydroxychloroquine	Antimalarial Drug	COVID-19
7	Bupropion	Depression	Smoking Cessation
8	Thalidomide	Morning Sickness	Multiple Myeloma
9	Chlorpromazine	Antimalarial Drug	Cancer
10	Aspirin	Analgesic	CVD and Cancer
11	Statins	Lipid Disorders	Cancer and COVID-19
12	Metformin	Type-2 Diabetes	Cancer
13	Raloxifene	Osteoporosis	Breast Cancer
14	Cardiac glycosides	Cardiac Conditions	Cancers
15	Chlorpromazine	Schizophrenia	Prostate Cancer
16	Penfluridol	Schizophrenia	Cancer
17	Fluspirilene	Schizophrenia	Cancer
18	Artemisinins	Antimalarial Drug	Cancer
19	DHA	Antimalarial Drug	Leukemia
20	Mebendazole	Parasitic Infections	Cancer
21	Itraconazole	Anti-Fungal	Angiogenesis & Lung Cancer
22	Ritonavir	HIV	Breast Cancer
23	Nelfinavir	HIV	Multiple Myeloma Cells
24	Doxycycline	Angiogenesis Inhibition	Cancer And COVID-19
25	Leflunomide	Rheumatoid Arthritis	Cancer
26	Auranofin	Arthritis	Cancers
27	Thalidomide	Sedative	Cancers
29	Favipiravir	Flu	COVID-19
40	Darunavir	HIV	COVID-19
41	Arbidol	Influenza	COVID-19
42	Tocilizumab	Rheumatoid Arthritis	Cancer and COVID-19
43	Nafamostat	Anti-Coagulant	COVID-19

Drug Repurposing Strategies and Methods

Drug repurposing can be done in two ways-experimental or computational (*In silico* drug repurposing - disease centric or drug centric). There are different types of drug repurposing strategies i.e. knowledge-based repurposing- target based, disease-based, pathway-based target mechanism

based, signature based and phenotype-based repurposing (17).The technological advancements will help to employ classification and segmentation algorithms for early disease diagnosis (18).

Technological applications for drug repurposing include Artificial Intelligence, Machine learning and Computational methods.

Artificial intelligence

Zhou et.al. (2020) has employed Artificial Intelligence (AI) combined with the network intelligence for the precision medicine discovery and development which is based on the hidden patterns based on the existing biomedical data (19). Denovo drug discovery helps to find the efficacy of the existing drugs by minimizing their side effects and it was stated by Sir James Black that they start with the basis of the old drug for the discovery of new drugs (20). The technique of drug repurposing is the most promising solution for the emergency pandemic like COVID-19. In the case of COVID-19, for the identification of it repurpose drugs the AI and network approaches are less effective due to the limited data available about the organism and which makes us understand how the basic knowledge is useful for the biomedicine research in the identification of the drugs (17).

Machine learning

It is of prime importance in the pharmaceutical industry to study the drugs mechanism of action, pharmacokinetic and pharmacodynamic properties. The other application of the Machine Learning algorithms is on the radiographic images analysis for accurate disease diagnosis based on the features selection (21). Machine learning algorithms can be employed to get better insights to mine the drug properties and activity in both time and cost-effective manner. Each characteristic of the drugs can be assumed as molecular fingerprints and the application of neural networks will help to understand the features in an effective manner. Yang et.al. (2022) has employed machine learning methods to employ Chinese traditional medical therapy as one of the drug repurposing approach in the treatment of COVID-19 (21). Many other machine learning algorithms such as UG-RNN (Update gGteRecurrent Neural Network) and GCN (Graph Convolution Network). Some are using deep-learning algorithms for the identification of both chemical and physical structures of the compounds while some are using reinforcement

algorithms for the identification of small molecule inhibitors against COVID-19 (22, 23). The studies of Yang et.al., (2022) are in agreement with the various studies, concluding that the application of machine learning algorithms has provided insight of traditional Chinese medicine application for COVID-19 treatment. Various network-based models can be integrated to employ text-based mining as well as structure-based mining studies in the small molecule identification. The application of the machine learning algorithms for drug repurposing studies was shown in the below Figure 3.

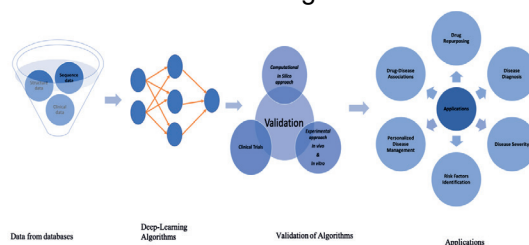


Figure 3. Application of Machine learning for Drug repurposing

Computational methods

The repurposing of the drugs has started long back and the applications of the computational approaches has gained importance. The computational methods were classified into target-based, knowledge-based, signature-based, network-based, phenotype-based repurposing and targeted mechanisms (6). Computational repurposing is also known as *in silico* drug repurposing. It was reported by Sanseau & Koehler (2011) that the computation repurposing can be either based on the disease (studying the associated drugs based on their properties) or targets (based on the compound's protein interactions based on the structural similarity of chemical entities and their binding sites- High-throughput screening of drugs for prediction of new indications (24).

The MER-SuMo approach was developed by the Moriaud et.al. for the identification of the new proteins based on the known compound off-target interactions. Cote

et.al. developed The Rare Disease Repurposing Database (RDBD) which constitutes the list of 200 repurposed drugs that can be used for treating the rare diseases complex and chronic diseases where the treatment is limited (24).

Farha & Brown (2020) worked on the repurposing of antimicrobial drugs, because the resistance towards the existing drugs is one of the potential threats across the world accounting for nearly 700000 deaths annually because of associated infectious diseases (malaria, pneumonia, Ebola etc.) and their number increases in the proceeding's years (15).

Virtual screening, docking and molecular dynamic and simulation studies are the other computational studies which were studied for screening of the compounds. It was understood that some of the drugs act on the causative agents like virus and bacteria whereas, some drugs act on the host by providing the immunity (25).

Genome wide association studies (GWAS)

The usage of GWAS for the new drug identification for complex diseases is based on the gene loci targets and the associated pathways. GWAS studies is the most common variants of the population. The data is collected by integrating omics data sets with the genes which are interconnected by various biological networks (26). Different ways of employing GWAS was summarised below:

By either mapping the genome for loci identification

IL-23 was identified as the repurposing candidate in treating Crohn's disease and the identified repurposed drug candidates are Ustekinumab and Risankizumab by Single Nucleotide Polymorphism (SNP) (27). The initiation of the SNP approach is its limited by size of the study.

Transcriptomic imputation

The transcriptomic repurposing of the GWAS study is based on mRNA expression, protein abundance and epigenetic modifications and can be analysed based on TWAS Z

score (28). The limitation associated with transcriptomic imputation is trait-associated expression changes.

Gene-set association

Gene set association repurposing is based on the genes associated with various biological networks and it was reported that bipolar disorder and the insulin secretion pathways are associated with each other. The other GWAS methods are mandolin randomization. Poly-gene scoring- helps for the heterogeneity of the individual disorders and their targets.

The software which is integrating the GWAS is the Open Targets Genetics resource which predicts variant genes. GREP framework- gene set association based on the GWAS functional loci and pathways. The DrugTargetor platform, for the identification of gene variants and matching drugs uses various drug repository databases like Drug Bank, DGIdb- drug gene interaction database (29). The Overview of GWAS association in repurpose drug discovery was shown in Figure4.

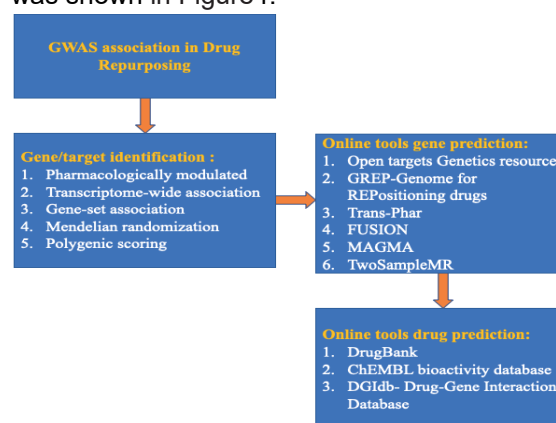


Figure 4. GWAS association in Drug repurposing
Databases Associated with Repurpose Drug Discovery

Many databases are available on the internet which constitutes the information associated with the pathways, diseases, some contain the drugs and other properties, some contain the information only about the repurposed

drugs, some contain the information of the gene targets (30). Most of the pharmaceutical companies have their own databases where they keep the drug data information secularly and in most cases this data will not be shared to the public because of various market associated risks. Some of the databases available are shown in the below Table 2.

Table 2. Databases and associated storage information

Database	Information
DepMap	Cancer data
cBioPortal	Cancers genomics data
Probes&Drugs portal	Bioactive compounds
DrugComb	Cancer data portal
Drug Target Commons (DTC)	Compound-target interaction profiles
IDAAPM	FDA approved drugs
PharmacODB	Pharmacogenomic studies
DisGeNet	Gene database
Drug Bank	Molecular information about drugs
ChEMBL	Chemical database of bioactive molecules
DGIdb	Drug-gene interactions

Validation of the repurposing will be done by using Computational methods-AUROC values, target based using PubMed, Clinical Trials/EHRs and experimental-(*in vivo* and *in vitro* validation).

For a better efficient repurposing drug development there is need for the better integration of data sources, genomic, biomedical and pharmacological data and this has gained importance because of personalized and precision medicine which accounts for heterogeneity and complexity to minimize drug toxicity (31).

Applications of the Drug repurposing

The Applications of the repurpose drug discovery is advantageous. It helps for

Rare disease drug identification

For the identification of the drug candidates to a specific disease which is rare and is less commonly observed among the individuals. Most of the pharma companies will not worry about the rare diseases because of the limited market.

Uncommon pandemic situations

Sudden pandemic situations like COVID-19, as there is no previous knowledge about the disease and there is an utmost concern as most of the people are dying and there is no time to conduct the clinical trial. Hence, the only available option is the drug repurposing by the *insilico* methods due to the limited time constraint and finding the repurpose of the existing drugs either individually or in combinations.

To overcome the adverse effects of the monotherapy by working on the combination therapy treatments (31).

Challenges of Drug Repurposing

Each and every drug discovery process will encounter challenges at any one stage or sometimes at all the stages of the drug discovery (32). Some of the reported challenges of the drug repurposing are:

Dosage limitations of the repurposed drug

The drug dosage can be similar to the original dosage or in some non-antibiotics

where the dosage is more than the antibiotic drug is causing adverse toxicity effects (ex: Anti-microbial compounds). Sometimes the repurposed drug may fail in demonstrating the new indication and the differences in the new benefit of the drug will affect the market.

Effect of pharmacokinetic properties

The pharmacokinetic profiles of the original drugs may affect the repurposed activity leading to impaired antimicrobial properties.

Need for clinical trial

Sometimes clinical trials need to be conducted to prove the efficacy of the approved drug. In some cases, the previous data cannot be considered for the regulatory approval of the repurposed drug and repetitive experiments may increase the cost of the drug and lack of efficient funding for the repurposed drug studies. Sometimes the results are not reliable because of data sensitivity to datasets from the previous studies.

Limited investments and Existing incentives

Breckenridge & Jacob (2019), have studied the legal and the regulatory barriers in the drug repurposing. Patents (protection of new drugs into the market) and the regulatory data exclusivity (prevents the usage of data for the purpose of generic applications) are the two intellectual property rights which are involved in the protection of the drug from the competition. The intellectual properties of the repurposed generic drugs will differ which limits the data of the drug for further studies (33).

Possible solutions to overcome the legal and regulatory barriers

The possible solution for the drug repurposing is:

The possible solution is to produce all the data information in the prescription and ensure the reimbursement which will allow the stakeholder to ensure the knowledge about the differentiation between the patented and unpatented drugs. Second medical use of the drug- if the company is ready to provide the

original data of the drug. Bypass exclusivity related incentives and provide incentives for the new drug developments for rare diseases.

Conclusion

Drug repurposing is one of the best alternative drug discovery processes and this has been proved from the literature studies in the pandemic situation for the identification of drugs to COVID-19. It was not only COVID-19, but drug repurposing studies have been performed on other diseases like cancer, Alzheimer's disease, Cardiovascular diseases and many others. Still, there is need to study in detail about various drugs to treat multiple diseases with in less time in an economical manner with high efficacy by integration of various genomic, proteomic, pathway data by using various computational tools.

References

1. Parvathaneni, V., et al., *Drug repurposing: a promising tool to accelerate the drug discovery process*. Drug discovery today, 2019. 24(10): p. 2076-2085.
2. Schuster, D., Laggner, C., & Langer, T. (2008). Why Drugs Fail—A study on side effects in new chemical entities. *Antitargets: Prediction and Prevention of Drug Side Effects*, 1-22.
3. Abideen, A. Z., Mohamad, F. B., & Hassan, M. R. (2020). Mitigation strategies to fight the COVID-19 pandemic—present, future and beyond. *Journal of Health Research*, 34(6), 547-562.
4. Pushpakom, S., Iorio, F., Eyers, P. A., Escott, K. J., Hopper, S., Wells, A., ... & Pirmohamed, M. (2019). Drug repurposing: progress, challenges and recommendations. *Nature reviews Drug discovery*, 18(1), 41-58.
5. Hernandez, J. J., Prysziak, M., Smith, L., Yanchus, C., Kurji, N., Shahani, V. M., & Molinski, S. V. (2017). Giving drugs a

- second chance: overcoming regulatory and financial hurdles in repurposing approved drugs as cancer therapeutics. *Frontiers in oncology*, 7, 273.
6. Karaman, B., & Sippl, W. (2019). Computational drug repurposing: current trends. *Current medicinal chemistry*, 26(28), 5389-5409.
 7. Pola, M., Rajulapati, S. B., Durthi, C. P., Erva, R. R., & Bhatia, M. (2018). In silico modelling and molecular dynamics simulation studies on L-Asparaginase isolated from bacterial endophyte of *Ocimum tenuiflorum*. *Enzyme and microbial technology*, 117, 32-40.
 8. Pola, M., Durthi, C. P., Rajulapati, S. B., & Erva, R. R. (2018). Modelling and optimization of L-Asparaginase production from *Bacillus stratosphericus*. *Current Trends in Biotechnology and Pharmacy*, 12(4), 390-405.
 9. Durthi, C. P., Pola, M., Rajulapati, S. B., Kola, A. K., & Kamal, M. A. (2020). Versatile and valuable utilization of amidohydrolase L-glutaminase in pharma and food industries: A review. *Current Drug Metabolism*, 21(1), 11-24.
 10. Pola, M., Durthi, C. P., & Rajulapati, S. B. (2019). Modeling and Optimization of L-Asparaginase production from novel *Bacillus stratosphericus* by soft computing techniques. *Current Trends in Biotechnology and Pharmacy*, 13(4), 438-447.
 11. Pola, M., Potla Durthi, C., Erva, R. R., & Rajulapati, S. B. (2019). Multi Gene Genetic Program Modelling on L-Asparaginase Activity of *Bacillus Stratosphericus*. *Chemical Product and Process Modeling*, 15(2), 20190046.
 12. Durthi, C. P., Pola, M., Rajulapati, S. B., & Kola, A. K. (2020). Insights into potent therapeutical antileukemic agent L-glutaminase enzyme under solid-state fermentation: a review. *Current Drug Metabolism*, 21(3), 211-220.
 13. Tripathi, M. K., Sharma, S., Singh, T. P., Ethayathulla, A. S., & Kaur, P. (2021). Computational intelligence in drug repurposing for COVID-19. *Computational Intelligence Methods in COVID-19: Surveillance, Prevention, Prediction and Diagnosis*, 273-294.
 14. Sleire, L., Førde, H. E., Netland, I. A., Leiss, L., Skeie, B. S., & Enger, P. Ø. (2017). Drug repurposing in cancer. *Pharmacological research*, 124, 74-91.
 15. Farha, M. A., & Brown, E. D. (2019). Drug repurposing for antimicrobial discovery. *Nature microbiology*, 4(4), 565-577.
 16. Simsek, M., Meijer, B., van Bodegraven, A. A., de Boer, N. K., & Mulder, C. J. (2018). Finding hidden treasures in old drugs: the challenges and importance of licensing generics. *Drug discovery today*, 23(1), 17-21.
 17. Dotolo, S., Marabotti, A., Facchiano, A., & Tagliaferri, R. (2021). A review on drug repurposing applicable to COVID-19. *Briefings in bioinformatics*, 22(2), 726-741.
 18. Tiwari, A., Sharan, T. S., Sharma, S., & Sharma, N. (2022). Deep learning-based automated multiclass classification of chest X-rays into Covid-19, normal, bacterial pneumonia and viral pneumonia. *Cogent Engineering*, 9(1), 2105559.
 19. Zhou, Y., Wang, F., Tang, J., Nussinov, R., & Cheng, F. (2020). Artificial intelligence in

- COVID-19 drug repurposing. *The Lancet Digital Health*, 2(12), e667-e676.
20. Yella, J. K., Yaddanapudi, S., Wang, Y., & Jegga, A. G. (2018). Changing trends in computational drug repositioning. *Pharmaceuticals*, 11(2), 57.
 21. Yang, F., Zhang, Q., Ji, X., Zhang, Y., Li, W., Peng, S., & Xue, F. (2022). Machine learning applications in drug repurposing. *Interdisciplinary Sciences: Computational Life Sciences*, 14(1), 15-21.
 22. Alok, T., Shiru, S., & Patnaik, R. (2019). Application of Neuroimaging Tools in Identification of Pinpoint Location of Blockage. *Advancement in the Pathophysiology of Cerebral Stroke*, 83-92.
 23. Tiwari, A., Tripathi, S., Pandey, D. C., Sharma, N., & Sharma, S. (2022). Detection of COVID-19 Infection in CT and X-ray images using transfer learning approach. *Technology and Health Care*, (Preprint), 1-14.
 24. Sanseau, P., & Koehler, J. (2011). Computational methods for drug repurposing. *Briefings in bioinformatics*, 12(4), 301-302.
 25. Fathima, A. J., Murugaboopathi, G., & Selvam, P. (2018). Pharmacophore mapping of ligand based virtual screening, molecular docking and molecular dynamic simulation studies for finding potent NS2B/NS3 protease inhibitors as potential anti-dengue drug compounds. *Current Bioinformatics*, 13(6), 606-616.
 26. Løset, M., Brown, S. J., Saunes, M., & Hveem, K. (2019). Genetics of atopic dermatitis: from DNA sequence to clinical relevance. *Dermatology*, 235(5), 355-364.
 27. Dugger, S. A., Platt, A., & Goldstein, D. B. (2018). Drug development in the era of precision medicine. *Nature reviews Drug discovery*, 17(3), 183-196.
 28. Hall, L. S., Medway, C. W., Pain, O., Pardiñas, A. F., Rees, E. G., Escott-Price, V., ... & O'Donovan, M. C. (2020). A transcriptome-wide association study implicates specific pre-and post-synaptic abnormalities in schizophrenia. *Human molecular genetics*, 29(1), 159-167.
 29. Konuma, T., Ogawa, K., & Okada, Y. (2021). Integration of genetically regulated gene expression and pharmacological library provides therapeutic drug candidates. *Human Molecular Genetics*, 30(3-4), 294-304.
 30. Masoudi-Sobhanzadeh, Y., Omid, Y., Amanlou, M., & Masoudi-Nejad, A. (2020). Drug databases and their contributions to drug repurposing. *Genomics*, 112(2), 1087-1095.
 31. Park, K. (2019). A review of computational drug repurposing. *Translational and clinical pharmacology*, 27(2), 59-63.
 32. Talevi, A., & Bellera, C. L. (2020). Challenges and opportunities with drug repurposing: finding strategies to find alternative uses of therapeutics. *Expert Opinion on Drug Discovery*, 15(4), 397-401.
 33. Breckenridge, A., & Jacob, R. (2019). Overcoming the legal and regulatory barriers to drug repurposing. *Nature reviews Drug discovery*, 18(1), 1-2.

Bioactive Components of *piper betel* Could be Potential anticancer Agents: A short Review on Pre-clinical Investigations and Practical Challenges

Bhabani Sankar Satapathy, Sangram Keshari Biswal, Laxmidhar Maharana, Snigdha Pattnaik*

School of Pharmaceutical Sciences,
Siksha 'O' Anusandhan Deemed to be University, Bhubaneswar, Odisha, India.
*Corresponding author: snigdhapattnaik@soa.ac.in

Abstract

The unmet treatment challenges such as intolerable adverse effects, massive immune suppression, and severe healthy tissue/organ toxicity with unaffordable treatment costs associated with conventional anticancer drug therapy have led to the exploration of complementary/alternative strategies to control the outbursting cases of cancer. In this context, plant-derived bioactive components have been increasingly popular as effective therapeutic options for the treatment of cancer. Phyto bioactive components (PBCs) derived from *Piper betel* have been shown to possess useful immune-modulatory, antioxidant, anti-inflammatory properties both *in vitro* and *in vivo*. At present, a large volume of pre-clinical studies have documented the beneficial effects of *Piper betel*-derived PBCs in various cancer therapy, either alone or in combination with established chemo drugs. The present review aims to provide a comprehensive research data on the therapeutic effectiveness of PBCs of *Piper betel* against various cancers to establish its druggability. The review would be useful to provide essential evidence-based support for furthering work on large scale formulation development as well as future clinical studies of *Piper betel*.

Key words: *Piper betel*, bioactive components, Therapeutic potential, Cancer therapy

1. Introduction

Application of phyto bioactive components (PBCs) for the treatment of cancer has been one of the emerging trends in drug delivery research. In view of the unavoidable adverse effect of conventional anticancer drugs associated with immune suppression and healthy tissue toxicity, plant based pharmaceuticals are being explored heavily to ameliorate treatment outcomes in cancer therapy. Cancer is a typical pathological state, where the cellular reproduction process goes out of control with formation of abnormal mass of cells. Due to the result of DNA damage of cells, irregular growth and division are observed in the cancer cell. In the present world, cancer has been recognized as the second deadliest disease followed by cardiovascular disease (1). According to WHO cancer takes nearly 10 million life in 2020 only (2). Around the world, one in five men and one in six women during their lifetime develop cancer and one in eight men and one in eleven women died due to cancer (3). The existing conventional treatments, *viz.* chemotherapy, surgery, radiation in combination have been showing uncountable limitations, severe

adverse effects with negligible improvements in quality of life post treatment. Surgery/radiation also has limited role in cancer like leukaemia and lymphomas (4). Further, existing anticancer drug therapy with the present methodology destroys the tumour tissue with great accuracy but fails to distinguish between the healthy and tumour cells (5). All conventional chemotherapeutic medications are severely cytotoxic and have a low therapeutic range. Due to their extreme cytotoxicity, they affect the microtubule organisation and cell survival (6). From the current clinical practice data, it is established that the synthetic chemotherapeutic agents have less specificity to cancer cells which lead to several adverse effects. Because the anticancer drug targets actively developing cells, it also has negative effect on normal cells that grow rapidly such as the hair follicles, gastrointestinal tract, and bone marrow (7). To overcome these setback, plant-derived anticancer agents with less toxicity and more specificity is highly needed. There are many plants that have been used for the research of cancer treatment for many years. Among 35000 potential plant species, 3000 species showed desired therapeutic activity against cancer according to National Cancer Institute (NCI) (8). Betel leaf (*Piper betel*) is one of the common plants among them and is well-known for its various anti-oxidant, antimicrobial and anti-inflammatory properties (9). According to various researchers, PBCs present in *Piper betel* have selective toxicity towards cancer cells too. Recent studies have shown effective anticancer potential of *Piper betel* derived PBCs in ameliorating cancer both *in vitro* and *in vivo*.

Thus, objective of the present review is to provide updated information on the anticancer properties of *Piper betel* and its important phyto constituents on different cancers. Updated research works of pre-clinical studies involving *Piper betel* derived PBCs on various cancer cells have been included. Along with that, we have briefly covered the crucial challenges in the clinical translation or vulnerability of PBCs for industrial scale production. We believe the

compiled reports on the anticancer activities of *Piper betel* would be helpful to provide useful insights in furthering research on its clinical aspects.

Betel leaf: Important bioactive constituents and traditional uses

Even in twenty-first century approximately 80 percent population in developing countries depends upon medicinal plant-based medicine as an affordable source (10). *Piper betel* (family: Piperaceae), a perennial, dioecious, evergreen, small shade-loving, aromatic root climber is one among Southeast Asia's most significant plants. In tropical and subtropical regions of the world this genus has been found largely distributed with wide range of traditional and medical applications (11). Betel vine is widely planted in Thailand, Sri Lanka, Malaysia, India, Nepal Taiwan, Pakistan, and other South-east Asian nations (12).

From various studies on betel leaf, many biologically active components have been reported (11). Phenol is one of such important components present in the leaf. The unique strong pungent aromatic flavours of the leaf are due to the presence of phenol and terpene-like compounds. Various significant PBCs which are present in *Piper betel* include chavibetol (betel-phenol; 3-hydroxy-4-methoxyallylbenzene), chavicol (p-allyl-phenol; 4-allyl-phenol), estragole (p-allyl-anisole; 4-methoxyallylbenzene), eugenol (allylguaiacol; 4-hydroxy-3-methoxy-allylbenzene; 2-methoxy-4-allyl-phenol), methyl eugenol (eugenol methyl ether; 3, 4-dimethoxyallylbenzene), hydroxycatechol (2, 4-dihydroxyallylbenzene) etc. Along with these, caryophyllene, p-cymene, cadinene, eugenol methyl ether, γ -lactone, tritriacontane, dotriacontanoic acid, allyl catechol cepharadione A etc. are too found in the betel leaf in varying amounts (13).

Use of betel leaves in India has been documented in various old books and in Ayurvedic manuscripts. The use of betel leaves from 1400 BC was also evidenced in Vatsyayan's

Kamasutra in which aphrodisiac activity of betel leaves has been mentioned (14). Betel leaves are also used in several rituals in Southeast Asian nations such as India, Sri Lanka, and Bangladesh. Betel leaf has traditionally been used to cure problems such as itching, otorrhoea, traumas, mastoiditis, leucorrhoea, mastitis, headache, constipation gum swelling, rheumatism, wounds, and conjunctivitis (15). The wound healing properties are also identified from Indian traditional and conventional medical systems. Betel leaf was recognized as a potent phyto medicine to assist the digestive process and shows a good effect for bronchitis treatment. Even it has traditional use as a flatus reliever to eradicate worms, bacteria. In India, betel leaf is very often chewed after meals, which shows moderate digestive stimulant activity (14). To cure cough, combination of *Piper betel* leaves and honey has been taken as a traditional herbal medication. Though, lots of medicinal effects of *Piper betel* were observed for several diseases from ancient times, but its therapeutic usefulness in cancer has been documented in twentieth century only (16).

Predicted mechanisms of *Piper betel* based PBCs for cancer prevention

Cancer is a typical disease and remains largely mysterious till today irrespective of eye-catching research progress in medical science. However, with the advancement of biotechnology, molecular engineering and pharmaceutical research, molecular insights of cancer progression is being unfolded slowly. In human bodies, free radicals in various forms such as reactive nitrogen species (RNS) and reactive oxygen species (ROS) are developed as a result of cellular metabolism. Excessive amounts of RNS/ROS lead to cytotoxicity, inflammation and even mutagenesis and thus have been identified as important molecular mechanism in cancer progression (17). *Piper betel* derived PBCs possess the ability to scavenge hydroxyl radical and superoxide radical. α , α -diphenyl- β -picryl hydrazyl (DPPH) radicals, superoxide radicals, and hydroxyl radicals have been

found effectively scavenged by ethanolic and aqueous extracts of betel leaf (18). In a study on the antioxidant effect of ethanolic extract of betel leaf, a significant decrease in extracellular nitric oxide production was observed (19).

Eugenol, one of the key ingredients of betel leaf possesses strong antioxidant properties. In lipopolysaccharide-stimulated mouse macrophage cells, eugenol inhibited COX-2 gene expression, which eventually led to the suppression of inflammatory responses (20). Hepatic level of retinol, ascorbic acid (antioxidant molecules), glutathione, Superoxide dismutases (SODs) is an antioxidant enzyme was also found to be significantly increased by the *Piper betel* leaf extract as reported by Choudhary et al. (21).

Peroxidative attacks by free radicals can lead to the destruction of poly-unsaturated fatty acids present in cell membranes, leading to cell membrane dysfunction (22). In an *in vitro* examination on rat liver mitochondria, alcoholic extract of the betel leaf prevented lipid peroxidation. *Piper betel* derived PBCs have been found to enhance the amount of Glutathione S-transferases (GST), another key enzyme which protects the cells from the effect of toxic metabolites. This enzyme system too works to fight against various carcinogenic metabolites and mutagens (23). When laboratory mice were treated with *Piper betel* leaf extract and its individual components like α -tocopherol, β -carotene and hydroxychavicol, the amount of GST was found to be increased in their liver (14). Studies on the structure-based effects of acetylation on benzene ring hydroxyl groups have revealed the anti-nitrosating action of the molecule, which indicates their potential for anti-mutagenic activities. In a report, both hydroxychavicol and eugenol (two major PBCs in *Piper betel*) were found to decrease nitrosation in a dose-dependent manner *in vitro* (18). Predicted mechanisms of *Piper betel* and its bioactive constituents in cancer prevention/treatment have been depicted in **Figure 1**.

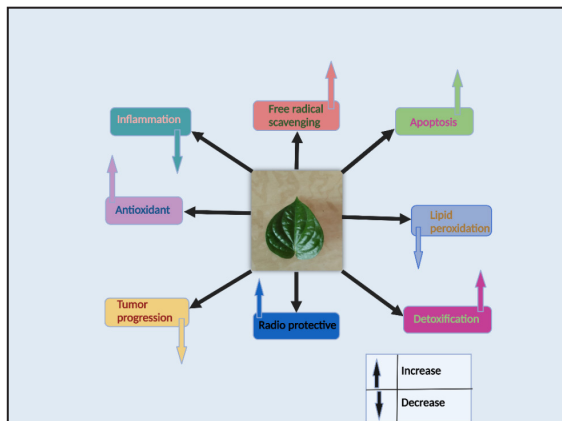


Figure 1. Mechanism of action of bioactive constituents of *Piper betel* in cancer prevention/treatment

Recent research progress on *Piper betel* based PBCs in cancer

Many studies have documented the anticancer potential of *Piper betel* derived PBCs *in vitro* and *in vivo*. The *in vitro* anticancer activity of *Piper betel* leaves in KB cell line (oral squamous carcinoma) was tested in a recent study by Sadiya R Veettil et al. 2022. For the study, aqueous extract of the dried betel leaves was used. *In vitro* cytotoxicity experiment was conducted in a 96 well tissue culture plate and the plates were examined using an inverted phase contrast tissue culture microscope for 72 hours for any visible morphological alterations in cells. Cell viability percentage was determined using the MTT method. *Piper betel* leaf extract showed significant cytotoxicity in the tested KB cells as evidenced in the form of noticeable changes in cellular morphology like vacuolization of cytoplasm, rounding/granulation and cell shrinkage. The study overall demonstrated that increase in the quantity of leaf extract reduced the percentage of survival of KB cells (24).

Microtubule is an important part to maintain the cytoskeleton of cells. Microtubules contribute to shape, dynamics, movement of cells and thus are considered partly responsible for the cancer cell migration. Aqueous extract *Piper betel* leaf showed substantial reduction in can-

cer cell migration (A549 cells) and modulation in microtubule structure *in vitro* (25). To evaluate effectiveness of anti-migration effect, results obtained with the experimental leaf extract was compared with that of 5-fluorouracil (5-FU), an established anticancer drug. For the study, *Piper betel* leaf extract and 5-FU at two different concentrations were taken. When the results of the study were compared, it was shown that both betel leaf extract and 5-FU inhibited cell migration at low quantities. However, betel leaf extract at relatively higher concentration (100 g/mL) was significantly more effective against migration than 5-FU. The morphology, structure, and tubulin network of human colorectal adenocarcinoma cells (HT29) treated with *Piper betel* leaf extract, 5-FU, and paclitaxel were examined. Paclitaxel treated cells and *Piper betel* leaf extract treated cells both showed similar morphologies of round shaped cells with long distorted spindle. These spindles are defects on the microtubule which prevent cell division and lead to apoptosis. The study concluded that *Piper betel* leaf extract induced microtubule polymerization whereas at relatively low concentration, it inhibited cell migration (25). Thus, *Piper betel* derived PBC was found as potential microtubule-targeting agent with anti-migratory effects on cancer cells.

Antioxidant and anticancer properties of betel leaf extract was studied in MCF-7 human breast cancer cells (26). The antioxidant activity of betel leaves extract was shown by DPPH radical scavenging capacity. The SRB technique was used to analyse the cytotoxicity of betel leaf extract in MCF-7 cells cultured in Dulbecco's Modified Eagle Medium (DMEM). The cells were plated in a culture dish at 37°C for 24 hours and for 48 hours with different dosages of betel leaf extract to examine its cytotoxic and anti-migratory effect. MCF-7 cell survival was reduced as the dosage of *Piper betel* leaf extract was increased. It was also shown that the betel leaf extract reduced cancer cell migration in a concentration dependent manner. Following the reasonable cytotoxic and anti-migratory

effects of betel leaf extract on MCF-7 cells, its local application was considered. As a result, a transdermal patch containing *Piper betel* leaf extract was developed for application to the intended breast area (26).

Similarly, another study was conducted on the anticancer efficacy of silver nano bio-conjugates synthesized from the methanolic extract of the *Piper betel* leaf. In 10:90 ratio, the methanolic extract of betel leaf or 100µg diluted purified eugenol was added to 1 mmol silver nitrate solution followed by exposure to sunlight and centrifugation. The anticancer activity was compared among the silver nano bio-conjugate and with the raw material like betel leaf extract or eugenol (27). Oral cancer cells (KB) along with non-cancerous buccal cells were used for the study. Both the cells were seeded as 10⁵ live cells/ml for further experiments. In the cell medium, the silver nano bio-conjugate synthesised from methanolic extract of betel leaf as well as eugenol was added. Both cancerous and non-cancerous cells were tested for viability with the MTT reduction assay. Results of MTT assay indicated after exposure to betel leaf extract, eugenol, and the experimental silver nano bio-conjugates, KB cells exhibited a dose-dependent reduction of cell viability. As compared to their non-nano raw material counterparts, silver nano bio-conjugates had reduced viability. Results overall depicted the improved anticancer effects, when extract and eugenol get administered in silver nano bio-conjugates. However, the viability of healthy buccal cells was unaffected by different doses of silver nano bio-conjugates and eugenol, which means that silver nano bio-conjugates are not harmful to healthy cells. Apoptosis study further confirmed higher anti-apoptotic activity of the experimental silver nano bio-conjugates than plain extract/eugenol. The nano bio-conjugates shifted cancer cells into S and G2/M phases, showing superior anticancer efficacy (27).

Methanolic extract of *Piper betel* leaf possessed antitumor efficacy against Ehrlich ascites carcinoma (EAC). The research was

conducted in Swiss albino mice bearing EAC and the median survival study along with the life span of cancer induced mice was estimated (28). The EAC cells were transplanted intra-peritoneally in Swiss albino female mice. After 24 hours of transplantation of EAC cells, the methanolic extracts were administered in different doses, viz. 25, 50, 100 mg/kg body weight for 9 days. The antitumor effect of the extract and fractions were evaluated by cell study from the mice as like viable and non-viable tumor cell count, tumor volume packed cell count. Haematological and biochemical parameters including haemoglobin content, RBC and WBC count, serum biochemical serum glutamate pyruvate transaminase (SGPT), serum glutamate oxaloacetate transaminase (SGOT), serum alkaline phosphatase (SALP), serum bilirubin, and total protein level were assessed. For antioxidant property, evaluation lipid peroxidation and catalase (CAT), reduced glutathione (GSH) and superoxide dismutase (SOD) levels were also calculated. The methanolic *Piper betel* leaf extract and 100 mg/kg body weight ethyl acetate fraction inhibited EAC cells significantly. Mice with EAC treated with betel leaf extract had a lower tumour volume, packed cells, and viable cell count, as well as a longer life time. Also, the haematological and serum biochemical profiles were found to remain in normal level as compared to EAC control mice. In case of methanolic extract and ethyl acetate fraction group, the lipid peroxidation get decreased and SOD, GSH, CAT levels were restored at normal level as compared to EAC control group. From the study, the antitumor effect of *Piper betel* leaf extract was well established (28).

Anti-carcinogenic properties of betel leaf extract was investigated by Toprani, R et al. in by using two different protocols in Swiss male mice. The effectiveness of *Piper betel* leaf extract against the standard carcinogen benzo[a]pyrene was studied in the first protocol using Wattenberg's stomach cancer model. *Piper betel* leaf extract was administered in eight weeks old male mice by intra-gastric instillation. In the second stage, effectiveness of *Piper betel*

leaf extract was determined against two tobacco-specific nitrosamines, N'-nitrosonornicotine (NNN) and 4-(methylnitrosamino)-1-(3-pyridyl)-1-butanone (NNK). Nitrosamines were administered in mice's tongue along with oral administration of the betel leaf extract with drinking water. Two different doses were used for NNN and one dose for NNK. In the first protocol, *Piper betel* leaf extract showed the reduction of tumorigenic effect of benzo[a]pyrene in the fore stomach tumour to very noteworthy range. In case of second protocol, the betel leaf extract treatment reduced the mortality of the animals. But the long term studies showed statistical significant difference in decreasing tumor volume in between NNN treated and betel leaf extract treated groups. The study thus evidenced the anti-carcinogenic effect of betel leaf extract *in vivo* against benzo[a]pyrene. Betel leaf derived PBCs were involved to minimize the toxicity caused by NNN and NNK (29). Anticancer effectiveness of *Piper betel* derived PBCs was also reported against prostate cancer cells. In the experiment by Rutugandha P. et al. *Piper betel* leaf extract was found to possess effective anticancer potential in prostate cancer therapy *in vivo*. For the study, 6 weeks old male mice prostate cancer cells (PC-3-luc) were inserted subcutaneously. At three different doses, the *Piper betel* leaf extract were administered orally in three different groups of animals along with the control group. The result showed that *Piper betel* leaf extracts significantly inhibited the prostate cancer cells proliferation in mice. To identify the main PBCs in the tested betel leaf extract, classical column chromatography was performed using solvents of different polarity strengths followed by thin layer chromatography. Among the fractions, F2 showed better *in vitro* effectiveness to inhibit prostate cancer proliferation almost three times than other treatment groups. Further, the F2 fraction was subjected to nuclear magnetic resonance analysis, mass spectrometry, and high-performance liquid chromatography, which confirmed that phenols, chavibetols (CHV) and hydroxychavicol (HC) were the principal PBCs. HC containing

sub-fraction was eight times more potent for inhibition of prostate cancer proliferation as compared to CHV containing sub-fraction. The study thus concluded that perhaps HC is a major component in *Piper betel* for the potential candidate of prostate cancer treatment (30). Anti-oxidant potential of *Piper betel* leaf extract was used to reduce growth of MCF-7 cells (31). For the determination of flavonoid and phenolic content of the leaf, colorimetric assay was used. To analyse the antioxidant activities of the plant extracts various assays like DPPH, FRAP, nitric oxide, superoxide anion and hydroxyl radical scavenging assays were used. The cell viability test was carried out using the MTT assay methods, with MCF-7 cancer cells on 96 well culture plates. After 24 h, the leaf extracts at various concentrations were added in each well. Among the tested extracts, ethyl acetate extract showed higher ferric reducing and free radical scavenging activity when measured with nitric oxide radicals, superoxide anion and DPPH. In case of hydroxyl radical scavenging activity it is second highest, just after aqueous extract. Pearson correlation analysis revealed no significant relationship between phenolic content and hydroxyl radical scavenging ability. Among all the betel leaf extract the phenolic content is maximum in ethyl acetate extract, even three times higher than hexane and sixteen times higher than methanol extract. But flavonoid amount is highest in methanolic extract. However, mostly the hexane and ethyl acetate extracts showed effective dose-dependent inhibition in the cytotoxicity assay against MCF-7 cells, with IC_{50} values of 65.00 ± 0.00 and 163.30 ± 2.89 g/ml, respectively (32). SOD and catalase activity were enhanced in MCF-7 cells treated with ethyl acetate fraction. The work in a nutshell overall depicted potential antioxidant and anti-proliferative activity of ethyl acetate fraction of betel leaf, which could be further investigated for further clinical feasibility.

A list of recently conducted research on *Piper betel* and its PBCs on various cancers has been depicted in **Table 1**.

Table 1 A list of recently conducted research on Piper betel and its PBCs on various cancers has been depicted

S . no	Form of formula-tion and used con-stituents	Type of can-cercancer cell /carcinogens	Result	Reference
1	<i>Piper betel</i> leaf ex-tract	Tobacco in-duced car-cinogenesis (NNN , NNK)	The constituents of betel leaf reduce the toxicity instigated by NNN and NNK.	Bhisey, R.A., at al. (2012)
2	<i>Piper betel</i> leaf extract eugenol, hydroxychavicol. -carotene and -to-copherol	bhide	Betel leaf extract like hydroxychavicol, -carotene, -tocopherol, eugenol, all significantly reduced the tumor growth. -carotene and -to-copherol show intense protection even in lower concentrations.	Gupta, R.K., at al. (2022)
3	<i>Piper betel</i> leaf extract with water, methanol, ethyl acetate, hexane	Breast cancer (MCF-7)	Ethyl acetate extracts showed maximum inhibi-tion of proliferation against the MCF-7 cell	Abraham at al. (2012)
4	Transdermal patch with <i>Piper betel</i> leaf extract	Breast cancer (MCF-7)	Transdermal patch shows prolonged anticancer effect compared to the leaf extract.	Boontha at al. (2019)
5	<i>Piper betel</i> leaf extract	Prostate can-cer	Piper betel leaf extracts significantly inhibit the human prostate implanted in mice. Hydroxy-chavicol is a major component in <i>Piper betel</i> for the potential candidate of prostate cancer treatment	Paranjpe at al. (2013)
6	<i>Piper betel</i> leaf ex-tract	Oral cancer (KB cell)	With the increase of the <i>Piper betel</i> leaf extract the cytotoxicity of KB cells also get increased.	Veettil at al. (2022)
7	Piper betel leaf methanolic extract and eugenol were used to create sil-ver nanobioconju-gates.	Oral cancer (KB cell)	The conjugated silver nano form shows higher anticancer properties compared to the respec-tive unconjugated form. And silvenano bio con-jugate are not cytotoxic for healthy cells.	Preethi at al. (2016)
8	Hydroxychavicol	Oral cancer (KB cell)	Hydroxichavicol promotes the inhibition of cell cycle, growth of KB cell, leads to apoptosis of KB cell	Chang at al. (2002)
9	Methanolic <i>Piper betel</i> leaf extract	Ehrlich ascites carcinoma (EAC)	Mice with EAC that were given betel leaf extract had a reduced tumour volume, packed cells, and viable cell count, as well as a longer life-time.	Alam at al. (2015)
10	Hydroxychavicol	p a n c r e a t i c cancer	Hydroxychavicol produced DNA damage, which caused pancreatic cancer cells to apoptosis.	Majumdar at al. (2019)

Challenges

Undoubtedly, emergence of phyto active components has boosted cancer research. As we discussed, multiple options are available for the fabrication of betel oil based PBCs with modified physiochemical characteristics. However, apart from the huge benefits that the phyto-medicine offers, there still exist many uncleared problems on their way for clinical application. Large scale synthesis, regulatory clearance followed by commercialization of such PBCs-based medicines need long term research collaboration with time-bound vision by pharmaceutical companies. Careful analysis of biocompatibility, therapeutic potential, structural stability, in vivo life span, biodistribution profile in healthy organs/tissues should be conducted along with long-term toxicity analysis (36). Though, many times, the formulation technologists and academic scientists argue that usually PBCs possess no/negligible side effects or toxicity profile as they belong to herbal origin. But, this argument clearly lacks scientific merit as no such regulatory bodies will ever accept this. Merely an herbal origin tag does not certify a component to be non-toxic or safe for human application. Also, the regulatory procedures are not streamlined in between Allopathic and Homeopathic/Ayurvedic medicine systems. Thus, formulation of PBCs must pass through toxicity testing protocol and must ensure its safty profile to get nod for commercial approval.

Another striking issue that is associated with PBCs is their versatile availability and yield percentage of active components. In many cases, the yield amount of active component remains too low from the plant raw materials used for extraction. Geographical distribution of the plant may vary, which also affects their active principles and contents. Many times, the low yield coupled with presence of variable active components in the plant material is not being able to meet the demand. In case of *Piper betel*, if we consider, then the yield percentage of essential oil from its leaves remains maximum up to 2 % w/v. However, this might vary from species to

species and largely depend on the geographical location. These factors also need to be considered for phyto fabrication. If the desired quantities of PBCs are not up to the mark, its proper way of plantation need to be planned, which ultimately would further add to the final cost of therapy. The extraction procedure or isolation of PBCs also needs up gradation with utilization of cutting-edge tools and flexible designs.

Despite eye-catching research advancements in drug delivery arena, use of phyto pharmaceuticals in novel delivery platforms stands a long way from clinical translation. Low drug loading capacity of nanocarriers along with stability issues of PBCs still an unsolved issue. Ligand-modified tailored nanocarriers though have put some promising clue for targeting of cancer, but such approach is yet to find its way for PBCs. The main reason is still the stability problem during manufacturing, and long term storage. Insufficient data are available till now on the in vivo efficacy of tailored nanocarriers loaded with PBCs over the plain nanocarrier formulations or the marketed conventional formulations for the treatment of cancer. Improved efficacy of PBCs loaded nanocarriers over conventional drugs has still remained marginal in pre-clinical study reports.

As discuseed before, large scale manufacturing of PBCs remains a key issue, as pharmaceutical companies hesitate to invest in them. Irrespective of voluminous in vitro/in vivo reports on the different phytopharmaceuticals at academic level, they yet to see day light at technology transfer. Lack of well-designed, optimized manufacturing procedure, standardized processing steps, improvement in material yield hijacks the transition from laboratory to industrial scale. For, pharma-companies, all therapeutic outcome claimed at in vivo stage are immaterial unless the clinical benefit is guaranteed.

Few specific points need to be considered seriously to avail the Piper betel-derived PBCs at bed side (37, 38).

a) Careful design and engineering of large scale

manufacturing process.

b) Toxicity analysis of PBCs-loaded carriers

c) In vitro/ in vivo correlation analysis

d) Continuous exchange of ideas between industry and academic scientists

e) Designing of collaborative research work between leading research laboratories considering the regulatory guidelines

Conclusion

It is an accepted fact that novel technology holds the potential to improve the therapeutic effectiveness of PBCs in cancer therapy. With the use of hyphenated technologies, advanced biomaterials, and well-designed formulation protocols, PBCs-based therapeutics would see day light in coming days. Use of *Piper betel* derived PBCs for the treatment of cancer is attracting attention of formulation scientists in recent days. It is quite evident that *Piper betel* and its constituents have a remarkable prospective to fight against breast cancer, oral cancer, prostate cancer. However, like the usual problems associated with clinical translation of other PBCs, further pre-clinical studies are too are highly warranted for *Piper betel* based therapeutics. In terms of biocompatibility, easy availability, safety profile etc. *Piper betel* derived PBCs could stand differently. Its wide range of availability across the geographical locations in India and long history of traditional uses could pave its patient compliance. Further investigations on the anticancer effectiveness of *Piper betel*-PBCs would help it to emerge as an effective alternative or complementary medicine for cancer application, which would in turn motivate the farmers for its wider cultivation. In many parts of India including Odisha, the large scale cultivation of the *Piper betel* would promote the socioeconomic status of the regions too. In a nut shell, *Piper betel*-PBCs based nanocarriers still have to pass through a long journey to find them in clinical stage as alternative treatment strategy for cancer. However, with advancement of technological inno-

vations and collaborative research strategies would make the challenges to be conquered in future.

Acknowledgments

The authors are very much grateful to Prof. Manoj Ranjan Nayak, President, Siksha 'O' Anusandhan (Deemed to be University) for providing necessary facilities and encouragement.

Disclosure statement

The authors of the article have no conflict of interest to declare.

References

1. Ferguson LR, Chen H, Collins AR, et al. Malhotra M, Meeker AK, Amedei A, Amin A, Ashraf SS. Genomic instability in human cancer: Molecular insights and opportunities for therapeutic attack and prevention through diet and nutrition. SICB. 2015 Dec 1 (Vol. 35, pp. S5-S24). Academic Press. <https://doi.org/10.1016/j.semcan.2015.03.005>
2. Cabasag CJ, Fagan PJ, Ferlay J, et al. Ovarian cancer today and tomorrow: A global assessment by world region and Human Development Index using GLOBOCAN 2020. IJC. 2022 Nov 1;151(9):1535-41.
3. Bray F, Ferlay J, Soerjomataram I, et al. Global cancer statistics 2018: GLOBOCAN estimates of incidence and mortality worldwide for 36 cancers in 185 countries. CA. 2018 Nov;68(6):394-424.
4. Johnson KK, Koshy P, Yang JL, et al. Pre-clinical cancer theranostics—from nanomaterials to clinic: the missing link. Adv. Funct. Mater. 2021 Oct;31(43):2104199. <https://doi.org/10.1002/adfm.202104199>
5. Mohan L. Plant-based drugs as an adjuvant to cancer chemotherapy. Altern. Med.-Updat. 2020 Oct 28.

6. Abeloff MD, Armitage JO, Niederhuber JE, et al. Review of clinical oncology. Philadelphia: Churchill Livingstone J. 2004. <https://doi.org/10.1016/j.ijrobp.2004.11.021>
7. Pérez-Herrero E, Fernández-Medarde A. Advanced targeted therapies in cancer: Drug nanocarriers, the future of chemotherapy. *Eur J Pharm Biopharm.* 2015 Jun 1;93:52-79.
8. Desai AG, Qazi GN, Ganju RK, et al. Medicinal plants and cancer chemoprevention. *Curr. Drug Metab..* 2008 Sep 1;9(7):581-91. <https://doi.org/10.2174/138920008785821657>
9. Pin KY, Chuah AL, Rashih AA, et al. Antioxidant and anti-inflammatory activities of extracts of betel leaves (*Piper betle*) from solvents with different polarities. *J. Trop. For. Sci..* 2010 Oct 1:448-55.
10. Mahady GB. Global harmonization of herbal health claims. *J Nutr.* 2001 Mar;131(3):1120S-3S. <https://doi.org/10.1093/jn/131.3.1120S>
11. Guha P, Nandi S. Essential oil of betel leaf (*Piper betle* L.): A novel addition to the world food sector. *Essential Oil Research: Trends in Biosynthesis, Analytics, J. Ind. Microbiol. Biotechnol..* 2019:149-96. https://doi.org/10.1007/978-3-030-16546-8_5
12. Punuri JB, Sharma P, Sibyala S, et al. Piper betle-mediated green synthesis of biocompatible gold nanoparticles. *Int. Nano Lett.* 2012 Dec;2:1-9. <https://doi.org/10.1186/2228-5326-2-18>
13. Haslan H, Suhaimi FH, Thent ZC, et al. The underlying mechanism of action for various medicinal properties of Piper betle (betel). *Clin Ter.* 2015 Sep 1;166(5):208-14. doi: 10.7417/CT.2015.1880
14. Biswas P, Anand U, Saha SC, et al. Betelvine (*Piper betle* L.): A comprehensive insight into its ethnopharmacology, phytochemistry, and pharmacological, biomedical and therapeutic attributes. *JCMM.* 2022 Jun;26(11):3083-119. <https://doi.org/10.1111/jcmm.17323> Agarwal T, Singh R, Shukla AD, et al. Comparative analysis of antibacterial activity of four Piper betle varieties. *Adv Appl Sc Res.* 2012;3(2):698-705. Chauhan ES, Aishwarya J, Singh A, Tiwari A. A review: Nutraceuticals properties of Piper betel (Paan). *Am J Phytomed Clin Ther.* 2016;4(2):28-41.
15. Maiuri AR, Savant SS, Podicheti R, et al. DNA methyltransferase inhibition reduces inflammation-induced colon tumorigenesis. *Clin. Epigenetics.* 2019 Dec 2;14(12):1209-23.
16. Rai MP, Thilakchand KR, Palatty PL, et al. Piper betel Linn (betel vine), the maligned Southeast Asian medicinal plant possesses cancer preventive effects: Time to reconsider the wronged opinion. *APJCP.* 2011 Jan 1;12(9):2149-56.
17. Ganguly S, Mula S, Chattopadhyay S, et al. An ethanol extract of Piper betle Linn. mediates its anti-inflammatory activity via down-regulation of nitric oxide. *J. Pharm. Pharmacol.* 2007 May;59(5):711-8. <https://doi.org/10.1211/jpp.59.5.0012>
18. Kim SS, Oh OJ, Min HY, et al. Eugenol suppresses cyclooxygenase-2 expression in lipopolysaccharide-stimulated mouse macrophage RAW264.7 cells. *Life Sci.* 2003 Jun 6;73(3):337-48. [https://doi.org/10.1016/S0024-3205\(03\)00288-1](https://doi.org/10.1016/S0024-3205(03)00288-1) Choudhary D, Kale RK. Antioxidant and non-toxic properties of Piper betle leaf extract: in vitro and in vivo studies. *Phytotherapy Research: IJTPR.* 2002 Aug;16(5):461-66. <https://doi.org/10.1002/ptr.1015> Devasagayam TP, Tilak JC, Bolor KK, et al. Free radicals

- and antioxidants in human health: current status and future prospects. *JAPI*. 2004 Oct 25;52(794804):4. Young SC, Wang CJ, Lin JJ, et al. Protection effect of piper betel leaf extract against carbon tetrachloride-induced liver fibrosis in rats. *Arch. Toxicol.* 2007 Jan;81:45-55. <https://doi.org/10.1007/s00204-006-0106-0>
19. Veettil SR, Sunil EA, Mukunda A, et al. Anticancer effect of Piper betle leaf extract on KB cell lines-an in vitro study. *OMPJ*. 2022 Jan 1;13(1).
 20. Looi ML, Wong AK, Gnappagasan SA, et al. Anti-migratory effects of Piper betle leaf aqueous extract on cancer cells and its microtubule targeting properties. *J Zhejiang Univ Sci B*. 2020 Sep;21(9):745. [10.1631/jzus.B2000278](https://doi.org/10.1631/jzus.B2000278)
 21. Boontha S, Taowkaen J, Phakwan T, et al. Evaluation of antioxidant and anticancer effects of Piper betle L (Piperaceae) leaf extract on MCF-7 cells, and preparation of transdermal patches of the extract. *Trop. J. Pharm. Res.* 2019;18(6):1265-72. [10.4314/tjpr.v18i6.17](https://doi.org/10.4314/tjpr.v18i6.17)
 22. Preethi R, Padma PR. Anticancer activity of silver nanobioconjugates synthesized from Piper betle leaves extract and its active compound eugenol. *Int J Pharm Pharm Sci*. 2016;8(9):201-5. <http://dx.doi.org/10.22159/ijpps.2016.v8i9.12993>
 23. Alam B, Majumder R, Akter S, Lee SH. Piper betle extracts exhibit antitumor activity by augmenting antioxidant potential. *Oncol. Lett.* 2015 Feb 1;9(2):863-68. <https://doi.org/10.3892/ol.2014.2738>
 24. Toprani R, Patel D. Betel leaf: Revisiting the benefits of an ancient Indian herb. *SAJC*. 2013 Jul;2(3):140.
 25. Paranjpe R, Gundala SR, Lakshminarayana N, et al. Piper betel leaf extract: anticancer benefits and bio-guided fractionation to identify active principles for prostate cancer management. *Carcinogenesis*. 2013 Jul 1;34(7):1558-66. <https://doi.org/10.1093/carcin/bgt066> Abraham NN, Kanthimathi MS, Abdul-Aziz A. Piper betle shows antioxidant activities, inhibits MCF-7 cell proliferation and increases activities of catalase and superoxide dismutase. *BMC complement. med. ther.* 2012 Dec;12(1):1-1. <https://doi.org/10.1186/1472-6882-12-220> Bhisey RA. Chemistry and toxicology of smokeless tobacco. *IJC*. 2012 Oct 1;49(4):364-72. [10.4103/0019-509X.107735](https://doi.org/10.4103/0019-509X.107735)
 26. Gupta RK, Guha P, Srivastav PP. Phytochemical and biological studies of betel leaf (Piper betle L.): Review on paradigm and its potential benefits in human health. *Acta Ecol. Sin.* 2022 Sep 27. <https://doi.org/10.1016/j.chnaes.2022.09.006>
 27. Chang MC, Uang BJ, Wu HL, et al. Inducing the cell cycle arrest and apoptosis of oral KB carcinoma cells by hydroxychavicol: roles of glutathione and reactive oxygen species. *Br. J. Pharmacol.* 2002 Feb;135(3):619-30. <https://doi.org/10.1038/sj.bjp.0704492>
 28. Majumdar AG, Subramanian M. Hydroxychavicol from Piper betle induces apoptosis, cell cycle arrest, and inhibits epithelial-mesenchymal transition in pancreatic cancer cells. *Biochem. Pharmacol.* 2019 Aug 1;166:274-91.
 29. Kumar LA, Pattnaik G, Satapathy BS, et al. Targeting to brain tumor: Nanocarrier-based drug delivery platforms, opportunities, and challenges. *J Pharm Bioallied Sci.* 2021 Apr;13(2):172. DOI: [10.4103/jpbs.JPBS_239_20](https://doi.org/10.4103/jpbs.JPBS_239_20)
 30. Katouzian I, Esfanjani AF, Jafari SM, et

- al. Formulation and application of a new generation of lipid nano-carriers for the food bioactive ingredients. *JFST*. 2017 Oct 1;68:14-25. <https://doi.org/10.1016/j.tifs.2017.07.017>
31. 31. Ravalika, V., and Sailaja, A.K. (2017). Formulation and evaluation of etoricoxib niosomes by thin film hydration technique and ether injection method. *Nano Biomed Eng*, 9(3): 242-248.
32. 32. Safwat, M.A., Soliman, G.M., Sayed, D., and Attia, M.A. (2016). Gold nanoparticles enhance 5-fluorouracil anti-cancer efficacy against colorectal cancer cells. *Int J Pharm*, 513: 648-658.
33. 33. John-Africa, L.B., Yahaya, T.A., and Isimi, C.Y. (2014). Anti-ulcer and wound healing activities of *Sida corymbosa* in rats. *Afr J Tradit Complement Altern Med*, 11(1): 87-92.
34. 34. Bayat, S., Amiri, N., Pishavar, E., Kalalinia, F., Movaffagh, J., and Hashemi, M. (2019). Bromelain-loaded chitosan nanofibers prepared by electrospinning method for burn wound healing in animal models. *Life Scie*, 229: 57-66.
35. 35. Nematollahi, M.H., Pardakhty, A., Torkzadeh-Mahanai, M., Mehrabani, M., and Asadikaram, G. (2017). Changes in physical and chemical properties of niosome membrane induced by cholesterol: a promising approach for niosome bilayer intervention. *RSC Adv*, 7(78): 49463-49472.
36. 36. Bhattacharya, M., Malinen, M.M., Lauren, P., Lou, Y.R., Kuisma, S.W., and Kanninen, L. (2012). Nanofibrillar Cellulose Hydrogel Promotes Three-Dimensional Liver Cell Culture. *J Control Release*, 164(3): 291-298.
37. 37. Pripem, A., Janpim, K., Nualkaew, S., and Mahakunakorn, P. (2016). Topical niosome gel of *Zingiber cassumunar* Roxb. extract for anti-inflammatory activity enhanced skin permeation and stability of compound. *AAPS Pharmscitech*, 17:631-9.